OFFICIAL JOURNAL OF THE SCIENTIFIC SOCIETY OF ANATOMISTS, HISTOLOGISTS, EMBRYOLOGISTS AND TOPOGRAPHIC ANATOMISTS OF UKRAINE

DOI: 10.31393
ISSN 1818-1295
eISSN 2616-6194

ВІСНИК МОРФОЛОГІЇ
REPORTS OF MORPHOLOGY

Vol. 30, №3, 2024

Scientific peer-reviewed journal in the fields of normal and pathological anatomy, histology, cytology and embryology, topographical anatomy and operative surgery, biomedical anthropology, ecology, molecular biology, biology of development

Published since 1993
Periodicity: 4 times a year

Vinnytsya · 2024

ВІСНИК МОРФОЛОГІЇ - REPORTS OF MORPHOLOGY

Founded by the "Scientific Society of Anatomists, Histologists, Embryologists, and Topographic Anatomists of Ukraine" and National Pyrogov Memorial Medical University, Vinnytsya in 1993

Certificate of state registration КВ №9310 from 02.11.2004

Professional scientific publication of Ukraine in the field of medical sciences in specialties 221, 222, 228, 229
According to the list of professional scientific publications of Ukraine, approved by the order of the Ministry of Education and Science of Ukraine No. 1188 of 24.09.2020
Professional scientific publication of Ukraine in the field of biological sciences in specialty 091
According to the list of professional scientific publications of Ukraine, approved by the order of the Ministry of Education and Science of Ukraine No. 1471 of 26.11.2020

Approved by the Academic Council of National Pyrogov Memorial Medical University, Vinnytsya, protocol №1 from 28.08.2024.

Indexation: Scopus, CrossRef, Index Copernicus, Google Schoolar Metrics, National Library of Ukraine Vernadsky

Address editors and publisher:
Pyrogov Str. 56,
Vinnytsya, Ukraine - 21018
Tel.: +38 (0432) 553959
E-mail: nila@vnmu.edu.ua

Computer page-proofs - Klopotovska L.O.
Translator - Gunas V.I.
Technical support - Levenchuk S.S.
Scientific editing - editorship

The site of the magazine - https://morphology-journal.com

CONTENT

DOI: 10.31393/morphology-journal-2024-30(3)-01 Reports of Morphology, Vol. 30, №3, Pages 5-14

ISSN 1818-1295 eISSN 2616-6194

REPORTS OF MORPHOLOGY

Official Journal of the Scientific Society of Anatomists, Histologists, Embryologists and Topographic Anatomists of Ukraine

journal homepage: https://morphology-journal.com

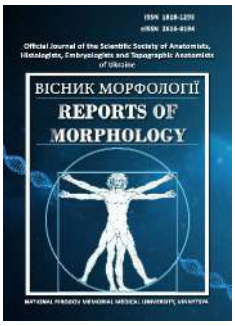

Structural changes in the organs of the lymphoid system in terms of induced carcinogenesis

Kramar S. B.[1], Soroka Yu. V.[1], Havryliuk-Skyba H. O.[2], Pyda V. P.[1], Nebesna Z. M.[1], Lisnychuk N. Ye.[1]

[1]I. Horbachevsky Ternopil National Medical University, Ternopil, Ukraine
[2]Bogomolets National Medical University, Kyiv, Ukraine

ARTICLE INFO
Received: 12 February 2024
Accepted: 20 June 2024

UDC: 616.411/428/438-091.8:616.345-006.6-06]-092.9

CORRESPONDING AUTHOR
e-mail: kramarsb@tdmu.edu.ua
Kramar S. B.

CONFLICT OF INTEREST
The authors have no conflicts of interest to declare.

FUNDING
This investigation is a part of the research project, which was funded by the Ministry of Health of Ukraine (Grant number 0119U002307).

DATA SHARING
Data are available upon reasonable request to corresponding author.

Colorectal cancer is the third most common cancer in the world. Despite recent therapeutic advances, it causes more than 500,000 deaths each year. The immune system plays a crucial role in protecting the body from cancer. However, cancer cells are able to evade immune detection and destruction. For example, they can downregulate antigen expression, produce immunosuppressive molecules, or recruit immune cells that perform regulatory or inhibitory functions. Understanding the complex interactions between the immune system and carcinogenesis is crucial for developing effective cancer treatments. The study aimed to determine the morphological changes in the thymus, spleen, and lymph nodes under N,N-dimethylhydrazine-induced carcinogenesis. The study was performed on 77 male outbred albino rats weighing 190-230 g, kept in standard vivarium conditions. Colon adenocarcinoma was modeled by administration of N,N-dimethylhydrazine hydrochloride for 30 weeks. To study the peculiarities of morphological and functional changes in lymphoid organs in the dynamics of colon tumor lesions, animals were withdrawn from the experiment every 30 days. Paraffin sections of the thymus, spleen, and lymph nodes 5-6 μm thick were made on a rotary microtome and stained with hematoxylin and eosin. The experimental investigation unveiled the character and extent of histological alterations within the lymphoid system organs under conditions of N,N-dimethylhydrazine-induced colon adenocarcinomatosis. As the experiment progressed, there was a noticeable escalation in the severity of detrimental and degenerative modifications observed in the thymus, spleen, and lymph nodes. These modifications were evident in the disruption of blood circulation within the examined organs, leading to vascular wall impairment and hemorrhaging, the disarray of morphofunctional elements and the development of fibrosis. Given the significant role played by the thymus, spleen, and lymph nodes in regulating carcinogenesis and maintaining immune balance, it is extremely important to delve into understanding the changes in their structure and function. Obtained results indicate that carcinogenesis is accompanied by pronounced morphological changes in the structural components of the lymphoid system organs, the degree of which increases in direct proportion to the duration of exposure to the oncogenic factor.

Keywords: *colon adenocarcinoma, spleen, thymus, lymph node, morphology.*

Introduction

Every year, 10 million new cases of malignant tumors are registered worldwide. This is one of the leading causes of death, which negatively affects life expectancy and causes irreversible losses to the population. According to the World Health Organization, by 2050, cancer incidence in the world will increase to 24.0 million cases, and mortality will reach 16.0 million registered cases [1, 24].

The development of any pathological process, especially carcinogenesis, occurs against the background of altered immune reactivity. Monitoring and correct interpretation of immunological test results, as well as understanding the peculiarities of morphological and functional changes in the organs of the lymphoid system, play an important role in the diagnosis and targeted treatment of tumors [7].

In many cases, the leading reason for developing various diseases is not the factor that caused a particular pathological state but rather disorders caused by altered,

excessive, or weakened immune processes. The immune system's role in carcinogenesis is complex and multifaceted, affecting every stage of the disease, from tumor development to treatment. Immune cells can act as inhibitors of tumor initiation and progression, as well as catalysts for proliferation, infiltration, and metastasis [12].

The presence of organized lymphoid structures is crucial for the proper functioning of adaptive immunity. Primary lymphoid organs, such as the thymus and red bone marrow, produce lymphocytes from immature progenitor cells. On the other hand, secondary lymphoid organs, including the spleen and lymph nodes, serve as a site for B- and T-cell activation and proliferation, as well as processes such as somatic hypermutation, affinity maturation, and immunoglobulin class switching. In addition, tissues affected by chronic inflammation can develop tertiary lymphoid organs, which include newly formed B-cell follicles and T-cell areas [6, 28].

The complex interaction mechanisms between a malignant tumor and the immune system reflect the most important function of the immune system - regulating cell regeneration and proliferation. Perhaps specific immunity is responsible not for destroying malignant cells but for regulating their growth and development. According to the latest scientific data, the mechanisms of nonspecific immune defense may play a crucial role in cancer prevention [3, 5, 23, 25].

Today, there is virtually no information on gradual changes in the structural organization of the lymphoid system in the dynamics of carcinogenesis. However, these changes may be crucial for inhibition or, conversely, cancer progression. Despite significant progress in understanding the basic mechanisms of carcinogenesis in recent years, many aspects still need to be clarified. Given that the thymus, spleen, and lymph nodes are among the most important organs that control carcinogenesis and determine immune homeostasis, further research into their structural and functional changes is more than justified.

Our work *aims* to determine the morphological changes in the thymus, spleen, and lymph nodes under N,N-dimethylhydrazine-induced carcinogenesis conditions.

Materials and methods

The study was conducted on 77 male outbred albino rats weighing 190-230 g, kept in standard vivarium conditions. The survival and weight of the animals were monitored throughout the experiment. Animals had free access to drinking water and a basic food diet ad libitum. The experimental animals were randomly divided into the following groups: control group (I); experimental group (II), which was administered the carcinogen for 30 weeks. After 30 weeks of administration of N,N-dimethylhydrazine dihydrochloride (DMH), all animals of group II were histologically confirmed to have colon adenocarcinoma in situ.

The N,N-dimethylhydrazine-induced (DMH-induced) carcinogenesis model is widely used in experimental oncology as the most widely used and 100 % reproducible model of neoplastic colon lesions. It has several morphological and molecular characteristics similar to sporadic human colorectal cancer [20].

Carcinogenesis was modeled by injection of N,N-dimethylhydrazine hydrochloride (Sigma-Aldrich Chemie, Japan, series D161802), pre-diluted with isotonic sodium chloride solution. The carcinogen was injected subcutaneously into the inter-lobar area at 7.9 mg/kg body weight once a week for 30 weeks. The control group of animals was weekly injected subcutaneously with saline at the rate of 0.1 ml per 100 g of body weight in a similar area of the body to simulate possible stress effects.

The administration of the carcinogen and the correction factor and the subsequent sampling of blood and organs for further studies were performed at the same time of day (10^{00}-12^{00}) in a special room.

To study the peculiarities of morphofunctional changes in lymphoid organs in the dynamics of colon tumor lesions, animals of the control and experimental groups were withdrawn from the experiment every 30 days (7 stages of the study).

All manipulations with experimental animals met international requirements. They were carried out following the requirements of the European Convention for the Protection of Vertebrate Animals Used for Experimental and Other Medical Purposes and were accredited by the Bioethics Committee of the I. Horbachevsky Ternopil National Medical University (Protocol No. 75 of 01.11.2023).

For histologic examination, pieces of the spleen, thymus, and lymph node were taken and fixed in a 10% neutral formalin solution. Tissues were processed in a closed vacuum histoprocessor LogosOne (Milestone, Italy). Paraffin sections 5-6 μm thick were made on a rotary microtome AMR400 (Amos, Australia) and stained with hematoxylin and eosin (Biognost, Croatia). Histological specimens were examined using a Nikon Eclipse Ci-E light microscope (Nikon, Japan) and photographed using a SIGETA M3CMOS 14000 camera (Sigeta, Ukraine).

Results

Histological studies of the thymus of white male rats showed that 1 and 2 months after the induction of oncogenesis, the structural components of the vascular bed of the organ expand. There is hemolysis of erythrocytes in the vessels. The thymus cortex is densely filled with lymphocytes, which causes its intensely basophilic color. In addition to lymphocytes, epithelial reticulocytes, components of the organ's stroma, are clearly visible in the medulla (Fig. 1).

At 3 and 4 months after the start of the experiment, microscopically, the lumens of capillaries, arterioles, and venules were dilated, with stasis and hemolysis of erythrocytes. The connective tissue interlobular trabeculae vessels have thickened walls (Fig. 2).

Stromal cells are better seen within the medulla of the

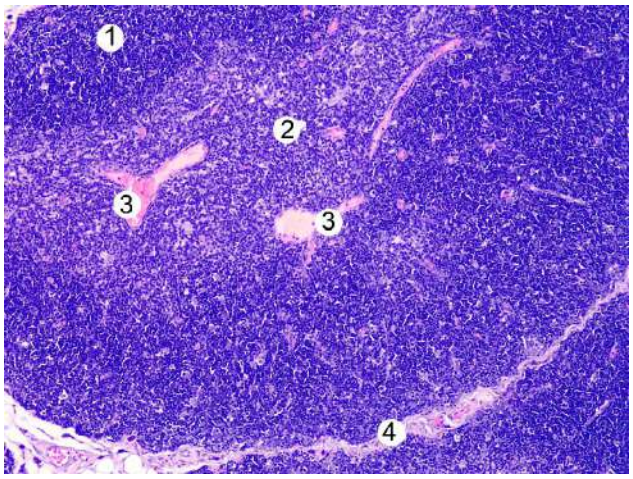

Fig. 1. Microscopic state of the thymus of animals after 2 months of chronic DMH exposure. Cortex (1) and medulla (2) of the lobule, blood vessels (3), interlobular trabeculae (4). Hematoxylin and eosin staining. Ocular x10, objective x10.

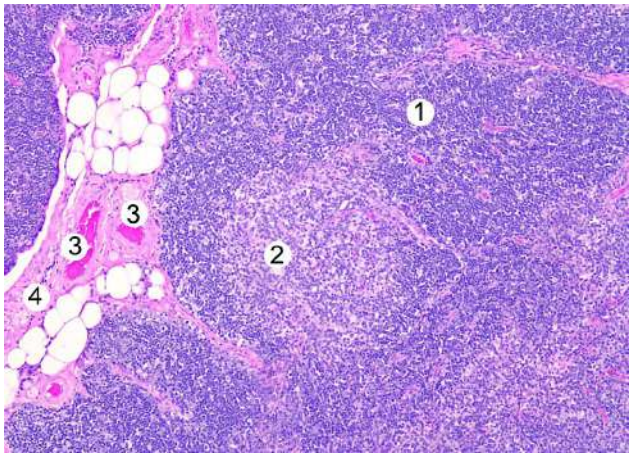

Fig. 2. Histological changes in the thymus of animals after 3 months of chronic DMH exposure. Cortex (1) and medulla (2) of the lobule, blood vessels (3), interlobular trabeculae (4). Hematoxylin and eosin staining. Ocular x10, objective x10.

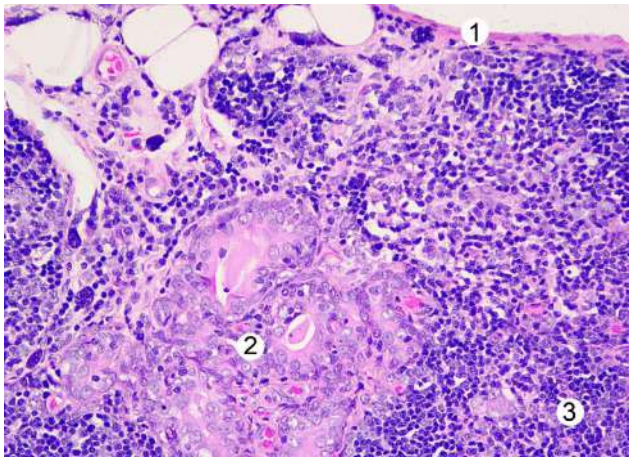

Fig. 3. Histological changes in the thymus of animals after 6 months of chronic DMH exposure. Capsule (1), thickened connective tissue trabeculae (2), cortex (3). Hematoxylin and eosin staining. Ocular x10, objective x20.

lobule. Epithelial reticulocytes at the light-optical level at this time of the experiment have a typical structure. Lymphocytes moderately fill the cortex and are unevenly distributed in the medulla of the lobule.

Histological examination at 5 and 6 months of the experiment revealed a tendency to fibrosis of the thymus lobules. In some fields of view, thickened layers of loose connective tissue were visible (Fig. 3).

The vessels in the interlobular trabeculae and the lobules were characterized by hemorrhage, stasis, thrombosis, and perivascular edema. The loose connective tissue of the interlobular septa contained many adipocytes (Fig. 4).

The hemocapillaries of the cortex are often overstretched and filled with hemolyzed oxyphilic contents. Among the components of the microcirculatory bed, there are vessels with stasis. Epithelial reticulocytes are enlarged. The cellular elements of the parenchyma are unevenly distributed in the lobules, which causes lucency in numerous areas, especially in the medulla.

After 7 months from the start of N,N-dimethylhydrazine hydrochloride administration, microscopic examination of the thymus of laboratory white rats revealed deepening of destructive changes in the components of the organ's vascular bed, manifested not only by overstretching of the lumens, thrombosis, and coagulation but also by damage to the vessel wall, leading to hemorrhages in the thymic parenchyma.

A large number of lobules look lucent, with a lower density of lymphoid cell elements in them (Fig. 5). In the medulla, layers of senescent epithelial reticulocytes in the form of Hassal's bodies are often seen.

After 1 and 2 months of the experiment, at the microscopic level, the spleen of the experimental animals showed full blood vessels and red pulp parenchyma. The trabecular arteries and veins are filled with blood formed elements and dilated, with microthrombi in some of them.

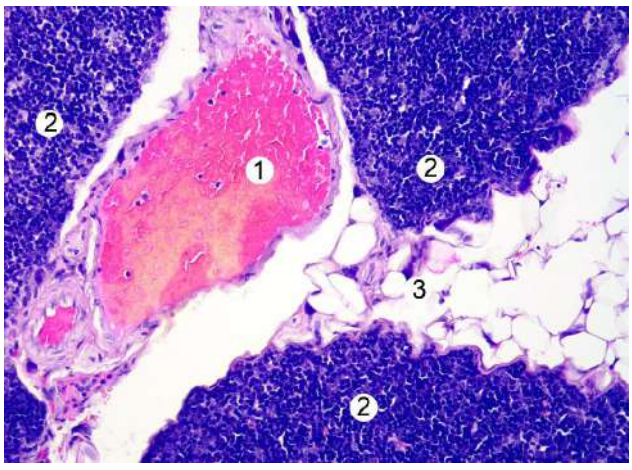

Fig. 4. Microscopic state of the thymus of animals after 6 months of chronic DMH exposure. Thrombus in the interlobular vein (1), lobule fragments (2), connective tissue with adipocytes (3). Hematoxylin and eosin staining. Ocular x10, objective x20.

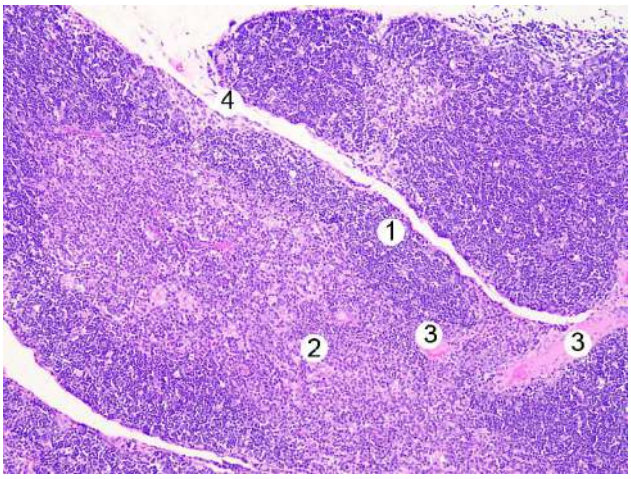

Fig. 5. Histological changes in the thymus of animals after 7 months of chronic DMH exposure. Cortex (1) and medulla (2) of the lobule, blood vessels (3), interlobular trabeculae (4). Hematoxylin and eosin staining. Ocular x10, objective x10.

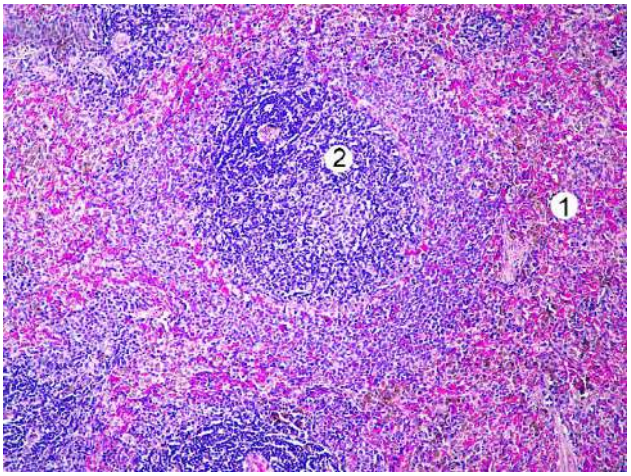

Fig. 6. Microscopic state of the spleen of animals after 1 month of chronic DMH exposure. Red pulp (1), white pulp lymph node (2) with clear zonation. Hematoxylin and eosin staining. Ocular x10, objective x10.

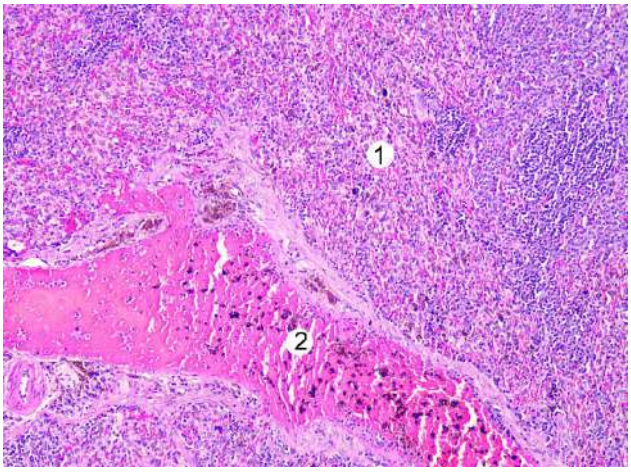

Fig. 7. Histological changes in the spleen of animals after 4 months of chronic DMH exposure. Red pulp (1), thrombosed vessel (2). Hematoxylin and eosin staining. Ocular x10, objective x10.

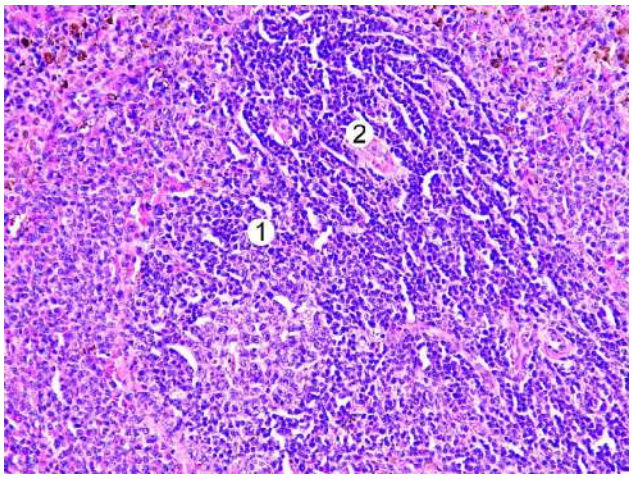

Fig. 8. Histological changes in the spleen of animals after 3 months of chronic DMH exposure. Lymph nodule of white pulp (1), central artery (2). Hematoxylin and eosin staining. Ocular x10, objective x20.

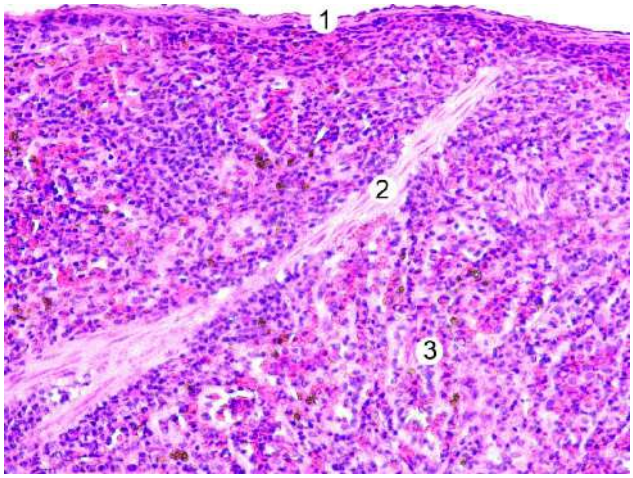

Fig. 9. Microscopic condition of the spleen of animals after 6 months of chronic DMH exposure. Spleen capsule (1), thickened trabeculae (2), red pulp (3). Hematoxylin and eosin staining. Ocular x10, objective x20.

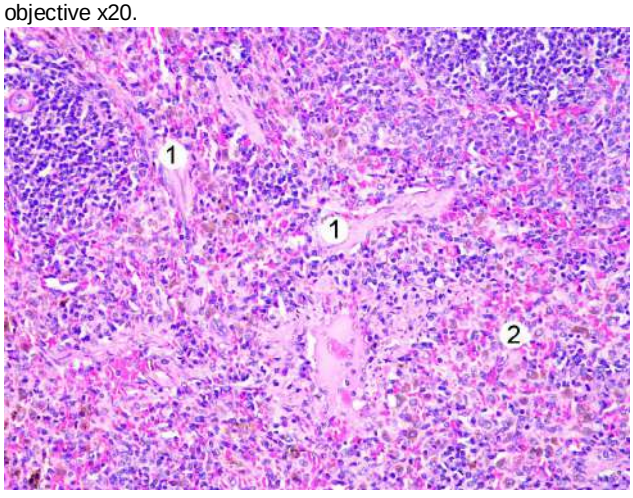

Fig. 10. Microscopic changes in the spleen of animals 7 months after chronic DMH exposure. Thickened trabeculae (1), red pulp (2). Hematoxylin and eosin staining. Ocular x10, objective x20.

Structural elements of the white pulp (lymph nodules) of different sizes, with well-defined zonation, are dispersed within the organ. Their reticular fibers are oriented eccentrically along the perimeter of the central artery. In the germinal center, stromal elements form a mesh in the lumens of which lymphocytes and plasma cells are located (Fig. 6).

At 3 and 4 months after the start of N,N-dimethylhydrazine dihydrochloride administration, histologically, splenic hyperplasia was observed due to stromal and parenchymal components. There is edema of reticular fibers in the stroma and trabeculae.

Microscopically, in many fields of view, the vessel lumens are thrombosed. Stasis was detected in the sinusoidal capillaries, indicating a slowing of blood flow in the organ. Macrophages with granules of hemosiderin pigment and lymphocytes were present in the lumens of the sinuses of the organ (Fig. 7).

At this time of the experiment, the red pulp is blood-filled, with the deposition of red blood cells and platelets. Hemolysis of red blood cells is often observed.

The lymph nodules of the white pulp are enlarged during these experimental periods, and there is an increase in the number and density of lymphocytes and plasmocytes of different sizes in their different zones (Fig. 8).

Significant changes in blood circulation were detected in the spleen 5 and 6 months after the induction of carcinogenesis by N,N-dimethylhydrazine dihydrochloride. In the dilated and full blood vessels, the adhesions of the cellular elements are noticeable. In the parenchyma of the organ, hemorrhages and excessive blood deposition were detected. The connective tissue capsule of the organ is thin, trabeculae are thickened, and stromal components are often fragmented (Fig. 9).

The white pulp's germinal centers and marginal zones are lucent due to the eviction of lymphocytes. The zonation of the nodules is disturbed.

After 7 months from the start of N,N-dimethylhydrazine dihydrochloride administration, microscopic examination revealed destructive and degenerative changes in the organ structure. The components of the spleen stroma were swollen and hypertrophied, manifested by thickening of the trabeculae. There was also a significant number of fibroblastic cells, leading to fibrosis (Fig. 10).

The organ parenchyma was unevenly blood-filled at the microscopic level. Both low-blooded and overstretched, excessively blood-filled vessels were observed, indicating congestion. Thrombosis of the microcirculatory vessels and hemolysis of erythrocytes were often detected. The red pulp contained macrophages with hemosiderin grains in the cytoplasm (Fig. 11).

Degeneration of lymphoid tissue is detected in the white pulp, manifested by a decrease in the volume of lymph nodules, hemorrhages in them, disappearance of germinal centers, and disorganization of the periarterial zone (Fig. 12).

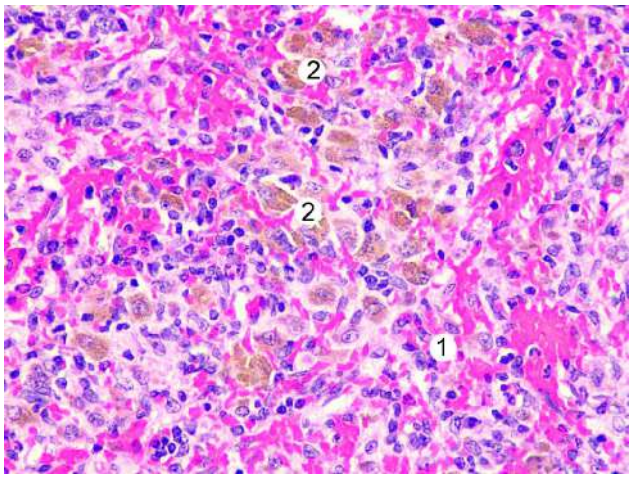

Fig. 11. Histological changes in the spleen of animals after 7 months of chronic DMH exposure. Red pulp (1), macrophages with hemosiderin grains (2). Hematoxylin and eosin staining. Ocular x10, objective x40.

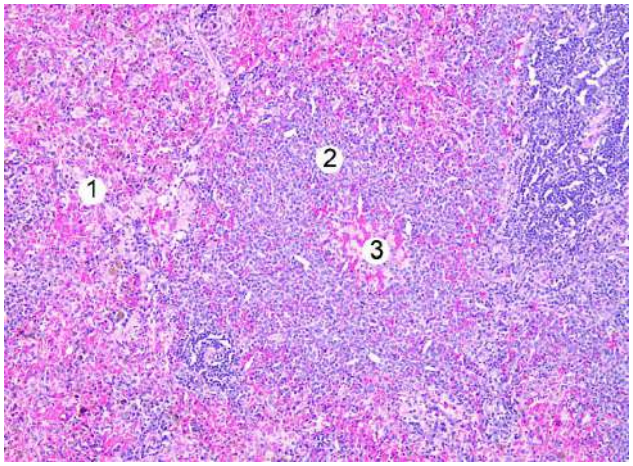

Fig. 12. Histological condition of the spleen of animals after 7 months of chronic DMH exposure. Red pulp (1), white pulp (2), hemorrhages (3). Hematoxylin and eosin staining. Ocular x10, objective x10.

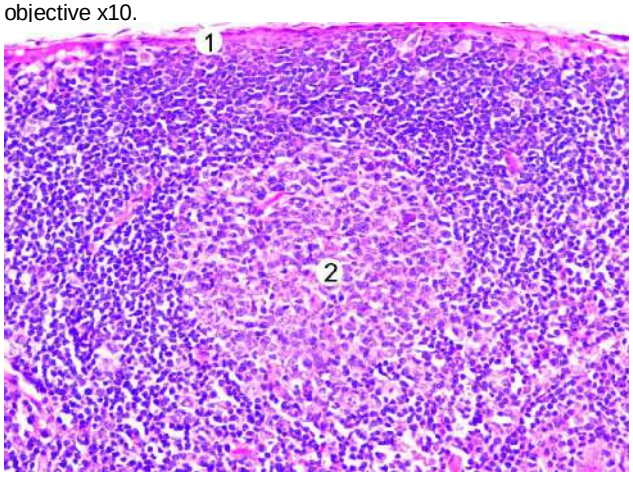

Fig. 13. Microscopic condition of the lymph node of animals after 1 month of chronic DMH exposure. Capsule (1), lymph nodule with a well-distinct germinal center (2). Hematoxylin and eosin staining. Ocular x10, objective x20.

The study of microscopic changes in the lymph nodes of white rats 1 and 2 months after the start of N,N-dimethylhydrazine dihydrochloride administration showed that the organ parenchyma is composed of cortex and medulla. The cortex consists of lymphoid nodules, among which secondary nodules dominate, with a germinal center containing mainly blast cells. Small lymphocytes are densely located in the marginal zone of the lymph nodule (Fig. 13).

The paracortical zone of the organ at this stage of the experiment is densely packed with small lymphocytes. The medullary sinuses are slightly dilated, with small lymphocytes, plasma cells, and macrophages in their lumen. The medullary cords are densely filled with lymphocytes and sometimes plasma cells. The cells of the reticular stroma retain their characteristic structural organization.

After 3 and 4 months of the experiment, the connective tissue capsule of the lymph node thickens. The germinal centers of the cortical lymph nodules are enlarged compared to the previous period, indicating an increase in the proliferative activity of lymphocytes (Fig. 14).

The vessels of the microcirculatory bed are dilated, and red blood cells are arranged in columns in their lumen. The lumens of the arteries and veins are filled with blood formed elements. Trabecular sinuses are moderately dilated, and the number of lymphocytes in their lumen increases compared to the previous period (Fig. 15).

At 5 and 6 months after the start of N,N-dimethylhydrazine dihydrochloride administration, the germinal centers of the lymph nodules are light and enlarged. Microscopically, they are dominated by medium-sized lymphocytes and lymphoblasts. There are also cells in a state of division and single destructively altered cells.

The components of the venous bed of the organ are deformed and dilated, full-blooded. Perivascular edema is present. Capillaries are dilated. The lumen of the medullary sinuses is filled mainly with small lymphocytes, macrophages, and reticular cells.

Compared to the experiment's previous terms, the node capsule's thickness continues to increase (Fig. 16).

Seven months after the induction of carcinogenesis in the lymph nodes, histologically, the deepening of destructive changes in the structural components of the organ was noted. The germinal centers of the cortical lymph nodules are lucent and enlarged and have intercellular layers (Fig. 17).

The trabecular and medullary sinuses are thickened due to the growth of loose connective tissue. The vessels of the organ retain full blood flow and have significantly dilated lumens, sometimes with wall destruction and hemorrhages. The wall of some arteries with signs of sclerosis. Hemocapillaries are dilated and full of blood (Fig. 18). There is perivascular and parenchymal edema. The medullary cords are densely filled with lymphoid cells, some of which have pathologically altered forms.

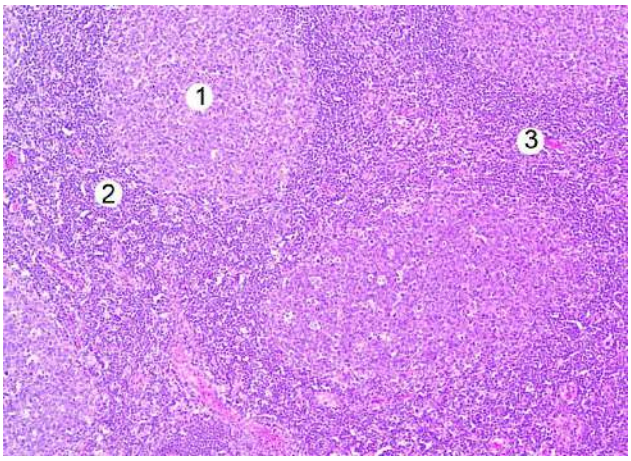

Fig. 14. Histological state of the lymph node of animals after 3 months of chronic DMH exposure. Germinal center (1) and marginal zone of the lymph nodule (2), blood-filled capillary (3). Hematoxylin and eosin staining. Ocular x10, objective x10.

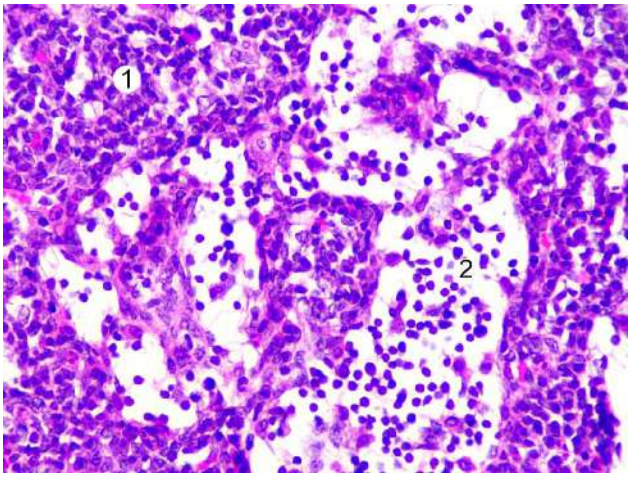

Fig. 15. Histological state of the medulla of the lymph node of animals after 4 months of chronic DMH exposure. Medullary cord (1) and medullary sinus (2). Hematoxylin and eosin staining. Ocular x10, objective x40.

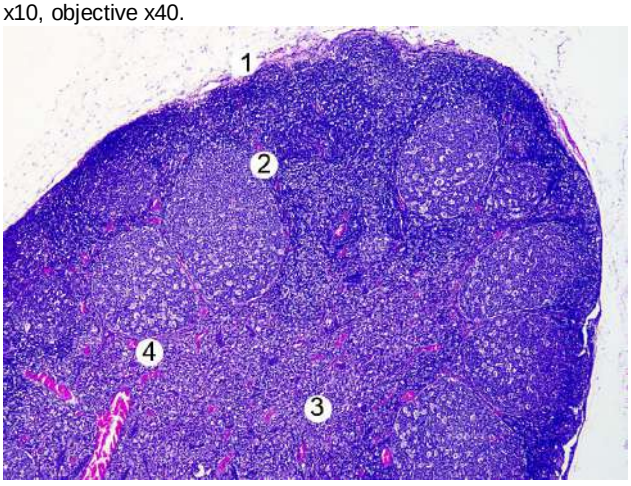

Fig. 16. Histological state of the lymph node of animals after 5 months of chronic DMH exposure. Capsule (1), cortex (2), medulla (3), blood vessels (4). Hematoxylin and eosin staining. Ocular x10, objective x4.

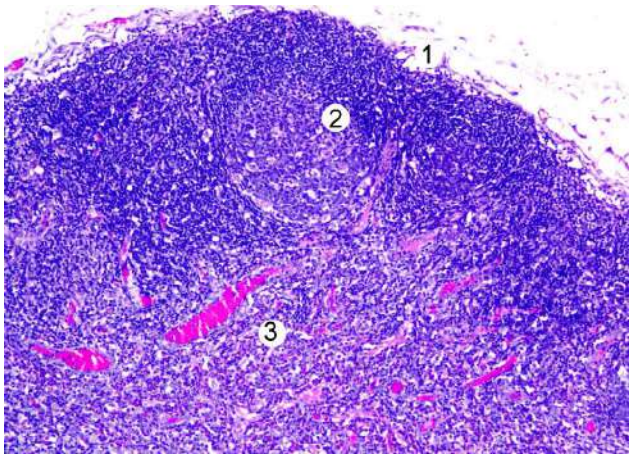

Fig. 17. Microscopic state of the lymph node of animals after 7 months of chronic DMH exposure. Capsule (1), lymph nodule (2), paracortical zone (3), blood vessels (4). Hematoxylin and eosin staining. Ocular x10, objective x10.

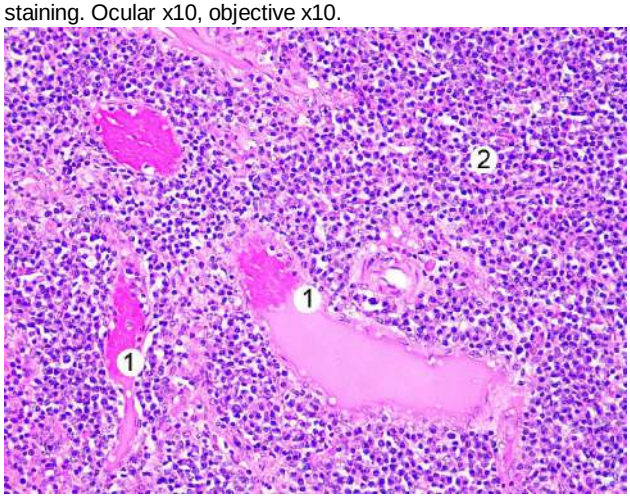

Fig. 18. Histological state of the lymph node of animals after 7 months of chronic DMH exposure. Blood vessels with hemolysis (1), lymphocytes (2). Hematoxylin and eosin staining. Ocular x10, objective x20.

Discussion

Thus, in the dynamics of the experiment, a significant increase in destructive and degenerative changes in the thymus, spleen, and lymph nodes was observed. These pathological processes were accompanied by impaired blood circulation in the studied lymphoid organs, leading to vascular wall damage and hemorrhages. The most pronounced disorganization of morphofunctional elements and the development of fibrosis in the thymus, spleen, and lymph nodes were observed after seven months of chronic DMH exposure.

Colorectal cancer is the third most common cancer in the world. Despite recent therapeutic advances, it causes more than 500,000 deaths each year. Therefore, there is a real need for therapeutic progress to reduce the risk of recurrence after surgery or to prolong the survival of patients with metastatic disease. Progress can be achieved by understanding the immune response's role and mechanisms in colorectal cancer and the development of immunotherapy [19].

The immune system plays a crucial role in protecting the body against cancer. However, cancer cells can find different ways to avoid immune detection and destruction. For example, they can downregulate antigen expression, produce immunosuppressive molecules, or recruit immune cells that perform regulatory or inhibitory functions. These complex mechanisms involve different cell types, signaling pathways, and molecules [31], which can lead to immune evasion and promote tumor growth and progression [10].

One important mechanism is the recognition and destruction of cancer cells by immune cells, such as T lymphocytes and natural killer cells. These cells can identify and target cancer cells that express abnormal or mutated proteins known as antigens. This process, known as immunosurveillance, is essential for preventing tumors from developing.

It has been found that the presence of lymphoid aggregates in the tumor microenvironment is associated with better survival outcomes for patients with colorectal cancer, and their density in the tumor microenvironment is associated with a reduced risk of tumor recurrence. These studies suggest that the organs of the lymphoid system, as well as the presence of lymphoid aggregates and lymphocytes in the tumor microenvironment, may play an important role in the immune response to colorectal cancer and can potentially be used as prognostic markers or therapeutic targets [15, 17, 22].

Recent studies have also emphasized the importance of the tumor microenvironment in shaping the immune response to cancer. The tumor microenvironment comprises various cell types, including cancer, immune, and stromal cells, as well as extracellular matrix components. Interactions between these components can either promote or suppress the immune response to cancer [32].

Understanding the complex interactions between the immune system and carcinogenesis is crucial for developing effective cancer therapies.

Lymph node metastasis is an important prognostic factor in colorectal cancer. It has long been established that colorectal carcinoma in situ has a low ability to metastasize to the lymph nodes, which is supported by the hypothesis that the normal colon mucosa lacks lymphatic vessels [6].

Structural and functional changes in the spleen in induced colorectal cancer have been studied by many researchers [4, 13, 16, 18]. However, today, there is no consensus on the role of the spleen in carcinogenesis. T. Toge and colleagues [27] found that T-suppressors, which can suppress the antitumor activity of the immune system, enter the bloodstream from the spleen. K. Noma and colleagues [16] also concluded that the spleen plays an

immunosuppressive role in gastric cancer, which contributes to the activation of cancer in the stomach.

L. Mellemkjaer and colleagues [13], in a large-scale scientific study, assessed the risk of developing cancer in patients with splenectomy due to traumatic injury (1103 patients) and splenectomy for other reasons (5212 patients). The authors concluded that there was no increased risk of cancer among patients who underwent splenectomy due to trauma. Among patients who underwent splenectomy for non-traumatic reasons, there was an excess of several specific types of cancer, but this can be largely explained by factors related to the underlying disease and/or treatment of this disease.

Published data vary in their interpretation of the effect of spleen cell culture on the activity of experimental oncological pathology development - either tumor progression or regression. The situation is similar in assessing spatial changes in the spleen - either reduction in size or tissue consolidation or splenomegaly [2, 18, 30].

The thymus is a rare site for metastasis of any malignant tumor, although cases of metastasis of breast, thyroid, testicular, and prostate cancer have been reported. It is believed that the histological structure of the thymus contributes significantly to its resistance to metastatic diseases. The involvement of the thymus in cellular immunity and the presence of the blood-thymus barrier usually prevent direct contact between its parenchyma and tumor cells or antigens [4, 8, 14, 21]. The function of T-cell immunity is key in regulating the onset and recurrence of cancer and stimulating the immune response against tumors [29]. Activated T cells enhance the immune response by secreting interferon (IFN)-γ or directly killing tumor cells through cytotoxic mechanisms [9, 11, 26]. There is a marked lack of reliable evidence on the impact of thymus function on carcinogenesis.

Since the condition of the organs under study largely determines the state of the body's immune homeostasis, we consider it advisable to conduct further immunohistochemical studies of the spleen, lymph nodes, and thymus to assess their functional capacity. Understanding the specifics of disorders in these organs can be the basis for the development of adequate and pathogenetically based methods of immunocorrection at all stages of treatment.

Conclusions

1. Carcinogenesis is accompanied by pronounced morphological changes in the structural components of the lymphoid system organs, the degree of which increases in direct proportion to the duration of exposure to the oncogenic factor.

2. Seven months after starting N,N-dimethylhydrazine hydrochloride administration, microscopic changes in the thymic vascular bed were found, manifested by lumen dilation, thrombosis, coagulation, wall damage, and hemorrhage. There was a decrease in the density of lymphocytes in thymic lobules and an increase in the number of Hassall's corpuscles.

3. In the spleen, at the final stage of induction of carcinogenesis, histologically, trabecular thickening, thrombosis of microcirculatory vessels, and hemolysis of erythrocytes, degeneration of lymphoid tissue, which was manifested by a decrease in the volume of lymph nodules and their disorganization, were detected.

4. In the lymph nodes at the late stages of the experiment, histologically, there was elucidation and enlargement of the germinal centers of the lymphoid nodules, dilation of the lumens of the vessels, sometimes with the destruction of their walls and hemorrhages, perivascular and parenchymal edema.

References

[1] Argiles, G., Tabernero, J., Labianca, R., Hochhauser, D., Salazar, R., Iveson, T., … & Taieb, J. (2020). Localised colon cancer: ESMO Clinical Practice Guidelines for diagnosis, treatment and follow-up. *Ann. Oncol.,* 31, 1291-1305. doi: 10.1016/j.annonc.2020.06.022

[2] Beheshti, A., Wage, J., McDonald, J. T., Lamont, C., Peluso, M., Hahnfeldt, P., & Hlatky, L. (2015). Tumor-host signaling interaction reveals a systemic, age-dependent splenic immune influence on tumor development. *Oncotarget,* 6(34), 35419-35432. doi: 10.18632/oncotarget.6214

[3] Berry, R. S., Xiong, M. J., Greenbaum, A., Mortaji, P., Nofchissey, R. A., Schultz, F. … & Hanson, J. A. (2017). High levels of tumor-associated neutrophils are associated with improved overall survival in patients with stage II colorectal cancer. *PLoS One,* 12(12), e0188799. doi: 10.1371/journal.pone.0188799

[4] Clark, S. L. (1962). The reticulum of lymph nodes in mice studied with the electron microscope. *American Journal of Anatomy,* 110(3), 217-257. doi: 10.1002/aja.1001100303

[5] De Vries, N. L., Swets, M., Vahrmeijer, A. L., Hokland, M., & Kuppen, P. J. (2016). The Immunogenicity of Colorectal Cancer in Relation to Tumor Development and Treatment. *International Journal of Molecular Sciences,* 17(7), 1030. https://doi.org/10.3390/ijms170710309

[6] Fogt, F., Zimmerman, R. L., Ross, H. M., Daly, T., & Gausas, R. E. (2004). Identification of lymphatic vessels in malignant, adenomatous, and normal colonic mucosa using the novel immunostain D2-40. *Oncol. Rep.*, 11(1), 47-50. doi: 10.3892/or.11.1.47

[7] Hanus, M., Parada-Venegas, D., Landskron, G., Wielandt, A. M., Hurtado, C., Alvarez, K., … & De la Fuente, M. (2021). Immune System, Microbiota, and Microbial Metabolites: The Unresolved Triad in Colorectal Cancer Microenvironment. *Front. Immunol.,* 12, 612826. doi: 10.3389/fimmu.2021.612826

[8] Lee, M., Choi, S. J., Yoon, Y. H., Kim, J. T., Baek, W. K., & Kim, Y. S. (2015). Metastatic thymic adenocarcinoma from colorectal cancer. *The Korean Journal of Thoracic and Cardiovascular Surgery,* 48(6), 447-451. doi: 10.5090/kjtcs.2015.48.6.447

[9] Li, L., Zhao, C., Kong, F., Li, Y. C., Wang, C., Chen, S., … & Wang, D. (2022). Calf Thymus Polypeptide Restrains the Growth of Colorectal Tumor via Regulating the Intestinal Microbiota-Mediated Immune Function. *Frontiers in pharmacology,* 13, 898906. doi: 10.3389/fphar.2022.898906

[10] Malka, D., Lievre, A., André, T., Taïeb, J., Ducreux, M., & Bibeau,

F. (2020). Immune scores in colorectal cancer: Where are we? *Eur. J. Cancer,* 140, 105-118. doi: 10.1016/j.ejca.2020.08.024. 19

[11] Mandai, M., Hamanishi, J., Abiko, K., Matsumura, N., Baba, T., & Konishi, I. (2016). Dual Faces of IFNγ in Cancer Progression: A Role of PD-L1 Induction in the Determination of Pro- and Antitumor Immunity. *Clin. Cancer Res.,* 22(10), 2329-2334. doi: 10.1158/1078-0432.ccr-16-0224

[12] Markman, J., & Shiao, S. (2014). Impact of the immune system and immunotherapy in colorectal cancer. *Journal of Gastrointestinal Oncology,* 6(2), 208-223. doi: 10.3978/j.issn.2078-6891.2014.077

[13] Mellemkjaer, L., Olsen, J. H., Linet, M. S., Gridley, G., & McLaughlin, J. K. (1995). Cancerrisiko efter splenektomi [Cancer risk after splenectomy]. *Ugeskr. Laeger,* 157(37), 5097-5100. PMID: 7502377

[14] Mushtaque, M., Naqash, S. H., Malik, A. A., Malik, R. A., Khanday, S. A., & Khan, P. S. (2011). Papillary carcinoma thyroid with metastasis to ectopic cervical thymus. *World J. Surg. Oncol.,* 9, 22. doi: 10.1186/1477-7819-9-22

[15] Müzes, G., Bohusné Barta, B., Sipos, F. (2022). Colitis and Colorectal Carcinogenesis: The Focus on Isolated Lymphoid Follicles. *Biomedicines,* 10(2), 226. doi: 10.3390/biomedicines10020226

[16] Noma, K., Yamaguchi, Y., Okita, R., Matsuura, K., & Toge, T. (2005). The spleen plays an immunosuppressive role in patients with gastric cancer: involvement of CD62L+ cells and TGF-beta. *Anticancer research,* 25(1B), 643-649. PMID: 15816640

[17] Ong, M. L., & Schofield, J. B. (2016). Assessment of lymph node involvement in colorectal cancer. *World J. Gastrointest. Surg.,* 8(3), 179-192. doi: 10.4240/wjgs.v8.i3.179

[18] Park, S., Kim, H. Y., Kim, H., Park, J. H., Kim, J. H., Kim, K. H., … & Kim, J. S. (2016). Changes in Noninvasive Liver Fibrosis Indices and Spleen Size During Chemotherapy: Potential Markers for Oxaliplatin-Induced Sinusoidal Obstruction Syndrome. *Medicine,* 95(2), e2454. doi: 10.1097/MD.0000000000002454

[19] Pernot, S., Terme, M., Voron, T., Colussi, O., Marcheteau, E., Tartour, E., & Taieb, J. (2014). Colorectal cancer and immunity: what we know and perspectives. *World J. Gastroenterol.,* 20(14), 3738-50. doi: 10.3748/wjg.v20.i14.3738

[20] Perše, M., & Cerar, A. (2011). Morphological and molecular alterations in 1,2 dimethylhydrazine and azoxymethane induced colon carcinogenesis in rats. *J. Biomed. Biotechnol.,* 11, 473-96. doi: 10.1155/2011/473964

[21] Peters, H. C., Liu, X., Iqbal, A., Cunningham, L. A., & Tan, S. A. (2017). Colorectal cancer metastasis to the thymus gland: rare presentation of colorectal cancer as anterior mediastinal mass. *Case Reports in Surgery,* 6581965 doi: 10.1155/2017/6581965

[22] Rodrigo-Calvo, M. T., Saez de Gordoa, K., Lopez-Prades, S., Archilla, I., Diaz, A., Berrios, M., … & Cuatrecasas, M. (2023). Tumour Cell Seeding to Lymph Nodes from In Situ Colorectal Cancer. *Cancers,* 15(3), 842. doi: 10.3390/cancers15030842

[23] Saleh, R., Taha, R. Z., Toor, S. M., Sasidharan, N. V., Murshed, K., Khawar, M., … & Elkord, E. (2020). Expression of immune checkpoints and T cell exhaustion markers in early and advanced stages of colorectal cancer. *Cancer Immunol. Immunother.,* 69(10), 1989-1999. doi: 10.1007/s00262-020-02593-w

[24] Siegel, R. L., Miller, K. D., Wagle, N. S., & Jemal, A. (2023). Cancer statistics. *CA: a Cancer Journal for Clinicians,* 73(1), 17-48. doi: 10.3322/caac.21763

[25] Sorrentino, C., D'Antonio, L., Fieni, C., Ciummo, S.L., & Di Carlo, E. (2021). Colorectal Cancer-Associated Immune Exhaustion Involves T and B Lymphocytes and Conventional NK Cells and Correlates With a Shorter Overall Survival. *Front. Immunol.,* 12, 778329. doi: 10.3389/fimmu.2021.778329

[26] Su, S., Zhao, J., Xing, Y., Zhang, X., Liu, J., Ouyang, Q., … & Song, E. (2018). Immune Checkpoint Inhibition Overcomes ADCP-Induced Immunosuppression by Macrophages. *Cell,* 175(2), 442-457.e23. doi: 10.1016/j.cell.2018.09.007

[27] Toge, T., Kuroi, K., Kuninobu, H., Yamaguchi, Y., Kegoya, Y, Baba, N., & Hattori, T. (1998). Role of the spleen in immunosuppression of gastric cancer: predominance of suppressor precursor and suppressor inducer T cells in the recirculating spleen cells. *Clin. Exp. Immunol.,* 74(3), 409-412. PMID: 2976622

[28] Väyrynen, J. P., Sajanti, S. A., Klintrup, K., Mäkelä, J., Herzig, K-H., Karttunen, T. J., & Makinen, M. (2014). Characteristics and significance of colorectal cancer associated lymphoid reaction. *International Journal of Cancer,* 134(9), 2126-2135. doi: 10.1002/ijc.28533

[29] Wang, W., Thomas, R., Sizova, O., & Su, D. M. (2020). *Thymic Function Associated With Cancer Development, Relapse, and Antitumor Immunity - A Mini-Review. Frontiers in Immunology,* 11, 773. doi: 10.3389/fimmu.2020.00773

[30] Wen, S. W., Everitt, S. J., Bedx, J., Chabrot, M., Ball, D. L., Solomon, B., … & Leimgruber, A. (2015). Spleen Volume Variation in Patients with Locally Advanced Non-Small Cell Lung Cancer Receiving Platinum-Based Chemo-Radiotherapy. *PloS One*, 10(11), e0142608. doi: 10.1371/journal.pone.0142608

[31] Zaborowski, A. M., Winter, D. C., & Lynch, L. (2021). The therapeutic and prognostic implications of immunobiology in colorectal cancer: a review. *Br. J. Cancer,* 125, 1341-1349. doi: 10.1038/s41416-021-01475-x

[32] Zhang, C., Wang, X-Y., Zuo, J-L., Wang, X-F., Feng, X-W., & Zhang, B. (2023). Localization and density of tertiary lymphoid structures associate with molecular subtype and clinical outcome in colorectal cancer liver metastases. *Journal for ImmunoTherapy of Cancer,* 11, e006425. doi: 10.1136/jitc-2022-006425.

СТРУКТУРНІ ЗМІНИ В ОРГАНАХ ЛІМФОЇДНОЇ СИСТЕМИ ЗА УМОВ ІНДУКОВАНОГО КАНЦЕРОГЕНЕЗУ

Крамар С. Б., Сорока Ю. В., Гаврилюк-Скиба Г. О., Пида В. П., Небесна З. М., Лісничук Н. Є.

Колоректальний рак - третє найпоширеніше онкологічне захворювання у світі. Незважаючи на останні терапевтичні досягнення, він спричиняє понад 500000 смертей щороку. Імунна система відіграє вирішальну роль у захисті організму від раку. Однак ракові клітини здатні уникати імунного виявлення та знищення. Наприклад, вони можуть знижувати експресію антигенів, виробляти імуносупресивні молекули або залучати імунні клітини, котрі виконують регуляторні або інгібуючі функції. Розуміння складних взаємодій між імунною системою та канцерогенезом має вирішальне значення для розробки ефективних методів лікування раку. Мета роботи - встановлення морфологічної перебудови тимуса, селезінки та лімфатичних вузлів в умовах N,N-диметилгідразин-індукованого канцерогенезу. Дослідження проводили на 77 самцях безпорідних щурів-альбіносів масою 190-230 г, котрих утримували у стандартних умовах віварію. Аденокарциному товстої кишки моделювали шляхом введення N,N-диметилгідразину гідрохлориду впродовж 30 тижнів. З метою вивчення

особливостей морфофункціональних змін лімфоїдних органів у динаміці пухлинних уражень товстої кишки тварин вилучали з експерименту кожні 30 днів. Парафінові зрізи тимуса, селезінки, лімфатичних вузлів товщиною 5-6 мкм виготовляли на роторному мікротомі і забарвлювали гематоксиліном та еозином. У результаті експериментального дослідження встановлено характер і ступінь гістологічних змін в органах лімфоїдної системи за N,N-диметилгідразин-індукованого аденокарциноматозу товстої кишки. В динаміці експерименту спостерігали помітне посилення вираженості деструктивних і дегенеративних змін у тимусі, селезінці та лімфатичних вузлах. Ці зміни проявлялися порушенням кровообігу досліджуваних органів, що призводило до ураження судинної стінки та крововиливів, а також до дезорганізації морфофункціональних елементів та розвитку фіброзу. Враховуючи значну роль, яку відіграють тимус, селезінка та лімфатичні вузли в регуляції канцерогенезу та підтримці імунного балансу, вкрай важливо заглибитися в розуміння змін, що відбуваються в їх структурі та функції. Отримані нами результати вказують на те, що канцерогенез супроводжується вираженими морфологічними змінами структурних компонентів органів лімфоїдної системи, ступінь яких зростає прямо пропорційно тривалості впливу онкогенного фактора.

Ключові слова: *аденокарцинома товстої кишки, селезінка, тимус, лімфатичний вузол, морфологія.*

Author's contribution

Kramar S. B. - data curation, investigation, methodology, visualization, conceptualization, writing - original draft.
Soroka Yu. V. - formal analysis, investigation, writing - review & editing.
Havryliuk-Skyba H. O. - methodology, investigation, visualization.
Pyda V. P. - investigation, writing - review & editing.
Nebesna Z. M. - conceptualization, investigation, visualization, writing - review & editing.
Lisnychuk N. Ye. - conceptualization, data curation, formal analysis, funding acquisition, methodology, project administration, supervision, validation, writing - review & editing.

DOI: 10.31393/morphology-journal-2024-30(3)-02 Reports of Morphology, Vol. 30, №3, Pages 15-24

ISSN 1818-1295 eISSN 2616-6194

REPORTS OF MORPHOLOGY

Official Journal of the Scientific Society of Anatomists, Histologists, Embryologists and Topographic Anatomists of Ukraine

journal homepage: https://morphology-journal.com

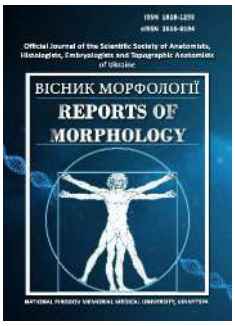

Girth sizes of the body in Ukrainian men and women with various forms of urticaria

Aladwan A. M. A., Dmytrenko S. V., Kyrychenko V. I., Glushak A. A., Prokopenko O. S., Ocheretna O. L., Gunas I. V.

National Pirogov Memorial Medical University, Vinnytsya, Ukraine

ARTICLE INFO

Received: 12 March 2024

Accepted: 04 July 2024

UDC: 616.514-037:572.087+612-071

CORRESPONDING AUTHOR

e-mail: amjad_aladwan@yahoo.com

Aladwan A. M. A.

CONFLICT OF INTEREST

The authors have no conflicts of interest to declare.

FUNDING

Not applicable.

DATA SHARING

Data are available upon reasonable request to corresponding author.

The relevance of studying body girth in patients with different forms of urticaria is due to the importance of anthropometric indicators in the diagnosis and prognosis of the disease. Urticaria, as one of the most common dermatological conditions, can present in various clinical forms, each of which may differently impact the body, particularly by altering body circumferences. Examining these indicators in Ukrainian men and women allows for the identification of gender-specific and individual characteristics, which could be crucial for improving treatment and prevention methods for urticaria. The purpose of the work is to establish the peculiarities and sex differences in body girth measurements in young Ukrainian men and women with acute and chronic mild and severe urticaria. Body girth measurements were determined in 40 Ukrainian men and 40 young women (25-44 years according to the age periodization of WHO, 2015) patients with acute (AU) and chronic (CU) urticaria of a mild (MU) and severe (SU) course. Urticaria was diagnosed according to the EAACI/GA²LEN/EuroGuiDerm/ APAAACI international guidelines. Anthropometric measurements were performed on the right side of the body. The girth sizes of the upper and lower limbs, neck and trunk were determined with a centimeter tape. As a control group, the girth measurements of the body of practically healthy Ukrainian men (n=82) and women (n=101) of young age were used, which were taken from the data bank of the research center of the National Pirogov Memorial Medical University, Vinnytsya. Statistical analysis of girth body dimensions was carried out in the license package "Statistica 6.0" using non-parametric estimation methods. When comparing the body girths of men or women with urticaria with practically healthy men or women, significantly larger values or a tendency towards larger values were established: in sick men, most of the girths of the upper limb (mainly in patients with AU/SU), hips, waist, chest during inhalation and at rest (in patients with AU/MU, AU/SU, CU/MU and CU/SU), neck (in patients with AU/MU, AU/SU and CU/MU); in sick women - shoulder girths in stressed and relaxed states, hips, thighs, neck, waist, chest during inhalation, exhalation and in a calm state (in patients with AU/MU, AU/SU, CU/MU and CU/SU), forearm in the lower part (in patients with AU/MU and CU/ MU), crus in the upper and lower part (in patients with AU/MU and CU/MU). When comparing the girths of the body between men and women with urticaria, only a few significant differences or trends were established: between the men, only larger values of the girths of the neck (in patients with AU/MU compared to AU/SU) and feet (in patients with AU/SU vs. CU/SU); between sick women - greater values of shoulder girths in tense and relaxed states, forearm in the lower part, hand, crus in the upper part, foot, thorax on exhalation and in a calm state (in patients with AU/MU compared to AU/SU), crus (in patients with CU/MU compared to CU/SU). Pronounced manifestations of sexual dimorphism of body girths between Ukrainian men and women with urticaria were also established: in sick men, larger values of hand and neck girths were found (in patients with AU/MU, AU/SU, CU/MU and CU/SU), shoulder girths in tense and relaxed states, forearms in the upper and lower part, feet, waist, chest during inhalation, exhalation and in a calm state (in patients with AU/SU), shoulder in a tense state (in patients with CU/ SU), forearm in the upper part (in patients with AU/MU), forearm in the lower part (in

patients with CU/MU); in female patients - larger values of hip girth (in patients with AU/MU) and hips (in patients with CU/MU).
Keywords: *skin diseases, urticaria, men, women, girth sizes of the body, sex differences.*

Introduction

Urticaria is a common skin disease with a tendency to a chronic course, in the development of which a key role is played by the activation of mast cells and basophils, which leads to the release of histamine and other inflammatory mediators. This causes dilation of blood vessels and an increase in the permeability of capillaries, which leads to the appearance of blisters and itching on the skin [22, 23]. Chronic urticaria is a significant challenge for the health care system, as patients with this disease often require frequent medical consultations and treatment. According to German authors, about 40 % of patients have concomitant diseases, such as asthma or allergic rhinitis. In addition, about 60 % of patients indicate a significant impact of the disease on the quality of life [28].

The prevalence of chronic urticaria in South Korea, according to the Korean Health Insurance Database 2010-2014, was: 0.55 % in 2014, with an increase of 0.13 % between 2010 and 2014. The incidence rate was higher among women (57.6 %) and among persons aged 40-59 years [18]. The prevalence of urticaria among children in Germany is approximately 3.4 %. The highest rates of morbidity are observed in children aged 6 to 10 years, where this rate reaches 4.8 %. Chronic urticaria is observed in 0.1 % of children [25]. In China, the overall prevalence of urticaria is 7.1 % of the population, with the highest incidence among people aged 40 to 49 years (9.5 %). Chronic urticaria is more common among women. It was also found that the southern regions have higher incidence rates [19]. In the United States, the prevalence of chronic urticaria is approximately 0.6 % among the adult population. Women, as in the data of previous studies, have a higher probability of the disease compared to men, and there is also an increased risk in the age category of 30-50 years [29]. The overall prevalence of urticaria is 0.6 % in the Polish population, with women suffering from this disease more often than men (0.7 % vs. 0.4 %), which is consistent with data from a previous study in China. The prevalence of acute urticaria is 0.5 %, and chronic urticaria is 0.1 %. The incidence of urticaria is higher among people over 60 years old [21].

M. M. Balp and co-authors [5] investigated the impact of chronic urticaria on patients in Brazil. Chronic urticaria significantly reduces the quality of life, in particular due to a decrease in physical and mental health indicators. Patients with chronic urticaria have 5 points lower mental health scores and 2.5 points lower physical health scores. There is also a significant increase in anxiety and sleep problems among patients. The results of research by Tzur Bitan D. and co-authors [27] showed that patients with urticaria have an increased risk of developing anxiety disorders and depression. In particular, 30 % of patients had symptoms of anxiety, while 25 % were diagnosed with depression. A survey of 401 patients from the UK, Germany, France, Italy and Spain found that more than 90 % of respondents with chronic urticaria experienced anxiety or depression, more than 70 % of patients experienced a significant negative impact on sleep, and more than 60 % reported decreased physical activity [6].

A study of 7,612 patients with idiopathic/spontaneous urticaria on the cost of medical resources for the treatment of the disease showed that individuals from this cohort had an average annual total cost per patient of $9,788 [8].

44 % of patients have a recurrence of urticaria within 10 years of initial treatment. Young age and a longer initial phase of the disease are factors that increase the risk of relapse. Patients requiring systemic corticosteroid treatment also have a higher risk of relapse [15]. Thus, urticaria is a serious challenge for health care and requires the development of mechanisms capable of predicting the risks of this disease, especially if possible during preventive examinations.

The purpose of the study is to establish the peculiarities and sex differences in body girth measurements in young Ukrainian men and women with mild and severe acute and chronic urticaria.

Materials and methods

On the basis of the Department of Skin and Venereal Diseases with a postgraduate course at the National Pirogov Memorial Medical University, Vinnytsya and the Military Medical Clinical Center of the Central Region, body girths were determined (according to the scheme of V. V. Bunak [14]) of 40 Ukrainian men and 40 young women age (25-44 years according to the age periodization of WHO, 2015) of patients with acute (AU) and chronic (CU) urticaria of a mild (MU) and severe (SU) course. Committee on Bioethics of National Pirogov Memorial Medical University, Vinnytsya (protocol No. 11 from 23.12.2021) found that the studies do not contradict the basic bioethical standards of the Declaration of Helsinki, the Council of Europe Convention on Human Rights and Biomedicine (1977), the relevant WHO regulations and laws of Ukraine.

The diagnosis of urticaria was made in accordance with the EAACI/GA^{2}LEN/EuroGuiDerm/APAAACI international guidelines for the definition, classification, diagnosis and treatment of urticaria (https://pubmed.ncbi.nlm.nih.gov/29336054/).

Anthropometric measurements were performed on the right side of the body. Body girth measurements were determined with a centimeter tape, the accuracy of which

was up to 0.5 cm, and the measurement limit was up to 100 measurements.

As a control group, body girth measurements of practically healthy Ukrainian men (n=82) and women (n=101) of the same age group were used, which were taken from the data bank of the research center of the National Pirogov Memorial Medical University, Vinnytsya.

Statistical analysis of body girths was carried out in the "Statistica 6.0" license package using non-parametric estimation methods. Means and standard square deviations were determined for each characteristic under study. The significance of the difference in values between independent quantitative values was determined using the Mann-Whitney U-test.

Results

It was established that the *girth of the shoulder in the tense state* is significantly greater or tends to greater values in men with AU/SU (36.10±4.12 cm, p<0.01), CU/MU (35.20±2.96 cm, p<0.05) and CU/ SU (35.70±5.03 cm, p=0.063) compared to healthy men (33.23±2.84 cm) (Fig. 1A). The value of this indicator is significantly higher or tends to higher values in women with AU/MU (35.20±4.83 cm, p<0.001), AU/SU (29.85±2.86 cm, p=0.076), CU/MU (34.25±4.71 cm, p<0.001) and CU/SU (30.75±3.39 cm, p<0.01) compared to healthy women (27.96±2.92 cm) (see Fig. 1A). In addition, the value of shoulder girth in the tense state is significantly greater (p<0.05) in women with AU/MU compared to women with AU/SU (see Fig. 1A). When comparing shoulder girth in a tense state between the respective groups of male and female patients, significantly higher values were established in male patients with AU/SU (p<0.01) and CU/SU (p<0.05) (see Fig. 1A).

Shoulder girth in a relaxed state is significantly greater only in men with AU/SU (32.40±3.92 cm, p<0.05) compared to healthy men (30.17±2.94 cm) (Fig. 1B). The value of this indicator is significantly higher or has a pronounced tendency to higher values in women with AU/MU (33.40±4.38 cm, p<0.001), AU/SU (28.50±2.72 cm, p=0.054), CU/MU (31.50± 4.84 cm, p<0.01) and CU/SU (29.40±3.20 cm, p<0.01) compared to healthy women (26.54±2.88 cm) (see Fig. 1B). In addition, the value of shoulder girth in a relaxed state is significantly greater (p<0.05) in women with AU/MU compared to women with AU/SU (see Fig. 1B). When comparing the shoulder girth in an unstressed state between the respective groups of male and female patients, only a significantly higher value was found in male patients with AU/SU (p<0.05) (see Fig. 1B).

There are no significant or trend differences in the *upper forearm circumference* between patients and healthy men or women (see Fig. 1C). Similarly, no significant or trend differences in this measurement are found between male or female patients (see Fig. 1C). However, when comparing the upper forearm circumference between the respective groups of male and female patients, significantly larger values are found in men with AU/MU (27.35±2.57 cm, p<0.05) and AU/SU (26.40±3.13 cm, p<0.01) compared to women (24.40±2.59 cm and 22.55±2.27 cm, respectively) (see Fig. 1C).

The circumference of the lower forearm is significantly greater or has a tendency towards greater values in men with AU/SU (18.40±1.56 cm, p<0.05) and CU/MU (18.65±2.17 cm, p=0.066) compared to healthy men (17.44±1.24 cm) (see Fig. 1D). This measurement is significantly larger in women with AU/MU (16.80±0.95 cm, p<0.001) and CU/MU (16.75±1.64 cm, p<0.01) compared to healthy women (15.47±1.14 cm) (see Fig. 1D). Additionally, the circumference of the lower forearm is significantly greater (p<0.01) in women with AU/MU compared to women with AU/SU (15.35±0.88 cm) (see Fig. 1D). When comparing the anteroposterior mid-sternum diameter between the respective groups of male and female patients, significantly larger values are observed in men with AU/SU (p<0.001) and CU/MU (p<0.05) (see Fig. 1D).

No significant or trend differences in *wrist circumference* were found between patients and healthy men or women (see Fig. 1E). It was found that this measurement is significantly larger (p<0.05) in women with AU/MU (19.05±0.72 cm) compared to women with AU/SU (18.30±0.67 cm) (see Fig. 1E). When comparing wrist circumference between the respective groups of male and female patients, significantly larger values (p<0.05-0.001) are observed in men with AU/MU (21.50±1.13 cm), AU/SU (22.05±1.25 cm), CU/MU (21.70±1.03 cm; compared to women - 18.85±1.11 cm) and CU/SU (21.05±2.15 cm; compared to women - 18.55±0.64 cm) (see Fig. 1E).

Thigh circumference is significantly larger or shows a pronounced tendency towards larger values in men with AU/MU (61.10±6.21 cm, p<0.001), AU/SU (61.30±4.62 cm, p<0.001), CU/MU (58.70±5.08 cm, p<0.01) and CU/SU (59.80±9.14 cm, p=0.052) compared to healthy men (53.25±4.49 cm) (see Fig. 2A). This measurement is significantly larger in women with AU/MU (66.50±8.24 cm, p<0.001), AU/SU (59.80±4.92 cm, p<0.001), CU/MU (66.80±7.94 cm, p<0.001) and CU/SU (62.50±7.26 cm, p<0.001) compared to healthy women (53.26±4.48 cm) (see Fig. 2A). When comparing thigh circumference between the respective groups of male and female patients, a significantly larger value is found only in women with CU/MU (p<0.05) (see Fig. 2A).

Thigh circumference is significantly larger only in men with AU/SU (103.2±7.9 cm, p<0.01) compared to healthy men (95.04±6.39 cm) (see Fig. 2B). This measurement is significantly larger or shows a tendency towards larger values in women with AU/MU (107.6±11.7 cm, p<0.001), AU/SU (99.40±7.57 cm, p<0.05), CU/MU (108.8±14.0 cm, p<0.01) and CU/SU (102.9±12.1 cm, p=0.061) compared to healthy women (95.08±6.95 cm) (see Fig. 2B). When comparing thigh circumference between the respective groups of male and female patients, a significantly larger

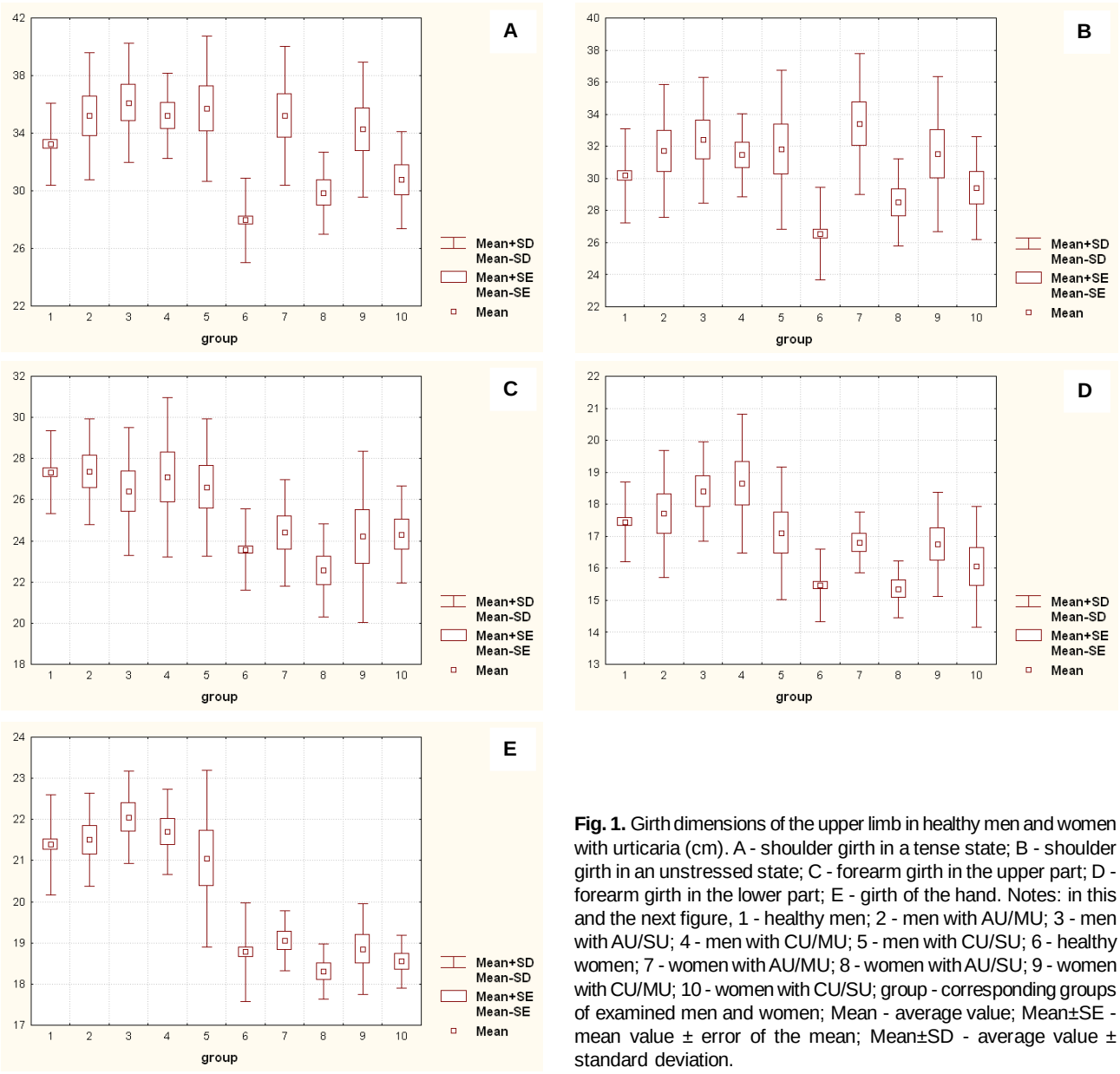

Fig. 1. Girth dimensions of the upper limb in healthy men and women with urticaria (cm). A - shoulder girth in a tense state; B - shoulder girth in an unstressed state; C - forearm girth in the upper part; D - forearm girth in the lower part; E - girth of the hand. Notes: in this and the next figure, 1 - healthy men; 2 - men with AU/MU; 3 - men with AU/SU; 4 - men with CU/MU; 5 - men with CU/SU; 6 - healthy women; 7 - women with AU/MU; 8 - women with AU/SU; 9 - women with CU/MU; 10 - women with CU/SU; group - corresponding groups of examined men and women; Mean - average value; Mean±SE - mean value ± error of the mean; Mean±SD - average value ± standard deviation.

value ($p<0.05$) is found only in women with AU/MU (compared to men with 98.60±8.07 cm) (see Fig. 2B).

Upper crus circumference is significantly larger in women with AU/MU (39.10±3.25 cm, $p<0.001$) and CU/MU (39.00±4.71 cm, $p<0.01$) compared to healthy women (34.85±2.94 cm) (see Fig. 2C). Additionally, this measurement is significantly larger ($p<0.05$) in women with AU/MU compared to women with AU/SU (36.10±2.23 cm) (see Fig. 2C). When comparing upper leg circumference between the respective groups of male and female patients, no significant or trend differences were found (see Fig. 2C).

Lower crus circumference is significantly larger only in men with AU/SU (25.50±2.47 cm, $p<0.01$) compared to healthy men (23.41±1.87 cm) (see Fig. 2D). This measurement is significantly larger in women with AU/MU (25.20±2.66 cm, $p<0.001$), AU/SU (23.70±2.00 cm, $p<0.05$) and CU/MU (25.45±3.62 cm, $p<0.01$) compared to healthy women (22.21±1.61 cm) (see Fig. 2D). Additionally, lower leg circumference at the distal part shows a tendency towards larger values ($p=0.076$) in women with CU/MU compared to women with CU/SU (23.05±1.80 cm) (see Fig. 2D). When comparing lower leg circumference at the distal part between the respective groups of male and female patients, no significant or trend differences were found (see Fig. 2D).

Foot circumference shows only a slight tendency towards smaller values in men with CU/SU (24.10±2.22 cm, $p=0.079$) compared to healthy men (24.96±1.46 cm) (see Fig. 2E). This measurement is significantly larger only

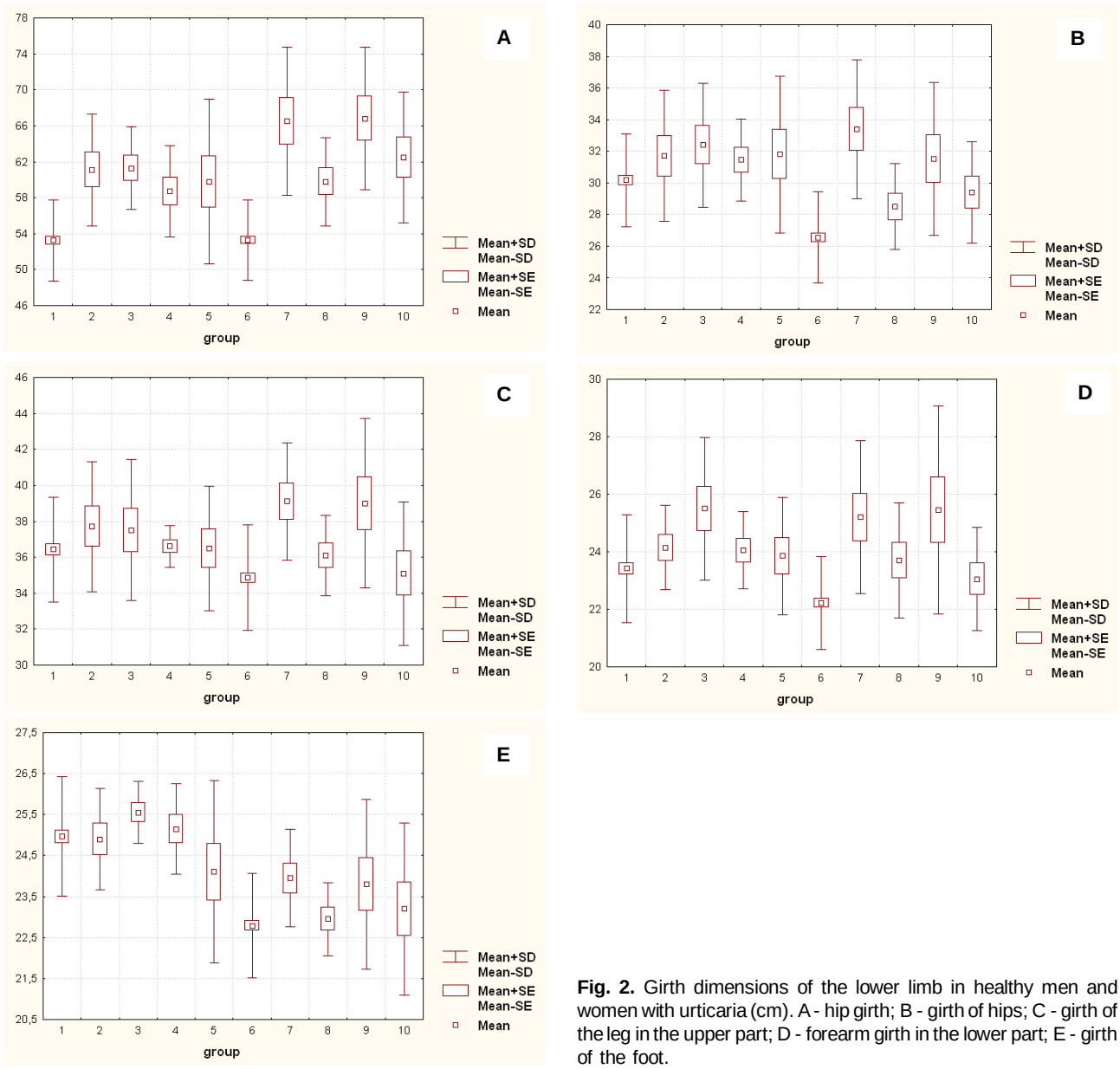

Fig. 2. Girth dimensions of the lower limb in healthy men and women with urticaria (cm). A - hip girth; B - girth of hips; C - girth of the leg in the upper part; D - forearm girth in the lower part; E - girth of the foot.

in women with AU/MU (23.95±1.19 cm, p<0.05) compared to healthy women (22.79±1.28 cm) (see Fig. 2E). Additionally, foot circumference is significantly larger (p<0.05) in men with AU/SU (25.55±0.76 cm) compared to men with CU/SU; and in women with AU/MU, there is a tendency towards larger values (p=0.076) compared to women with AU/SU (22.95±0.90 cm) (see Fig. 2E). When comparing foot circumference between the respective groups of male and female patients, only men with AU/SU show a significantly larger value (p<0.001) (see Fig. 2E).

Neck circumference is significantly larger in men with AU/MU (40.80±2.97 cm, p<0.001), AU/SU (42.30±3.27 cm, p<0.001) and CU/MU (40.20±1.99 cm, p<0.001) compared to healthy men (37.67±1.92 cm) (see Fig. 3A). This measurement is also significantly larger in women with AU/MU (35.90±3.93 cm, p<0.001), AU/SU (33.40±1.90 cm, p<0.01), CU/MU (35.20±2.90 cm, p<0.001) and CU/SU (33.90±2.38 cm, p<0.01) compared to healthy women (31.96±1.45 cm) (see Fig. 3A). Additionally, neck circumference is significantly larger (p<0.05) in men with AU/SU compared to men with AU/MU (see Fig. 3A). Among the respective groups of male and female patients, significant larger values of neck circumference were found in men with AU/MU (p<0.05), AU/SU (p<0.001), CU/MU (p<0.01) and CU/SU (40.10±4.79 cm, p<0.01) (see Fig. 3A).

Waist circumference is significantly larger in men with AU/MU (90.50±13.89 cm, p<0.01), AU/SU (97.60±13.38 cm, p<0.001), CU/MU (89.50±12.29 cm, p<0.01) and CU/SU (93.90±18.90 cm, p<0.01) compared to healthy men

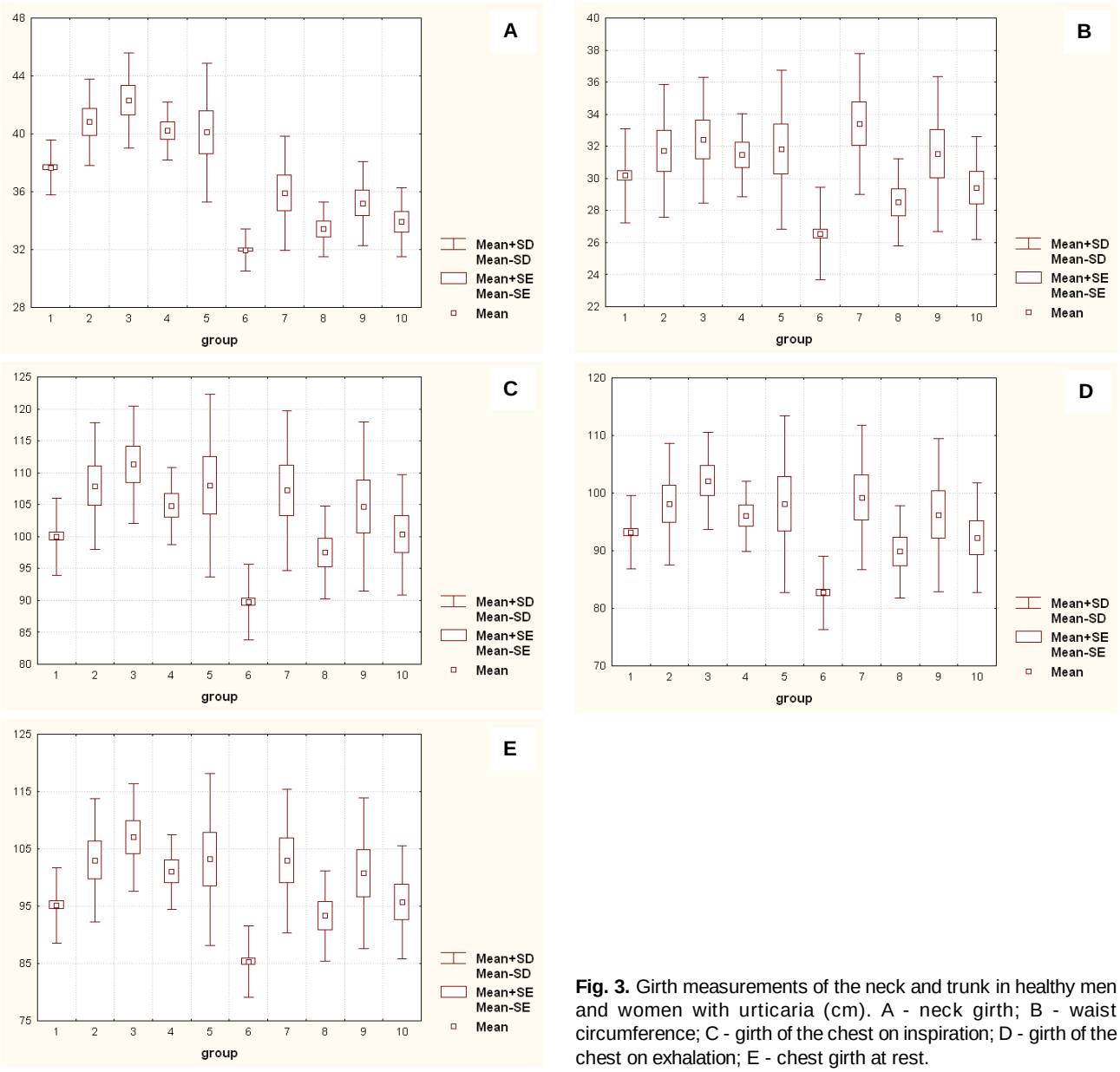

Fig. 3. Girth measurements of the neck and trunk in healthy men and women with urticaria (cm). A - neck girth; B - waist circumference; C - girth of the chest on inspiration; D - girth of the chest on exhalation; E - chest girth at rest.

(79.48±7.32 cm) (see Fig. 3B). This measurement is also significantly larger in women with AU/MU (92.40±19.81 cm, p<0.001), AU/SU (76.00±20.24 cm, p<0.05), CU/MU (88.20±20.53 cm, p<0.001) and CU/SU (83.80±12.04 cm, p<0.001) compared to healthy women (68.98±6.29 cm) (see Fig. 3B). When comparing waist circumference between corresponding groups of male and female patients, only men with AU/SU have a significantly larger value (p<0.01) (see Fig. 3B).

The chest circumference on inhalation is significantly larger in men with AU/MU (107.9±9.9 cm, p<0.01), AU/SU (111.3±9.2 cm, p<0.001), CU/MU (104.8±6.1 cm, p<0.05) and CU/SU (108.0±14.3 cm, p<0.05) compared to healthy men (100.0±6.0 cm) (see Fig. 3C). This measurement is also significantly larger in women with AU/MU (107.2±12.6 cm, p<0.001), AU/SU (97.50±7.23 cm, p<0.01), CU/MU (104.7±13.2 cm, p<0.001) and CU/SU (100.3±9.4 cm, p<0.001) compared to healthy women (89.75±5.88 cm) (see Fig. 3C). When comparing chest circumference on inhalation between corresponding groups of male and female patients, only men with AU/SU have a significantly larger value (p<0.01) (see Fig. 3C).

The chest circumference on exhalation is significantly larger only in men with AU/SU (102.1±8.5 cm, p<0.01) compared to healthy men (93.18±6.39 cm) (see Fig. 3D). This measurement is significantly larger in women with AU/MU (99.20±12.52 cm, p<0.001), AU/SU (89.80±7.98 cm, p<0.01), CU/MU (96.20±13.26 cm, p<0.001) and CU/SU (92.20±9.52 cm, p<0.01) compared to healthy women (82.68±6.33 cm) (see Fig. 3D). Additionally, chest

circumference on exhalation shows a trend towards larger values (p=0.070) in women with AU/MU compared to women with AU/SU (see Fig. 3D). When comparing chest circumference on exhalation between corresponding groups of male and female patients, only men with AU/SU have a significantly larger value (p<0.01) (see Fig. 3D).

The chest circumference at rest is significantly larger in men with AU/MU (103.0±10.8 cm, p<0.01), AU/SU (107.0±9.3 cm, p<0.001), CU/MU (101.0±6.5 cm, p<0.05) and CU/SU (103.2±15.0 cm, p<0.05) compared to healthy men (95.20±6.57 cm) (see Fig. 3E). This measurement is significantly larger in women with AU/MU (102.9±12.5 cm, p<0.001), AU/SU (93.30±7.90 cm, p<0.01), CU/MU (100.7±13.1 cm, p<0.001) and CU/SU (95.70±9.81 cm, p<0.01) compared to healthy women (85.34±6.20 cm) (see Fig. 3E). Additionally, chest circumference at rest shows a trend towards larger values (p=0.065) in women with AU/MU compared to women with AU/SU (see Fig. 3E). When comparing chest circumference at rest between corresponding groups of male and female patients, only men with AU/SU have a significantly larger value (p<0.01) (see Fig. 3E).

Discussion

Thus, *compared to healthy men*: the size of *upper arm circumferences in both tensed and relaxed states and lower forearm circumference* is significantly larger (p<0.05-0.001) in men with AU/SU (8.64 %, 7.39 % and 5.50 %, respectively); *upper arm circumference in the tensed* state is significantly larger (p<0.05) or shows a trend towards larger values (p=0.063) in men with CU/MU (5.93 %) and CU/SU (7.43 %); *upper forearm circumference* shows a trend towards larger values (p=0.066) in men with CU/MU (6.94 %); *thigh circumference* is significantly larger (p<0.01-0.001) or shows a trend towards larger values (p=0.052) in men with AU/MU (14.74 %), AU/SU (15.12 %), CU/MU (10.23 %) and CU/SU (12.30 %); *thigh and lower crus circumferences* are significantly larger (p<0.01 in both cases) in men with AU/SU (8.59 % and 8.93 %, respectively); *foot circumference* shows a trend towards smaller values (p=0.079) in men with CU/SU (3.45 %); *waist circumference*, *chest circumference on inhalation, and at rest* are significantly larger (p<0.05-0.001) in men with AU/MU (13.86 %, 7.90 % and 8.19 %, respectively), AU/SU (22.80 %, 11.30 % and 12.39 %, respectively), CU/MU (12.61 %, 4.80 % and 18.35 %, respectively) and CU/SU (18.14 %, 8.00 % and 8.40 %, respectively); *neck circumference* is significantly larger (p<0.001 in all cases) in men with AU/MU (8.31 %), AU/SU (12.29 %) and CU/MU (6.72 %); *chest circumference on exhalation* is significantly larger (p<0.01) in men with AU/SU (9.57 %).

When compared to healthy women: the size of upper arm circumferences in both tensed and relaxed states is significantly larger (p<0.01-0.001) or shows a trend towards larger values (p=0.054-0.076) in women with AU/MU (25.89 % and 25.85 %, respectively), AU/SU (6.76 % and 7.39 %, respectively), CU/MU (22.50 % and 18.69 %, respectively) and CU/SU (9.98 % and 10.78 %, respectively); *forearm circumference in the lower part* is significantly larger (p<0.01-0.001) in women with AU/MU (8.60 %) and CU/MU (8.27 %); *thighs and thigh circumferences* are significantly larger (p<0.05-0.001) or show a trend towards larger values (p=0.061) in women with AU/MU (24.86 % and 13.17 %, respectively), AU/SU (12.28 % and 4.54 %, respectively), CU/MU (25.42 % and 14.43 %, respectively) and CU/SU (17.35 % and 8.22 %, respectively); *crus circumferences in the upper and lower parts and foot circumference* are significantly larger (p<0.05-0.001) in women with AU/MU (12.20 %, 13.46 % and 5.09 %, respectively); *crus circumferences in the upper and lower parts* are significantly larger (p<0.01 in both cases) in women with CU/MU (11.91 % and 14.59 %, respectively); only the *lower part of crus circumference* is significantly larger (p<0.05) in women with AU/SU (6.71 %); *neck, waist, and chest circumferences on inhalation, exhalation, and at rest* are significantly larger (p<0.05-0.001) in women with AU/MU (12.33 %, 33.95 %, 19.44 %, 19.98 % and 20.58 %, respectively), AU/SU (4.51 %, 10.18 %, 8.64 %, 8.61 % and 9.33 %, respectively), CU/MU (10.14 %, 27.86 %, 16.66 %, 16.35 % and 18.00 %, respectively) and CU/SU (6.07 %, 21.48 %, 11.75 %, 11.51 % and 12.14 %, respectively).

When comparing body circumferential dimensions among Ukrainian men with *urticaria*, only significantly larger values (p<0.05 in both cases) were found for *neck circumference* in patients with AU/MU compared to those with AU/SU (3.68 %) and *foot circumference* in patients with AU/MU compared to those with CU/SU (6.02 %). Among women with AU/MU compared to those with AU/SU, significantly larger (p<0.05-0.01) or trending larger values (p=0.065-0.076) were observed for *upper arm circumferences in both tensed* (17.92 %) and *relaxed states* (17.19 %), *forearm circumference in the lower part* (9.45 %), wrist circumference (4.10 %), *upper crus circumference* (8.31 %), *foot circumference* (4.36 %), *chest circumference on exhalation* (10.47 %) and *at rest* (10.29 %); as well as a trend towards larger values (p=0.076) for *lower crus circumference* in women with CU/MU compared to women with CU/SU (10.41 %).

Significant manifestations of *sexual dimorphism* in body circumferential dimensions were established between Ukrainian men and women with *urticaria*: significantly larger values (p<0.05-0.001) for *wrist and neck circumferences* in men with AU/MU (12.86 % and 13.65 %, respectively), AU/SU (20.49 % and 26.65 %, respectively), CU/MU (15.12 % and 14.20 %, respectively) and CU/SU (13.48 % and 18.29 %, respectively); significantly larger values (p<0.05-0.001) for *upper arm circumferences in both tensed* (20.94 %) and *relaxed states* (13.68 %), *forearm circumferences in the upper* (17.07 %) and *lower parts* (19.87 %), *foot circumference* (11.33%), *waist circumference* (28.42%), *chest circumference on inhalation* (14.15%), *exhalation* (13.70 %) and *at rest* (14.68 %) in men with AU/SU; significantly larger values (p<0.05 in both cases) for

forearm circumference in the upper part (12.09 %) in men with AU/MU and *thigh circumference* (9.13 %) in women with AU/MU; significantly larger values ($p<0.05$ in both cases) for *forearm circumference in the lower part* (11.34 %) in men with CU/MU and *thigh circumference* (13.80 %) in women with CU/MU; significantly larger value ($p<0.05$) for *upper arm circumference in the tensed state* (16.10 %) in men with CU/SU.

The connection between the risk of occurrence or features of the course of various dermatological diseases and the features of anthropometric indicators has been highlighted in various works over the last decade. Thus, it was established that patients with chronic idiopathic urticaria have a significantly higher BMI compared to control groups. In particular, in patients with chronic idiopathic urticaria, the average BMI is 28.5±3.2, which indicates a potential association between this form of urticaria and increased BMI [1]. Another study found that 42 % of patients with chronic idiopathic urticaria had a body mass index greater than 30, indicating obesity, compared to 24 % of controls [9]. Data from laboratory studies also indicate the existence of a connection with increased body weight. Patients with chronic urticaria have 25 % higher leptin levels and 15 % lower adiponectin levels compared to controls [26].

Similar trends were found for other dermatological diseases, and this applies to all age categories. A study by Darlenski R. and co-authors [10] showed that obesity is associated with various skin problems, including acne, psoriasis and eczema. Obese patients have been found to have a 30 % greater risk of developing these diseases compared to normal weight patients. 60 % of obese children have skin diseases such as acanthosis nigricans and stretch marks [11]. Elderly patients with increased BMI more often have skin lesions, such as dermatophytosis and stretch marks. In particular, 50 % of patients with a BMI over 30 had skin lesions, compared to 20 % of patients with a normal BMI [20].

In the studies of Khasawneh A. R. et al. [16] among the parameters associated with an unfavorable prognosis of the development of the generalized fatty form of seborrheic dermatitis of varying degrees of severity, the muscle component of body weight according to the methods of Matiegka and the American Institute of Nutrition, the fat component of body weight (both in men and women) and mesomorphic and ectomorphic components of the somatotype (only in women). 27 % of patients with atopic eczema suffer from obesity, compared to 18 % in the control group [3].

Men with severe psoriasis have thicker skin folds compared to those with mild psoriasis. The average thickness of skin folds in patients with severe psoriasis was 25 mm, while in patients with mild psoriasis it was 18 mm. Also, taking into account the somatotype shows that patients with the endomorphic type have a greater thickness of skin folds [2]. A high BMI and abdominal obesity are associated with an increased risk of psoriasis. It has been found that each additional unit of BMI increases the risk of psoriasis by 2 %, and people with high levels of abdominal obesity have a 25 % greater risk of developing psoriasis [4]. Severe forms of psoriasis are associated with more pronounced changes in body composition, in particular, with an increase in BMI by 2.5 units compared to mild forms of the disease [7]. In patients with psoriasis who are obese, the frequency of severe forms of the disease is 25 % higher compared to non-obese patients. It has also been established that each additional unit of BMI increases the risk of psoriasis by 5 % [12].

Acanthosis nigricans is also strongly associated with obesity and elevated insulin levels. In particular, 70 % of patients with acanthosis nigricans have a BMI greater than 25, and insulin levels were 20 % higher compared to controls [13].

A high BMI is associated with more severe forms of acne. In patients with a BMI greater than 25, the severity of acne is 40 % higher compared to patients with a normal BMI. In particular, 60 % of obese patients have severe forms of acne, compared to 30 % in the control group [17]. Obese adolescents have a 30 % higher risk of developing acne compared to normal-weight adolescents. Specifically, 25 % of obese adolescents have moderate or severe acne, compared to 18 % in the control group [24].

Atopic dermatitis is also significantly associated with obesity. The overall risk of atopic dermatitis is 40 % higher in overweight people and 60 % higher in obese people compared to controls [30].

Conclusion

1. In patients with acute and chronic urticaria of mild and severe course of Ukrainian men and women of young age, significantly higher values or tendencies towards higher values were established, compared to healthy men or women, numerous discrepancies in body girth sizes - higher values in patients (more pronounced in women). Between sick men and sick women, only isolated differences in girth of the body were established (also more pronounced in women).

2. Pronounced manifestations of sexual dimorphism of girth body sizes between sick men and women were established - in most cases, greater values in men.

References

[1] Aamir, I. S., Choudry, U. K., & Mannan, N. (2016). Association between chronic idiopathic urticaria and body mass index. *Pakistan Journal of Physiology,* 12(1), 35-37. doi: 10.69656/pjp.v12i1.424

[2] Al-Qaraleh, O. B. A. R. (2020). Skinfold thickness in men with mild and severe psoriasis without and taking into account the somatotype. *Biomedical and Biosocial Anthropology*, (40), 48-53. doi: 10.31393/bba40-2020-08

[3] Ascott, A., Mansfield, K. E., Schonmann, Y., Mulick, A., Abuabara, K., Roberts, A., ... & Langan, S. M. (2021). Atopic eczema and

obesity: a population-based study. *British Journal of Dermatology,* 184(5), 871-879. doi: 10.1111/bjd.19597

[4] Aune, D., Snekvik, I., Schlesinger, S., Norat, T., Riboli, E., & Vatten, L. J. (2018). Body mass index, abdominal fatness, weight gain and the risk of psoriasis: a systematic review and dose-response meta-analysis of prospective studies. *European journal of epidemiology,* 33, 1163-1178. doi: 10.1007/s10654-018-0366-z

[5] Balp, M. M., Lopes da Silva, N., Vietri, J., Tian, H., & Ensina, L. F. (2017). The burden of chronic urticaria from Brazilian patients' perspective. *Dermatology and therapy,* 7, 535-545. doi: 10.1007/s13555-017-0191-4

[6] Balp, M. M., Vietri, J., Tian, H., & Isherwood, G. (2015). The impact of chronic urticaria from the patient's perspective: a survey in five European countries. *The Patient-Patient-Centered Outcomes Research,* 8, 551-558. doi: 10.1007/s40271-015-0145-9

[7] Blake, T., Gullick, N. J., Hutchinson, C. E., & Barber, T. M. (2020). Psoriatic disease and body composition: A systematic review and narrative synthesis. *PloS one,* 15(8), e0237598. doi: 10.1371/journal.pone.0237598

[8] Broder, M. S., Raimundo, K., Antonova, E., & Chang, E. (2015). Resource use and costs in an insured population of patients with chronic idiopathic/spontaneous urticaria. *American journal of clinical dermatology*, 16, 313-321. doi: 10.1007/s40257-015-0134-8

[9] Choudhary, D., & Shrestha, S. Y. (2020). Association of Obesity with Chronic Idiopathic Urticaria at Birat Medical College and Teaching Hospital. *Birat Journal of Health Sciences,* 5(2), 1087-1090. doi: 10.3126/bjhs.v5i2.31411

[10] Darlenski, R., Mihaylova, V., & Handjieva-Darlenska, T. (2022). The link between obesity and the skin. *Frontiers in nutrition,* 9, 855573. doi: 10.3389/fnut.2022.855573

[11] Hasse, L., Jamiolkowski, D., Reschke, F., Kapitzke, K., Weiskorn, J., Kordonouri, O., ... & Ott, H. (2023). Pediatric obesity and skin disease: cutaneous findings and associated quality-of-life impairments in 103 children and adolescents with obesity. *Endocrine Connections,* 12(9), e230235. doi: 10.1530/EC-23-0235

[12] Jensen, P., & Skov, L. (2017). Psoriasis and obesity. *Dermatology,* 232(6), 633-639. doi: 10.1159/000455840

[13] Jorwal, P., Keshwani, P., & Verma, R. (2014). Association of acanthosis nigricans with anthropometric and biochemical parameters in young Indian males. *Ann Nigerian Med,* 8, 65-68. doi: 10.4103/0331-3131.153354

[14] Kalmin, O. V., & Galkina, T. N. (2020). *Медицинская антропология [Medical anthropology].* Высшее образование: Специалитет=Higher education: Specialist.

[15] Kim, J. K., Har, D., Brown, L. S., & Khan, D. A. (2018). Recurrence of chronic urticaria: incidence and associated factors. *The Journal of Allergy and Clinical Immunology: In Practice*, 6(2), 582-585. doi: 10.1016/j.jaip.2017.07.012

[16] Khasawneh, A. R., Serheta, I. V., Vadzyuk, S. N., Khapitska, O. P., & Bondar, S. A. (2022). Somatotypological parameters of the body in men and women with seborrheic dermatitis of varying severity. *Вісник Вінницького національного медичного університету=Reports of Vinnytsia National Medical University,* 26(2), 209-214. doi: 10.31393/reports-vnmedical-2022-26(2)-06

[17] Lajevardi, V., Ghodsi, S. Z., Daneshpazhooh, M., Kazemi, H., Aryanian, Z., & Goodarzi, A. (2014). The relationship between body mass index and the severity of acne. Iranian Journal of *Dermatology,* 17(1), 13-17.

[18] Lee, N., Lee, J. D., Lee, H. Y., Kang, D. R., & Ye, Y. M. (2017). Epidemiology of chronic urticaria in Korea using the Korean Health Insurance Database, 2010-2014. *Allergy, asthma & immunology research,* 9(5), 438-445. doi: 10.4168/aair.2017.9.5.438

[19] Li, J., Mao, D., Liu, S., Liu, P., Tian, J., Xue, C., ... & Zhang, J. (2022). Epidemiology of urticaria in China: a population-based study. *Chinese Medical Journal,* 135(11), 1369-1375. doi: 10.1097/CM9.0000000000002172

[20] Pepple, E. F., Amadi, E. S., Otike-Odibi, B., & Bell-Gam, H. I. (2022). Body Mass Index (BMI) and Cutaneous Lesions among the Elderly Patients in a Tertiary Hospital in Rivers State. *European J Nutr Food Saf,* 14(10), 15-22. doi: 10.9734/EJNFS/2022/v14i1030535

[21] Raciborski, F., Klak, A., Czarnecka-Operacz, M., Jenerowicz, D., Sybilski, A., Kuna, P., & Samoliński, B. (2018). Epidemiology of urticaria in Poland-nationally representative survey results. *Advances in Dermatology and Allergology/Postepy Dermatologii i Alergologii,* 35(1), 67-73. doi: 10.5114/ada.2018.73165

[22] Saini, S. S. (2014). Chronic spontaneous urticaria: etiology and pathogenesis. *Immunology and Allergy Clinics,* 34(1), 33-52. doi: 10.1016/j.iac.2013.09.012

[23] Sanchez-Borges, M., Ansotegui, I. J., Baiardini, I., Bernstein, J., Canonica, G. W., Ebisawa, M., ... & Martell, J. A. O. (2021). The challenges of chronic urticaria part 1: Epidemiology, immunopathogenesis, comorbidities, quality of life, and management. *World Allergy Organization Journal,* 14(6), 100533. doi: 10.1016/j.waojou.2021.100533

[24] Snast, I., Dalal, A., Twig, G., Astman, N., Kedem, R., Levin, D., ... & Levi, A. (2019). Acne and obesity: A nationwide study of 600,404 adolescents. *Journal of the American Academy of Dermatology,* 81(3), 723-729. doi: 10.1016/j.jaad.2019.04.009

[25] Staubach, P., Mann, C., Peveling-Oberhag, A., Lang, B. M., Augustin, M., Hagenström, K., ... & Petersen, J. (2021). Epidemiology of urticaria in German children. *JDDG: Journal der Deutschen Dermatologischen Gesellschaft,* 19(7), 1013-1019. doi: 10.1111/ddg.14485

[26] Trinh, H. K. T., Pham, D. L., Ban, G. Y., Lee, H. Y., Park, H. S., & Ye, Y. M. (2016). Altered systemic adipokines in patients with chronic urticaria. *International archives of allergy and immunology*, 171(2), 102-110. doi: 10.1159/000452626

[27] Tzur Bitan, D., Berzin, D., & Cohen, A. (2021). The association of chronic spontaneous urticaria (CSU) with anxiety and depression: a nationwide cohort study. *Archives of Dermatological Research,* 313(1), 33-39. doi: 10.1007/s00403-020-02064-3

[28] Weller, K., Maurer, M., Bauer, A., Wedi, B., Wagner, N., Schliemann, S., ... & Staubach, P. (2022). Epidemiology, comorbidities, and healthcare utilization of patients with chronic urticaria in Germany. *Journal of the European Academy of Dermatology and Venereology,* 36(1), 91-99. doi: 10.1111/jdv.17724

[29] Wertenteil, S., Strunk, A., & Garg, A. (2019). Prevalence estimates for chronic urticaria in the United States: A sex-and age-adjusted population analysis. *Journal of the American Academy of Dermatology,* 81(1), 152-156. doi: 10.1016/j.jaad.2019.02.064

[30] Zhang, A., & Silverberg, J. I. (2015). Association of atopic dermatitis with being overweight and obese: a systematic review and metaanalysis. *Journal of the American Academy of Dermatology,* 72(4), 606-616. doi: 10.1016/j.jaad.2014.12.013

ОСОБЛИВОСТІ ОБХВАТНИХ РОЗМІРІВ ТІЛА В УКРАЇНСЬКИХ ЧОЛОВІКІВ І ЖІНОК ХВОРИХ НА РІЗНІ ФОРМИ КРОПИВ'ЯНКИ

Аладван А. М. А., Дмитренко С. В., Кириченко В. І., Глушак А. А., Прокопенко О. С., Очеретна О. Л., Гунас І. В.

Актуальність дослідження обхватних розмірів тіла у пацієнтів з різними формами кропив'янки зумовлена значущістю антропометричних показників у діагностиці та прогнозуванні перебігу захворювання. Кропив'янка, як одна з найпоширеніших дерматологічних патологій, може мати різні клінічні форми, кожна з яких може по-різному впливати на організм, зокрема на зміну обхватних розмірів тіла. Вивчення цих показників у чоловіків та жінок українського походження дозволяє виявити статеві та індивідуальні особливості, що можуть мати важливе значення для покращення методів лікування та профілактики кропив'янки. Мета роботи - встановити особливості та статеві розбіжності обхватних розмірів тіла в українських чоловіків і жінок молодого віку хворих на гостру та хронічну кропив'янку легкого й тяжкого перебігу. Проведено визначення обхватних розмірів тіла у 40 українських чоловіків і 40 жінок молодого віку (25-44 роки згідно вікової періодизації ВООЗ, 2015) хворих на гостру (ГК) та хронічну (ХК) кропив'янку легкого (ЛП) і тяжкого (ТП) перебігу. Встановлення діагнозу кропив'янки проводили відповідно до міжнародного керівництва EAACI/GA²LEN/EuroGuiDerm/APAAACI. Антропометричні вимірювання проводили на правій частині тіла. Сантиметровою стрічкою визначали обхватні розміри верхніх і нижніх кінцівок, шиї та тулуба. В якості контрольної групи використані обхватні розміри тіла практично здорових українських чоловіків (n=82) і жінок (n=101) молодого віку, які були взяті з банку даних науково-дослідного центру Вінницького національного медичного університету ім. М. І. Пирогова. Статистичний аналіз обхватних розмірів тіла проведений у ліцензійному пакеті "Statistica 6.0" з використанням непараметричних методів оцінки. При порівнянні обхватних розмірів тіла у хворих на кропив'янку чоловіків або жінок із практично здоровими чоловіками або жінками встановлені достовірно більші або тенденція до більших значень: у хворих чоловіків - більшості обхватів верхньої кінцівки (переважно у хворих на ГК/ТП), стегна, талії, грудної клітки на вдиху та у спокійному стані (у хворих на ГК/ЛП, ГК/ТП, ХК/ЛП і ХК/ТП), шиї (у хворих на ГК/ЛП, ГК/ТП і ХК/ЛП); у хворих жінок - обхватів плеча у напруженому та ненапруженому станах, стегна, стегон, шиї, талії, грудної клітки на вдиху, на видиху та у спокійному стані (у хворих на ГК/ЛП, ГК/ТП, ХК/ЛП і ХК/ТП), передпліччя у нижній частині (у хворих на ГК/ЛП і ХК/ЛП), гомілки у верхній і нижній частині (у хворих на ГК/ЛП і ХК/ЛП). При порівнянні обхватних розмірів тіла між хворими на кропив'янку чоловіками або жінками встановлені лише поодинокі достовірні або тенденції розбіжностей: між хворими чоловіками - лише більші значення обхватів шиї (у хворих на ГК/ЛП порівняно з ГК/ТП) та стопи (у хворих на ГК/ТП порівняно з ХК/ТП); між хворими жінками - більші значення обхватів плеча у напруженому та ненапруженому станах, передпліччя у нижній частині, кисті, гомілки у верхній частині, стопи, грудної клітки на видиху та у спокійному стані (у хворих на ГК/ЛП порівняно з ГК/ТП), гомілки у нижній частині (у хворих на ХК/ЛП порівняно з ХК/ТП). Також встановлені виражені прояви статевого диморфізму обхватних розмірів тіла між хворими на кропив'янку українськими чоловіками та жінками: у хворих чоловіків - більші значення обхватів кисті та шиї (у хворих на ГК/ЛП, ГК/ТП, ХК/ЛП і ХК/ТП), обхватів плеча у напруженому та ненапруженому станах, передпліччя у верхній та нижній частині, стопи, талії, грудної клітки на вдиху, на видиху та у спокійному стані (у хворих на ГК/ТП), плеча у напруженому стані (у хворих на ХК/ТП), передпліччя у верхній частині (у хворих на ГК/ЛП), передпліччя у нижній частині (у хворих на ХК/ЛП); у хворих жінок - більші значення обхвату стегон (у хворих на ГК/ЛП) та стегна (у хворих на ХК/ЛП).

Ключові слова: *шкірні захворювання, кропив'янка, чоловіки, жінки, обхватні розміри тіла, статеві розбіжності.*

Author's contribution

Aladwan A. M. A. - research, review writing and editing, methodology and writing of the original draft.
Dmytrenko S. V. - conceptualization, supervision.
Kyrychenko V. I. - software, resources.
Glushak A. A. - data visualization, resources.
Prokopenko O. S. - data visualization, resources.
Ocheretna O. L. - software, resources.
Gunas I. V. - formal analysis and validation.

DOI: 10.31393/morphology-journal-2024-30(3)-03 Reports of Morphology, Vol. 30, №3, Pages 25-32

ISSN 1818-1295 eISSN 2616-6194

REPORTS OF MORPHOLOGY

Official Journal of the Scientific Society of Anatomists, Histologists, Embryologists and Topographic Anatomists of Ukraine

journal homepage: https://morphology-journal.com

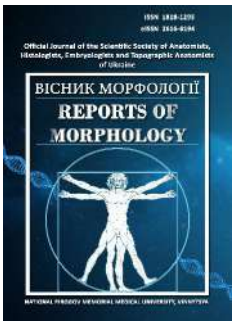

Dynamics of changes in the representation of mesenchymal cells in the forming glial scar during dexamethasone application

Graboviy O. M., Mervinsky T. S., Savosko S. I., Yaremenko L. M.
Bogomolets National Medical University, Kyiv, Ukraine

ARTICLE INFO
Received: 18 January 2024
Accepted: 08 July 2024

UDC: 576.32/.36:577.175.5:[616.831-005.1-085:615.212]-092

CORRESPONDING AUTHOR
e-mail: xabalas1@gmail.com
Mervinsky T. S.

CONFLICT OF INTEREST
The authors have no conflicts of interest to declare.

FUNDING
The study was carried out within the framework of the funding of fundamental research of the Ministry of Health of Ukraine "The study of restorative processes in the brain and nerve trunk during modulation of accumulation and differentiation of mesenchymal stem cells" number 0123U101051. Implementation period: 2023-2025.

DATA SHARING
Data are available upon reasonable request to corresponding author.

Mesenchymal stem cells are involved in cellular responses in the injured brain after a stroke. The formation of a glial scar is a local response in the brain to damage, and mesenchymal stem cells may be involved in the processes of scar formation. Mesenchymal stem cells express a range of membrane markers, the expression profile of which obviously changes as they differentiate and depends on the microenvironment in which these cells are located. However, it is still unclear where the stem cells in the damaged brain originate from - whether they come from a resident source or from the bone marrow, although an increase in CD34$^+$ cells in the blood of stroke patients is a well-known fact. In this study, we consider the hypothesis regarding the appearance of mesenchymal stem cells in the brain during a stroke and their potential involvement in the formation of a glial scar. The aim of the study is to investigate the involvement of CD44$^+$, CD68$^+$, CD90$^+$, and CD146$^+$ cells in the formation of a glial scar during hemorrhagic stroke and the changes in their representation under the effect of dexamethasone. To achieve this goal, we simulated hemorrhagic stroke in rats and compared the results of immunohistochemical detection of CD44$^+$, CD68$^+$, CD90$^+$, and CD146$^+$ cells in the area of glial scar formation against the dexamethasone administration. We obtained convincing results of differences in the activity and timing of migration of cells expressing CD44 compared to cells expressing CD68, CD90, and CD146. There is a tendency indicating a dependence between the detection of CD44$^+$ cells and the extent of the damage, while the detection of CD68$^+$, CD90$^+$, and CD146$^+$ cells is strongly correlated and increases under the effect of dexamethasone. Cells expressing CD44 were the main participants in the infiltrating pool of cells in the acute phase, but dexamethasone delayed the peak accumulation of CD44$^+$ cells in the forming scar. There were some changes in the detection of these cells around the hemorrhage during dexamethasone treatment, which may indicate its modulating effect on mesenchymal stem cells during glial scar formation. The more frequent detection of CD68$^+$, CD90$^+$, and CD146$^+$ cells can be considered a manifestation of the potential modification by dexamethasone of cellular reactions involved in glial scar formation in the brain after a stroke. The study of the roles of specific immunophenotypes of mesenchymal stem cells in the areas of glial scar formation following hemorrhagic stroke opens new perspectives in the study of brain recovery processes.

Keywords: *glial scar, brain vascular injury, stroke, brain damage, brain recovery, dexamethasone, mesenchymal stem cells.*

Introduction

Damage to the central nervous system (CNS) leads to a range of complex cellular and molecular responses [26]. One of them is the formation of a glial scar, which consists of reactive glia and other cells surrounding the area of significant brain tissue damage [5]. Its physiological role is ambiguous, with both negative and positive aspects. The predominance of these aspects is determined by the heterogeneity of the cellular composition of the glial scar and the extent of reactive astrogliosis [11]. This largely depends on the severity of the brain injury, which triggers an inflammatory response accompanied by swelling, infiltration of inflammatory hematogenous cells, and neuroinflammation [2, 14, 18].

During the glial scar formation, not only glial cells but

also non-resident cells, such as mesenchymal stem cells, are involved [29]. The migration of non-resident cells, which are not neurogenic but rather mesenchymal, into the injured brain is still insufficiently studied [13]. It is known that there is an active presence of $CD44^+$ cells in the affected area, as well as cells involved in angiogenesis, resident and hematogenous macrophages, such as $Iba\text{-}1^+$ and $CD68^+$ cells [23, 28]. It is evident that a rather heterogeneous population of cells migrates to the damaged areas of the brain, each with different properties and different effects on the recovery processes. On the other hand, their involvement in brain damage repair may be determined by the microenvironment, hematoma volume, inflammatory factors, and other conditions. The role of these cells in the elimination of hemorrhages, simulation of the peri-lesion environment, and their direct or indirect involvement, through cytokine secretion, in formation of the glial scar cannot be underestimated [19].

Mesenchymal stem cells do not have a unique immunophenotypic profile of their own; however, they are known to express a range of antigens, including CD34, CD44, CD68, CD90, and CD146. These could represent different populations of non-resident cells in the brain injury area, such as $CD146^+/34^-$ pericytes [12], mesenchymal stem cells $CD44^+/CD90^+/CD34^-$, and monocytes/macrophages $CD68^+$ [30]. This indicates that studying the involvement of endogenous stem cells in brain injury is an intriguing, but complex task.

In clinical practice, corticosteroids are often used to reduce swelling in brain injury [8], which in many cases can save patients' lives. Based on the general understanding of the mechanism of the corticosteroids action, it was logical to assume that reducing microcirculation disturbances and inflammatory infiltration would lead to a decrease in the severity of astrogliosis. However, the opposite is observed - an increase in the level of astrogliosis in the affected area [27].

This raises the question of how non-resident mesenchymal cells behave in brain areas adjacent to the damaged regions under the effect of corticosteroids. Evaluating these cellular responses could reveal potential targets for influencing glial scar formation, which is a crucial factor in improving recovery after brain injuries.

The aim of this study is to investigate the involvement of $CD44^+$, $CD68^+$, $CD90^+$, and $CD146^+$ cells in the formation of a glial scar during hemorrhagic stroke and the changes in their representation under the effect of dexamethasone.

Materials and methods

The study was held using the male Wistar rats (average body weight of 205.6±7.1 g) in the vivarium of the Bogomolets National Medical University (Kyiv, Ukraine). The rats were divided into three main groups: the sham-operated group (SH) (n=40), the hemorrhagic stroke group (HS) (n=40), and the hemorrhagic stroke + dexamethasone group (HS+D) (n=40). The studies were approved by the Bioethics Committee on Human or Animal Research of Bogomolets National Medical University (No. 160, dated 22.09.2022).

Hemorrhagic stroke in the brains of rats was simulated by injecting autologous blood (0.02 ml, without coagulants, using a 1.0 ml syringe in a fixation frame, with a repeated injection of the same volume after 10 minutes). In the SH group, the trepanation hole and needle insertion were simulated without blood injection. Dexamethasone was administered as a single daily subcutaneous injection at a dose of 10 mg/kg at 1, 2, and 3 days. The animals in each main group were randomly divided into subgroups of 8 rats for each of the 5 observation periods (1, 3, 10, 30, and 60 days post-surgery).

The rats were euthanized by administering a lethal dose of sodium thiopental. Afterward, access to the animal's heart was made for intracardiac perfusion (using 200 ml of physiological saline and 200 ml of 4 % formaldehyde and 0.9 % sodium chloride solution). The brain was then removed and placed in the latter solution (pH 7.4, 24 hours, 4°C). Brain fragments 3 mm thick were collected from each sample by making two frontal cuts (at the level of the needle insertion path). The brain samples were dehydrated in isopropanol and embedded in paraffin (Leica Surgipath Paraplast Regular). Immunohistochemical studies were conducted on 4 µm-thick frontal brain sections according to the manufacturer's antibody protocol.

The authors used mouse monoclonal antibody CD44 (Abcam, ab238464, USA), mouse monoclonal antibody CD68 (Abcam, ab201340, USA), mouse monoclonal antibody CD90 (Abcam, ab225, USA), and rabbit polyclonal antibody CD146 (Abcam, ab203118, USA). All antibodies were diluted at a 1:200 ratio. Nuclei were stained with Gill's hematoxylin. We detected the reaction products using a diaminobenzidine-based detection system (EnVision FLEX; Dako, Glostrup, Denmark). Brain sections were incubated with the antibodies at 24°C (with primary antibodies for 20 minutes and secondary antibodies for 10 minutes, respectively). Rat brain sections with positive protein expression were used as positive controls; for negative controls, all procedures were performed except for the use of primary antibodies. The samples were examined under an Olympus BX51 microscope, and photographs were taken with an Olympus C3040ZOOM digital camera using Olympus DP-Soft 3.2 software (Olympus, Tokyo, Japan).

The number of $CD44^+$, $CD68^+$, $CD90^+$, and $CD146^+$ cells was evaluated using a 4-point scale, where: 0 points = absence of labeled cells; 1 point (low) = single cells; 2 points (moderate) = groups of cells around the hemorrhage; 3 points (high) = numerous infiltrates inside and around the hemorrhage. A score was assigned to each sample based on the identified regions of interest (ROIs) with the studied cells (in 3 fields/sections per sample). The average value obtained from the ROIs of each sample was used for correlation analysis.

The researchers cut the brain at the level of the needle introduction track (visually visible on the surface of the hemisphere). Coronal sections with a thickness of 2 mm

were obtained, and the area of hemorrhage (for days 1 and 3) and the area of the haemorrhage (for days 10, 30, and 60) were calculated. The area was multiplied by the thickness of the section(s) to obtain the total volume of the hematoma or lesion. Lesions in sections with an eliminated thrombus included degenerative tissue (such as lacunae with or without erythrocytes or hemosiderin, and degenerated tissue).

The statistical analysis was by StatPlus software (7.0) (AnalystSoft Inc.), by univariate analysis (ANOVA) with Bonferroni post hoc test and correlation analysis (Spearman's rank correlation coefficient, rho). The strength and direction of the correlations were determined according to Chaddock's scale (up to 0.3 - negligible; 0.3-0.5 - weak; 0.5-0.7 - moderate; 0.7-0.9 - strong). Differences between groups were considered statistically significant at $p<0.05$.

Results

In the frontal brain sections of rats after simulated HS, a hematoma was detected in all cases, while in the SH group rats, only the needle insertion track didn't show the hematoma formation. At 30 and 60 days after the blood injection into the brain, the hematoma and blood clot were no longer observed, which indicated complete elimination of cellular debris and hemosiderin, and a developed cavity (pseudocyst) in place of the hematoma. A glial scar was developing around the perimeter of the pseudocyst.

The assessment of changes in brain lesion volume after HS under the effect of dexamethasone showed that calculations of areas with hematomas at 1, 3, and 10 days, and calculations of brain necrosis areas at 30 and 60 days of the experiment, did not show a significant difference in lesion volume between the HS group and the HS+D group ($p\geq0.20$) (Table 1). In the latter two time points, a smaller lesion volume was observed in the HS group compared to day 1. In the overall sample of hematomas reproduced in the rats, the volumes were similar, and therefore, in the brains of randomly assigned rats in the HS and HS+D groups, there were no statistical differences.

The perimeter of the hematoma and later in the wall of the pseudocyst showed infiltration of $CD44^+$, $CD68^+$, $CD90^+$, and $CD146^+$ cells (Fig. 1). The cellular response around the hematoma was almost uniform across the entire perimeter. Some differences on the lateral and medial sides of the hematoma or the needle insertion track in the brain were not significant enough to create substantial variations.

The dynamical pattern of $CD44^+$ cell content differed between the groups of rats: from the appearance of isolated cells or small groups of $CD44^+$ immunopositive cells in the needle insertion track in the SH group, to the presence of a significant number of cells in the HS group in 3 and 10 days. In the HS+D group, the peak accumulation of these cells was observed 30 days after simulating HS. $CD44^+$ cells were detected around the hematoma during all measurements.

In the HS group, there was a significant decrease in the intensity of cell migration to the glial scar formation area at 60 days compared to the periods after the 3rd ($p=0.01$) and 10th days ($p=0.04$). In the HS+D group, a positive dynamic in the accumulation of $CD44^+$ cells in the glial scar was observed at 30 days (1 day vs. 30 days, $p=0.02$). No statistical difference between the HS and HS+D groups was found for each observation period, but dexamethasone delayed the peak accumulation of $CD44^+$ cells in the affected area (Fig. 2).

$CD68^+$ cells were detected in the perihematomal area in smaller numbers compared to $CD44^+$ cells. Instances of isolated cells were observed in the HS group in 10, 30, and 60 days, while in the HS+D group, the first isolated cells around the hematoma were registered in 3 days and then in 10, 30, and 60 days, similar to the HS group. The results of the analysis by 3-point scale showed no significant difference between the HS and HS+D groups, and in the HS group, they were not detected at all.

$CD90^+$ cells were also occasionally detected in the area of glial scar formation. In the HS group, their migration to the scar was rare at 10 and 30 days, and only at 60 days we observed focal accumulations of cells observed around the pseudocyst. In contrast, in the HS+D group, the migration of $CD90^+$ cells to the scar was more intense, with a peak accumulation at 30 days (HS vs. HS+D, $p=0.01$).

$CD146^+$ cells were detected around individual thin-walled vessels and within the glial scar of the pseudocyst as isolated cells or occasionally in small focal groups at 10, 30, and 60 days after simulating HS. In the HS+D group, the migration activity of $CD146^+$ cells was somewhat more intense, although no significant difference was found between the comparison groups.

A correlation analysis between the volume of the lesion and the intensity of cell migration of the studied immunophenotypes found no convincing statistical evidence of a direct relationship between the lesion volume and the appearance of the studied cells in the area of glial scar formation (for each observation period, rho>0.41, p>0.41; in the overall sample of observations, rho>0.12, p>0.47), except for the Spearman correlation coefficient analysis in the case of $CD44^+$ cell infiltration at 3 days in the

Table 1. Volume of brain lesion (mm^3) in rats after SH and HS (M±m).

Group	Day of experiment				
	1	3	10	30	60
SH	1.920±0.320	2.070±0.908	2.010±0.190	0.740±0.083	0.810±0.221
HS	26.17±2.27*	17.38±1.72*	19.70±3.53*	16.52±3.36*†	16.85±0.71*†
HS+D	21.55±2.15*	18.75±4.20*	18.33±1.97*	16.99±2.93*	17.34±1.32*

Note: * - $p<0.05$ compared to SH; † - $p<0.05$ compared to day 1.

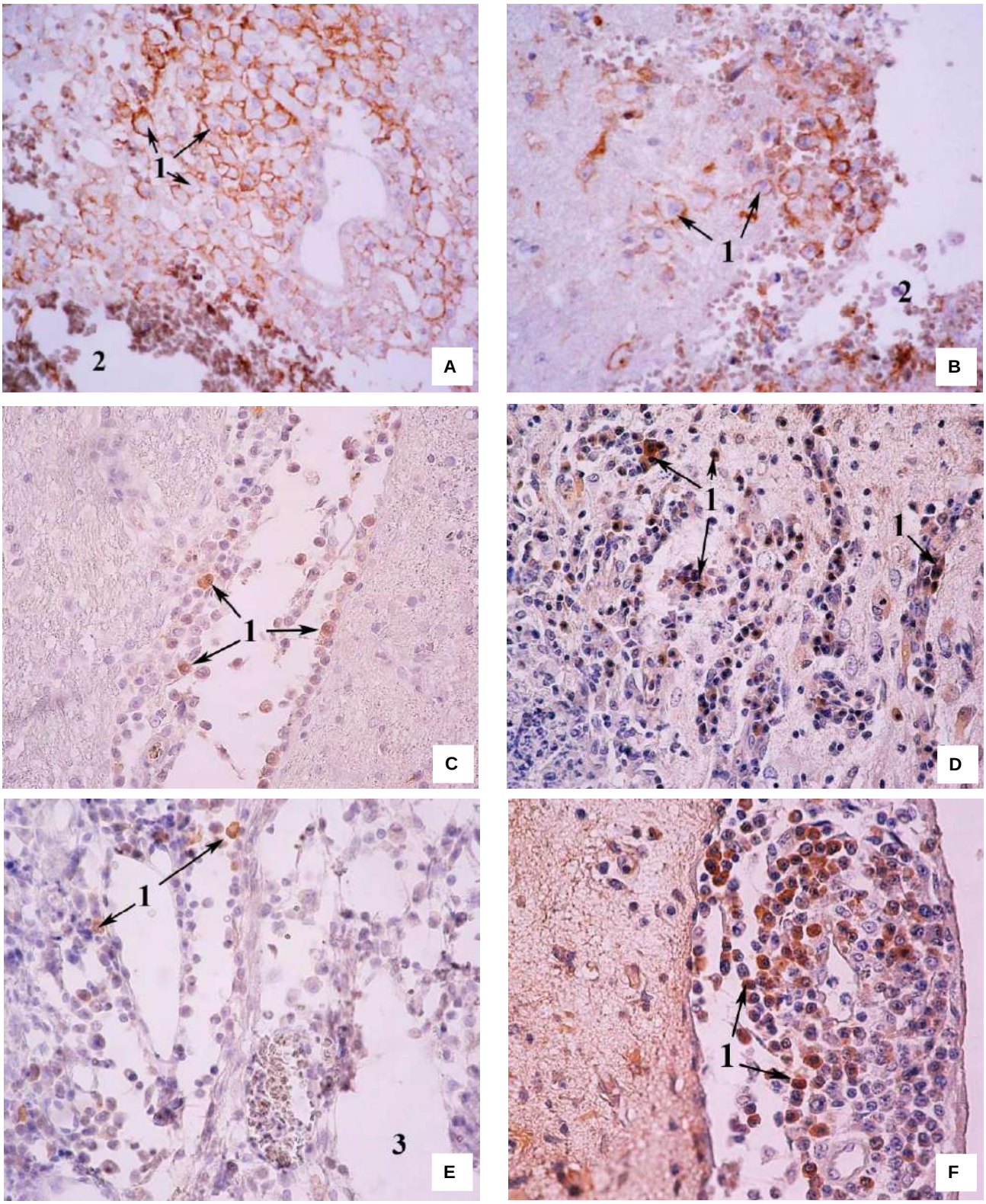

Fig. 1. CD44$^+$, CD68$^+$, CD90$^+$ and CD146$^+$ cells in the area of glial scar formation in the brains of rats in the HS and HS+D groups. 1 - cells with positive immune response, 2 - hemorrhage area, 3 - pseudocyst. A - CD44$^+$ cells in the HS group, 3 days; B - CD44$^+$ cells in the HS+D group, 3 days; C - CD68$^+$ cells in the HS group, 10 days; D - CD68$^+$ cells in the HS+D group, 10 days; E - CD90$^+$ cells in the HS group, 10 days; F - CD90$^+$ cells in the HS+D group, 10 days; G - CD146$^+$ cells in the HS group, 60 days; H - CD146$^+$ cells in the HS+D group, 60 days. Immunohistochemistry, nuclei stained with Gill's hematoxylin, X400.

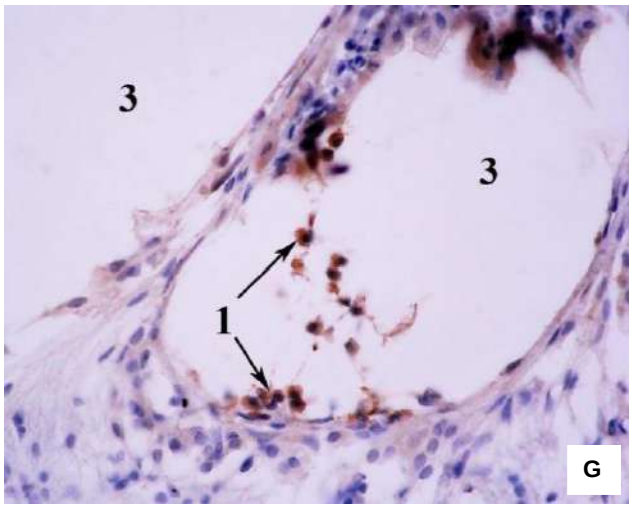

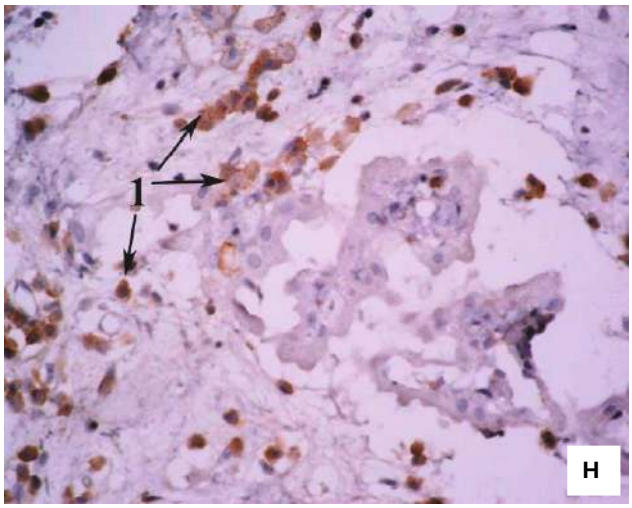

Continuation of fig. 1.

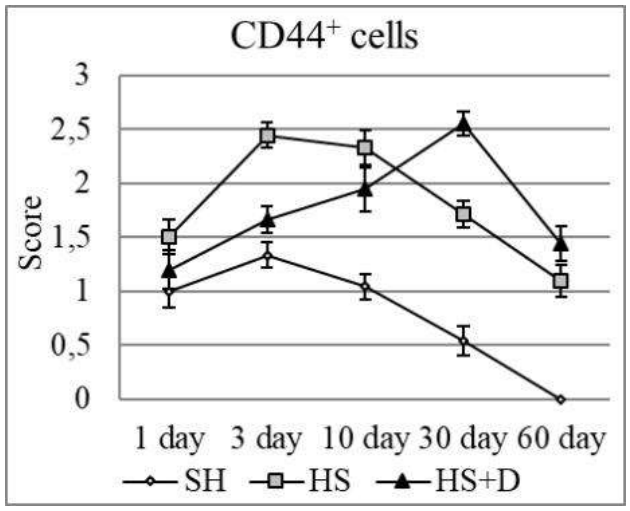

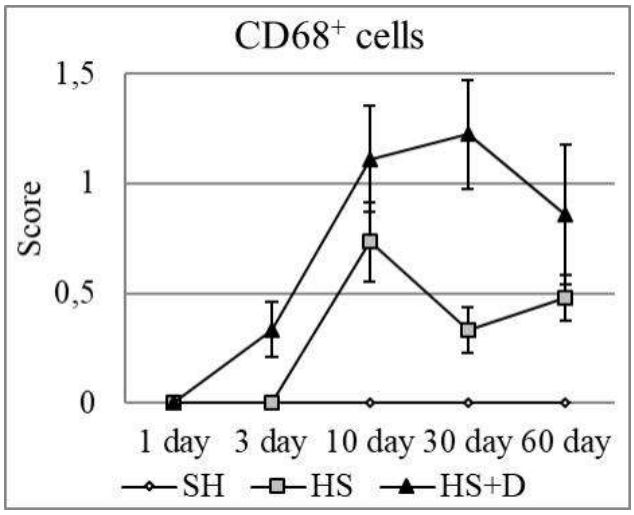

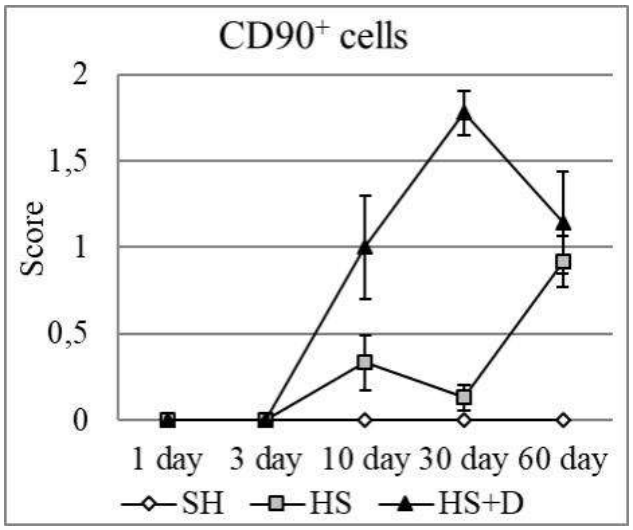

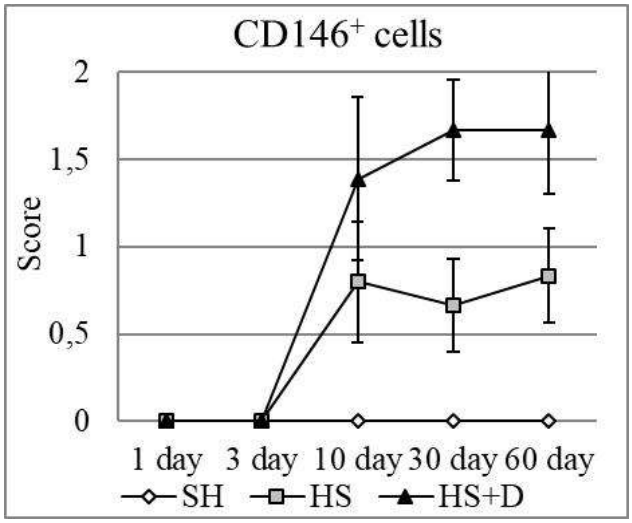

Fig. 2. Quantitative assessment of $CD44^+$, $CD68^+$, $CD90^+$, and $CD146^+$ cells in glial scars surrounding the damaged brain tissue area (M±m).

HS+D group (rho=0.89, p=0.04; in the overall sample of observations, rho>0.14, p>0.48). This can be explained by the fact that the migration of $CD44^+$ cells at the border of the hematoma and scar, or pseudocyst and scar, was a dynamic

Table 2. Correlation between cells with identified CD markers in the combined study. (HS / HS+D).

Cells vs. Cells	Spearman's rho/p-value		
	HS	HS+D	total study
$CD68^+$ vs. $CD90^+$	0.59/0.01	0.56/0.01	0.53/0.01
$CD68^+$ vs. $CD146^+$	0.79/0.01	0.61/0.01	0.63/0.01
$CD90^+$ vs. $CD146^+$	0.61/0.01	0.82/0.01	0.73/0.01
$CD44^+$ vs. $CD68^+$	0.11/0.53	0.54/0.01	0.32/0.01
$CD44^+$ vs. $CD90^+$	-0.13/0.44	0.47/0.01	0.12/0.03
$CD44^+$ vs. $CD146^+$	0.09/0.61	0.57/0.01	0.27/0.03

phenomenon, starting with an initial increase in $CD44^+$ cell migration in the acute phase and declining to rare occurrences at 60 days in the pseudocyst after complete hematoma elimination. Noteworthy, the overall sample of observations in the SH group showed a dependence of the activity of $CD44^+$ cell migration on the volume of penetrating brain injury (for each observation period, rho>0.47, p>0.24; in the overall sample of observations, rho=0.53, p=0.01). A similar trend was observed after HS, but in the perifocal area of the hematoma, outside the glial scar.

$CD68^+$, $CD90^+$ and $CD146^+$ cells were mainly detected at 10 days following HS simulation. Although their appearance was associated with the area of glial scar around the pseudocyst, no significant correlation with the volume of the pseudocyst was found. This lack of correlation can be attributed to their infrequent appearance, which was insufficient for a robust statistical analysis.

We decided to determine the overall biological relationship between the appearance of the studied cells at the border with the hematoma during glial scar formation. To do this, we combined the data variation series from the HS and HS+D groups to obtain more statistical data. A correlation was established between the intensity of migration of $CD68^+$, $CD90^+$ and $CD146^+$ cells, ranging from weak to strong. A weak correlation was also found between $CD44^+$ and $CD68^+$ cells (Table 2). In the HS+D group, the correlation between $CD44^+$ cells and the other three immunophenotypes was significant.

Discussion

Mesenchymal stem cells are considered a potential therapeutic target for the treatment of ischemic brain injury [6, 15]. Previous studies have shown that an increased number of $CD34^+$ cells in peripheral blood immediately after a stroke directly correlates with functional recovery [7, 17, 22]. However, these studies only confirm the presence of stem cells, their association with certain parameters, or their appearance in the brain in experimental settings. It is crucial to study their differentiation into tissue structures of the damaged organ [1, 3, 16].

Experimental studies and immunohistochemical detection of cells based on specific clusters of differentiation (CD) can help with this. However, this presents another challenge, as mesenchymal stem cells do not consistently express a single CD marker profile, and their expression changes as they differentiate. The study is limited to the cells expressing CD44, CD68, CD90, and CD146.

Our hypothesis was that CD44, CD68, and CD90 could be markers of mesenchymal stem cells in the brain, while cells expressing CD146 might be associated with the regeneration of blood vessels in the brain. Additionally, CD68 may be expressed by microglial cells, which could simultaneously be considered as a hypothetical differentiation of stem cells into microglia. The results showed that $CD44^+$ cells were more frequently detected in the area of scar formation around the hemorrhage compared to CD68, CD90, or CD146 cells, particularly before the hemorrhage was eliminated. Meanwhile, $CD68^+$ cells began to appear after the hematoma was eliminated and during scar formation. We concluded that cells expressing CD68 are a rather heterogeneous population, and accurately determining whether they belong to mesenchymal stem cells or are already differentiated into microglial cells requires further investigation.

It is important to note that dexamethasone delayed the migration of $CD44^+$ cells to the area of glial scar formation around the hematoma, which facilitated the appearance of cells expressing CD68, CD90, or CD146. The presence of $CD44^+$ cells in the brain during stroke and neuroinflammation is well documented [23]. The accumulation of $CD44^+$ cells was delayed as the hematoma and cellular debris were eliminated, and dexamethasone slowed down these cellular reactions. Dexamethasone is a powerful anti-inflammatory agent and has been shown to be effective in promoting post-traumatic recovery in a model of acute spinal cord compression injury [24].

Dexamethasone prevents the loss of proliferative potential and the typical phenotype of human mesenchymal stem cells, promotes angiogenesis, and thus may modify the responses of mesenchymal cells of different immunophenotypes in the damaged brain [25]. Despite the active migration of $CD44^+$ cells to the hematoma and their potential involvement in hematoma simulation, CD44 is considered a membrane marker of mesenchymal stem cells [21], so their role in the recovery processes around the hematoma or pseudocyst still needs to be explored.

CD68 is a marker of hematopoietic stem cells and tissue macrophages/microglial cells, and it is detected in neuroinflammation and stroke as cells with a pro-inflammatory phenotype [20]. However, the role of mesenchymal stem cells expressing CD68 remains poorly understood.

CD146 has been considered a receptor for cell adhesion between endothelial cells and pericytes, which is expressed by hematopoietic cells and newly formed hemocapillaries [4]. We hypothesized that angiogenesis around the hemorrhage would be accompanied by the appearance of cells expressing CD146, which should be associated with vascular differentiation and the restoration of the blood-brain barrier. In this study, cells expressing CD146 were observed

specifically around thin-walled newly formed blood vessels and in the areas of the glial scar forming in the lumen of the pseudocyst. The appearance of these cells around the vessel walls occurred much later than expected and was quite focal. This phenomenon deserves further attention, as angiogenesis and the state of the blood-brain barrier in the brain after injury are critical factors in potential recovery. Additionally, there was a trend toward the recruitment of $CD146^+$ cells under dexamethasone administration, but their role in vascular system recovery also needs further investigation.

The role of CD90+ cells in the brain remains the least understood, as their appearance was quite rare, and the migration of these cells coincided with the appearance of cells expressing CD68 and CD146. Therefore, the possibility of co-expression of several surface CD markers on certain populations of mesenchymal cells in the glial scar should be considered.

The results of this study suggest that dexamethasone may modify the formation of the glial scar in the brain, highlighting the importance of further investigation into the role of specific immunophenotypes of mesenchymal stem cells in the cellular reactions within the glial scar after hemorrhagic stroke, particularly around the formed pseudocyst.

Conclusion

1. The presence of cells expressing CD44, CD68, CD90, and CD146 around the hematoma in the brain is evidence of the involvement of mesenchymal stem cells in the formation of the glial scar during hemorrhagic stroke.

2. The mesenchymal stem cell representation in the scar is characterized by the early appearance of $CD44^+$ cells, followed by their replacement with cells expressing CD68, CD90, and CD146 markers.

3. The peak migration of $CD44^+$ cells to the glial scar was delayed with the application of dexamethasone, while the appearance of $CD68^+$, $CD90^+$ and $CD146^+$ cells tended to increase, particularly 30 days after brain injury.

References

[1] Ahn, S. Y., Sung, D. K., Kim, Y. E., Sung, S., Chang, Y. S., & Park, W. S. (2021). Brain-derived neurotropic factor mediates neuroprotection of mesenchymal stem cell-derived extracellular vesicles against severe intraventricular hemorrhage in newborn rats. *Stem Cells Translational Medicine,* 10(3), 374-384. doi: 10.1002/sctm.20-0301

[2] Bao, Y., Qin, L., Kim, E., Bhosle, S., Guo, H., Febbraio, M., … & Cho, S. (2012). CD36 is Involved in Astrocyte Activation and Astroglial Scar Formation. *Journal of Cerebral Blood Flow & Metabolism,* 32(8), 1567-1577. doi: 10.1038/jcbfm.2012.52

[3] Bashyal, N., Kim, M. G., Jung, J. H., Acharya, R., Lee, Y. J., Hwang, W. S., … & Suh-Kim, H. (2023). Preclinical Study on Biodistribution of Mesenchymal Stem Cells after Local Transplantation into the Brain. *International Journal of Stem Cells,* 16(4), 415-424. doi: 10.15283/ijsc23062

[4] Chen, J., Luo, Y., Hui, H., Cai, T., Huang, H., Yang, F., … & Yan, X. (2017). CD146 coordinates brain endothelial cell-pericyte communication for blood-brain barrier development. *Proceedings of the National Academy of Sciences of the United States of America,* 114(36), E7622-E7631. doi: 10.1073/pnas.1710848114

[5] Clain, J., Couret, D., Bringart, M., Lecadieu, A., Meilhac, O., Lefebvre d'Hellencourt, C., & Diotel, N. (2024). Metabolic disorders exacerbate the formation of glial scar after stroke. *The European Journal of Neuroscience*, 59(11), 3009-3029. doi: 10.1111/ejn.16325

[6] Dabrowska, S., Andrzejewska, A., Strzemecki, D., Muraca, M., Janowski, M., & Lukomska, B. (2019). Human bone marrow mesenchymal stem cell-derived extracellular vesicles attenuate neuroinflammation evoked by focal brain injury in rats. *Journal of Neuroinflammation*, 16(1), 216. doi: 10.1186/s12974-019-1602-5

[7] Dunac, A., Frelin, C., Popolo-Blondeau, M., Chatel, M., Mahagne, M. H., & Philip, P. J. (2007). Neurological and functional recovery in human stroke are associated with peripheral blood CD34+ cell mobilization. *Journal of Neurology,* 254, 327-332. doi: 10.1007/s00415-006-0362-1

[8] Guennoun, R., Zhu, X., Fréchou, M., Gaignard, P., Slama, A., Liere, P., & Schumacher, M. (2019). Steroids in Stroke with Special Reference to Progesterone. *Cellular and Molecular Neurobiology,* 39(4), 551-568. doi: 10.1007/s10571-018-0627-0

[9] Guo, Y., Peng, Y., Zeng, H., & Chen, G. (2021). Progress in Mesenchymal Stem Cell Therapy for Ischemic Stroke. *Stem Cells International,* 10, 1-24. doi: 10.1155/2021/9923566

[10] He, J. Q., Sussman, E. S., & Steinberg, G. K. (2020). Revisiting Stem Cell-Based Clinical Trials for Ischemic Stroke. *Frontiers in Aging Neuroscience,* 12, 575990. doi: 10.3389/fnagi.2020.575990

[11] He, Y., Liu, X., & Chen, Z. (2020). Glial Scar - a Promising Target for Improving Outcomes After CNS Injury. *Journal of Molecular Neuroscience,* 70, 340-352. doi: 10.1007/s12031-019-01417-6

[12] Hörl, S., Ejaz, A., Ernst, S., Mattesich, M., Kaiser, A., Jenewein, B., … & Zwerschke, W. (2017). CD146 (MCAM) in human cs-DLK1-/cs-$CD34^+$ adipose stromal/progenitor cells. *Stem Cell Research*, 22, 1-12. doi: 10.3389/fncel.2020.546659

[13] Huang, L., Nakamura, Y., Lo, E. H., & Hayakawa, K. (2019). Astrocyte Signaling in the Neurovascular Unit After Central Nervous System Injury. *International Journal of Molecular Sciences,* 20(2), 282. doi: 10.3390/ijms20020282

[14] Koyama, R., & Shichita, T. (2023). Glial roles in sterile inflammation after ischemic stroke. *Neuroscience Research,* 187, 67-71. doi: 10.1016/j.neures.2022.10.002

[15] Li, J., Zhang, Q., Wang, W., Lin, F., Wang, S., & Zhao, J. (2021). Mesenchymal stem cell therapy for ischemic stroke: A look into treatment mechanism and therapeutic potential. *Journal of Neurology,* 268(11), 4095-4107. doi: 10.1007/s00415-020-10138-5

[16] Mitkari, B., Nitzsche, F., Kerkelä, E., Kuptsova, K., Huttunen, J., Nystedt, J., … & Jolkkonen, J. (2014). Human bone marrow mesenchymal stem/stromal cells produce efficient localization in the brain and enhanced angiogenesis after intra-arterial delivery in rats with cerebral ischemia, but this is not translated to behavioral recovery. *Behavioural Brain Research*, 259, 50-59. doi: 10.1016/j.bbr.2013.10.030

[17] Mizuno, T., Hoshino, T., Ishizuka, K., Toi, S., Takahashi, S., Wako, S., … & Kitagawa, K. (2024). Association of circulating CD34+ cells level and prognosis after ischemic stroke. *International Journal of Stroke: Official Journal of the International Stroke Society,* 19(4), 460-469. doi: 10.1177/

17474930231217192
[18] Nicaise, A. M., D'Angelo, A., Ionescu, R. B., Krzak, G., Willis, C. M., & Pluchino, S. (2022). The role of neural stem cells in regulating glial scar formation and repair. *Cell Tissue Research,* 387(3), 399-414. doi: 10.1007/s00441-021-03554-0
[19] Noh, J. E., Oh, S. H., Park, I. H., & Song, J. (2020). Intracerebral Transplants of GMP-Grade Human Umbilical Cord-Derived Mesenchymal Stromal Cells Effectively Treat Subacute-Phase Ischemic Stroke in a Rodent Model. *Frontiers in Cellular Neuroscience,* 14, 546659. doi: 10.3389/fncel.2020.546659
[20] Rahmanian, A., Salehi, A., Kamali-Sarvestani, E., Ahrari, I., Mohamadhoseini, E., Jamali, M., & Ghahramani, S. (2024). CD68 Antigen and Cerebral Aneurysms: A Case-Control Study. *Journal of Neurological Surgery Part A: Central European Neurosurgery,* 85(2), 142-146. doi: 10.1055/s-0043-1761944
[21] Ramos, T., Sánchez-Abarca, L. I., Muntión, S., Preciado, S., Puig, N., López-Ruano, G., … & del Cañizo, C. (2016). MSC surface markers (CD44, CD73, and CD90) can identify human MSC-derived extracellular vesicles by conventional flow cytometry. *Cell Communication and Signaling,* 14, 2. doi: 10.1186/s12964-015-0124-8
[22] Rigato, M., & Fadini, G. P. (2018). Circulating Stem/Progenitor Cells as Prognostic Biomarkers in Macro- and Microvascular Disease: A Narrative Review of Prospective Observational Studies. *Current Medicinal Chemistry*, 25(35), 4507-4517. doi: 10.2174/0929867324666170920154020
[23] Sawada, R., Nakano-Doi, A., Matsuyama, T., Nakagomi, N., & Nakagomi, T. (2020). CD44 expression in stem cells and niche microglia/macrophages following ischemic stroke. *Stem Cell Investigation*, 7, 4. doi: 10.21037/sci.2020.02.02
[24] Sharma, A., Tiwari, R., Badhe, P., & Sharma, G. (2004). Comparison of methylprednisolone with dexamethasone in treatment of acute spinal injury in rats. *The Indian Journal of Experimental Biology*, 42(5), 476-480.
[25] Xiao, Y., Peperzak, V., van Rijn, L., Borst, J., & de Bruijn, J.D. (2010). Dexamethasone treatment during the expansion phase maintains stemness of bone marrow mesenchymal stem cells. *Journal of Tissue Engineering and Regenerative Medicine,* 4(5), 374-386. doi: 10.1002/term.250
[26] Yaremenko, L., Grabovoi, A., Cherkasov, V., Lakhtadyr, T., & Shepelev, E. (2020). Reactions of astrocytes and microglia of the sensorimotor cortex at ligation of the carotid artery, sensitization of the brain antigen and their combination. *Georgian Medical News,* 304-305, 122-127.
[27] Ye, X., Zou, G., Hou, J., Bi, H., Zhou, C., Wang, R., Xu, Y., … Huang, C. (2020). Dexamethasone does not ameliorate gliosis in a mouse model of neurodegenerative disease. *Biochemistry and Biophysics Reports,* 24, 100817. doi: 10.1016/j.bbrep.2020.100817
[28] Yoon, J. S., Jo, D., Lee, H. S., Yoo, S. W., Lee, T. Y., Hwang, W. S., … & Suh-Kim, H. (2018). Spatiotemporal Protein Atlas of Cell Death-Related Molecules in the Rat MCAO Stroke Model. *Experimental Neurobiology,* 27(4), 287-298. doi: 10.5607/en.2018.27.4.287
[29] Zhang, Y., Dong, N., Hong, H., Qi, J., Zhang, S., & Wang, J. (2022). Mesenchymal Stem Cells: Therapeutic Mechanisms for Stroke. *International Journal of Molecular Sciences*, 23, 2550. doi: 10.3390/ijms23052550
[30] Xhang, X., Ma, Z., Zhu, G., Lu, Y, & Yang, J. (2021). New perspective into mesenchymal stem cells: Molecular mechanisms regulating osteosarcoma. *Journal of Bone Oncology,* 29, 100372. doi: 10.1016/j.jbo.2021.100372

ДИНАМІКА ЗМІН ПРЕДСТАВНИЦТВА МЕЗЕНХІМАЛЬНИХ КЛІТИН У ГЛІАЛЬНОМУ РУБЦІ, ЩО ФОРМУЄТЬСЯ, ПРИ ВВЕДЕННІ ДЕКСАМЕТОЗОНА

Грабовий О. М., Мервінський Т. С., Савосько С. І., Яременко Л. М.

Мезенхімальні стовбурові клітини беруть участь у клітинних реакціях у пошкодженому мозку після інсульту. Розвиток гліального рубця є місцевою реакцією у мозку на пошкодження і мезенхімальні стовбурові клітини можуть бути залучені у процеси формування рубця. Мезенхімальні стовбурові клітини експресують ряд мембранних маркерів, профіль експресії яких очевидно змінюється по мірі їх диференціації і залежить від мікрооточення в яке потрапили ці клітини. В свою чергу, не зрозуміло звідки у пошкодженому мозку з'являються стовбурові клітини, вони походять від резидентного джерела, чи їх кісткового мозку, хоча підвищення CD34⁺ клітин у крові хворих з інсультом є відомим. У цій роботі ми розглядаємо гіпотезу про появу мезенхімальних стовбурових клітин у мозку при інсульті та їх потенційну участь у формуванні гліального рубця. Мета роботи - дослідити участь CD44⁺, CD68⁺, CD90⁺ та CD146⁺ клітин у формуванні гліального рубця при геморагічному інсульті та зміни їх представництва при дії дексаметазону. Для реалізації даної мети нами у щурів змодельовано геморагічний інсульт і проведено порівняння результатів імуногістохімічного виявлення CD44⁺, CD68⁺, CD90⁺ і CD146⁺ клітин у ділянці формування гліального рубця на тлі введення дексаметазону. Отримано переконливі результати, які вказують на різницю в активності та термінах виявлення клітин, що експресують CD44, і клітин, що експресують CD68, CD90 і CD146. Має місце тенденція залежності між виявленням CD44⁺ клітин і об'ємом ураження, а виявлення CD68⁺, CD90⁺ і CD146⁺ клітин має сильну залежність і зростає під дією дексаметазону. Клітини, які експресують CD44, були основними учасниками інфільтраційного пулу клітин у гострому періоді, але дексаметазон відтермінував пік накопичення CD44⁺ клітин у рубці, що формується. Мали місце деякі зміни у виявленні цих клітин навколо крововиливу під час дії дексаметазону, що може свідчити про його модулюючу дію на мезенхімальні стовбурові клітини при формуванні гліального рубця. Частіше виявлення CD68⁺, CD90⁺ і CD146⁺ клітин можна розглядати як прояв потенційної модифікації дексаметазоном клітинних реакцій у формуванні гліального рубця у мозку після інсульту. Дослідження ролі окремих імунофенотипів мезенхімальних стовбурових клітин у ділянках формування гліального рубця після геморагічного інсульту розкриває нові перспективи у вивченні відновних процесів у мозку.

Ключові слова: *гліальний рубець, судинні ураження мозку, інсульт, пошкодження мозку, відновлення мозку, дексаметазон, мезенхімальні стовбурові клітини.*

Author's contribution

Graboviy O. M. - conceptualization, administration.
Mervinsky T. S. - data visualization, project administration, research, formal analysis and validation, methodology and writing of the original draft.
Savosko S. I. - supervision, software.
Yaremenko L. M. - resources, data visualization, resources, review writing and editing.

DOI: 10.31393/morphology-journal-2024-30(3)-04 Reports of Morphology, Vol. 30, №3, Pages 33-43

ISSN 1818-1295 eISSN 2616-6194

REPORTS OF MORPHOLOGY

Official Journal of the Scientific Society of Anatomists, Histologists, Embryologists and Topographic Anatomists of Ukraine

journal homepage: https://morphology-journal.com

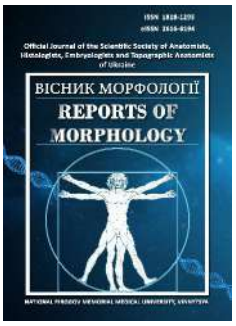

Regression models of computed tomographic dimensions necessary for building the correct shape of the dental arch in Ukrainian young men and young women with a physiological bite without taking into account the type of face, depending on the features of teleroentgenometric indicators according to the Ricketts method and computed tomographic dimensions of teeth

Brotskyi N. O.[1], Dmitriev M. O.[1], Cherkasova L. A.[2], Smiiukha O. A.[1], Beliaiev E. V.[1], Moroz V. V.[2], Vakhovskyi V. V.[1]

[1]National Pirogov Memorial Medical University, Vinnytsya, Ukraine
[2]Bogomolets National Medical University, Kyiv, Ukraine

ARTICLE INFO

Received: 21 February 2024
Accepted: 19 July 2024

UDC: 611.314:611.714+616.714.1-071.3

CORRESPONDING AUTHOR

e-mail: opdihatopa@gmail.com
Brotskyi N. O.

CONFLICT OF INTEREST

The authors have no conflicts of interest to declare.

FUNDING

Not applicable.

DATA SHARING

Data are available upon reasonable request to corresponding author.

Orthodontics plays a crucial role in ensuring facial aesthetic harmony and functional correctness of the dentoalveolar system. Cephalometric analysis is an essential tool in orthodontic treatment planning, as its parameters vary significantly depending on the patient's age, sex, and nationality. Understanding these differences is critically important for accurate diagnosis and effective treatment across different populations. The aim of the study is to construct and analyze regression models of computed tomography dimensions necessary for constructing the correct shape of the dental arch in Ukrainian young men and young women with a physiological bite, depending on the specific cephalometric parameters according to the Ricketts method and computed tomography tooth dimensions. In the licensed software OnyxCeph³™ version 3DPro, primary computed tomography scans of Ukrainian young men (n=41) and young women (n=68) with physiological bites were analyzed, obtained from the database of the Department of Pediatric Dentistry and the Research Center of the National Pirogov Memorial Medical University, Vinnytsya. According to the Ricketts method, "dental," "skeletal and dentoskeletal," "soft tissue aesthetics," "craniofacial relationships," and "internal structures" indicators were determined on lateral cephalograms. Morphometric parameters of upper and lower jaw teeth were determined in the mesiodistal and buccolingual directions on computed tomography scans, as well as distances necessary for constructing correct dental arch forms. Regression models of the linear dimensions necessary for constructing the correct dental arch shape, depending on the specific cephalometric parameters according to the Ricketts method and computed tomography tooth dimensions, were constructed using the licensed "Statistica 6.0" package. It was found that in Ukrainian young men, all 18 possible reliable regression models were constructed with a coefficient of determination greater than 0.6 (R^2= from 0.617 to 0.833, $p<0.001$ in all cases); while in Ukrainian young women, only 6 reliable regression models were constructed with a coefficient of determination greater than 0.6 (R^2= from 0.605 to 0.793, $p<0.001$ in all cases). When analyzing the percentage of inclusion in the regression equations of cephalometric parameters and computed tomography tooth dimensions, it was found that in Ukrainian young men, cephalometric parameters and crown width in the mesiodistal direction were most frequently included in the models (26.67 % each), distance from the incisal edge to the apex of the tooth root (13.33 %), and crown width in the buccolingual direction (10.00 %); while in Ukrainian young women, cephalometric parameters and crown width in the mesiodistal direction were most frequently included in the models (21.95 % each), crown width in the buccolingual direction (14.63 %), and distance from the incisal edge to the apex of the tooth root (9.76 %). When analyzing the percentage of inclusion in the regression equations of

respective teeth, it was found that in Ukrainian young men, upper incisors were most frequently included in the models (20.00 % - 8.33 % central incisors and 11.67 % lateral incisors), lower incisors (13.33 % - 4.17 % central incisors and 9.17 % lateral incisors), upper canines (10.83 %), and upper premolars (10.00 % - 2.50 % first premolars and 7.50 % second premolars); while in Ukrainian young women, upper incisors were most frequently included in the models (29.27 % - 21.95 % central incisors and 7.32 % lateral incisors) and lower premolars (12.20 % - 4.88 % first premolars and 7.32 % second premolars). Thus, in Ukrainian young men and young women with a physiological bite, highly informative reliable regression models of linear dimensions necessary for constructing the correct dental arch shape, depending on the specific cephalometric parameters according to the Ricketts method and computed tomography tooth dimensions, were constructed using regression analysis.

Keywords: *dentistry, teleroentgenometry according to the Ricketts method, computed tomographic dimensions of teeth, dental arches, regression models, Ukrainian young men and young women, physiological bite.*

Introduction

Orthodontics plays a key role in maintaining the health of the maxillofacial system, and studies show that various occlusal abnormalities and dental pathologies have a significant impact on quality of life and overall health. The overall prevalence of malocclusion (bite abnormalities) among different population groups varies significantly depending on age and geographic location [16]. According to a systematic review and meta-analysis by Lombardo G. et al. [15], the global prevalence of malocclusion among children of different ages ranges from 39-93 %, which emphasizes the importance of early diagnosis and treatment of orthodontic problems. P. Balachandran and C. Janakiram [5] in their work note that among children aged 8-15 years in India, the prevalence of malocclusion is 40-78 %, which indicates a significant need for preventive and therapeutic measures among young people.

One important aspect of orthodontic health is reducing the risk of traumatic dental injury in patients with large anterior overlap. J. P. Schatz et al. [25] found that a large overjet is a significant risk factor for traumatic dental injuries, and patients with this factor have a 50% greater risk of injury compared to those without similar abnormalities. It is important to note that sociocultural and economic factors also influence the prevalence and severity of dental abnormalities such as crowding. According to a study by Kenessey D. E. and colleagues [13], sociocultural factors such as diet, oral care, and access to health services largely determine the prevalence of crowding in the population.

Crowding of teeth is an important problem associated with the presence of impacted third molars. T. C. Wei et al. [30] found that among patients with lower anterior crowding, the prevalence of impacted third molars is as high as 65 %, indicating the need for early diagnosis and possibly surgical intervention to prevent further complications.

Problems with an excessive number of teeth, in particular overcrowding, are another significant orthodontic pathology. According to a study by Demiriz L. and colleagues [8, 9], the prevalence of supernumerary teeth in the population is approximately 1-3 %, and their number and location can cause serious aesthetic and functional problems. T. Finkelstein et al. [12] note that among Israeli patients with orthodontic problems, supernumerary teeth occur in 2.8 % of cases, with the highest number of cases occurring among children and youth. Other studies [3, 28] confirm these data, showing that supernumerary teeth are most often found in the maxillary region and require special attention during orthodontic treatment.

Also, according to a study by Vani N. V. et al. [29], the prevalence of other dental anomalies such as impacted or missing teeth in the adult population of Saudi Arabia is about 10 %. S. Patil and S. Maheshwari [22] reported that in North India such anomalies are common and can complicate the orthodontic treatment process, especially in adult patients.

Cephalometric analysis, as a key tool in orthodontic diagnostics, allows for the effective detection and classification of various orthodontic pathologies, which contributes to the development of individualized treatment plans for each patient. Thanks to this approach, a wide range of occlusal abnormalities and other dental pathologies can be overcome, increasing the effectiveness of orthodontic intervention and improving the general health of patients.

The purpose of the study is to build and analyze regression models of computed tomography dimensions necessary for building the correct form of the dental arch in Ukrainian young men and young women with a physiological bite, depending on the features of teleroentgenometric indicators according to the Ricketts method and computed tomography dimensions of teeth.

Materials and methods

The initial computed tomography scans of 41 Ukrainian young men (aged 17 to 21) and 68 Ukrainian young women (aged 16 to 20) with physiological occlusion closely approximating orthognathic occlusion, who had no history of prior orthodontic treatment, complaints regarding the functioning of the temporomandibular joint, ENT organ pathologies, surgical interventions, or trauma, were obtained from the database of the Department of Pediatric

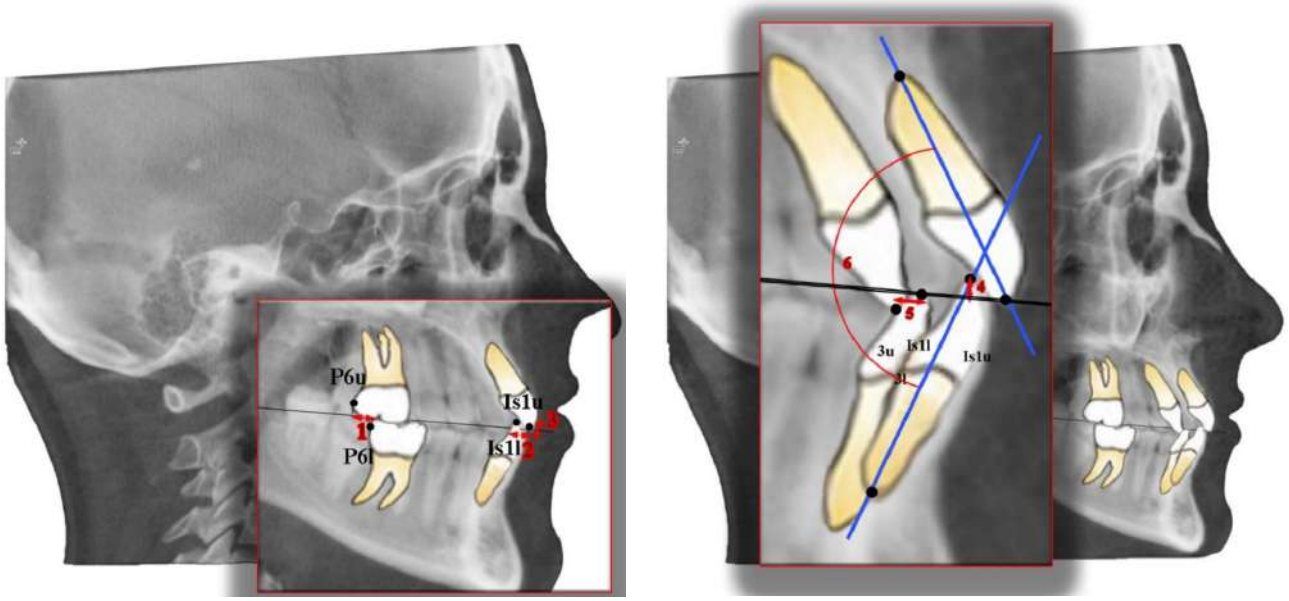

Fig. 1. "Dental indicators" determined by the cephalometric method of Ricketts R. M.: 1 - distance 6u-6l (mm); 2 - distance Overjet (mm); 3 - distance Overbite (mm); 4 - distance 1l-OcP (mm); 5 - distance 3u-3l (mm); 6 - angle Max1-Mand1 (°).

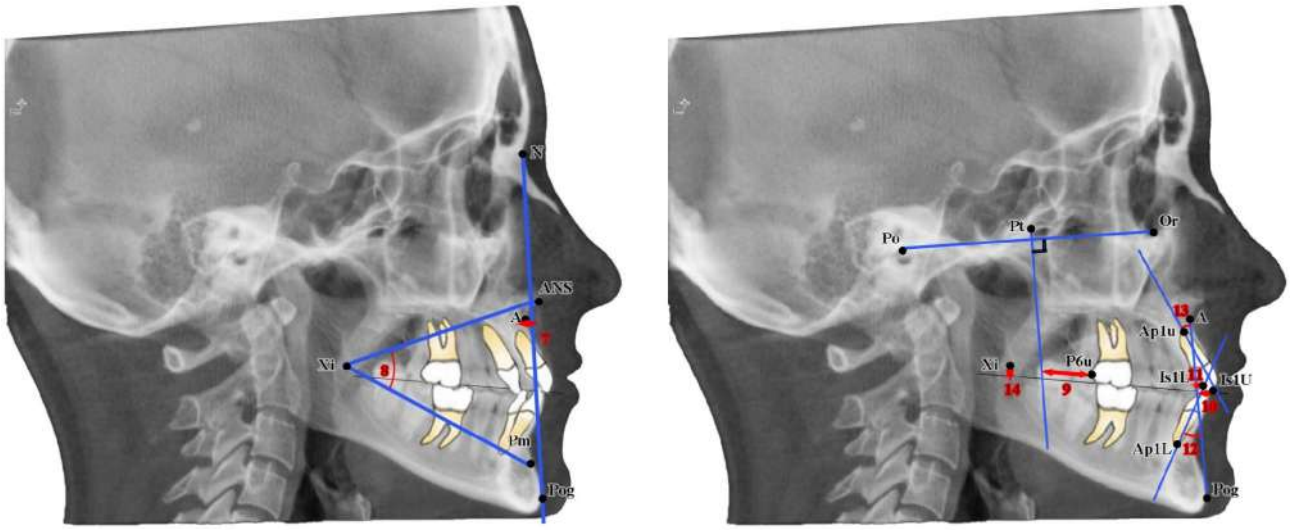

Fig. 2. "Skeletal and dental-skeletal" indicators determined by the cephalometric method of Ricketts R. M.: 7 - distance A-NPog (mm); 8 - angle ANS-Xi-PM (°); 9 - distance 6u-PTV (mm); 10 - distance 1l-APog (mm); 11 - distance 1u-APog (mm); 12 - angle Mand1-APog (°); 13 - angle Max1-APog (°); 14 - distance Xi-OcP (mm).

Dentistry and Research Center at Pirogov National Medical University, Vinnytsya. All examinations of the young men and women were conducted based on the principle of voluntary informed consent. The Bioethics Committee of Pirogov National Medical University, Vinnytsya (protocol No. 8 dated 30.09.2021), determined that the conducted studies do not contradict the basic bioethical norms of the Helsinki Declaration, the Council of Europe Convention on Human Rights and Biomedicine (1977), relevant WHO provisions, and the laws of Ukraine.

All the young men and women who underwent dental radiological studies for various reasons at the private dental clinic "Vinintermed" and at the "Maxillofacial Diagnostic Center Planmeca 3D" underwent cephalometric (generator voltage 90 kV, current 10 mA, exposure time 0.1 s, effective radiation dose up to 0.001 mSv) and computed tomography (generator voltage 60-90 kV, current 4-5 mA, exposure time 13.5 s, effective radiation dose up to 0.11-0.48 mSv) using the dental cone-beam CT scanner Veraviewepocs 3D Morita (Japan) and Planmeca ProMax 3D Mid, manufactured by Planmeca OY (Finland). The 3D image studies were conducted using the i-Dixel One Volume Viewer software (Ver.1.5.0) by J Morita Mfg. Cor, and Planmeca Romexis Viewer (ver. 3.8.3.R 15.12.14) by Planmeca OY. In addition

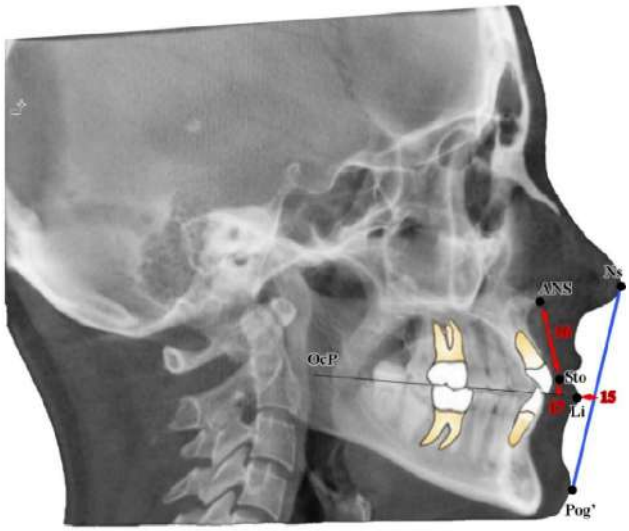

Fig. 3. Indicators of "soft tissue aesthetics" according to the cephalometric technique of Ricketts R. M.: 15 - distance Li-NsPog' (mm); 16 - distance ANS-sto (mm); 17 - distance sto-OcP (mm).

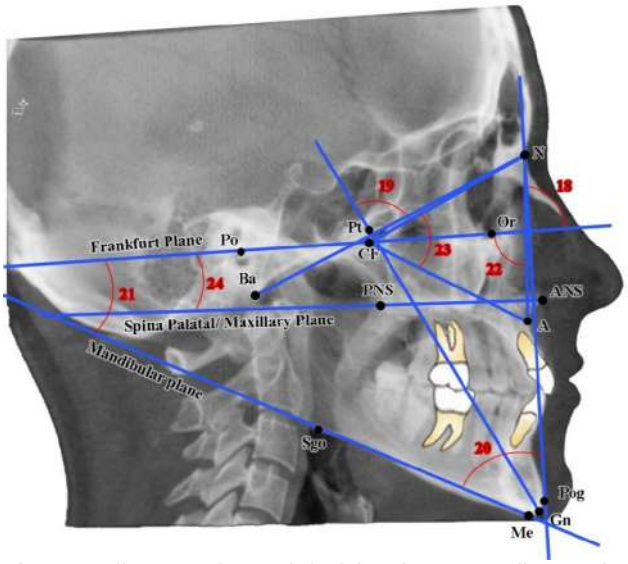

Fig. 4. Indicators of "craniofacial ratios" according to the cephalometric technique of Ricketts R. M.: 18 - angle NPog-POr (°); 19 - angle NBa-PtG (°); 20 - angle MeSgo-NPog (°); 21 - angle MeSgo-POr (°); 22 - angle POr-NA (°); 23 - angle N-CF-A (°); 24 - angle POr-SpP (°).

to the standard cephalograms, cephalograms with points marked on 3D objects created in the 3D Slicer v5.4.0 software were used. Further analysis and processing of the cephalograms were performed using the licensed OnyxCeph³™ software, version 3DPro, by Image Instruments GmbH, Germany. For the analysis of the lateral cephalograms, Ricketts R. M.'s method [24] was chosen.

Using Ricketts R. M.'s method, we determined "dental" indicators (Fig. 1), "skeletal and dento-skeletal" indicators (Fig. 2), "soft tissue aesthetics" indicators (Fig. 3), "craniofacial relationships" indicators (Fig. 4), and "internal structures" indicators (Fig. 5).

The following morphometric parameters of the teeth were studied:

For teeth that typically have a single root, such as the incisors and canines of the upper and lower jaws, measurements were taken in the mesiodistal (Md) and vestibulo-oral (Vo) directions to determine the following: crown width (MdK, VoK) and height (MdLK, VoLK), dentinoenamel junction width (MdC, VoC), root length (MdLR, VoLR), and overall tooth length (MdLD) (Fig. 6).

Since the premolars and molars have multiple roots, the measurement of some parameters is quite variable. Therefore, it was decided to measure only the crown portion and the total tooth length based on the vestibular root, which is usually the longest. For the premolars, in addition to the crown characteristics (mesiodistal and vestibulo-oral dimensions similar to those of incisors and canines), the length of the tooth was measured from the tips of the vestibular cusp to the apex of the vestibular root (Fig. 7).

Since the geometry of the first molars' roots is quite variable, with frequent curvatures and deformations, we consider it impractical to measure their lengths and related dimensions.

Considering that previous studies [18] found no significant differences or trends when comparing the computed tomography dimensions of corresponding teeth on the right and left sides, we use the average values of the corresponding teeth on the upper and lower jaws in our further research. Thus, in our study: 11 or 41 refers to the upper or lower central incisors, 12 or 42 to the upper or lower lateral incisors, 13 or 43 to the upper or lower canines, 14 or 44 to the upper or lower first premolars, 15 or 45 to the upper or lower second premolars, and 16 or 46 to the upper or lower first molars.

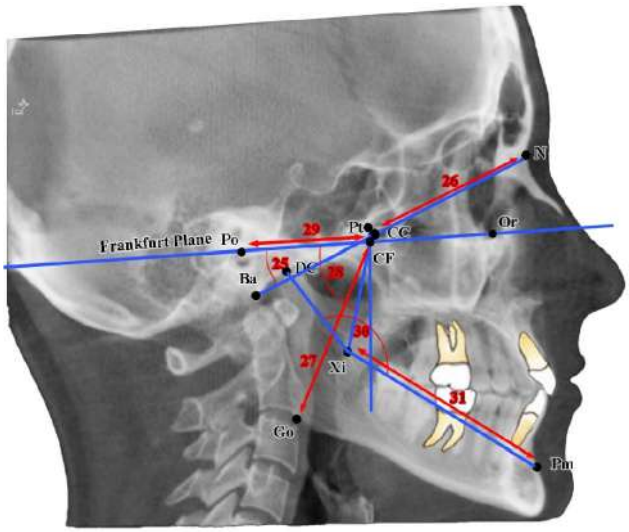

Fig. 5. Indicators of "internal structures" according to the Ricketts R. M. cephalometric method: 25 - angle POr-NBa (°); 26 - distance N-CC (mm); 27 - distance Go-CF (mm); 28 - angle POr-CFXi (°); 29 - distance P-PTV (mm); 30 - angle DC-Xi-Pm (°); 31 - distance Xi-Pm (mm).

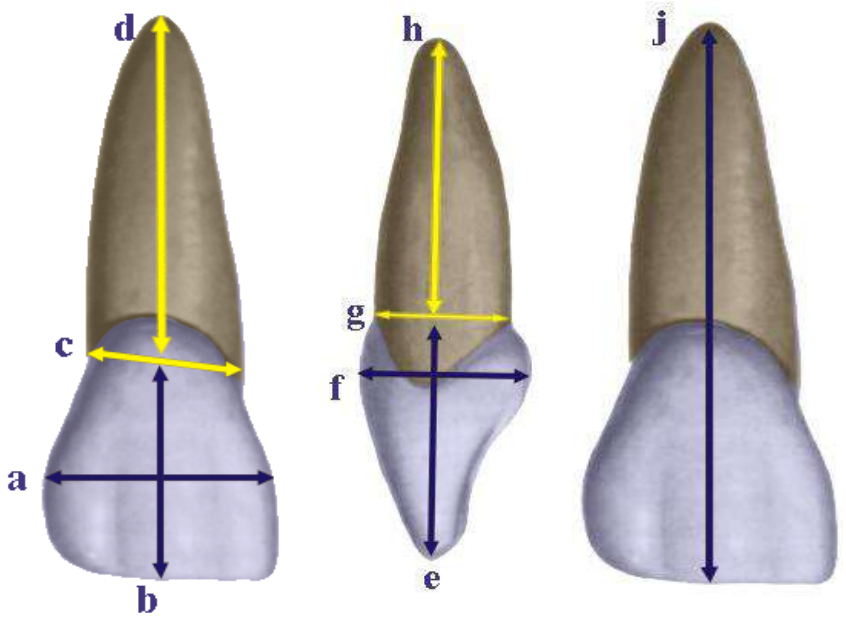

Fig. 6. Determination of morphometric indicators of incisors and canines in the mesio-distal (1) and vestibulo-oral (2) directions. a - tooth crown width; b - the height of the tooth crown; c - the width of the dentino-enamel border; d - root length; e - the height of the tooth crown; f - tooth crown width; g - the width of the dentino-enamel border; h - the length of the root; j - the length of the corresponding incisor or canine.

Fig. 7. Determination of the length of the first and second premolar teeth. k is the length of the corresponding premolar tooth.

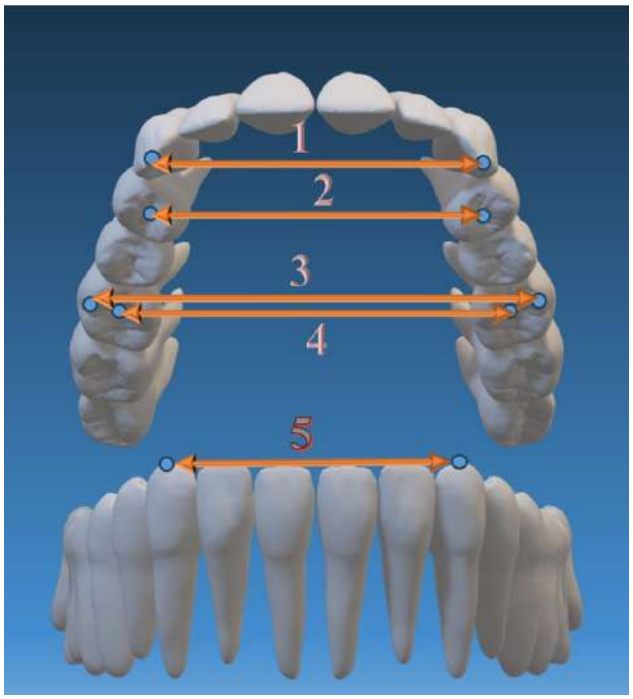

Fig. 8. Parameters of dental arches in the transverse plane. 1 - distance 13_23Bugr; 2 - distance PonPr; 3 - distance VestBM; 4 - distance PonM; 5 - distance 33_43Bugr.

A fundamental difference in understanding the parameters of dental arches is the realization that dental arches form a three-dimensional structure. Therefore, to determine the characteristics of the dental arches, we conducted the following measurements:

In the transverse plane, measurements were taken of the distances between the cusp tips of the canines on the lower (33_43Bugr) and upper (13_23Bugr) jaws, the vestibular medial cusps of the first molars (VestBM) on the

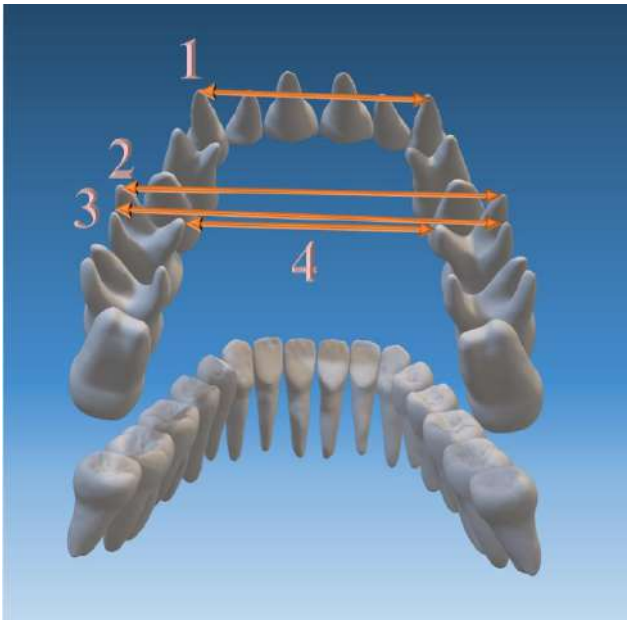

Fig. 9. Parameters of dental arches in the transverse plane. 1 - distance 13_23Apx; 2 - distance napx_6; 3 - distance dapx_6; 4 - distance mapex_6.

upper jaw, premolar (PonPr) and molar (PonM) points according to Pon (Fig. 8). Additionally, on the upper jaw, distances were measured between the apices of the canines (13_23Apx), between the medial (napx_6), distal (dapx_6), and palatal (mapex_6) roots of the first molars (Fig. 9). On the lower jaw, measurements included the distances between the apices of the canines (33_43Apx) and between the medial (mapx_46) and distal (dapx_46) roots of the first molars (Fig. 10).

In the sagittal plane, the distances were measured between the incisal point and the midpoints of the canine (DL_C), premolar (DL_F), and molar (DL_S) lines (Fig. 11).

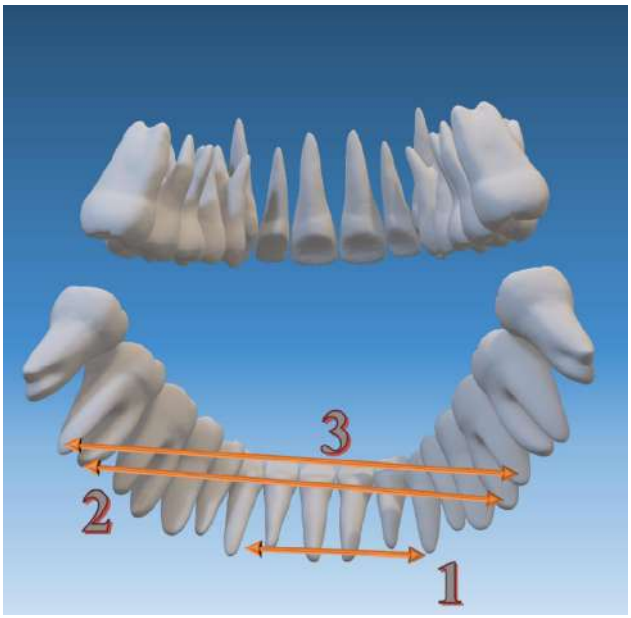

Fig. 10. Parameters of dental arches in the transverse plane. 1 - distance 33_43Apx; 2 - distance mapx_46; 3 - distance dapx_46.

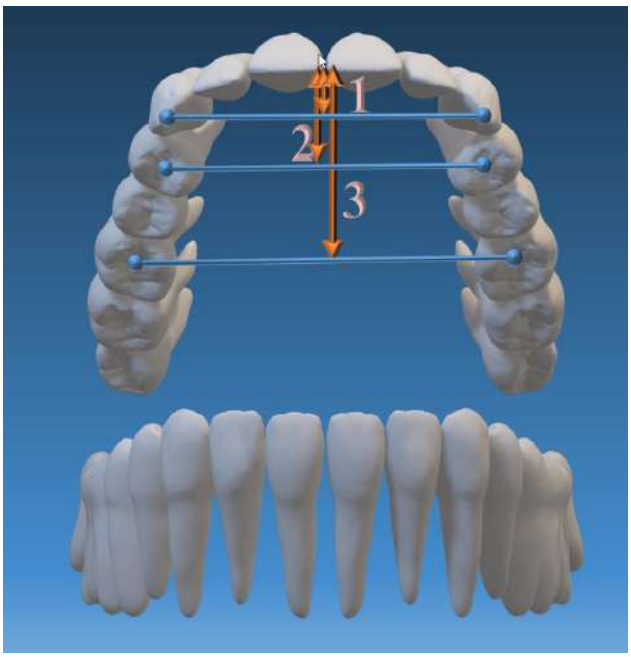

Fig. 11. Parameters of dental arches in the sagittal plane. 1 - distance DL_C; 2 - distance DL_F; 3 - distance DL_S.

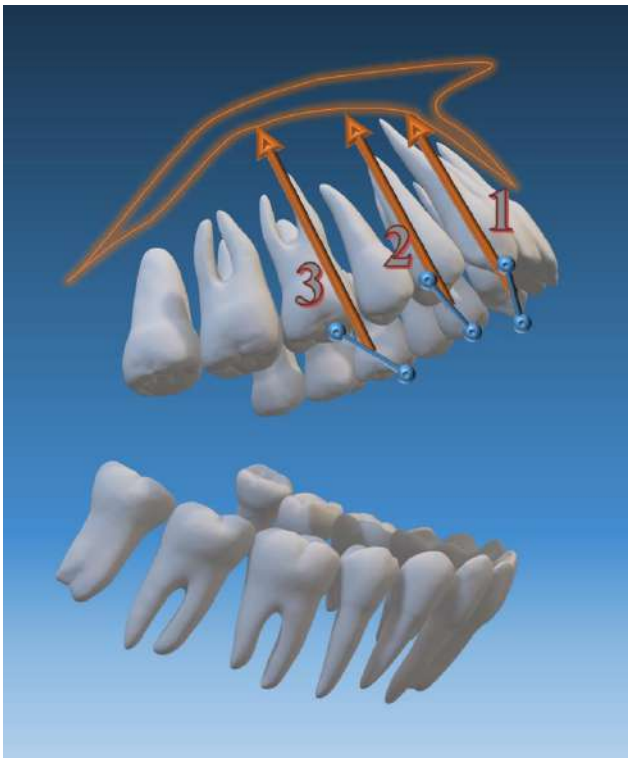

Fig. 12. Parameters of dental arches in the vertical plane. 1 - distance GL_1; 2 - distance GL_2; 3 - distance GL_3.

In the vertical plane, the distance from the occlusal plane to the palate was determined at the level of the canine (GL_1), premolar (GL_2), and molar (GL_3) lines (Fig. 12).

Using the method of step-by-step regression analysis in the licensed statistical package "Statistica 6.0", the parameters necessary for building the correct shape of the dental arch were modeled. When conducting a step-by-step regression analysis, the following algorithm was followed: the coefficient of determination of the regression polynomial R^2 (indicates the dependence of the corresponding indicator on a set of other indicators) should be at least 0.60; the value of Fisher's criterion (F-criterion) should exceed 3.0; the number of free terms in the equation should be minimal; simulations should be carried out under constant logical control to prevent equations based on random unclear connections.

Results

Built in Ukrainian young men and young women with a physiological bite, regression models of the linear dimensions necessary for building the correct shape of the dental arch, depending on the features of the teleroentgenometric indicators according to the Ricketts method and the computed tomographic dimensions of the teeth, have the form of the following linear equations:

distance DL_C (young men regardless of face type) =

2.943 + 0.721 x MdK11 + 0.207 x MdLD14 + 0.971 x MdC11 - 0.330 x MdLD42 - 0.043 x Max1-Mand1 + 0.175 x MdLD15 (R^2=0.823, $F_{(6.33)}$=25.58, p<0.001, Std.Error of estimate=0.562);

distance GL_1 (young men regardless of face type) = 31.66 + 0.552 x A-NPog - 0.283 x Max1-APog + 1.724 x MdK11 - 2.291 x MdK46 - 0.225 x N-CF-A + 0.412 x MdLD13 - 0.814 x MdLR12 + 1.547 x VoC42 (R^2=0.781, $F_{(8.31)}$=13.80, p<0.001, Std.Error of estimate=1.248);

distance DL_F (young men regardless of face type) = -5.377 + 1.453 x MdK11 + 0.850 x MdK13 + 1.597 x MdK42 - 0.351 x VoLK42 + 1.152 x MdC42 - 0.090 x POr-CFXi (R^2=0.774, $F_{(6.33)}$=18.83, p<0.001, Std.Error of estimate=0.760);

distance GL_2 (young men regardless of face type) = 18.72 - 0.833 x sto-OcP + 1.462 x MdLK13 + 0.531 x A-NPog - 0.686 x MdLD45 - 0.586 x MdLR12 + 0.338 x VoLR13 (R^2=0.699, $F_{(6.33)}$=12.79, p<0.001, Std.Error of estimate=1.558);

distance PonPr (young men regardless of face type) = -10.30 + 1.483 x MdK12 + 3.813 x MdK42 - 1.743 x VoC42 + 1.937 x MdK15 + 0.830 x MdK13 + 1.356 x MdK41 + 0.129 x Xi-OcP (R^2=0.792, $F_{(7.32)}$=17.36, p<0.001, Std.Error of estimate=1.010);

distance DL_S (young men regardless of face type) = 0.454 + 1.547 x MdK11 + 0.969 x MdK13 + 0.877 x VoK46 + 0.194 x A-NPog + 0.095 x Xi-Pm - 0.045 x Max1-Mand1 (R^2=0.811, $F_{(6.33)}$=23.55, p<0.001, Std.Error of estimate=0.829);

distance GL_3 (young men regardless of face type) = 22.89 - 0.620 x sto-OcP - 0.233 x Li-NsPog' + 1.458 x MdK11 - 1.141 x MdK16 - 0.475 x MdLD45 + 0.762 x MdLK13 (R^2=0.617, $F_{(6.33)}$=8.85, p<0.001, Std.Error of estimate=1.411);

distance PonM (young men regardless of face type) = 4.301 + 2.483 x VoK15 + 1.717 x VoLK41 + 1.414 x MdLK12 - 0.638 x MdLD45 - 0.232 x POr-SpP + 0.173 x N-CC (R^2=0.794, $F^{(6.33)}$=21.17, p<0.001, Std.Error of estimate=1.269);

distance 13_23Bugr (young men regardless of face type) = 9.415 + 2.591 x MdK12 + 2.043 x MdK13 - 0.522 x VoLR12 - 0.783 x VoK14 + 1.520 x MdK41 + 1.502 x MdC41 - 1.102 x VoC41 (R^2=0.797, $F_{(7.32)}$=17.96, p<0.001, Std.Error of estimate=1.001);

distance 13_23Apx (young men regardless of face type) = -11.61 + 1.140 x 1l-OcP + 0.302 x N-CC - 0.301 x P-PTV + 0.370 x A-NPog + 0.693 x MdLK42 + 0.097 x Max1-Mand1 - 0.329 x MdLD15 (R^2=0.689, $F_{(7.31)}$=9.80, p<0.001, Std.Error of estimate=1.430);

distance VestBM (young men regardless of face type) = 14.06 + 1.778 x VoK15 + 0.200 x Go-CF + 0.816 x MdLD44 - 0.475 x MdLD14 - 0.414 x MdLD42 + 1.716 x MdK44 (R^2=0.816, $F_{(6.33)}$=24.45, p<0.001, Std.Error of estimate=1.223);

distance napx_6 (young men regardless of face type) = 40.33 - 2.791 x 3u-3l + 0.231 x Xi-Pm - 0.864 x MdLD13 + 4.832 x MdK44 - 2.370 x VoK46 + 0.595 x VoLR43 - 1.909 x MdC12 (R^2=0.740, $F_{(7.32)}$=13.03, p<0.001, Std.Error of estimate=1.782);

distance dapx_6 (young men regardless of face type) = -23.59 + 2.126 x VoK15 + 2.002 x MdK46 - 4.501 x MdC13 + 1.071 x VoLK13 + 2.363 x MdK12 + 2.766 x MdK15 + 3.040 x VoC13 - 0.219 x Max1-APog (R^2=0.750, $F_{(8.31)}$=11.64, p<0.001, Std.Error of estimate=2.383);

distance mapex_6 (young men regardless of face type) = -29.64 + 2.731 x MdK45 + 0.252 x Xi-Pm + 3.581 x MdK15 - 0.385 x sto-OcP + 1.481 x MdK11 + 0.415 x MdLD44 (R^2=0.833, $F_{(6.33)}$=27.42, p<0.001, Std.Error of estimate=1.434);

distance 33_43Bugr (young men regardless of face type) = 0.595 + 1.743 x MdK12 - 0.766 x 1l-OcP + 1.618 x MdK42 - 0.396 x MdLR11 + 1.040 x MdK15 + 1.040 x MdC42 (R^2=0.733, $F_{(6.33)}$=15.08, p<0.001, Std.Error of estimate=0.820);

distance 33_43Apx (young men regardless of face type) = -5.526 + 1.073 x MdLD43 + 5.369 x VoC12 - 3.689 x VoK12 - 0.439 x VoLR12 - 1.051 x MdC11 + 1.398 x VoK43 - 1.664 x MdC12 - 0.364 x sto-OcP (R^2=0.733, $F_{(8.31)}$=10.65, p<0.001, Std.Error of estimate=1.340);

distance mapx_46 (young men regardless of face type) = 15.07 + 1.469 x MdLK12 + 3.314 x MdK45 + 2.561 x VoK16 - 0.669 x MdLD45 - 1.750 x VoK46 + 0.972 x MdC43 (R^2=0.730, $F_{(6.32)}$=14.45, p<0.001, Std.Error of estimate=1.556);

distance dapx_46 (young men regardless of face type) = 29.23 + 5.498 x MdK44 - 0.275 x MeSgo-NPog - 3.948 x VoK11 + 0.649 x MdLD13 - 0.176 x Mand1-APog + 1.452 x VoK16 + 0.748 x 1l-OcP + 0.145 x DC-Xi-Pm (R^2=0.733, F^2=10.29, p<0.001, Std.Error of estimate=1.670);

distance GL_1 (young women regardless of face type) = 4.691 - 0.336 x Max1-APog + 1.188 x MdK11 - 1.038 x VoK45 + 1.435 x VoLK42 - 1.563 x VoLK41 + 2.484 x VoK43 + 0.513 x 1u-APog - 1.218 x VoC43 (R^2=0.624, F^2=12.22, p<0.001, Std.Error of estimate=1.210);

distance DL_F (young women regardless of face type) = 3.620 + 1.295 x MdK11 + 0.187 x Li-NsPog' + 0.774 x VoK12 - 0.067 x MeSgo-POr + 0.249 x VoLR11 - 0.177?MdLD14 (R^2=0.658, $F_{(6.61)}$=19.56, p<0.001, Std.Error of estimate=0.845);

distance DL_S (young women regardless of face type) = 2.740 + 0.865 x MdK11 + 0.416 x 1u-APog + 1.108 x MdK16 + 0.842 x VoK11 - 0.176 x 3u-3l + 0.213 x MdLK11 (R^2=0.793, $F_{(6.61)}$=38.95, p<0.001, Std.Error of estimate=0.783);

distance 13_23Apx (young women regardless of face type) = 13.15 + 2.420 x MdK11 + 0.852 x MdLD45 - 0.319 x MdLD43 + 0.236 x Xi-OcP + 1.476 x MdK12 - 1.683 x MdK14 - 1.145?VoC11 - 0.348 x MdLD14 (R^2=0.605, $F(_{8.59})$=11.30, p<0.001, Std.Error of estimate=1.643);

distance mapx_46 (young women regardless of face type) = 16.20 + 1.601 x MdK16 - 0.076 x MdC43 - 0.406 x Li-NsPog' + 1.014 x MdLK13 + 1.666 x MdC13 + 1.699 x MdK41 - 1.008 x VoK44 (R^2=0.630, $F_{(7.54)}$=13.14, p<0.001, Std.Error

of estimate=1.775);

distance dapx_46 (young women regardless of face type) = 30.48 + 0.927 x MdLD45 - 0.549 x VoLK11 - 0.573 x Li-NsPog' + 2.827 x MdC12 + 0.495 x MdLK41 - 1.060 x VoK44 (R^2=0.703, $F_{(6.55)}$=21.69, p<0.001, Std.Error of estimate=1.853);

where, here and in the following equations, R^2 - coefficient of determination; $F_{(!)}$=! - critical $_{(!)}$ and obtained (!) Fisher's test value; p - confidence level; Std.Error of estimate - standard error of estimate.

The coefficients of determination for the regression equations of the *distances DL_C, GL_2, PonPr, GL_3, PonM, 13_23Bugr, VestBM, napx_6, dapx_6, mapex_6, 33_43Bugr, and 33_43Apx* in young women, without considering the type of face, range from 0.237 to 0.533, and therefore do not have significant practical relevance.

Discussion

Thus, in Ukrainian young men with a physiological bite, all 18 possible reliable (p<0.001 in all cases) regression models of linear dimensions necessary for the construction of a correct dental arch shape were built, depending on the specific features of the Ricketts cephalometric indicators and the computed tomographic sizes of teeth, with a coefficient of determination greater than 0.6 (R^2 ranging from 0.617 to 0.833). When analyzing the percentage of Ricketts cephalometric indicators and computed tomographic sizes of teeth included in the regression equations for young men, it was found that the most frequently included variables are: Ricketts cephalometric indicators and the mesiodistal width of the tooth crown (each accounting for 26.67 % of all independent variables), the distance from the incisal edge to the apex of the tooth root (13.33 % of all independent variables), and the buccolingual width of the tooth crown (10.00 % of all independent variables). When analyzing the percentage of inclusion of specific teeth in the regression equations for young men, the most frequently included teeth are: upper incisors (20.00 % of all independent variables - 8.33 % central incisors and 11.67 % lateral incisors), lower incisors (13.33 % of all independent variables - 4.17 % central incisors and 9.17 % lateral incisors), upper canines (10.83 % of all independent variables), and upper premolars (10.00 % of all independent variables - 2.50 % first premolars and 7.50 % second premolars).

In Ukrainian young women with a physiological bite, out of 18 possible regression models, only 6 reliable (p<0.001 in all cases) regression models of linear dimensions necessary for the construction of a correct dental arch shape were built, depending on the specific features of the Ricketts cephalometric indicators and the computed tomographic sizes of teeth, with a coefficient of determination greater than 0.6 (R^2 ranging from 0.605 to 0.793). When analyzing the percentage of Ricketts cephalometric indicators and computed tomographic sizes of teeth included in the regression equations for young women, it was found that, similar to young men, the most frequently included variables are: Ricketts cephalometric indicators and the mesiodistal width of the tooth crown (each accounting for 21.95 % of all independent variables), the buccolingual width of the tooth crown (14.63 % of all independent variables), and the distance from the incisal edge to the apex of the tooth root (9.76 % of all independent variables). When analyzing the percentage of inclusion of specific teeth in the regression equations for young women, the most frequently included teeth are: upper incisors (29.27 % of all independent variables - 21.95 % central incisors and 7.32 % lateral incisors) and lower premolars (12.20 % of all independent variables - 4.88 % first premolars and 7.32 % second premolars). The coefficients of determination for other reliable (p<0.001 in all cases) regression equations for young women range from 0.237 to 0.533, and therefore the constructed models do not have significant practical relevance in dentistry.

In their research, Marchenko A. V. and others [20] created mathematical models that allow predicting teleroentgenographic parameters according to the Schwarz method depending on the main cephalometric indicators in Ukrainian boys and girls with different types of faces and models of individual linear dimensions necessary for building the correct forms of dental arches in young men with a wide face [17]. This study made it possible to create a database for the assessment of cephalometric parameters depending on the type of face, which is important for the accuracy of diagnosis and planning of orthodontic treatment.

In the study of Chernysh A. V. [7], regression models were proposed, which are used to determine individual cephalometric indicators according to the Ricketts method. The use of such models significantly increases the accuracy of assessment and prediction of craniofacial characteristics, which, in turn, contributes to improving the results of orthodontic treatment.

In her study, Drachevska I. Y. [11] developed regression models for determining individual teleroentgenographic indicators using the Ricketts method in young Ukrainians with different facial types. This study highlights the importance of considering individual anthropometric characteristics during orthodontic treatment planning.

E. J. Bae et al. [4] studied changes in long-term craniofacial growth in patients with normal occlusion using the Ricketts analysis. The study showed that with age there are significant changes in the position of the upper and lower jaws, which can affect the need for orthodontic correction even in patients without obvious bite pathologies.

I. Perez et al. [23] used the Ricketts method to determine sex in Peruvians by applying logistic regression analysis. The study showed that this method can be effectively used for forensic purposes, as it allows to determine sex with high accuracy based on cephalometric data.

M. Chacon et al. [6] investigated the effect of a mandibular protraction device on dento-skeletal and

esthetic parameters using the Ricketts analysis. They found that the use of this device significantly improves the aesthetic profile of patients and corrects malocclusion.

O. Otuyemi et al. [21] investigated the preference for the Ricketts E-line profile among orthodontists, orthodontist trainees and students in Nigeria. They found that orthodontists and students have different perceptions of the ideal facial profile, which can influence orthodontic treatment planning approaches.

M. Sivagnanam and J. M. Cheong [27] conducted a pilot study to establish the cephalometric norms of the upper and lower lips to E-lineage Ricketts in a Malay female population in Kuantan City. They found that ethnic characteristics significantly affect facial parameters, which emphasizes the need to create individual norms for different populations.

Q. A. Marianna [18] in her study studied the relationship between Ricketts' E-line and facial profile in patients with open bite. Research has shown that occlusal anomalies can significantly affect the aesthetic appearance of the face, and correction of such anomalies is important to achieve a harmonious profile.

I. E. Alroudhan et al. [1] investigated the craniofacial morphometry of a northern Saudi population using Ricketts analysis. They found significant differences in facial parameters compared to other populations, highlighting the importance of considering ethnic characteristics during orthodontic treatment.

P. K. Shah et al. [26] conducted an aesthetic facial analysis among Nepalese. They found that the facial parameters determined by the Ricketts method can differ significantly from the generally accepted norms, which emphasizes the importance of individualizing the approach to each patient.

In general, cephalometric analysis, especially according to the Ricketts method, is an extremely important tool for the diagnosis and planning of orthodontic treatment [2, 10, 14]. It allows taking into account individual anthropometric and ethnic characteristics of patients, which significantly increases the effectiveness of treatment and improves the aesthetic appearance of the face.

Conclusion

1. Using regression analysis, highly informative (with a coefficient of determination greater than 0.6) reliable models of linear dimensions necessary for constructing the correct shape of the dental arch were developed for Ukrainian young men and young women with a physiological bite, without considering facial type, based on specific cephalometric parameters according to the Ricketts method and computed tomography tooth dimensions. In young men, all 18 possible models were built with R^2 values ranging from 0.617 to 0.833; in young women, only six models were reliable, with R^2 values ranging from 0.605 to 0.793.

2. When analyzing the percentage of inclusion of cephalometric parameters according to the Ricketts method and computed tomography tooth dimensions in the regression equations, it was found that in young men, the models most frequently included cephalometric parameters and crown width in the mesiodistal direction (26.67 % each), the distance from the incisal edge to the apex of the tooth root (13.33 %), and crown width in the buccolingual direction (10.00 %). In young women, the most frequent inclusions were cephalometric parameters and crown width in the mesiodistal direction (21.95 % each) and crown width in the buccolingual direction (14.63 %).

3. When analyzing the percentage of inclusion of specific teeth in the regression equations, it was found that in young men, the models most frequently included upper incisors (20.00 %), lower incisors (13.33 %), upper canines (10.83 %), and upper premolars (10.00 %). In young women, the most frequent inclusions were upper incisors (29.27 %) and lower premolars (12.20 %).

References

[1] Alroudhan, I. E., Kundi, I., Alam, M. K., Albalawe, M. A., Alsharari, K. N., & Alrwaili, A. M. (2021). Evaluation of craniofacial morphometry of northern Saudi Arabian population, using Rickett's analysis: A descriptive cross-sectional study. *Journal of International Oral Health,* 13(2), 136-143. doi: 10.4103/jioh.jioh_291_20

[2] Al-Taee, R., Al-Saedi, A. I. L., & Nahidh, M. (2021). Cephalometric Assessment of Iraqi Sample from Basrah City for Orthodontic and Surgical Treatment Planning. *Indian Journal of Forensic Medicine & Toxicology,* 15(2), 1829-1836. doi: 10.37506/ijfmt.v15i2.14605

[3] Ata-Ali, F., Ata-Ali, J., Peñarrocha-Oltra, D., & Peñarrocha-Diago, M. (2014). Prevalence, etiology, diagnosis, treatment and complications of supernumerary teeth. *Journal of clinical and experimental dentistry,* 6(4), e414-e418. doi: 10.4317/jced.51499

[4] Bae, E. J., Kwon, H. J., & Kwon, O. W. (2014). Changes in longitudinal craniofacial growth in subjects with normal occlusions using the Ricketts analysis. *The Korean Journal of Orthodontics,* 44(2), 77-87. doi: 10.4041/kjod.2014.44.2.77

[5] Balachandran, P., & Janakiram, C. (2021). Prevalence of malocclusion among 8-15 years old children, India-A systematic review and meta-analysis. *Journal of oral biology and craniofacial research,* 11(2), 192-199. doi: 10.1016/j.jobcr.2021.01.011

[6] Chacon, M., Henriques, J. F. C., Vedovello Filho, M., Menezes, C. C. D., Vedovello, S. A. S., Venezian, G. C., & Lucato, A. S. (2018). Dentoskeletal and aesthetic effects of mandibular protraction appliance (MPA) using Ricketts analysis. *Revista de Odontologia da UNESP,* 47, 7-11. doi: 10.1590/1807-2577.05717

[7] Chernysh, A. V. (2018). Regression models of individual cephalometric indicators used in the method of RM Ricketts. *Biomedical and Biosocial Anthropology,* (32), 56-62. doi: 10.31393/bba32-2018-08

[8] Demiriz, L., Durmuslar, M. C., & Misir, A. F. (2015). Prevalence and characteristics of supernumerary teeth: A survey on 7348 people. *Journal of International Society of Preventive and Community Dentistry*, 5(Suppl 1), S39-S43. doi: 10.4103/2231-0762.156151

[9] Demiriz, L., Misir, A. F., & Durmuslar, M. C. (2015). The prevalence and the characteristics of supernumerary teeth of children and young adolescents from north-western region of Turkey. *Br J Med Med Res*, 7(5), 369-377. doi: 10.9734/BJMMR/2015/16422

[10] Drachevska, I. Y. (2020). Features and modern aspects of the use of teleroentgenographic indicators determined by Steiner, Ricketts and Downs methods (analysis of scientific literature). *Reports of Vinnytsia National Medical University,* 24(2), 321-324. doi: 10.31393/reports-vnmedical-2020-24(2)-21

[11] Drachevska, I. Y. (2021). Regression models of individual teleradiographic indicators according to Ricketts method in Ukrainian young men and young women with different face types. *Reports of Vinnytsia National Medical University,* 25(2), 238-246. doi: 10.31393/reports-vnmedical-2021-25(2)-09

[12] Finkelstein, T., Shapira, Y., Pavlidi, A. M., Schonberger, S., Blumer, S., Sarne, O., & Shpack, N. (2019). Prevalence and characteristics of supernumerary teeth in Israeli orthodontic patients. *Journal of clinical pediatric dentistry*, 43(4), 244-251. doi: 10.17796/1053-4625-43.4.4

[13] Kenessey, D. E., Vlemincq-Mendieta, T., Scott, G. R., & Pilloud, M. A. (2023). An anthropological investigation of the sociocultural and economic forces shaping dental crowding prevalence. *Archives of Oral Biology,* 147, 105614. doi: 10.1016/j.archoralbio.2023.105614

[14] Koval, S., Garladinne, L., & Isayev, A. (2021). Cephalometric soft tissue lip measurements in adults in different populations and ethnic groups: a systematic review. *J Dent Oral Disord Ther,* 9(1), 1-11. doi: 10.15226/jdodt.2021.001122

[15] Lombardo G., Vena F., Negri P., Pagano S., Barilotti C., Paglia L., ... & Cianetti S. (2020). Worldwide prevalence of malocclusion in the different stages of dentition: A systematic review and meta-analysis. *European journal of paediatric dentistry,* 21, 115-122. doi: 10.23804/ejpd.2020.21.02.05

[16] Mahn, E., Walls, S., Jorquera, G., Valdés, A. M., Val, A., & Sampaio, C. S. (2018). Prevalence of tooth forms and their gender correlation. *Journal of Esthetic and Restorative Dentistry,* 30(1), 45-50. doi: 10.1111/jerd.12341

[17] Marchenko, A. V., Shinkaruk-Dykovytska, M. M., Pozur, T. P., Gunas, V. I., & Orlovskiy, V. O. (2020). Models of individual linear dimensions necessary for the construction of the correct form of dental arches in young men with a wide face, depending on the features of odontometric and cephalometric indicators. *Wiadomosci Lekarskie* (Warsaw, Poland: 1960), 73(6), 1103-1107. doi: 10.36740/WLek202006104

[18] Marianna, Q. A. (2017). Commitment of the Aesthetic Line of Ricketts and the Facial Profile in Patients with Open Bite without Growth. *EC Dental Science*, 7, 228-234.

[19] Marchenko, A. V., Gunas, I. V., Petrushanko, T. O., Serebrennikova, O. A., & Trofimenko, Yu. Yu. (2017). Computer-tomographic characteristics of root length incisors and canines of the upper and lower jaws in boys and girls with different craniotypes and physiological bite. *Wiadomosci Lekarskie* (Warsaw, Poland: 1960), 70(3 pt 1), 499-502. PMID: 28711896

[20] Marchenko, A. V., Prokopenko, O. S., Dzevulska, I. V., Zakalata, T. R., & Gunas, I. V. (2021). Mathematical modeling of teleroentgenographic parameters according to the method of Schwarz AM depending on the basic cephalometric parameters in Ukrainian young men and young women with different face types. *Wiadomosci Lekarskie* (Warsaw, Poland: 1960), 74(6), 1488-1492. PMID: 34159943

[21] Otuyemi, O., Afolabi, D., & Oyewole, T. (2022). Ricketts' E-line profile preferences among Nigerian orthodontists, orthodontic trainees, and a young undergraduate students' population. *Nigerian Journal of Clinical Practice,* 25(4), 541-547. doi: 10.4103/njcp.njcp_1873_21

[22] Patil, S., & Maheshwari, S. (2014). Prevalence of impacted and supernumerary teeth in the North Indian population. *Journal of clinical and experimental dentistry,* 6(2), e116-e120. doi: 10.4317/jced.51284

[23] Perez, I., Chavez, A. K., & Ponce, D. (2016). Applicability of the Ricketts' posteroanterior cephalometry for sex determination using logistic regression analysis in Hispano American Peruvians. *Journal of forensic dental sciences*, 8(2), 121-126. doi: 10.4103/0975-1475.186371

[24] Ricketts, R. M. (1972). The value of cephalometrics and computerized technology. *Angle Orthod,* (42), 179-199. doi: 10.1043/0003-3219(1972)042<0179:TVOCAC>2.0.CO;2

[25] Schatz, J. P., Ostini, E., Hakeberg, M., & Kiliaridis, S. (2020). Large overjet as a risk factor of traumatic dental injuries: a prospective longitudinal study. *Progress in orthodontics,* 21, 1-6. doi: 10.1186/s40510-020-00341-5

[26] Shah, P. K., Shrestha, S., & Rokaya, D. (2022). Facial esthetic analysis of Nepalese subjects. *The Open Dentistry Journal,* 16(1), e187421062111191. doi: 10.2174/18742106-v16-e2111191

[27] Sivagnanam, M., & Cheong, J. M. (2023). Establishing cephalometric norms of upper and lower lips to Rickett's E-line in the Malay female population of Kuantan city: a pilot study. *IIUM Journal of Orofacial and Health Sciences*, 4(1), 26-32. doi: 10.31436/ijohs.v4i1.164

[28] Syriac, G., Joseph, E., Rupesh, S., Philip, J., Cherian, S. A., & Mathew, J. (2017). Prevalence, characteristics, and complications of supernumerary teeth in nonsyndromic pediatric population of South India: A clinical and radiographic study. *Journal of pharmacy & bioallied sciences,* 9(Suppl 1), S231-S236. doi: 10.4103/jpbs.JPBS_154_17

[29] Vani, N. V., Saleh, S. M., Tubaigy, F. M., & Idris, A. M. (2016). Prevalence of developmental dental anomalies among adult population of Jazan, Saudi Arabia. *The Saudi Journal for Dental Research,* 7(1), 29-33. doi: 10.1016/j.sjdr.2015.03.003

[30] Wei, T. C., Soemantri, E. S. S., & Sunaryo, I. R. (2016). Prevalence of third molar impaction in patient with mandibular anterior teeth crowding. *Padjadjaran Journal of Dentistry,* 28(3), 159-163. doi: 10.24198/pjd.vol28no3.13673

РЕГРЕСІЙНІ МОДЕЛІ КОМП'ЮТЕРНО-ТОМОГРАФІЧНИХ РОЗМІРІВ НЕОБХІДНИХ ДЛЯ ПОБУДОВИ КОРЕКТНОЇ ФОРМИ ЗУБНОЇ ДУГИ В УКРАЇНСЬКИХ ЮНАКІВ І ДІВЧАТ ІЗ ФІЗІОЛОГІЧНИМ ПРИКУСОМ БЕЗ УРАХУВАННЯ ТИПУ ОБЛИЧЧЯ В ЗАЛЕЖНОСТІ ВІД ОСОБЛИВОСТЕЙ ТЕЛЕРЕНТГЕНОМЕТРИЧНИХ ПОКАЗНИКІВ ЗА МЕТОДОМ RICKETTS І КОМП'ЮТЕРНО-ТОМОГРАФІЧНИХ РОЗМІРІВ ЗУБІВ

Броцький Н. О., Дмитрієв М. О., Черкасова Л. А., Сміюха О. А., Беляєв Е. В., Мороз В. В., Ваховський В. В.

Ортодонтія відіграє ключову роль у забезпеченні естетичної гармонії обличчя та функціональної правильності зубо-щелепної системи. Цефалометричний аналіз є важливим інструментом у плануванні ортодонтичного лікування, оскільки його параметри значно варіюють залежно від віку, статі та національності пацієнта. Розуміння цих відмінностей є критично важливим для точного діагнозу та ефективного лікування в різних популяціях. Мета роботи - побудувати та провести аналіз регресійних моделей комп'ютерно-томографічних розмірів необхідних для побудови коректної форми зубної дуги в

українських юнаків і дівчат із фізіологічним прикусом в залежності від особливостей телерентгенометричних показників за методом Ricketts і комп'ютерно-томографічних розмірів зубів. В ліцензійному програмному забезпеченні OnyxCeph³™ версії 3DPro проведено аналіз первинних комп'ютерних томограм українських юнаків (n=41) і дівчат (n=68) із фізіологічним прикусом, які були отримані з банку даних кафедри стоматології дитячого віку та науково-дослідного центру Вінницького національного медичного університету ім. М. І. Пирогова. За методом Ricketts на бокових телерентгенорамах визначали "зубні", "скелетні та зубо-скелетні" показники, показники "естетики м'яких тканин", показники "черепно-лицевих співвідношень" та показники "внутрішніх структур". На комп'ютерних томограмах визначали морфометричні параметри зубів верхньої та нижньої щелеп у мезіо-дистальному та вестибуло-оральному напрямках, а також відстані необхідні для побудови коректної форми зубних дуг. Регресійні моделі лінійних розмірів необхідних для побудови коректної форми зубної дуги в залежності від особливостей телерентгенометричних показників за методом Ricketts і комп'ютерно-томографічних розмірів зубів побудовані за допомогою ліцензійного пакету "Statistica 6.0". Встановлено, що в українських юнаків побудовані усі 18 можливих достовірних регресійних моделей із коефіцієнтом детермінації більшим 0,6 (R^2= від 0,617 до 0,833, p<0,001 в усіх випадках); а в українських дівчат - лише 6 достовірних регресійних моделей із коефіцієнтом детермінації більшим 0,6 (R^2= від 0,605 до 0,793, p<0,001 в усіх випадках). При аналізі відсотку входження до регресійних рівнянь телерентгенометричних показників і комп'ютерно-томографічних розмірів зубів встановлено: в українських юнаків найбільш часто до моделей входять телерентгенометричні показники та ширина коронки зуба у мезіо-дистальному напрямку (по 26,67 %), відстань від ріжучого краю до апексу кореня зуба (13,33 %) та ширина коронки зуба у вестибуло-оральному напрямку (10,00 %); а в українських дівчат - телерентгенометричні показники та ширина коронки зуба у мезіо-дистальному напрямку (по 21,95 %), ширина коронки зуба у вестибуло-оральному напрямку (14,63 %) та відстань від ріжучого краю до апексу кореня зуба (9,76 %). При аналізі відсотку входження до регресійних рівнянь відповідних зубів встановлено: в українських юнаків найбільш часто до моделей входять верхні різці (20,00 % - 8,33 % присередні різці та 11,67 % бічні різці), нижні різці (13,33 % - 4.17 % присередні різці та 9,17 % бічні різці), верхні ікла (10,83 %) та верхні малі кутні зуби (10,00 % - 2,50 % перші та 7,50 % другі); а в українських дівчат - верхні різці (29,27 % - 21,95 % присередні різці та 7,32 % бічні різці) та нижні малі кутні зуби (12,20 % - 4,88 % перші та 7,32 % другі). Таким чином, в українських юнаків і дівчат із фізіологічним прикусом без урахування типу обличчя за допомогою регресійного аналізу побудовані високоінформативні достовірні моделі лінійних розмірів необхідних для побудови коректної форми зубної дуги в залежності від особливостей телерентгенометричних показників за методом Ricketts і комп'ютерно-томографічних розмірів зубів.

Ключові слова: *стоматологія, телерентгенометрія за методом Ricketts, комп'ютерно-томографічні розміри зубів, зубні дуги, регресійні моделі, українськи юнаки та дівчата, фізіологічний прикус.*

Author's contribution

Brotskyi N. O. - research, review writing and editing, methodology and writing of the original draft.
Dmitriev M. O. - conceptualization, supervision.
Cherkasova L. A. - software.
Smiiukha O. A. - data visualization.
Beliaiev E. V. - formal analysis.
Moroz V. V. - validation and resources.
Vakhovskyi V. V. - validation and resources.

DOI: 10.31393/morphology-journal-2024-30(3)-05 Reports of Morphology, Vol. 30, №3, Pages 44-51

ISSN 1818-1295 eISSN 2616-6194

REPORTS OF MORPHOLOGY

Official Journal of the Scientific Society of Anatomists, Histologists, Embryologists and Topographic Anatomists of Ukraine

journal homepage: https://morphology-journal.com

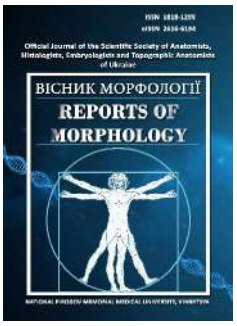

Remodeling of the structural components of the capsule and glomerular zone of the adrenal glands cortex of white rats under the influence of a complex of food additives at the late terms of the experimental study

Donchenko S. V., Bilash S. M., Koptev M. M., Pronina O. M., Oliinichenko Ya. O., Pirog-Zakaznikova A. V., Oleksiienko V. V., Mamai O. V.

Poltava State Medical University, Poltava, Ukraine

ARTICLE INFO

Received: 14 March 2024

Accepted: 20 July 2024

UDC: 611.453-031-018:613.29-092.9-024.76

CORRESPONDING AUTHOR

e-mail: donchsveta77@gmail.com

Donchenko S. V.

CONFLICT OF INTEREST

The authors have no conflicts of interest to declare.

FUNDING

Not applicable.

DATA SHARING

Data are available upon reasonable request to corresponding author.

With food additives, we can add flavour to food, extend its shelf life, and make it look good. However, even small amounts of these additives can lead to diseases of various organs and systems. The aim of our work is to establish metrics and morphological changes in the structure of the capsule and the glomerular zone of the cortex of the adrenal glands of rats at the later stages of the experimental study under the conditions of consumption of a complex of food additives: monosodium glutamate, sodium nitrite and Ponceau 4R. The control group of rats consumed oral drinking water and saline. The rats of the experimental groups were orally administered once a day with a 10 % solution of sodium nitrite (E250), sodium glutamate (E621) or Ponceau 4R. The dosages of food additives were two times lower than the permissible norm in food. The rats were withdrawn from the experiment after 8, 12 and 16 weeks. The adrenal glands were removed for the study. Paraffin sections were stained with hematoxylin and eosin, and semi-thin sections with toluidine blue, and examined using a light microscope Biorex with a digital microphoto attachment DSM 900. Ultrathin sections were examined in a TEM-125 K electron microscope. For morphometric analysis, the structure of the capsule and the glomerular zone of the cortex of the adrenal glands of rats at the later stages of the experimental study was studied. The study results were analysed using the software package "InStat". At the late stages of the experimental study, the adrenal capsule underwent irreversible changes. The average thickness of the adrenal connective tissue capsule decreased by the end of the 16th week of the experimental research. Similarly, the average thickness of the cortex decreased with each subsequent week relative to the control values, indicating significant structural and functional disorders. The average thickness of the glomerular zone of the adrenal cortex periodically changed as a compensatory reaction in response to the administration of a complex of food additives to rats. The phenomena of nucleus pyknosis and sludge syndrome were detected, which indicated compensatory and adaptive processes at the microscopic level. The analysis of electron micrographs revealed destroyed granular endoplasmic reticulum cisternae and mitochondrial remnants. Thus, it has been established that using a complex of food additives (monosodium glutamate, sodium nitrite and Ponceau 4R) directly affects the adrenal glands of rats. This effect causes structural changes in the cortex and medulla, causing alteration and hypertrophy of cells in these areas. Additionally, hyperhydration of the connective tissue stroma and compensatory-restorative reactions aimed at transcription factors and internal mechanisms of nitric oxide formation were recorded.

Keywords: *monosodium glutamate, morphology, medulla, adrenal glands, sodium nitrite, Ponceau 4R, cortical substance, hemomicrocirculatory bed, rats, morphological and functional changes, submicroscopic changes, endocrinocytes.*

Introduction

Taste plays an essential role in human life, not only as a pleasure from tasty food but also as a protective function, helping to determine the suitability and safety of products [1, 2, 10]. Our daily diet often contains foods containing

additives that give various products unique characteristics, ranging from intense flavours to attractive presentations. Even though food additives in low concentrations harm our health, no one is in a hurry to give up such food [3, 16]. The popularity of tasty foods is only growing.

Food additives are natural or synthetic substances added to products to improve their taste and preserve their appearance for a long time [5]. Many such additives have emerged due to the need to produce food in large quantities to provide people with food. However, they are very different from home cooking [27]. Food additives are necessary to enhance the taste and preserve the presentation of products, and they should not harm the human body [12, 18]. However, unscrupulous manufacturers may provide false information about the finished product on labels, often preventing us from choosing a healthy and safe product in the supermarket [13].

Today, there are many food additives that consumers are not even aware of. In Europe, the use and production of food additives have grown by 2 %. In particular, the demand for various sweeteners has increased [4]. According to European and international classification standards (INS), the content of food additives in products is denoted by the "E" index.

We are investigating some of the most common food additives: monosodium glutamate (E621), monosodium nitrite (E250), and Ponceau 4R (E124). They harm health, contributing to the development of serious diseases of organs and systems [20]. The most common negative effects of food additives include schizophrenia, anxiety, epilepsy, depression, migraines, Alzheimer's and Parkinson's diseases, hypotension, asthma, nausea, heart palpitations, and other symptoms [8, 9]. Studies show that the complex of monosodium glutamate, sodium nitrite, and Ponceau 4R affects the brain activity of rats with impaired spatial orientation, memorization, and learning ability [7, 30].

The effect of food additives on the adrenal glands is of particular importance [29]. With the development of diagnostic methods for the study of diseases, more and more diseases are attributed to the adrenal glands, which are the basis of our study [11, 20].

The purpose of the study is to establish the metric and morphological changes in the structure of the capsule and the glomerular zone of the rat's adrenal glands cortex at the late stages of the experimental study under the conditions of the use of a complex of food additives: sodium glutamate, sodium nitrite and Ponceau 4R.

Materials and methods

The experimental study was carried out on 80 white outbred rats. The Law of Ukraine "On the Protection of Animals from Cruelty" (No. 3447-IV dated 21.02.2006) and the European Convention on the Protection of Vertebrate Animals Used for Research and Other Scientific Purposes (Strasbourg, 1986) ensured compliance with ethical principles regarding animals. According to the decision of the Commission on Bioethics of the Poltava State Medical University (protocol No. 178 dated 24.12.2019), no violations of moral and ethical norms during research were detected.

The control group of rats used oral drinking water and physiological saline. Rats of experimental groups were orally administered a 10 % solution of sodium nitrite (E250), monosodium glutamate (E621) at a dose of 20 mg/kg in 0.5 ml of distilled water, Ponceau 4R at a dose of 5 mg/kg in 0.5 ml of distilled water once a day. Dosages of food additives were two times lower than the permissible norm in food products. After 8, 12 and 16 weeks, the rats were removed from the experiment using ether anaesthesia followed by euthanasia.

Adrenal glands were fixed in a neutral formalin solution, after which they were embedded in paraffin. Subsequently, the prepared sections were stained with hematoxylin and eosin and studied using a Viorex light microscope with a DSM 900 digital photomicroscope. The studied material was fixed in glutaraldehyde and sealed in EPON-812 to obtain semi-thin sections. Ready sections were stained with toluidine blue. For morphometric analysis, the structure of the capsule and glomerular zone of the adrenal glands rats cortex was studied at the late stages of the experimental study.

Ultrathin sections for electron microscopic examination, made on an LKB-3 ultramicrotome, were stained with a 1 % aqueous solution of uranyl acetate and contrasted with lead citrate according to the Reynolds method. Then, they were examined in an electron microscope TEM-125 K (serial number 38-76, TU 25-07-871-70) at an accelerating voltage of 50-75 kV.

The research results were statistically analyzed on a computer using the "InStat" software package, which is designed for data processing in medical-biological and epidemiological studies.

Results

It was morphometrically determined and statistically confirmed that the connective tissue capsule of the adrenal glands at the late stages of the experimental study underwent degenerative changes, became thinner and, due to such transformations, partially failed to perform its functions. After the 8th week of the experiment, the average thickness of the connective tissue capsule decreased statistically significantly ($p<0.05$) by 1.78 times compared to the control indicators.

After the 12th week of observation of laboratory animals, the above indicator statistically significantly ($p<0.05$) decreased by 2.48 times compared to the control indicators, and compared to the previous observation period, statistically significantly ($p<0.05$) decreased by 1.39 times, which indicated the continuation of degenerative changes in the connective tissue capsule in response to the administration of a complex of food dietary supplements to laboratory animals.

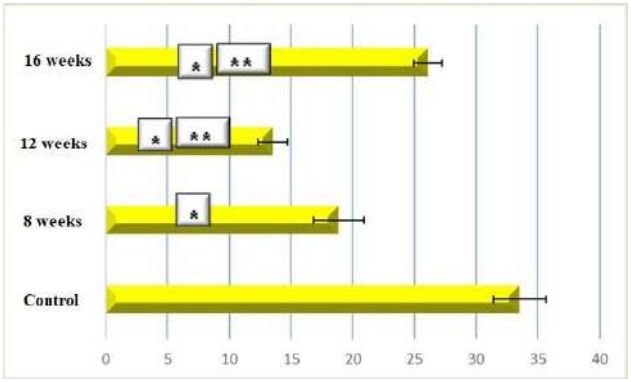

Fig. 1. Morphometric characteristics of changes in the average thickness of white rats' connective tissue capsule of the adrenal glands at the late stages of the experimental study (μm). * - statistically significant difference at p<0.05 compared to control indicators; ** - statistically significant difference at p<0.05 compared to the previous observation period.

After the 16th week of the experimental study, the average thickness of the connective tissue capsule of the adrenal glands decreased statistically significantly (p<0.05) by 1.29 times compared to the control indicators, and compared to the previous observation period, it increased statistically significantly (p<0.05) by 1.93 times, which indicates about the continuation of degenerative changes of the connective tissue capsule in response to the administration of a complex of dietary supplements to laboratory animals, but it should be noted that the above indicator did not approach the indicators of the control group of animals until the end of the observations of the laboratory animals (Fig. 1).

At the light-optical level, when analyzing histological preparations after the 8th week of the experimental study, it was determined that significant thinning of the connective tissue capsule is associated with adipose tissue dystrophy, which is a structural element of the adrenal gland capsule in rats of the control group. In parallel with this, it was determined that the number of fibroblastic diferon cells located between collagen and reticular fibers decreased in the composition of the capsule, and the latter had signs of disorganization and chaotic arrangement (Fig. 2A).

It is worth noting that after the 16th week of the experiment, the restoration of adipose tissue in the composition of the capsule was determined, but not in total volume compared to the histological preparations of the control group. However, the number of fibroblastic diferon cells was still significantly reduced. Collagen and reticular fibres in the composition of the connective tissue capsule acquired signs of hyperhydration and were oriented chaotically, which visually created signs of its expansion, but structurally, the connective tissue capsule had signs of destruction (Fig. 2B).

The average thickness of the cortex of the adrenal glands at the late stages of the experimental study reliably decreased, which indicated destructive processes and was confirmed by the statistical analysis data. After the 8th week of the experiment, the average thickness of the cortex decreased statistically significantly (p<0.05) by 1.27 times compared to the control indicators. After the 12th week of observation of laboratory animals, the above indicator was statistically significantly (p<0.05) reduced by 1.51 times compared to the control indicators, and compared to the previous period of observation, it decreased by 1.18 times (p<0.05). After the 16th week of the experimental study, the average indicator of the thickness of the cortex statistically significantly (p<0.05) decreased by 1.54 times compared to the control indicators, and compared to the previous period of observation, it also decreased by 1.93 times and by the end of the experiment remained 1.54 times smaller compared to by the control group, which indicated significant structural disorders, which will cause functional disorders in the future (Fig. 3).

It was morphometrically determined and statistically confirmed that the glomerular zone of the adrenal gland

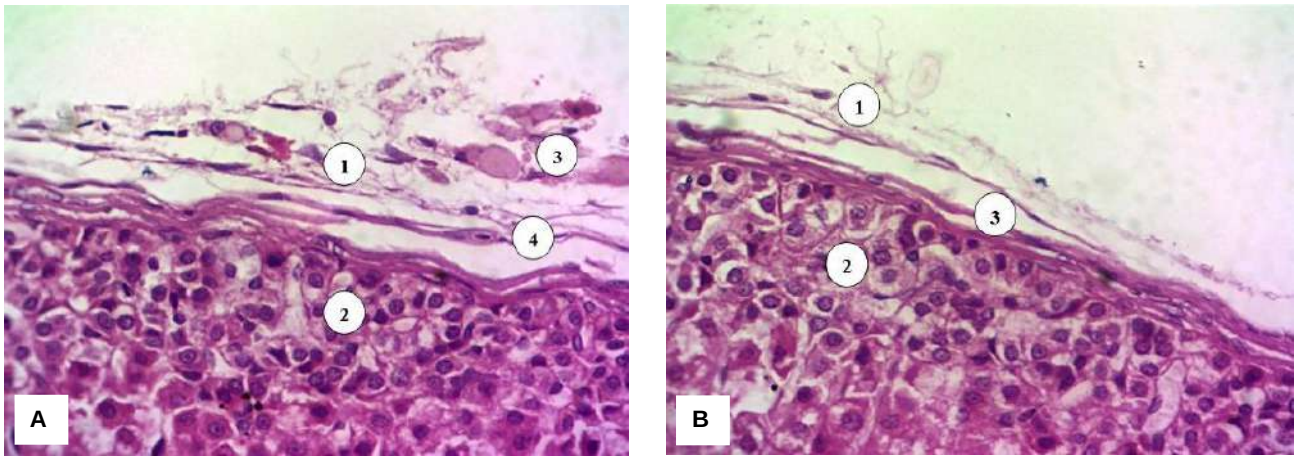

Fig. 2. Remodeling of the structural components of the connective tissue capsule in the late stages: A - after the 8th week of the experimental study; B - after the 16th week of the experimental study. 1 - connective tissue capsule; 2 - glomerular zone; 3 - elements of restored adipose tissue; 4 - fibrous component of the capsule. Hematoxylin-eosin. Eyepiece x10, lens x40.

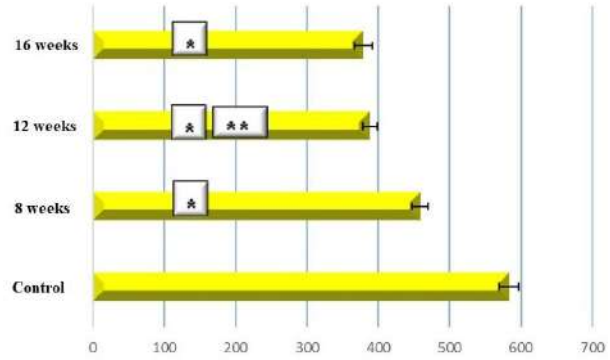

Fig. 3. Morphometric characteristics of changes in the average thickness of the cortex of the adrenal glands of white rats at the late stages of the experimental study (μm). * - statistically significant difference at p<0.05 compared to control indicators; ** - statistically significant difference at p<0.05 compared to the previous observation period.

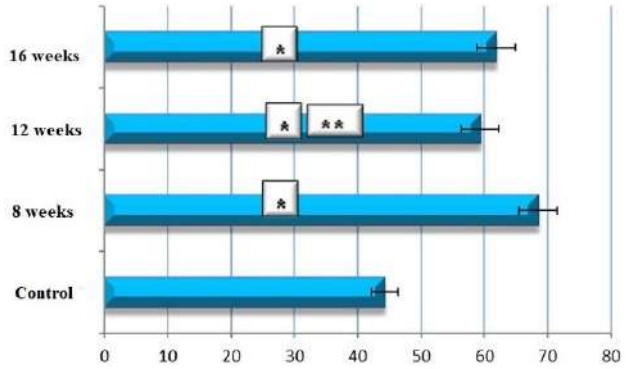

Fig. 4. Morphometric characteristics of changes in the average thickness of the glomerular zone of the adrenal glands cortex of white rats at the late stages of the experimental study (μm). * - statistically significant difference at p<0.05 compared to control indicators; ** - statistically significant difference at p<0.05 compared to the previous observation period.

cortex also underwent specific degenerative changes. After the 8th week of the experiment, the indicator of the average thickness of the glomerular zone of the cortex increased statistically significantly (p<0.05) by 1.55 times compared to the control indicators. After the 12th week of observation of laboratory animals, the above indicator statistically significantly (p<0.05) also increased by 1.34 times compared to the control indicators, and compared to the previous period of observation, it decreased statistically significantly (p<0.05) by 1.15 times. After the 16th week of the experimental study, the average index of the thickness of the glomerular zone of the cortex increased statistically significantly (p<0.05) by 1.39 times compared to the control indicators. Compared to the previous observation period, it also increased by 1.93 times. It remained 1.39 times larger until the end of the experiment compared with the control group, indicating significant structural changes aimed at compensatory reactions in response to administering a complex of dietary supplements to laboratory animals (Fig. 4).

At the light-optical level, during the analysis of histological preparations of the glomerular zone of the cortex of the adrenal glands, we determined that after 8 weeks of administration of a complex of food dietary supplements to laboratory animals, an active accumulation of lipid inclusions was visualized in the cytoplasm of corticocytes, and the average number of light endocrinocytes significantly exceeded dark endocrinocytes. However, it should be noted that the nuclei of light corticocytes were determined with the phenomena of pyknosis, and microvascular loops around the glomeruli were visualized with signs of sludge syndrome (Fig. 5).

The described morphological changes indicate compensatory and adaptive processes at the microscopic level in response to long-term administration of a complex

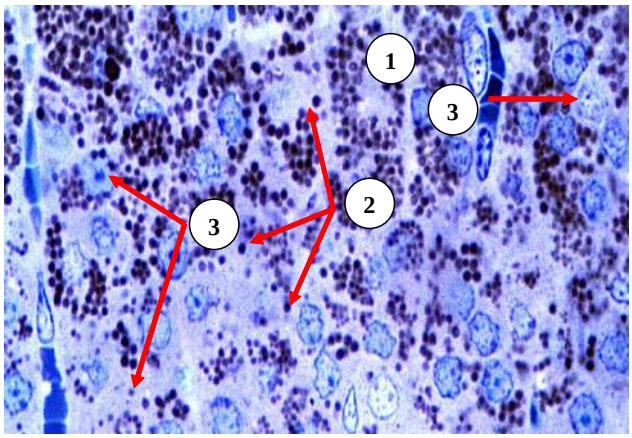

Fig. 5. Remodeling of the structural components of the glomerular zone of the adrenal glands of white rats after 8 weeks of experimental research. 1 - the surface part of the glomerular zone of the cortex; 2 - oxyphilic corticocytes; 3 - microvascular loops. Semi-thin cut. Toluidine blue. Eyepiece x10, lens x20.

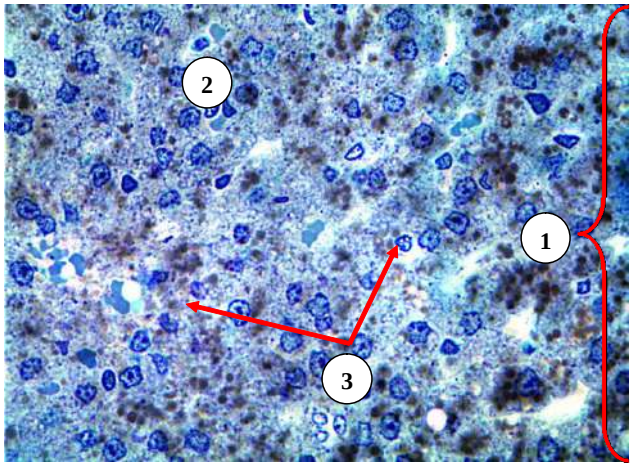

Fig. 6. Remodelling of the structural components of the glomerular zone of the adrenal glands of white rats after 16 weeks of experimental research. 1 - glomerular zone of the cortex; 2 - corticocytes of the glomerular zone; 3 - microvessels of the loop with signs of perivascular edema. Semi-thin sections. Toluidine blue. Eyepiece x10, lens x20.

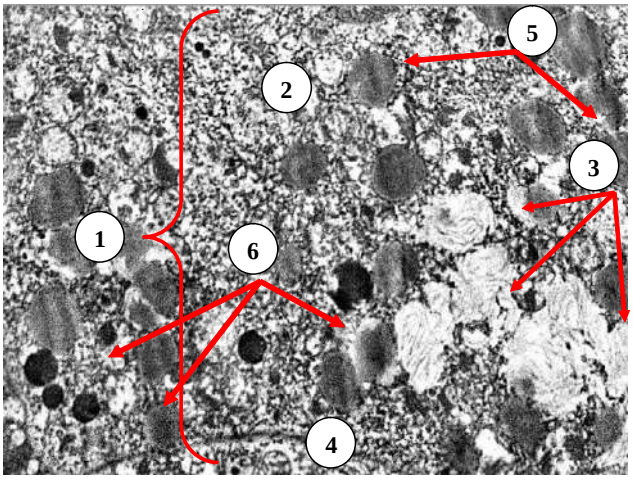

Fig. 7. Subcellular changes in the cytoplasm of corneocytes in the composition of white rats' adrenal gland cortex glomerular zone after the 16th week of the experimental study. 1 - glomerular zone; 2 - cytoplasm of adrenocorticocytes of the glomerular zone; 3 - apoptotic transformations of synthetic organelles; 4 - corticocyte nucleus; 5 - depleted lipid inclusions; 6 - lipid inclusions with accumulated content. Electrogram. x14000.

of food dietary supplements, enhancement of their functional activity with the active synthesis of aldosterone, corresponding effect on the distal convoluted tubules of the nephron, and enhancement of removal of the harmful factor from the body through the kidneys.

After the 16th week of the experimental study, we determined that the average number of secretory granules in the cytoplasm of light corticocytes sharply decreased, and their cytolemma did not contrast against the background of the parenchyma of the glomerular zone. Dark corticocytes were visualized singly. Lipid inclusions lost their contrast, which indicates their emptying, and microvessels were identified with signs of perivascular edema (Fig. 6).

We determined significant subcellular degenerative changes when analyzing electronograms at the ultramicroscopic level after the 16th week of the experimental study. In the cytoplasm of the corticocytes of the glomerular zone, destroyed cisterns of the granular endoplasmic reticulum were visualized on the spot, and myeloid bodies were determined in the place of mitochondria (compared to the electronograms of the control group of animals), which indicates apoptotic processes in the cytoplasm of the corticocytes of the glomerular zone. Lipid inclusions, which ensured the energy exchange of corticocytes, were visualized as empty, and only a small part of them contrasted against the background of the cytoplasm with fine-grained osmiophilic content (Fig. 7).

Thus, when conducting an experimental study within 16 weeks, it was established that the synthetic apparatus of corticocytes of the glomerular zone underwent significant degenerative changes, which led to a decrease or complete absence of its functional activity.

Discussion

The adrenal glands have long attracted the attention of scientists due to their complex structure, large number of hormones, extensive innervation, and numerous functions [28]. They are a prime example of paracrine interactions between cortex and medulla, which are histogenetically distinct tissues. The adrenal glands play an essential role in the hypothalamic-pituitary-adrenal system and as endocrine organs that serve as a source of stem cells capable of cortex regeneration [13]. They provide adaptive responses and regulate all metabolic processes in the human body, being the main stress-relieving system. Treatment and diagnosis of adrenal diseases remain an urgent medical and social problem [24]. Due to the widespread use of modern imaging methods, the detection of adrenal diseases is becoming more common and possible at early stages [6]. The main method of diagnosis is magnetic resonance imaging, which allows to determine the nature of neoplasms - malignant or benign, to avoid unnecessary surgical interventions and to detect the disease at an early stage, even before the onset of clinical symptoms.

The adrenal glands, a subject of extensive research by scientists globally, are of significant interest due to their susceptibility to various chemicals. Our research has shown that experimentally induced diabetes in rats led to an increase in reticular fibers and impaired steroidogenesis, loss of parallel arrangement of the cells of the fascicular zone, capillary dilation and overflow, and nuclear apoptosis [9]. We've also found that sodium glutamate depletes intracellular glutathione levels and reduces the ability of cells to protect themselves from oxidative stress [12]. Furthermore, sodium glutamate caused an increase in the size of the adrenal glands and cortex hypertrophy [15]. Sodium nitrite causes vasodilation and a large number of accumulated apoptotic cells [17]. Long-term use of the food supplement Ponceau 4R caused adrenal hypotrophy [19]. These findings have profound implications for understanding the effects of various chemicals on adrenal gland health and function, underscoring the importance of our research.

Researchers have meticulously examined the effects of exogenous factors on the adrenal glands. Under conditions of chronic hyperglycemia, they found destroyed endocrinocytes, signs of cell cytoplasmic edema, and filled and dilated vessels, indicating a violation of microcirculation. The capsule was thickened and stratified, and pycnosis was observed in the cell nuclei. The vessels were full-blooded, with erythrocyte sludge syndrome and perivascular edema [21]. This thorough research provides a comprehensive understanding of the effects of exogenous factors on the adrenal glands.

Under conditions of prolonged exposure to heavy metal salts, the integrity of the adrenal capsule was impaired in

some places, the vessels of the capsule were dilated with signs of full blood, the morphological structure of the walls of arteries and arterioles was disturbed, their muscular membrane was thickened, and endothelial cells with hyperchromic, hypertrophied nuclei were edematized. The glomerular and fascicular zones were slightly reduced. The cells of these zones had indistinct membrane shapes, their nuclei were hyperchromic. The reticular zone was enlarged, the walls of the venules were thickened, and sludge syndrome was observed [23].

Under the influence of experimental extracellular dehydration in the adrenal glands, morphological changes in the vascular bed were observed due to polycythemic hypovolemia and hypoxia. There was a violation of vascular blood filling, blood stasis, and increased vascular wall permeability [22].

The effect of chronic stress on the adrenal glands causes their hypertrophy, exhaustion and circulatory disorders. There were signs of perivascular edema and punctate hemorrhages, and proliferation of connective tissue between the cortex and medulla. During acute stress, there was hypertrophy of the organ, changes in the parenchymal-stromal ratio and the size of the nuclei. Adrenal hypertrophy was also observed under the influence of ionizing radiation [14]. In tobacco intoxication, changes in the reticular zone occurred, namely its expansion, as a reaction to adaptation. When the daylight hours changed, the activation of the fascicular zone and the suppression of the glomerular and reticular zones occurred, indicating an excessive production of corticosteroids and a hypoproduction of aldosterone and steroid hormones.

As a result of the combined effect of ionization and heavy metals, significant dystrophic and destructive processes, suppression of glandular activity, and impaired adaptive responses occurred in the adrenal glands.

Our observations during the modeling of streptozotocin-induced diabetes revealed significant changes in the adrenal cortex. These included thickening of all areas, an increase in the size of endocrinocytes and their nuclei, and high levels of cortisol in the blood. Additionally, we detected hemodynamic disorders of the microcirculatory system [25].

Exposure to low temperatures has a profound impact on the adrenal glands. In the early stages of the experiment, we observed swelling of cellular structures and organ parenchyma with areas of vasospasm. Subsequently, compensatory changes in the components of the gland were observed, and in the later stages, compensatory and restorative processes with signs of regeneration processes were detected [26].

In acute inflammation, hyperemia of the adrenal glands was observed. Histological examination revealed haemorrhages. General hypoxia and overheating also cause irreversible morphological changes in the adrenal glands [29]. Antineoplastic drugs significantly disrupt the morphology and function of the adrenal glands. Under the influence of cytostatics, lipid inclusions were almost completely absent in the cells of the fascicular zone, and glucocorticoids were synthesized in small amounts. The secretion of adrenaline and noradrenaline decreased in the medulla [10, 11].

Studies of the adrenal glands after influenza A (H1N1) and COVID-19 have revealed edema and partial destruction of the cortex and medulla [24]. In combination with COVID-19, hypoxia is accompanied by the accumulation of lipofuscin granules in the cytoplasm of endocrine cells, a marker of lipid-free radical oxidation activation.

Conclusion

1. The result of this experiment showed that the action of any exogenous and endogenous factors is accompanied by non-specific changes in the body. In our case, the effect of a complex of food additives on the adrenal glands triggers adaptive and compensatory mechanisms in response to this stress stimulus.

2. It was established that in the early stages of the experimental study, the influence of irritating factors caused initial destructive changes, and in the later stages, irreversible degenerative disorders occurred.

References

[1] Akimov, O. Y., & Kostenko, V. O. (2016). Functioning of nitric oxide cycle in gastric mucosa of rats under excessive combined intake of sodium nitrate and fluoride. *Ukr Biochem J,* 88(6), 70-5. doi: 10.15407/ubj88.06.070

[2] Banerjee, A., Mukherjee, S., & Maji, B. K. (2021). Worldwide flavor enhancer monosodium glutamate combined with high lipid diet provokes metabolic alterations and systemic anomalies: an overview. *Toxicology Reports*, 8, 938-961. doi: 10.1016/j.toxrep.2021.04.009

[3] Benbow, T., Teja, F., Sheikhi, A., Exposto, F. G., Svensson, P., & Cairns, B. E. (2022). Peripheral N-methyl-D-aspartate receptor activation contributes to monosodium glutamate-induced headache but not nausea behaviours in rats. *Scientific reports,* 12, 13894. doi: 10.1038/s41598-022-18290-w

[4] Blais, A., Rochefort, G. Y., Moreau, M., Calvez, J., Wu, X., Matsumoto, H., & Blachier, F. (2019). Monosodium glutamate supplementation improves bone status in mice under moderate protein restriction. *JBMR Plus*, 3(10), e10224. doi: 10.1002/jbm4.10224

[5] Bumeister, V. I., Sikora, V. Z., Yarmolenko, O. S., & Prykhodko, O. O. (2022). Morphological changes of the adrenal gland in rats under conditions of experimental chronic hyperglycemia. *Bulletin of Problems in Biology and Medicine,* 3(166), 350-355. doi: 10.29254/2077-4214-2022-3-166-350-355

[6] Butnariu, M., & Sarac, I. (2019). What is sodium glutamate and what effects it has on health. *Journal of Applied Biotechnology and Bioengineering,* 6(5), 223-226. doi: 10.15406/jabb.2019.06.00195

[7] Chazelas, E., Pierre, F., Druesne-Pecollo, N., Esseddik, Y., de Edelenyi, F. S., & Agaesse, C. (2022). Nitrites and nitrates from food additives and natural sources and cancer risk: results from the NutriNet-Sante cohort. *International Journal of Epidemiology,* 51(4), 1106-1119.

[8] Dong, Y., Xuexiu, J., Mengyuan, D., Han, F., Shi, F., Tanikawa,

H., & Hiroki, T. (2020). Life cycle assessment of cleaner production measures in monosodium glutamate production: A case study in China. *Journal of Cleaner Production*, 270, 122-126. doi: 10.1016/j.jclepro.2020.122126

[9] Ernstsen, C., Christensen, S. L., Olesen, J., & Kristensen, D. M. (2021). No additive effect of combining sumatriptan and olcegepant in the GTN mouse model of migraine. *Cephalalgia,* 41(3), 329-339. doi: 10.1177/0333102420963857

[10] Hryntsova, N. B., Romaniyk, A. M. & Bumeister, V. I. (2019). Morphological rearrangements of the rat's adrenal cortex under conditions of prolonged exposure to heavy metal salts and non-hormonal correction. *Morphologia,* 13(3), 26-31. doi: 10.26641/1997-9665.2019.3.26-31

[11] Hryntsova, N. B., Romanyuk, O. K., Volkova, M. V., Romaniyk, A. M., & Bumeister, V. I. (2018). Морфологічні та морфометричні перебудови судин клубочкової та пучкової зони кори наднирників щурів за умов експериментальної позаклітинної дегідратації середнього ступеня. [Morphological and morphometric transformations of the glomerulosa and fascscblate zonnes blood vessels of the adrenal cortex of rats under conditions of experimental extracellular dehydration of middle degree]. *Art of Medicine,* 3(7), 35-38.

[12] Kinash, O. V., Yeroshenko, G. A., Shevchenko, K. V., Lisachenko, O. D., Donets, I. M., Kinash, P. M., & Hryhorenko A. S. (2021). Вплив глутамату натрію на організм людини і тварин [Effects of sodium glutamate on human and animal]. *Вісник проблем біології і медицини=Bulletin of problems biology and medicine*, 3(161), 49-52. doi: 10.29254/2077-4214-2021-3-161-49-52

[13] Kouzuki, M., Taniguchi, M., Suzuki, T., Nagano, M., Nakamura, S., & Katsumata, Y. (2019). Effect of monosodium L-glutamate (umami substance) on cognitive function in people with dementia. *Eur J Clin Nutr,* 73(2), 266-275. doi: 10.1038/s41430-018-0349-x

[14] Kulbitska, V. V., & Nebesna, Z. M. (2022). Субмікроскопічні зміни ендокриноцитів кіркової речовини надниркових залоз через 14 діб після змодельованої опікової травми [Submicroscopic changes of endocrinocytes of the adrenal gland 14 days after the simulated burn injury]. *Вісник медичних і біологічних досліджень=Bulletin of Problems in Biology and Medicine,* 2, 30-34. doi: 10.11603/bmbr.2706-6290.2022.2.13064

[15] Kulbitska, V., Nebesna, Z., & Trach Rosolovska, S. (2020). Adrenal glands: morphofunctional reorganization based on the influence of exogenous and endogenous factors. *Journal of Education, Health and Sport,* 10(1), 354-364. doi: 10.12775/JEHS.2020.10.01.037

[16] Kulbitska, V. V., Nebesna, Z. M., & Shuturma, O. Ya. (2021). Гістологічні зміни надниркових залоз у пізні терміни після експериментальної термічної травми та застосування подрібненого субстрату ліофілізованої ксеношкіри [Histological changes of the adrenal gland in the late period after experimental thermal injury and application of lyophilized xenograft skin substrate]. *Оригінальні дослідження=Original research,* 2(8), 40-44. doi: 10.11603/bmbr.2706-6290.2021.2.12337

[17] Leulescu, M., Lacobescu, G., Bojan, M., & Rotaru, P. (2019). Ponceau 4R azoic red dye. *Journal of Thermal Analysis and Calorimetry,* 138, 2091-2101. doi: 10.1007/s10973-019-08680-0

[18] Magerowski, G., Giacona, G., Patriarca, L., Papadopoulos, K., Garza-Naveda, P., & Radziejowska, J. (2018). Neurocognitive effects of umami: association with eating behavior and food choice. *Neuropsychopharmacology*, 43(10), 2009-2016. doi: 10.1038/s41386-018-0044-6

[19] Martami, F, & Holton, K. F. (2023). Targeting Glutamate Neurotoxicity through Dietary Manipulation: Potential Treatment for Migraine. *Nutrients,* 15(18), 3952. doi: 10.3390/nu15183952

[20] Millan, S., Satish, L., Bera, K., & Sahoo, H. (2019). Binding and inhibitory effect of the food colorants Sunset Yellow and Ponceau 4R on amyloid fibrillation of lysozyme. *New Journal of Chemistry,* 9, 3956-3968. doi: 10.1039/C8NJ05827J

[21] Mustafina, H. M., Starchenko, I. I., Fylenko, B. M., Koka, V. M., Cherniak, V. V., Roiko, N. V., & Proskurnya, S. A. (2022). Morphological features of the liver parenchyma in the experimental supplementation of ration with the food additives. *Wiadomosci Lekarskie,* 75(6), 1525-1528. doi: 10.36740/WLek202206117

[22] Mustafina, H. M., Starchenko, I. I., Koka, V. M., Lukachina, Y. I., & Chernyak, V. V. (2021). Сучасні уявлення про вплив окремих харчових добавок на організм людини [Modern concepts about impact of different food additives on the human body]. *Актуальні проблеми сучасної медицини=Actual Problems of the Modern Medicine: Bulletin of Ukrainian Medical Stomatological Academy,* 21(1), 194-198. doi: 10.31718/2077-1096.21.1.194

[23] Oluwole, D. T., Oladipupo, S. E., Ajayi, L. O., Alabi, O. D., Amos, V., & Akanbi, G. (2024). Disruptive consequences of monosodium glutamate on male reproductive function: A review. *Current Research in Toxicology,* 6, 100148. doi: 10.1016/j.crtox.2024.100148

[24] Othman, S. I., & Jumah, M. B. (2019). Histomorphological Changes in Monosodium Glutamate Induced Hepato-renal Toxicity in Mice. *International Journal of Pharmacology,* 15(4), 449-456. doi: 10.3923/ijp.2019.449.456

[25] Tovkay, O. (2019). Diagnostic and treatment algorithm of comprehensive surgical management of patients with adrenal tumors. *International Journal of Endocrinology,* 15(8), 603-609. doi: 10.22141/2224-0721.15.8.2019.191682

[26] Wang, C. X., Zhang, Y., Li, Q. F., Sun, H. L., Chong, H. L., & Jiang, J. X. (2021). The Reproductive Toxicity of Monosodium Glutamate by Damaging GnRH Neurons Cannot Be Relieved Spontaneously Over Time. *Drug Design, Development and Therapy*, 15, 3499-3508. doi: 10.2147/DDDT.S318223

[27] Yachmin, A. I., Yeroshenko, G. A., Shevchenko, K. V., Hapon, S. V., Vatsenko, A. V., & Ulanovska-Tsyba, N. A. (2022). Ultrastructural characteristics of the rat gastric fundic wall after the impact of the complex of food additives. *Світ медицини та біології=World of Medicine and Biology,* 2(80), 252-255. doi: 10.26724/2079-8334-2022-2-80-252-255

[28] Yan, L., Dong, X., & Xue, L. (2018). Neurogenic dural inflammation induced by inflammatory soup combined with CGRP: A modified animal model of migraine. *Int. J. Clin. Exp. Med.,* 11, 9126-9134. doi: 10.1177/03331024211017882

[29] Yeroshenko, G. A., Grygorenko, A. S., Shevchenko, K. V., Lysachenko, O. D., Maksymenko, N. T., & Vatsenko, A. V. (2022). The features of the normal ultrastructure of the rat duodenum and under the combined effect of the food additives complex. *Wiad Lek,* 75(6), 1466-1470. doi: 10.36740/WLek202206107

[30] Zanfirescu, A., Ungurianu, A., Tsatsakis, A. M., Nitulescu, G. M., Kouretas, D., & Veskoukis, A. (2020). A review of the alleged health hazards of monosodium glutamate. *Comprehensive Reviews in Food Science and Food Safety,* 18(4), 1111-1134. doi: 10.1111/1541-4337.12448

РЕМОДЕЛЮВАННЯ СТРУКТУРНИХ КОМПОНЕНТІВ КАПСУЛИ ТА КЛУБОЧКОВОЇ ЗОНИ КІРКОВОЇ РЕЧОВИНИ НАДНИРКОВИХ ЗАЛОЗ БІЛИХ ЩУРІВ ПРИ ДІЇ КОМПЛЕКСУ ХАРЧОВИХ ДОБАВОК НА ПІЗНІХ ТЕРМІНАХ ЕКСПЕРИМЕНТАЛЬНОГО ДОСЛІДЖЕННЯ

Донченко С. В., Білаш С. М., Коптев М. М., Проніна О. М, Олійніченко Я. О., Пирог-Заказникова А. В., Олексієнко В. В., Мамай О. В.

Завдяки харчовим добавкам ми можемо додавати їжі певних смакових властивостей, подовжувати термін її зберігання та робити її привабливою на вигляд. Проте, навіть невеликі кількості цих добавок можуть призвести до захворювань різних органів та систем. Мета нашої роботи - встановити метричні та морфологічні зміни структури капсули та клубочкової зони кіркової речовини надниркових залоз щурів на пізніх етапах експериментального дослідження за умов вживання комплексу харчових добавок: глутамату натрію, нітриту натрію та Понсо 4R. Контрольна група щурів вживала перорально питну воду та фізіологічний розчин. Щурам дослідних груп 1 раз на добу перорально вводили 10 % розчин нітриту натрію (Е250), глутамату натрію (Е621) або Понсо 4R. Дозування харчових добавок були у 2 рази меншими, ніж допустима норма у харчових продуктах. Через 8, 12 і 16 тижнів щурів виводили з експерименту. Для дослідження вилучали надниркові залози. Виготовлені парафінові зрізи забарвлені гематоксиліном і еозином, а напівтонкі зрізи - толуїдиновим синім, вивчали за допомогою світлового мікроскопа Biorex з цифровою мікрофотонасадкою DCM 900. Ультратонкі зрізи досліджували в електронному мікроскопі ПЕМ-125 К. Для морфометричного аналізу вивчали структуру капсули та клубочкової зони кіркової речовини надниркових залоз щурів на пізніх етапах експериментального дослідження. Статистичний аналіз результатів дослідження проводили з використанням програмного пакета "InStat". Встановлено, що на пізніх термінах експериментального дослідження капсула надниркових залоз зазнала незворотних змін. Середній показник товщини сполучнотканинної капсули надниркових залоз зменшувався до кінця 16 тижня експериментального дослідження. Аналогічно показник середньої товщини кіркової речовини із кожним наступним тижнем зменшувався відносно контрольних значень, що свідчило про значні структурні та функціональні порушення. Середній показник товщини клубочкової зони кіркової речовини надниркових залоз періодично змінювався, як компенсаторна реакція у відповідь на введення щурам комплексу харчових добавок. Виявлені явища пікнозу ядер, сладж-синдрому, що свідчило про компенсаторно-пристосувальні процеси на мікроскопічному рівні. Під час аналізу електронограм зафіксовані зруйновані цистерни гранулярної ендоплазматичної сітки та залишки мітохондрій. Таким чином, встановлено, що вживання комплексу харчових добавок (глутамату натрію, нітриту натрію та Понсо 4R) має безпосередній вплив на надниркові залози щурів. Цей вплив викликає структурні зміни в кірковій та мозковій речовині, спричиняючи альтерацію та гіпертрофію клітин цих зон. Додатково зафіксовано гіпергідратацію сполучнотканинної строми та компенсаторно-відновлювані реакції, спрямовані на транскрипційні фактори та внутрішні механізми утворення оксиду азоту.

Ключові слова: *глутамат натрію, морфологія, мозкова речовина, надниркові залози, нітрит натрію, Понсо 4R, кіркова речовина, гемомікроциркуляторне русло, щури, морфофункціональні зміни, субмікроскопічні зміни, ендокриноцити.*

Author's contribution

Donchenko S. V. - research, methodology and writing of the original draft, data visualization.
Bilash S. M. - conceptualization, research, review writing and editing.
Koptev M. M. - formal analysis and validation.
Pronina O. M. - project administration.
Oliinichenko Ya. O. - software, resources.
Pirog-Zakaznikova A. V. - data visualization.
Oleksiienko V. V. - formal analysis and validation, resources.
Mamai O. V. - software, conceptualization.

DOI: 10.31393/morphology-journal-2024-30(3)-06 **Reports of Morphology, Vol. 30, №3, Pages 52-62**

ISSN 1818-1295 eISSN 2616-6194

REPORTS OF MORPHOLOGY

Official Journal of the Scientific Society of Anatomists, Histologists, Embryologists and Topographic Anatomists of Ukraine

journal homepage: https://morphology-journal.com

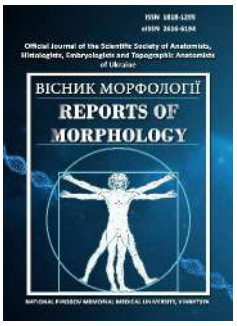

Therapeutic potential of mesenchymal stromal cells on morphological parameters in the hippocampus of rats with brain ischemia-reperfusion modeling

Konovalov S. V.[1], Moroz V. M.[1], Yoltukhivskyy M. V.[1], Gadzhula N. G.[1], Gusakova I. V.[1], Deryabina O. G.[2,3], Kordium V. A.[2,3]

[1]National Pirogov Memorial Medical University, Vinnytsya, Ukraine
[2]State Institute of Genetic and Regenerative Medicine, National Academy of Medical Sciences of Ukraine, Kyiv, Ukraine
[3]Institute of Molecular Biology and Genetics, National Academy of Sciences of Ukraine, Kyiv, Ukraine

ARTICLE INFO
Received: 04 March 2024
Accepted: 22 July 2024

UDC: 612.8:611.81:616.12:599.323.4

CORRESPONDING AUTHOR
e-mail: gadzhula@vnmu.edu.ua
Gadzhula N. G.

CONFLICT OF INTEREST
The authors have no conflicts of interest to declare.

FUNDING
Not applicable.

DATA SHARING
Data are available upon reasonable request to corresponding author.

Ischemic stroke is an extremely important pathology with high mortality, in which more than 50 % of patients with occlusion of the main vessels remain disabled, despite early reperfusion therapy by thrombolysis or thrombectomy. As part of the regenerative strategy, stem cell transplantation in ischemic stroke became a new impetus. Cell therapy with the use of mesenchymal stromal cells demonstrated encouraging results regarding endogenous mechanisms of neuroregeneration in response to ischemic damage to brain structures. The aim of the research is to study the influence of mesenchymal stromal cells of various genesis, lysate of mesenchymal stromal cells obtained from Wharton's jelly umbilical cord and citicoline on the dynamics of morphological changes in the hippocampal CA1 region of rats with acute cerebral ischemia-reperfusion according to light microscopy and micromorphometry data. The experiment was carried out using 200 male Wistar rats, which were subjected to ischemia-reperfusion by reversible 20-minute bilateral occlusion of the internal carotid arteries. Animals with modeled pathology were intravenously transplanted with mesenchymal stromal cells of various genesis (from Wharton's jelly of the human umbilical cord, human and rat adipose tissue), and rat embryonic fibroblasts, lysate of mesenchymal stromal cells and citicoline were injected. Histological analysis of rat brain sections was performed on the 7th and 14th day of the experiment. Statistical analysis was performed using "Statistica 6.0" (StatSoft® Snc, USA). The significance of differences was assessed using the Student's t-test and the nonparametric Mann-Whitney U test. During the study, it was found that modeled ischemia-reperfusion in rats caused almost complete degeneration of the structure of the pyramidal layer of hippocampal CA1 region, gave uniformity to the structure of the radiant layer, infiltration of microglia, contributed to the disruption of the arrangement of apical dendrite bundles and narrowing of blood vessels as a result of perivascular edema. Also, the modeled pathology reduced the total number of neuronal nuclei in the hippocampal CA1 area, the overwhelming majority of which had signs of pathological changes. Transplantation of mesenchymal stromal cells of various origins, lysate of mesenchymal stromal cells and citicoline contributed to a significant increase in the number of neuronal nuclei in the hippocampal CA1 zone and nuclei that did not undergo pathological changes. The most positive effect was found in the transplantation of mesenchymal stromal cells from human Wharton's jelly-derived cells. Thus, both in the subacute and recovery periods of ischemic stroke in rats, the transplantation of human Wharton's jelly-derived mesenchymal stromal cells was significantly surpassed the reference drug citicoline in its ability to reduce the number of pathologically changed nuclei by 1.5 times ($p<0.05$). At the same time, the number of pathologically unchanged nuclei significantly exceeded the number of nuclei with signs of karyorrhexis and karyopyknosis, so it would be advisable to use mesenchymal stromal cells of various genesis, lysate or citicoline in conditions of acute cerebral ischemia-reperfusion, taking into account their ability to

reduce the volume of the infarct. In the future, an injectable drug will be created from the most effective culture of mesenchymal stromal cells in terms of cerebroprotective properties for cell therapy of patients with acute ischemic stroke.
Keywords: *mesenchymal stromal cells, neurons, hippocampus, ischemia-reperfusion, rats.*

Introduction

Ischemic stroke is a global problem of humanity, because it leads to a high mortality, in which more than 50 % of patients with occlusion of the main vessels remain disabled, despite the earliest possible thrombolytic therapy [13, 14, 21]. Every year, about 150,000 cases of stroke occur in our country, among which more than 100,000 cases end in death of patients from stroke or other cerebral circulation disorders. The majority of patients (80%) who have survived after the stroke later suffer from physical disorders, cognitive and psychological disorders, and socio-economic challenges, which imposes a considerable burden of this pathology on the state budget [17]. Among patients with ischemic stroke, every third person is of working age, and every tenth patient will be able to recover and fully return to normal life. Of the ischemic stroke patients, every third is of working age, and every tenth patient will be able to recover and completely return to normal life [21]. Therefore, assistance with acute cerebrovascular accident (ACVA) is the main focus of the Medical Guarantee Program with financing at an increased tariff [16, 17].

A sign of destructive-degenerative injury of cellular structure in central nervous system's tissue in the formation of a focus of ischemia as a result of ACVA is a decrease in the density of neurons, as well as their nucleic acid content. A decrease in brain blood supply results in insufficient supply of oxygen (O_2) and glucose to it. At the same time, a decrease in the level of glucose contributes to the activation of glycolysis and, accordingly, suppression of the formation of adenosine triphosphate in the brain. As a result of the loss of potassium ions (K+) by nerve cells and the accumulation of sodium ions (Na+) and water (H_2O), brain tissue inflammation occurs [26]. In emergency stroke therapy, there is a need quickly restore the perfusion of the ischemic area [1]. It should be noted that even early reperfusion does not always live up to doctors' expectations, as reperfusion injury of neurons often occurs after recanalization of the occluded artery. Therefore, the development of modern drugs to promote cerebroprotection is of primary importance in order to improve the results of prevention and treatment of ischemic stroke. At present, encouraging results have been obtained from recent experiments on the ability of mesenchymal stromal cells (MSCs) to prevent the appearance of plastic exchange disorders and the loss of their structural components by neurons, which may be a sign of their cerebroprotective effect in acute brain ischemia [6, 10, 28]. However, such researches are limited, and rarely comparative. From literary sources, it is known that the study of the influence of mesenchymal stromal cells in the treatment of ischemic stroke has been conducted for the past two decades. MSCs are derived from adipose tissue, tooth buds and tooth pulp, bone marrow, liver or umbilical cord, umbilical cord blood and placenta. Various stem cells have been tested in animal models of ischemic stroke as monotherapy [19]. Bone marrow-derived cells have been well studied in recent years, as have adipose-derived MSCs, and only a few studies have been carried out with placental cells [3, 20]. Therefore, in our study, as in other experiments, researchers used both allogeneic [27] and xenogeneic [18] MSCs, but we compared the cerebroprotective effect of both allogeneic and xenogeneic MSCs from several sources. The optimal dose of MSC transplantation in ischemic stroke in rats was determined by Chen Y. et al. [5] and was 105-106 cells per animal, which corresponded to the number of cells intravenously transplanted into rodents in our study. MSCs obtained from Wharton's human umbilical cord blood cells (HUC-MSCs), due to their unique beneficial properties, have the best clinical perspectives in use. They do not have ethical and legal concerns, do not induce oncogenesis, they are easy to obtain in large quantities (multipotent, proliferative and hypoimmunogenic).

The above-mentioned data regarding the presence of cerebroprotective effect of MSCs in case of cerebral ischemia-reperfusion injury became the basis for carrying out this experimental study.

The purpose of the research is to study the influence of mesenchymal stromal cells of various genesis, lysate of mesenchymal stromal cells obtained from Wharton's jelly umbilical cord and citicoline on the dynamics of morphological changes in the hippocampal CA1 region of rats with acute cerebral ischemia-reperfusion according to light microscopy and micromorphometry data.

Materials and methods

The experiment was carried out in 200 4-month-old male Wistar rats weighing between 160-190 g, which were subjected to transient bilateral 20-minute ischemia-reperfusion of the internal carotid arteries. The animals were a brood of the vivarium of National Pirogov Memorial Medical University (Vinnytsya, Ukraine) and were kept in standard conditions with free access to feeder. An experimental model of ischemia-reperfusion was made by placing ligatures on the internal carotid arteries (ICA) bilaterally under propofol "Propofol-Novo" anesthesia (Novofarm-Biosintez LLC, Ukraine) at the dose of 60 mg/kg lasting 20 minutes. The chosen model reflects the clinical manifestations of cerebral infarction and is adequate for experimental study of potential neuroprotective

Table 1. Distribution of rats by experimental groups during therapeutic administration of the studied substances.

Group of animals	Number of animals	Treatment
Group 1	10	intact rats
Group 2	10	sham-operated rats + 0.9 % sodium chloride solution, 2 ml/kg
Group 3	40	ischemia-reperfusion + 0.9 % sodium chloride solution, 2 ml/kg
Group 4	20	ischemia-reperfusion + HUC-MSCs, 106 cells/animal
Group 5	20	ischemia-reperfusion + rat embryonic fibroblasts, 106 cells/animal
Group 6	25	ischemia-reperfusion + MSCs from human adipose tissue, 106 cells/animal
Group 7	25	ischemia-reperfusion + MSCs from rat adipose tissue, 106 cells/animal
Group 8	25	ischemia-reperfusion + cell lysate from HUC-MSCs, 0.2 ml/animal
Group 9	25	ischemia-reperfusion + Citicoline, 250 mg/kg

substances [9]. Rats were separated into 9 groups (Table 1).

Group 1 included intact animals. Group 2 consisted of pseudo/sham-operated rats, which were sequentially subjected to the following interventions (anesthesia, skin incision and vessel preparation) without subsequent ligation of ICA to reduce the impact of the traumatic experimental conditions. Group 3 included rats with control pathology; they were subjected to 20-minute cerebral ischemia by ligatures placing on the ICA. In 20 minutes the ligatures were removed from the ICA (reperfusion) and a 0.9 % saline solution was injected into the femoral vein (2 ml/kg). The same dose of physiological solution was administered to group 2 rats. In the group 4 the rats were transplanted with 106 HUC-MSCs immediately after ischemia-reperfusion. In the group 5 of animals with ischemia-reperfusion a single transplantation with 106 cells/animal of rat embryonic fibroblasts was used. Group 6 of rats with ischemia-reperfusion were transplanted with 106 cells/animal derived from human adipose tissue MSCs. Group 7 of rats were injected with 106 cells/animal derived from rat adipose MSCs after ischemia-reperfusion. Group 8 of animals with ischemia-reperfusion was injected with 0.2 ml/animal of lysate derived from human Wharton's jelly MSCs. Group 9 of rats immediately after ischemia-reperfusion administered a single dose (250 mg/kg) of the reference drug citicoline "Neuroxon" (Arterium Corporation, Ukraine). Citicoline was chosen among all available drugs due to its ability to enhance neuroregenerative processes in the rat experiment and to improve cognitive and memory functions in patients with cerebral ischemia [4, 15, 24].

To analyze the influence of mesenchymal stromal cells of different origin, cell lysate from HUC-MSCs and citicoline on the dynamics of destructive changes in the CA1 area of the hippocampus, the brain of rats was removed immediately after decapitation using propofol anesthesia with an overdose of pentobarbital ("Penbital", Bioveta JSC, Czech Republic, 100 mg/kg) in 7 days (subacute period of ischemia) and 14 days (recovery period) after ischemia-reperfusion [12, 27]. The brains of rats were fixed with a 4% solution of formaldehyde within 24 hours. After fixation, the brains were washed in water, passed through ethanol of ascending concentration and xylene, and after standard histological processing, embedded in Paraplast Plus© (Leica Scientific (McCormick©), USA). The sections at 5 μm thickness were made on a rotary microtome. Deparaffinized sections were stained according to the Nissl staining method. Digital images of frontal brain sections of experimental animals obtained with a BX-51 microscope (Olympus, Japan) were analyzed using the ImageJ computer program (1.48 v software, freeware license, Rasband, USA, 2015). In hippocampal CA1 region, the total neuronal nuclei numbers per 1 mm^2 was estimated, and the ratio of the number of unchanged neuronal nuclei and nuclei with pathological changes (karyopyknosis and karyorrhexis) was also determined.

When carrying out the study, the methodological recommendations of SEC of Ministry of Health of Ukraine and bioethics requirements in relation to the National "General Ethical Principles of Experiments on Animals" approved by the First National Congress of Bioethics (Kyiv, Ukraine, 2001) and the Law of Ukraine dated 21.11.2006 No. 3447-IV "On the Protection of Animals from Cruelty" were taken into account.

Bioethics Committee of National Pirogov Memorial Medical University, Vinnytsya (protocol No. 2 dated 31.01.2024) established that the research materials do not contradict the basic moral and ethical standards of the Helsinki Declaration, the Council of Europe Convention on the Protection of Vertebrate Animals Used in the Experiment dated 18.03.1986, standards of the Directive of the Council of the European Communities 86/609/EEC dated 24.11.1986. The study is a fragment of the initiative research work "Pathogenetic substantiation of the expediency of use stem cells of various origins in the treatment of acute cerebral ischemia (experimental study)", state registration No. 0120U101861.

Statistical analysis of the obtained data was performed using Microsoft© Exel©-2010 and "Statistica 6.0" (StatSoft® Snc, USA) software. The significance of differences was assessed using the Student's t-test and unpaired nonparametric Mann-Whitney U test. Differences between the measured parameters were considered statistically significant at $p<0.05$.

Results

The lack of differences and clear visualization of all zones and layers in the hippocampus of intact and sham-operated animals during histological examination of frontal paraffin sections of rat brains identified the latter as the control group (Fig. 1).

Basal dendrites of pyramidal neurons formed the ascending layer of the CA1 zone in rat hippocampus, and pyramidal neurons' bodies - a dense layer made of 3-5 rows of pyramidal cells. Pyramidal neurons had a nucleus containing a single nucleolus and euchromatin in enough amount (see Fig. 1).

Unbranched apical dendrites of pyramidal neurons were radially oriented in the radiant layer. Their thin endings formed a lacunose-molecular layer, in which a large number of blood vessels were visualized. Blood vessels wall was formed by endotheliocytes with heterochromic nuclei.

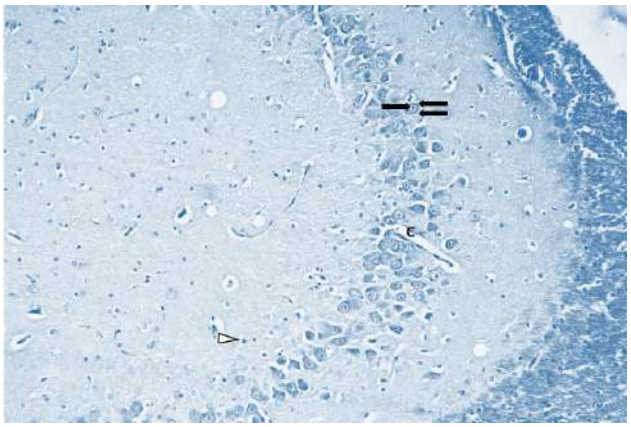

Fig. 1. The figure shows the fragment of CA1 zone in rat hippocampus in the group of pseudo-operated animals. Pyramidal neuronal nucleus is pointed out with a double arrow, while its nucleolus - with a single one. The astrocyte nucleus is shown by a white triangle. C letter indicates a blood vessel lumen. Staining according to Nissl. x200.

On day 7 after ischemia-reperfusion in the control group of rats, a visible devolution in the pyramidal layer took place in the part of the hippocampal slices made in the CA1 zone, in particular puckered hyperchromic neuronal bodies with acidophilic cytoplasm and also karyopyknosis and karyorrhexis were well visible (Fig. 2A).

It should be emphasized that intense infiltration with microglial cells took place in the pyramidal and radiant layers of the CA1 zone in the hippocampus. While the structure of the radiant layer became homogeneous, the architecture of the apical dendrites forming beams was affected (Fig. 2A). There was edema of the intercellular space, as well as pronounced perivascular edema and narrowing of the vessel lumen. In some rats with ischemia-reperfusion modeling hemorrhage and hyaline masses formation, sludge of red blood cells (RBCs) and destruction were visualized.

In fourteen days after ischemia-reperfusion modeling, degeneration of the CA1 pyramidal layer also was clear in the hippocampus (Fig. 2B). The destructive changes manifestations in the CA1 zone were analogous as that in seven days after ischemia-reperfusion injury, i.e., the structure of the radiant layer of the CA1 hippocampal zone also was connatural, intercellular edema and pronounced perivascular edema persisted, the arrangement of apical dendrites strands was affected (see Fig. 2B).

On the 7th day after HUC-MSCs transplantation to the rats with ischemia-reperfusion modeling (it's the study group 4) against the background of the above-mentioned changes found in the pyramidal layer of the CA1 zone, lots of unharmed pyramidal neurons was detected (Fig. 3A). Microglial infiltration of the radiant and pyramidal layers was almost not observed. 3-5 ordered rows of pyramidal neuronal bodies were noticed in the pyramidal layer. Midst pathologically unchanged euchromatic nuclei of pyramidal neurons having one nucleolus, there were also

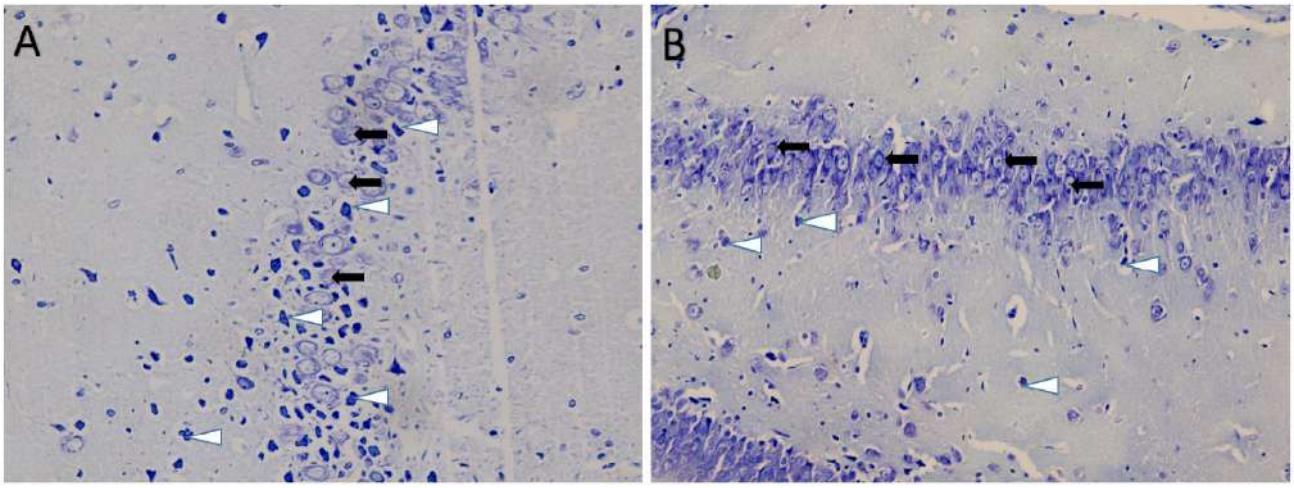

Fig. 2. The figure shows the degeneration of the pyramidal layer in the CA1 hippocampal zone on day 7 (**A**) and day 14 (**B**) after ischemia-reperfusion modeling. In neurons, their bodies are puckered and hyperchromic, their cytoplasm is acidophilic (pointed out with triangles). Separate neurons, the structure of which is preserved, are pointed out with arrows. Intercellular edema is visible. Staining according to Nissl x200.

heterochromatic and pyknotic nuclei with pronounced perinuclear edema. Apical dendrites shaped ordered strands. The vascular wall in capillaries was lined with endotheliocytes having heterochromatic nuclei. Next to some capillaries perivascular edema was visible.

On the 14th day after ischemia-reperfusion and subsequent transplantation of HUC-MSCs, in the CA 1 zone of the rat hippocampus the cytoarchitectonics was analogous to investigated on the 7th day: in particular, pyramidal neurons were orderly oriented and formed unceasing beams, euchromatin nucleoli were obvious in their nuclei (Fig. 3B). We could also see damaged hyperchromic neuronal bodies containing acidophilic cytoplasm. Apical dendrites of neurons in this layer formed radially directed unbranched structured beams and endothelial cells with heterochromatic nuclei were very noticeable in the vascular wall.

In the group of rats with ischemia-reperfusion and consequent transplantation of rat embryonic fibroblasts on the day 7 after ischemia-reperfusion modeling, both pyramidal neurons with euchromatin nuclei and one nucleolus and harmed hyperchromic neurons having karyopyknosis features and acidophilic cytoplasm took place in the hippocampal CA1 zone (Fig. 4A). The cytoarchitectonics of the radiant layer in the CA1 zone of the rat hippocampus was disturbed: the apical dendrites of neurons did not form orderly unceasing beams, narrowing

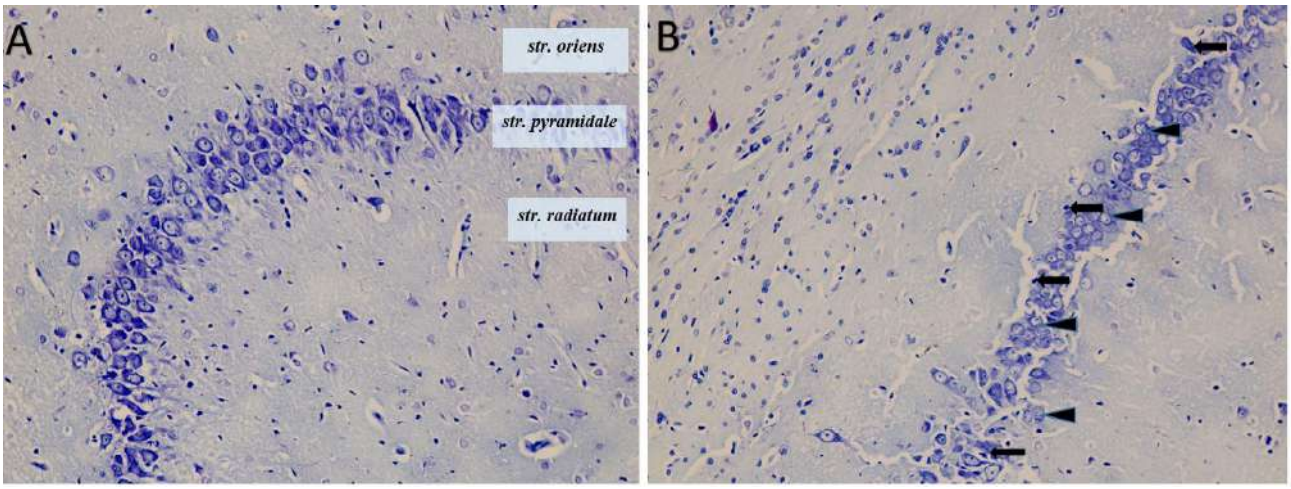

Fig. 3. A - the figure shows the pyramidal layer in the CA1 area of rat hippocampus on the day 7 after ischemia-reperfusion and consequent Wharton's jelly-derived MSCs transplantation. A considerable number of unharmed neurons is in the pyramidal layer, while radially oriented apical dendrites arrange straight beams in the radiant layer. **B** - on the figure 3B the pyramidal layer in the CA1 area on the day 14 after ischemia-reperfusion and consequent transplantation of human MSCs is given. It is clearly visible that the neuronal nuclei contain large euchromatin amount, one or two nucleoli and are well ordered forming beams. Neurons which have a preserved structure are pointed out with triangles, while the damaged hyperchromic neurons having acidophilic cytoplasm - with arrows. Staining according to Nissl. x200.

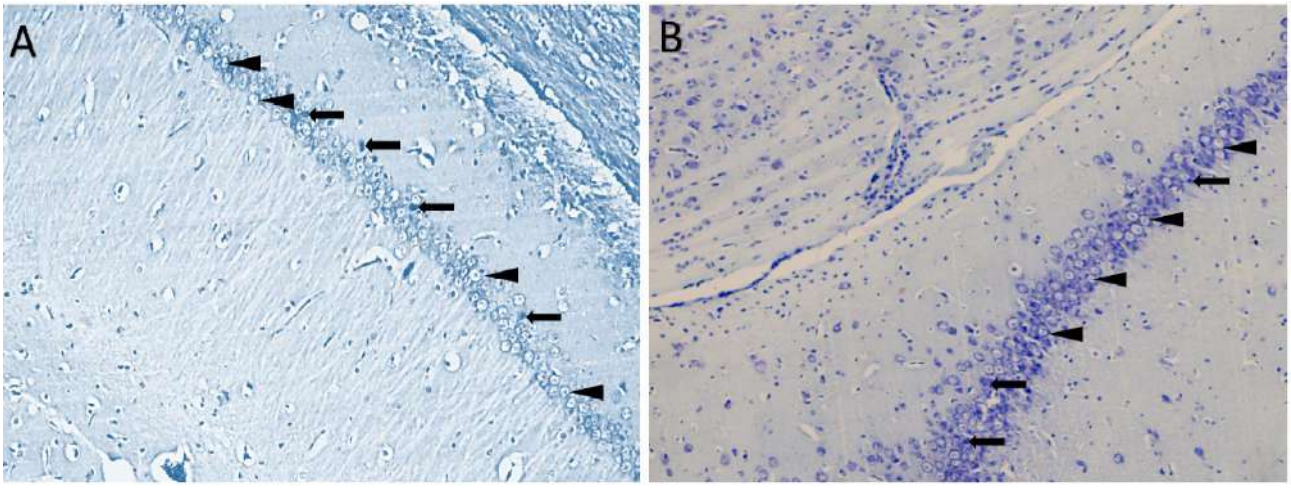

Fig. 4. A - the figure shows the pyramidal layer in the CA1 zone of the rat hippocampus on the day 7 after ischemia-reperfusion and consequent transplantation of rat embryonic fibroblasts. Pyramidal neurons containing euchromatin nuclei are pointed with triangles, and damaged hyperchromic neurons with karyopyknosis features and acidophilic cytoplasm are marked with arrows. Perivascular edema is observed. **B** - the pyramidal layer of the CA1 hippocampal zone on the day 14 after ischemia-reperfusion and consequent transplantation of rat embryonic fibroblasts. Disorganization of the radiant layer takes place. Perivascular edema persists. Stasis and RBCs sludge are observed in blood capillaries. Endotheliocytes of the capillary wall are characterized by heterochromatic nuclei. Staining according to Nissl. x200.

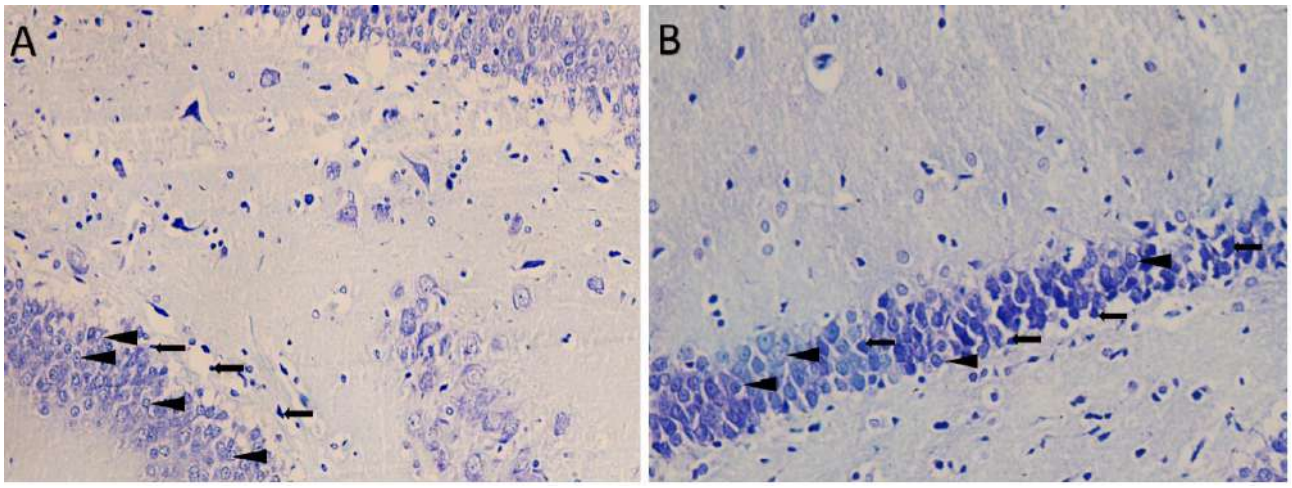

Fig. 5. The picture shows the pyramidal layer of the CA1 hippocampal zone on day 7 (**A**) and day 14 (**B**) after ischemia-reperfusion modeling and consequent MSCs transplantation of the cells obtained from human adipose tissue. Neurons with a preserved structure are pointed with triangles, while damaged ones - with arrows. Staining according to Nissl. A - x200, B - x400.

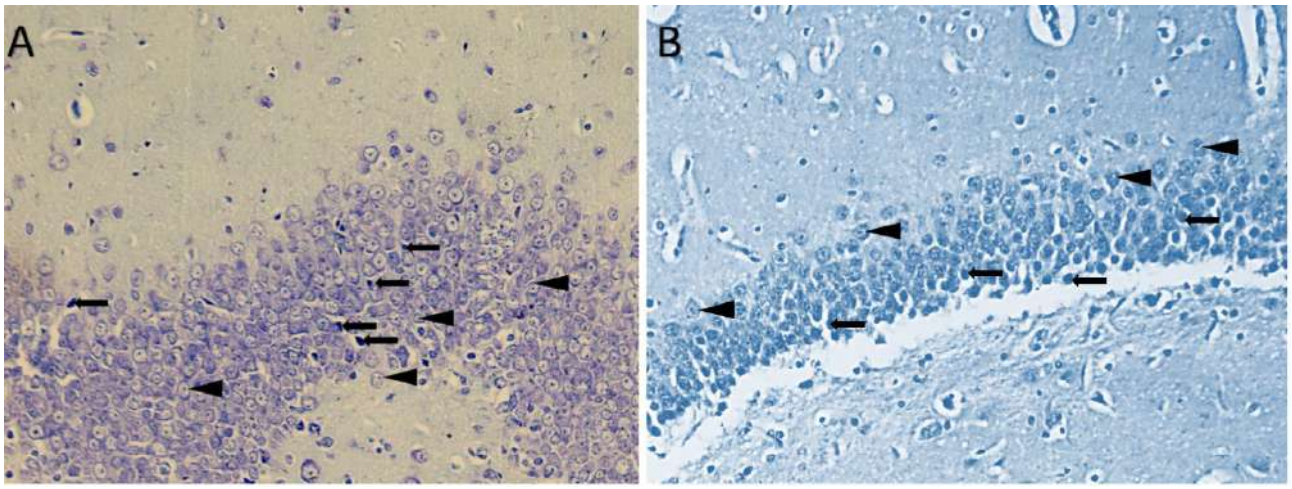

Fig. 6. The figure shows the pyramidal layer of the CA1 hippocampal zone in rats on day 7 (**A**) and day 14 (**B**) after ischemia-reperfusion followed by transplantation of stem cells obtained from rat adipose tissue. **A** - the neuronal nuclei are saturated in euchromatin and have a well-visible nucleolus. Infiltration of the pyramidal layer with microglia does not occur. Unharmed neurons are pointed out with triangles, while the damaged ones - with arrows. **B** - pyramidal neurons nuclei are saturated with euchromatin and have a well-visible nucleolus. Apical dendrites are well oriented. Intercellular swelling takes place. Unchanged pyramidal neurons are pointed out by triangles, damaged neurons - by arrows. Staining according to Nissl. x200.

of blood vessels was observed, in the lumen of which visible RBCs were, perivascular edema occurred also.

On the 14th day after ischemia-reperfusion modeling followed by rat embryonic fibroblasts transplantation in the CA1 zone of rat hippocampus pyramidal neurons were ordered forming straight beams made of some layers of pyramidal cells (Fig. 4B). Their nuclei were abundant with euchromatin, with one nucleolus. Solitary heterochromatic or bulging nuclei were between such the nuclei. The radiant layer, although it looked disorganized, but, unlike the 7th day, it showed straight beams built from apical dendrites. In a part of the blood vessels, the lumen was narrowed, perivascular edema took place.

In the group of rats with ischemia-reperfusion modeling and the subsequent transplantation of MSCs obtained from human adipose tissue on the 7th day in the CA1 hippocampal zone pyramidal neurons fit tightly to each other, forming straight beams (Fig. 5A). Neuronal nuclei with excess euchromatin and one or two nucleoli could be seen. Only solitary nuclei of pyramidal neurons demonstrated characteristics of karyopyknosis and swelling. Although the apical dendrites showed an organized structure, it was different from that of the sham-operated animals. Endothelial cells of the vascular wall had heterochromatic nuclei.

In the animals of this group, on the 14th day after ischemia-reperfusion modeling and transplantation of MSCs from human adipose tissue, pathologically unchanged nuclei of neurons were observed in the CA1 hippocampal zone, they were situated in several rows. Howsoever, considerable heterochromatization of pyramidal neuronal nuclei and nuclear swelling were occasionally (Fig. 5B).

In the radiant layer the apical dendrites formed straight beams. Intercellular swelling took place. Simultaneously, blood vessels were narrowed, inside the vessels RBC sludge was as well as accumulation of blood plasma proteins, perivascular edema also present.

In seven days after ischemia-reperfusion modeling followed by transplantation of stem cells from rat adipose tissue pyramidal neurons were arranged in a dense layer of 3-5 ordered cellular rows in the CA1 area of the rat hippocampus (Fig. 6A). Their nuclei contained a large amount of euchromatin with a well-defined nucleolus. Among pathologically unchanged euchromatic nuclei of pyramidal neurons we also could observed single heterochromatic and pyknotic ones. There was no microglial infiltration in the pyramidal layer. The capillary wall from the inside was covered with endotheliocytes with heterochromatic nuclei. In some of the capillaries perivascular edema occurred.

In fourteen days after ischemia-reperfusion modeling followed by transplantation of MSCs from rat adipose tissue pyramidal neurons in the CA1 hippocampal zone formed straight, well-ordered beams, their nuclei were euchromatic, with one nucleolus (Fig. 6B). Unitary harmed hyperchromic bodies of pyramidal cells having acidophilic cytoplasm were well visible. Most of apical dendrites were ordered, slight swelling was noticeable between them. Blood capillaries were filled with blood, endotheliocytes in the vascular wall contained heterochromatic nuclei. Perivascular edema was less intensive (compared to the day 7).

When analyzing results obtained during the examination of the rat group that received cell lysate of HUC-MSCs after ischemia-reperfusion, it was found that in seven days after treatment pyramidal neurons (in the CA1 area of rat

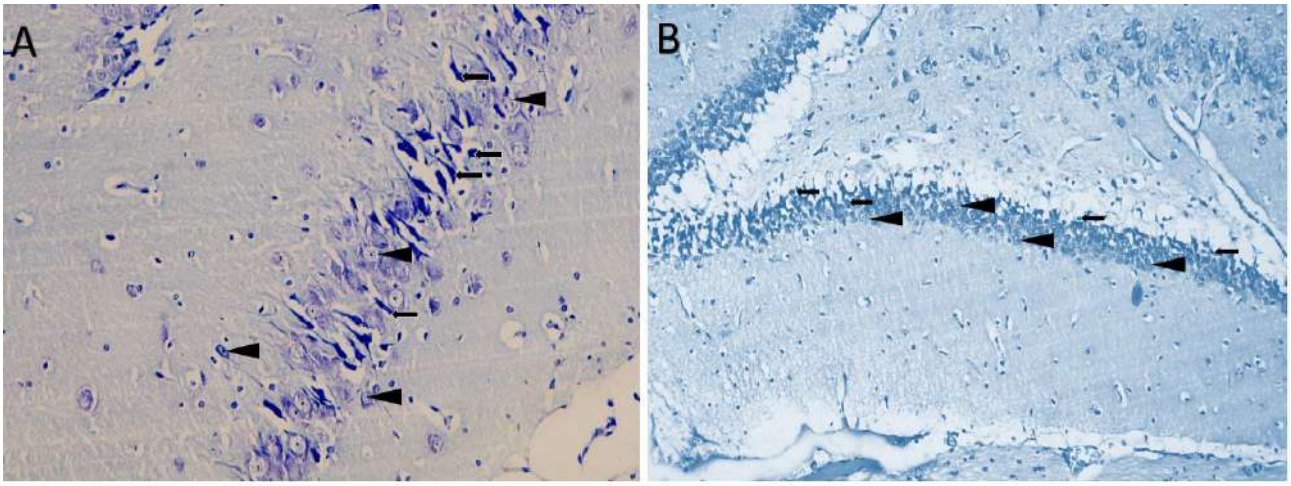

Fig. 7. The figure shows pyramidal layer in the CA1 zone of rat hippocampus on the day 7 (**A**) and day 14 (**B**) after ischemia-reperfusion modeling and subsequent HUC- MSCs lysate injection. Pyramidal neurons in the hippocampus are not situated compactly and are placed enough chaotically; unharmed neurons are pointed out with triangles, while affected hyperchromic neuronal bodies - with arrows. Staining according to Nissl. A - x400, B - x100.

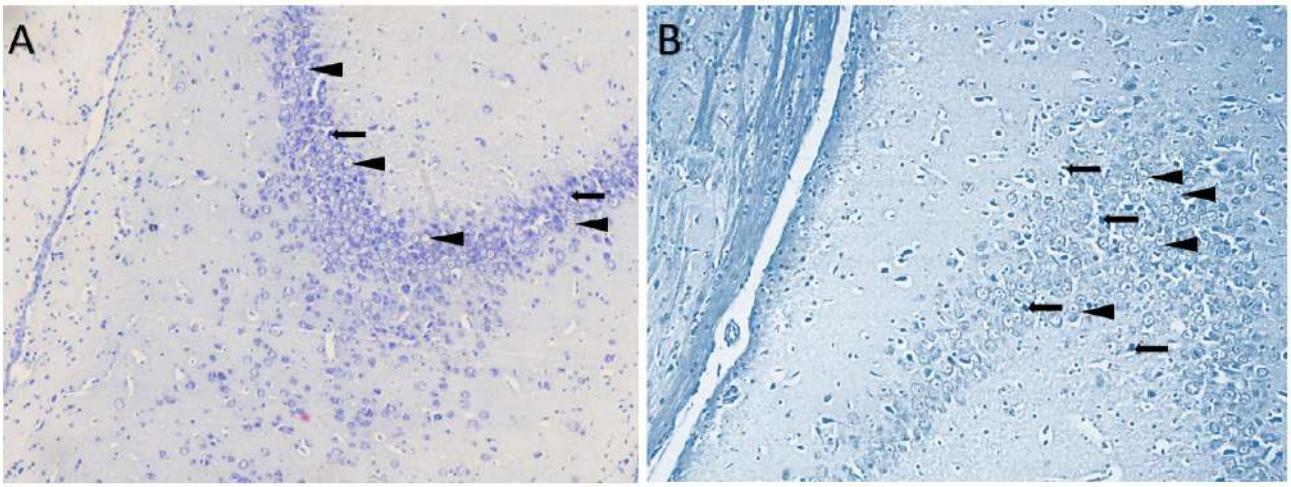

Fig. 8. The figure shows changes of the pyramidal layer in the CA1 zone of the rat hippocampus on the day 7 (**A**) and day 14 (**B**) after ischemia-reperfusion and subsequent citicoline administration. **A** - lots of neurons are affected. Homogenization as well as microvacuolation in the radiant layer is. Unharmed neurons are pointed out with triangles, while the affected hyperchromic neuronal bodies - with arrows. **B** - pyramidal neurons are situated loosely. Neurons with non-changed structure are pointed out by triangles, damaged hyperchromic neuronal bodies - by arrows. Staining according to Nissl. x200.

hippocampus) were located chaotically, in two-three layers significantly different from those in the pyramidal layer in sham-operated rats, pyramidal neurons were both hyperchromic and intact (Fig. 7A). In the radiating layer, parallelism of apical dendrites was not. The radiant layer was visualized neatly. Pyramidal and radiating layers were infiltrated with microglia. Perivascular edema was visible in some areas of the lacunose-molecular layer, the blood vessels lumen was narrowed, blood plasma proteins were accumulated in blood vessels, RBCs sludge was observed. The vascular wall contained endotheliocytes, nuclei of which were enriching in heterochromatin.

In fourteen days after ischemia-reperfusion modeling followed by administration of cell lysate of HUC-MSCs, we could observe disarrangement in the pyramidal layer of the CA1 area; it lost its density, the nervous cells were lying loosely (Fig. 7B). Hyperchromic neurons also met between the unharmed ones. Apical dendrites sent their collaterals into the radiant layer.

In seven days after ischemia-reperfusion and immediately subsequent citicoline administration in the radiant layer of the CA1 hippocampal area, alternation of homogenization with microvacuolation and normal fibrous structure were. We could see such the picture next to the layer of pyramidal cells (Fig. 8A), last one contained a lot of harmed hyperchromic neurons having acidophilic cytoplasm. Infiltration with microglia was insignificant.

In fourteen days after ischemia-reperfusion modeling and treatment with citicoline in the hippocampal CA1 region of rats, pyramidal neurons were loosely located, affected hyperchromic neurons having acidophilic cytoplasm were found enough (Fig. 8B). The rats with citicoline administration on day 14 after treatment had greater number of unharmed neurons in the pyramidal layer compared to such the group on day 7. Homogenization in the radiant layer was preserved, perivascular edema also.

When analyzing the morphometric parameters, it was established that the total number of neuronal nuclei in 1 mm^2 of the CA1 hippocampal zone in the rats with modeled ischemia-reperfusion (without treatment) compared to sham-operated animals decreased by more than 2 times and amounted to an average of 1627±179 nuclei on the 7th day and 1740±254 nuclei on the 14th day (Table 2). Most of these nuclei were subject to destruction: in the subacute follow-up period, 95.8% of the nuclei were pathologically altered (karyorrhexis and karyopyknosis), in the recovery period - 91.5%.

The use of MSCs, cell lysate of HUC-MSCs, and citicoline as a therapy for ischemia-reperfusion brain injury in rats contributed to a significant reduction of pathological damage to the nuclei of neurons in the hippocampal CA1 region, which in turn increased the number of intact neurons compared to a group of animals with control pathology. These results demonstrate the neuroprotective properties of the studied substances, among which the best protective effect on neurons during cerebral ischemia-reperfusion in rats was MSC transplantation derived from human Wharton's jelly. The number of neuronal nuclei in the hippocampal CA1 zone in this group of rats approached the number of nuclei in the group of sham-operated animals and on the 7th day after transplantation was on average 3226±260 nuclei, and on the 14th day - 3329±213 nuclei, while the number of pathologically unchanged nuclei significantly exceeded the number of nuclei with signs of destruction: on the 7th day - 90.20±12.01 and 15.60±3.51; on the 14th day - 105.20±7.40 and 16.40±7.40, respectively ($p<0.05$), compared to the control.

HUC-MSCs demonstrated a significantly better neuroprotective effect than the reference drug citicoline. Thus, in the research periods in the group of rats treated with citicoline (250 mg/kg, intravenously), significantly lower values of the intact neuronal nuclei number and higher

Table 2. Morphometric analysis of hippocampal CA1 region in rats with modeled ischemia-reperfusion.

Period	Group 2	Group 3	Group 4	Group 5	Group 6	Group 7	Group 8	Group 9
The total number of neuronal nuclei in 1 mm^2 of hippocampal CA1 region								
7th day	3977±234	1627±179*$	3226±260*#$	2773±300*#	2802±199*#	3123±242*#$	2673±182*#	2456±201*#
14th day		1740±254*$	3329±213*#$	2875±204*#	2929±204*#	3230±318*#$	2720±226*#	2553±180*#
The total number of nuclei								
7th day	128.3±9.40	23.67±7.79*	105.80±14.0*#	83.60±6.99*#$	95.40±15.45*#$	91.50±17.35*#$	89.00±9.25*#$	68.50±10.97*#
14th day		37.33±6.28*	121.60±12.30#$	88.67±3.39*#$	99.80±3.90*#$	96.83±19.59*#$	89.83±8.30*#$	79.33±4.84*#
The number of intact neuronal nuclei								
7th day	128.3±9.40	1.00±0.89*#	90.20±12.01*#$	60.00±4.30*#	70.20±1.92*#$	70.50±12.44*#$	55.33±8.59*#$	37.67±6.41*#
14th day		3.170±1.17*	105.20±7.40*#$	66.00±6.10*#	75.00±1.87*#$	76.50±14.01*#$	58.67±4.89*#$	45.50±3.27*#
The number of damaged neuronal nuclei (karyorrhexis and karyopyknosis)								
7th day	0	22.67±7.28*	15.60±3.51*$	23.60±2.88*$	25.20±13.70*	21.00±5.83*$	33.67±1.97*#	30.83±5.74*#
14th day		34.17±5.42*	16.40±7.40*#$	22.67±3.67*#$	24.80±2.77*#$	20.33±6.02*#$	31.17±5.67*	33.83±2.86*

Notes: * - $p<0.05$ relative to group 2 (sham-operated rats); # - $p<0.05$ relative to group 3 (control pathology); $ - $p<0.05$ relative to group 9 (citicoline).

pathologically changed nuclei values were observed - 30.83±5.74 on day 7 and 45.50±3.27 on day 14, compared to the group of rats that HUC-MSCs were injected (37.67±6.41 and 33.83±2.86 respectively, $p<0.05$). From the given data, it can be seen that both in the subacute and recovery periods of acute ischemic stroke in rats, transplantation of HUC-MSCs significantly exceeded the reference drug citicoline in its ability to reduce the number of pathologically altered nuclei by 1.5 times ($p<0.05$). An analogous pattern was observed when using lysate of HUC-MSCs: the ratio of the intact nuclei number to pathologically changed ones was 55.33±8.59 and 33.67±1.97 on the 7th day and 58.67±4.89 and 31.17±5.67 on the 14th day, which was significantly different from the group of animals that were injected with HUC-MSCs.

Discussion

Thus, the results of the conducted research demonstrate the presence of expressive cerebroprotective properties in MSCs (106 cells/animal, intravenously) in conditions of ischemia-reperfusion caused by acute brain ischemia. The best result among MSCs of various origins was found in HUC-MSCs. In our opinion, in the acute period of ischemia-reperfusion, MSCs contributed to preserving the area and density of intact neurons of hippocampal CA1 region due to the improvement of brain perfusion. This may occur due to the presence of a modulating effect of MSCs on the processes of necrosis and neuroapoptosis in the ischemic penumbra zone.

Cerebral ischemia-reperfusion involves many complex pathological processes, including oxidative stress, blood-brain barrier disruption, mitochondrial dysfunction, inflammation, and apoptosis, leading to neuronal cell death and impairment of sensory, motor, and cognitive functions [13].

The study demonstrated that intravenous xenogeneic and allogeneic transplantation of MSCs obtained from adipose tissue, HUC-MSCs and cell lysate of HUC-MSCs, rat embryonic fibroblasts, and citicoline in modeled ischemia-reperfusion in rats reduced the extent of ischemia-reperfusion injury of the brain.

Researchers proved that transplantation of MSCs after cerebral ischemia in animals improved brain function, effectively protected and restored neurons in ischemic-reperfusion brain damage [2, 18, 20]. This is caused by the fact that MSCs release a wide range of trophic and immunomodulatory cytokines, which are called the MSC secretome, which has significant potential for treating degenerative brain diseases through the induction of neurogenesis, angiogenesis, and endogenous neuroprotection [2, 11, 25].

MSCs derived from adipose tissue are available and easily obtained in large quantities. The effectiveness and safety of MSCs obtained from human adipose tissue in stroke treatment has been proven in many experimental studies [8]. It has been shown that MSC transplantation reduced apoptosis and loss of neurons due to their death, thereby demonstrating a significant protective effect on them through inactivation of KDM6B/BMP2/BMF in rats with cerebral ischemia [30].

In many researches, the effectiveness of HUC-MSCs in ischemic stroke has been studied. It has been reported that transplantation of HUC-MSCs into rats with ischemic stroke reduced neuroinflammation, enhanced neuroregeneration and protection of vascular endothelium, which resulted in a reduction in infarct volume [7, 23, 28, 29].

In the above-mentioned studies, the effects of MSCs obtained from a single cell culture were studied, but we compared the action of both allogeneic and xenogeneic cells obtained from two sources. Paracrine factor variations of different classes of MSCs promote various possibilities for nerve tissue recovery. MSCs derived from human Wharton's jelly or adipose tissue act differently on the population of cells of the central nervous system, in which HUC-MSCs demonstrate a more pronounced positive effect on metabolism and neurons' density in the hippocampal CA1 zone [22]. We also revealed a neuroprotective effect of MSCs lysate obtained from HUC-MSCs in animals with modeled ischemia-reperfusion of ICA. These data suggest that HUC-MSCs are an effective and safe source of therapy for experimental reversible cerebral ischemia.

In further studies, it is planned to prove the cerebroprotective effect of MSCs in ischemia-reperfusion model of the brain in rats. To identify the most effective class of stem cells in terms of neuroprotective properties among the studied MSCs, in order to subsequently create an injectable drug for intravenous transplantation in the treatment of patients with acute ischemic stroke.

Conclusions

1. Acute cerebral ischemia-reperfusion in rats in the subacute and recovery periods led to almost complete degeneration of the pyramidal layer of hippocampal CA1 region; caused the infiltration of microglia in the pyramidal and radiate layers, that disrupted the arrangement of apical dendrites bundles; formed edema surround the blood vessels with their subsequent narrowing. Also, in the studied periods of modeled ischemia-reperfusion in rats, the total number of neuronal nuclei in 1 mm^2 of hippocampal CA1 zone was significantly reduced, of which the vast majority had signs of pathological changes.

2. Mesenchymal stromal cells, cell lysate of HUC-MSCs, and citicoline have pronounced neuroprotective properties, due to a significant increase in the number of neuronal nuclei in the hippocampal CA1 region in rats and nuclei that were not pathologically altered, compared to a group of animals with ischemia-reperfusion without administered treatment. HUC-MSCs had the best neuroprotective effect among the studied stem cells and substances.

3. The use of MSCs of various genesis, lysate of HUC-MSCs, or citicoline in conditions of acute cerebral ischemia in rats caused a decrease in the volume of ischemic-reperfusion injury in the hippocampus, which may indicate the feasibility of their use in the therapy of ischemic stroke.

References

[1] Albers, G. W., Marks, M. P., Kemp, S., Christensen, S., Tsai, J. P., Ortega-Gutierrez, S., … & DEFUSE 3 Investigators (2018). Thrombectomy for Stroke at 6 to 16 Hours with Selection by Perfusion Imaging. *The New England Journal of Medicine,* 378(8), 708-718. doi: 10.1056/NEJMoa1713973

[2] Asgari Taei, A., Dargahi, L., Khodabakhsh, P., Kadivar, M., & Farahmandfar, M. (2022). Hippocampal neuroprotection mediated by secretome of human mesenchymal stem cells against experimental stroke. *CNS Neuroscience & Therapeutics,* 28(9), 1425-1438. doi: 10.1111/cns.13886

[3] Barzegar, M., Vital, S., Stokes, K. Y., Wang, Y., Yun, J. W., White, L. A., … & Alexander, J. S. (2021). Human placenta mesenchymal stem cell protection in ischemic stroke is angiotensin converting enzyme-2 and masR receptor-dependent. *Stem Cells* (Dayton, Ohio), 39(10), 1335-1348. doi: 10.1002/stem.3426

[4] Bustamante, A., Giralt, D., Garcia-Bonilla, L., Campos, M., Rosell, A., & Montaner, J. (2012). Citicoline in pre-clinical animal models of stroke: a meta-analysis shows the optimal neuroprotective profile and the missing steps for jumping into a stroke clinical trial. *Journal of Neurochemistry*, 123(2), 217-225. doi: 10.1111/j.1471-4159.2012.07891.x

[5] Chen, Y., Peng, D., Li, J., Zhang, L., Chen, J., Wang, L., & Gao, Y. (2023). A comparative study of different doses of bone marrow-derived mesenchymal stem cells improve post-stroke neurological outcomes via intravenous transplantation. *Brain Research,* 1798, 148161. doi: 10.1016/j.brainres.2022.148161

[6] Donders, R., Bogie, J. F. J., Ravanidis, S., Gervois, P., Vanheusden, M., Maree, R., … & Hellings, N. (2018). Human Wharton's Jelly-Derived Stem Cells Display a Distinct Immunomodulatory and Proregenerative Transcriptional Signature Compared to Bone Marrow-Derived Stem Cells. *Stem Cells and Development,* 27(2), 65-84. doi: 10.1089/scd.2017.0029

[7] Fu, Y. S., Yeh, C. C., Chu, P. M., Chang, W. H., Lin, M. A., & Lin, Y. Y. (2022). Xenograft of Human Umbilical Mesenchymal Stem Cells Promotes Recovery from Chronic Ischemic Stroke in Rats. *International Journal of Molecular Sciences*, 23(6), 3149. doi: 10.3390/ijms23063149

[8] Gutierrez-Fernandez, M., Otero-Ortega, L., Ramos-Cejudo, J., Rodriguez-Frutos, B., Fuentes, B., & Diez-Tejedor, E. (2015). Adipose tissue-derived mesenchymal stem cells as a strategy to improve recovery after stroke. *Expert Opinion on Biological Therapy,* 15(6), 873-881. doi: 10.1517/14712598.2015.1040386

[9] Gündüz, Z. B., Aktas, F., Vatansev, H., Solmaz, M., & Erdogan, E. (2021). Effects of amantadine and topiramate on neuronal damage in rats with experimental cerebral ischemia-reperfusion. *Advances in Clinical and Experimental Medicine: Official Organ Wroclaw Medical University,* 30(10), 1013-1023. doi: 10.17219/acem/138327

[10] He, J. Q., Sussman, E. S., & Steinberg, G. K. (2020). Revisiting Stem Cell-Based Clinical Trials for Ischemic Stroke. *Frontiers in Aging Neuroscience,* 12, 575990. doi: 10.3389/fnagi.2020.575990

[11] Hu, Y., Chen, W., Wu, L., Jiang, L., Qin, H., & Tang, N. (2019). Hypoxic preconditioning improves the survival and neural effects of transplanted mesenchymal stem cells via CXCL12/CXCR4 signalling in a rat model of cerebral infarction. *Cell Biochemistry and Function,* 37(7), 504-515. doi: 10.1002/cbf.3423

[12] Lee, M. C., Jin, C. Y., Kim, H. S., Kim, J. H., Kim, M. K., Kim, H. I., … & Woo, Y. J. (2011). Stem cell dynamics in an experimental model of stroke. *Chonnam Medical Journal*, 47(2), 90-98. doi: 10.4068/cmj.2011.47.2.90

[13] Lindsay, M. P., Norrving, B., Sacco, R. L., Brainin, M., Hacke, W., Martins, S., ... & Feigin, V. (2019). World Stroke Organization (WSO): Global Stroke Fact Sheet 2019. *International Journal of Stroke: Official Journal of the International Stroke Society*, 14(8), 806-817. doi: 10.1177/1747493019881353

[14] Martin, S. S., Aday, A. W., Almarzooq, Z. I., Anderson, C. A. M., Arora, P., Avery, C. L., … & Palaniappan, L. P. (2024). 2024 Heart disease and stroke statistics: a report of US and global data from the American Heart Association. *Circulation*, 149, e347-e913. doi: 10.1161/CIR.0000000000001209

[15] Mehta, A., Mahale, R., Buddaraju, K., Javali, M., Acharya, P., & Srinivasa, R. (2019). Efficacy of Neuroprotective Drugs in Acute Ischemic Stroke: Is It Helpful? *Journal of Neurosciences in Rural Practice,* 10(4), 576-581. doi: 10.1055/s-0039-1700790

[16] Ministry of Health of Ukraine. (2023). Наказ МОЗ України "Про затвердження Порядку організації надання медичної допомоги пацієнтам із гострим мозковим інсультом" від 15.06.2023 р. № 1091 зі змінами від 07.07.2023 № 1239 [Order of the Ministry of Health of Ukraine "On approval of the Procedure for providing medical care to patients with acute cerebral stroke" dated June 15, 2023 № 1091 with changes from July 7, 2023 № 1239]. URL: https://zakon.rada.gov.ua/laws/show/z1118-23#Text

[17] Ministry of Health of Ukraine. (2024). У 2024 році лікування гострого мозкового інсульту є пріоритетом в програмі медичних гарантій [In 2024, the treatment of acute stroke is a priority in the medical guarantee program]. Retrieved from: https://krml3.lic.org.ua/novyny/bezoplatna-diahnostyka-ta-likuvannia-insultu-u-2024-rotsi/

[18] Moisan, A., Favre, I., Rome, C., De Fraipont, F., Grillon, E., Coquery, N., … & Detante, O. (2016). Intravenous Injection of Clinical Grade Human MSCs After Experimental Stroke: Functional Benefit and Microvascular Effect. *Cell Transplantation,* 25(12), 2157-2171. doi: 10.3727/096368916X691132

[19] Nam, H. S., Kwon, I., Lee, B. H., Kim, H., Kim, J., An, S., ... & Heo, J. H. (2016). Effects of mesenchymal stem cell treatment on the expression of matrix metalloproteinases and angiogenesis during ischemic stroke recovery. *PLoS One* 11(1), e0144218. doi: 10.1371/journal.pone.0146628

[20] Namestnikova, D. D., Gubskiy, I. L., Cherkashova, E. A., Sukhinich, K. K., Melnikov, P. A., Gabashvili, A. N., … & Yarygin, K. N. (2023). Therapeutic Efficacy and Migration of Mesenchymal Stem Cells after Intracerebral Transplantation in Rats with Experimental Ischemic Stroke. *Bulletin of Experimental Biology and Medicine*, 175(1), 116-125. doi: 10.1007/s10517-023-05822-1

[21] Paul, S., & Candelario-Jalil, E. (2021). Emerging neuroprotective strategies for the treatment of ischemic stroke: An overview of clinical and preclinical studies. *Experimental Neurology,* 335, 113518. doi: 10.1016/j.expneurol.2020.113518

[22] Ribeiro, C. A., Fraga, J. S., Grãos, M., Neves, N. M., Reis, R. L., Gimble, J. M., … & Salgado, A. J. (2012). The secretome of stem cells isolated from the adipose tissue and Wharton jelly acts differently on central nervous system derived cell populations. *Stem Cell Research & Therapy,* 3(3), 18. doi: 10.1186/scrt109

[23] Russo, E., Lee, J. Y., Nguyen, H., Corrao, S., Anzalone, R., La

Rocca, G., & Borlongan, C. V. (2020). Energy Metabolism Analysis of Three Different Mesenchymal Stem Cell Populations of Umbilical Cord Under Normal and Pathologic Conditions. *Stem Cell Reviews and Reports,* 16(3), 585-595. doi: 10.1007/s12015-020-09967-8

[24] Secades, J. J., & Gareri, P. (2022). Citicoline: pharmacological and clinical review, 2022 update. Citicolina: revisión farmacológica y clinica, actualización 2022. *Revista de neurologia*, 75(s05), S1-S89. doi: 10.33588/rn.75s05.2022311

[25] Son, J. W., Park, J., Kim, Y. E., Ha, J., Park, D. W., Chang, M. S., & Koh, S. H. (2019). Glia-Like Cells from Late-Passage Human MSCs Protect Against Ischemic Stroke Through IGFBP-4. *Molecular Neurobiology,* 56(11), 7617-7630. doi: 10.1007/s12035-019-1629-8

[26] Stokum, J. A., Gerzanich, V., & Simard, J. M. (2016). Molecular pathophysiology of cerebral edema. *Journal of Cerebral Blood Flow and Metabolism: Official Journal of the International Society of Cerebral Blood Flow and Metabolism*, 36(3), 513-538. doi: 10.1177/0271678X15617172

[27] Toyoshima, A., Yasuhara, T., Kameda, M., Morimoto, J., Takeuchi, H., Wang, F., … & Date, I. (2015). Intra-Arterial Transplantation of Allogeneic Mesenchymal Stem Cells Mounts Neuroprotective Effects in a Transient Ischemic Stroke Model in Rats: Analyses of Therapeutic Time Window and Its Mechanisms. *PloS One,* 10(6), e0127302. doi: 10.1371/journal.pone.0127302

[28] Wu, K. J., Yu, S. J., Chiang, C. W., Lee, Y. W., Yen, B. L., Hsu, C. S., … & Wang, Y. (2018). Wharton' jelly mesenchymal stromal cell therapy for ischemic brain injury. *Brain Circulation,* 4(3), 124-127. doi: 10.4103/bc.bc_16_18

[29] Zhang, L., Wang, L. M., Chen, W. W., Ma, Z., Han, X., Liu, C. M., … & Zhang, X. H. (2017). Neural differentiation of human Wharton's jelly-derived mesenchymal stem cells improves the recovery of neurological function after transplantation in ischemic stroke rats. *Neural Regeneration Research,* 12(7), 1103-1110. doi: 10.4103/1673-5374.211189

[30] Zhang, Y., Liu, J., Su, M., Wang, X., & Xie, C. (2021). Exosomal microRNA-22-3p alleviates cerebral ischemic injury by modulating KDM6B/BMP2/BMF axis. *Stem Cell Research & Therapy,* 12(1), 111. doi: 10.1186/s13287-020-02091-x

ТЕРАПЕВТИЧНИЙ ПОТЕНЦІАЛ МЕЗЕНХІМАЛЬНИХ СТРОМАЛЬНИХ КЛІТИН НА МОРФОЛОГІЧНІ ПОКАЗНИКИ У ГІПОКАМПІ ЩУРІВ ІЗ МОДЕЛЬНОЮ ІШЕМІЄЮ-РЕПЕРФУЗІЄЮ ГОЛОВНОГО МОЗКУ

Коновалов С. В., Мороз В. М., Йолтухівський М. В., Гаджула Н. Г., Гусакова І. В., Дерябіна О. Г., Кордюм В. А.

Ішемічний інсульт є вкрай важливою патологією з високою летальністю, при якій понад 50 % хворих з оклюзією магістральних судин залишаються інвалідами, незважаючи на якомога ранню реперфузійну терапію шляхом тромболізису чи тромбектомією. У рамках регенеративної стратегії новим поштовхом стала трансплантація стовбурових клітин при ішемічному інсульті. Обнадійливі результати щодо ендогенних механізмів нейровідновлення у відповідь на ішемічне пошкодження структур головного мозку продемонструвала клітинна терапія з використанням мезенхімальних стромальних клітин. Мета дослідження - вивчення впливу МСК різного походження, лізату МСК отриманих із Вартонових драглів пуповини людини та цитиколіну на динаміку морфологічних змін у зоні СА1 гіпокампа щурів із гострою церебральною ішемією-реперфузією за даними світлової мікроскопії та мікроморфометрії. Експеримент проведено з використанням 200 самців щурів лінії Вістар, яким здійснено ішемію-реперфузію шляхом оборотної 20-и хвилинної білатеральної оклюзії внутрішніх сонних артерій. Тваринам із модельованою патологією внутрішньовенно трансплантували МСК різного походження (з Вартонових драглів пуповини людини, з жирової тканини людини та щура), вводили ембріональні фібробласти щура, лізат МСК із Вартонових драглів людини, цитиколін. Гістологічний аналіз зрізів головного мозку щурів проводили на 7 та 14 добу експерименту. Статистичну обробку виконували за допомогою "Statistica 6.0" (StatSoft® Snc, США). Достовірність відмінностей визначали з використання t-критерію Ст'юдента, непараметричного U критерію Манна-Уітні. Під час дослідження встановлено, що модельна ішемія-реперфузія у щурів викликала майже повну дегенерацію пірамідного шару СА1 зони гіпокампу та надала однорідності структури променистому, інфільтрацію мікроглії, порушення розташування тяжів апікальних дендритів, звуження кровоносних судин у наслідок периваскулярного набряку. Також, змодельована патологія зменшувала загальну кількість ядер нейронів СА1 зони гіпокампа, переважна більшість з яких мали ознаки патологічних змін. Трансплантація мезенхімальних стромальних клітин різного походження, лізату мезенхімальних стромальних клітин та цитиколіну сприяли достовірному збільшенню кількості ядер нейронів у СА1 зоні гіпокампа та ядер, які не зазнавали патологічних змін. Найкращий позитивний ефект виявлено при трансплантації мезенхімальних стромальних клітин із Вартонових драглів людини. Таким чином, як у підгострому, так і відновлювальному періодах ішемічного інсульту в щурів, трансплантація мезенхімальних стромальних клітин Вартонових драглів людини вірогідно перевершувала референс-препарат цитиколін за здатністю зменшувати кількість патологічно змінених ядер у 1,5 рази (p<0,05). При цьому кількість патологічно неушкоджених ядер значно перевищувала кількість ядер з ознаками каріорексису та каріопікнозу, тому доцільно було б застосовувати мезенхімальні стромальні клітини різного походження, лізат або цитиколін в умовах гострої ішемії-реперфузії головного мозку, враховуючи їх здатність зменшувати обсяг інфаркту. У подальшому буде створений ін'єкційний препарат, із найбільш ефективної за церебропротекторними властивостями культури мезенхімальних стромальних клітин для клітинної терапії хворих на гострий ішемічний інсульт.

Ключові слова: *мезенхімальні стромальні клітини, нейрони, гіпокамп, ішемія-реперфузія, щури.*

Author's contribution

Konovalov S. V. - conceptualization, research, methodology and writing of the original draft, data visualization, resources, software.
Moroz V. M. - conceptualization, formal analysis and validation, supervision, project administration.
Yoltukhivskyi M. V. - conceptualization, project administration, review writing and editing.
Gadzhula N. G. - formal analysis and validation, writing the article, editing.
Gusakova I. V. - writing the article.
Deryabina O. G. - formal analysis and validation, editing.
Kordium V. A. - conceptualization, formal analysis and validation.

DOI: 10.31393/morphology-journal-2024-30(3)-07 Reports of Morphology, Vol. 30, №3, Pages 63-79

ISSN 1818-1295 eISSN 2616-6194

REPORTS OF MORPHOLOGY

Official Journal of the Scientific Society of Anatomists, Histologists, Embryologists and Topographic Anatomists of Ukraine

journal homepage: https://morphology-journal.com

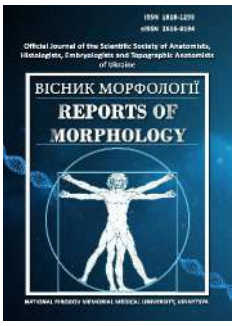

The morphological structure of prostate gland under the condition of experimental prostatopathy and after using of cholecalciferol in the different schemes of hypofertility correction

Marakhovskyi I. O., Smolienko N. P., Korenieva Ye. M., Bielkina I. O., Brechka N. M., Boiko M. O., Laryanovska Yu. B., Bondarenko V. O.

SI "V. Danilevsky Institute for Endocrine Pathology Problems of NAMS of Ukraine", Kharkiv, Ukraine

ARTICLE INFO

Received: 19 February 2024

Accepted: 02 August 2024

UDC: 616-03/
612.61:616.6+616.69:611.018

CORRESPONDING AUTHOR

e-mail: ihor1marahovskiy@gmail.com
Marakhovskyi I. O.

CONFLICT OF INTEREST

The authors have no conflicts of interest to declare.

FUNDING

The work was carried out in accordance with the scientific of the SI "V. Danilevsky Institute for Endocrine Pathology Problems of the National Academy of Medical Sciences of Ukraine": "Determination of the role of vitamin D deficiency in the development of genital gland dysfunction, justification of approaches to their therapy" (state registration number - 01179U102381). The institution that finances the study is the National Academy of Medical Sciences of Ukraine.

DATA SHARING

Data are available upon reasonable request to corresponding author.

The impact of negative factors, stress, and modern living conditions damages men's health and leads to infertility. Prostatitis is often a cause of hypofertility. It is now shown that vitamin D may play a role in regulating the functioning of reproductive system organs. The aim of the study was to determine the effect of cholecalciferol on the histological structure of the prostate gland in rats with experimental prostatitis and after its application alone or in combination with a prostate protector. Experimental prostatitis was induced by cold intraoperative damage to the prostate gland. To correct prostatitis, vitamin D_3 (cholecalciferol) was administered orally at a dose of 4000 IU. The prostate protector (Prostatilen, Pr) and its pharmaceutical composition, as well as vitamin $D3_3$, were administered rectally. Rats with modeled prostatitis were divided into groups: EP (cold experimental prostatitis without treatment); EP + seed oil (on the background of experimental prostatitis, animals received a solvent - apricot kernel oil); EP + vit D_3 (per os) (on the background of experimental prostatitis, animals received vitamin D_3); EP + Pr (rec) (on the background of experimental prostatitis, males were administered Prostatilen per rectum); EP + vit. D_3 (per os) + Pr (rec) (on the background of experimental prostatitis, animals received vitamin D_3 (per os) and Prostatilen gel (per rectum)); EP + (vit. D_3 + Pr) (rec) (on the background of experimental prostatitis, rats were administered Prostatilen gel with vitamin D3 per rectum). Intact animals (Intact group) and sham-operated rats (Control group) were used as controls. Paraffin sections of the prostate gland were stained with hematoxylin, eosin, and Van Gieson's method. In addition to the review microscopy of the ventral lobes of the prostate gland and the isthmus between them, the power of histochemical reactions was measured, the severity of inflammation and fibrosis was assessed, the number of terminal sections of the prostatic glands with a visually unchanged state, with lumen expansion, and with wall destruction was counted, the longitudinal diameter of the acini and the height of the epithelial cells of the prostatic glands were measured. Statistical analysis of the results was performed using the standard software package "Statistica 6.0" with the use of Student's t-test and nonparametric analog of one-way analysis of variance - Kruskal-Wallis test, as well as Mann-Whitney test. It was found that rats with experimental prostatitis exhibit pronounced changes in the morphological structure of the prostate gland. The prostate-protective effect of vitamin D per os at a dose of 4000 IU was established, which reduced the manifestations of atrophic and destructive processes, signs of tissue inflammation, and coarsening of the prostate gland stroma. Signs of fibrosis development in the prostate gland in males of this group were reduced, and the number of destructive changes and the longitudinal diameter of the terminal sections of the prostatic glands of prostate ventral lobe in rats with experimental prostatitis were decreased. Thus, the addition of cholecalciferol to the basic therapy for infertility has a more pronounced corrective effect on the morphological structure of the prostate than the separate use of cholecalciferol and the prostate protector. Combining basic therapy with vitamin D enhances the prostate-protective properties of the latter and is promising for restoring reproductive function overall.

Keywords: *vitamin D, histostructure, morphometric indices, cholecalciferol, prostate gland, prostatitis.*

Introduction

Reduced fertility is not only a significant medical issue but also a major social problem that affects individuals, their families, and society as a whole. The relevance of this topic is driven by the increasing cases of infertility [1, 4, 12], which are rapidly rising during wartime and are likely to continue growing in the post-war period. This concerns all men, especially combatants and veterans. The problem is associated with the impact of numerous additional negative factors, including stress and modern living conditions, which damage men's health [17].

The prostate gland (PG) plays a significant role in maintaining reproductive ability [25], which makes the treatment of PG disorders one of the main directions in urology and andrology. Chronic prostatitis affects 30 % to 45 % of men of various ages. Restoring PG function is essential because this pathology can lead to generative problems [7] and the development of erectile dysfunction [8]. It is well known that the PG is a target organ for sex hormones, and changes in their blood levels affect its structural and functional state [8]; conversely, prostatopathies are often associated with impaired reproductive function and lead to hypofertility [9, 25]. As an accessory sex gland, the PG has endocrine functions, participating in converting the primary male sex hormone into dihydrotestosterone, and exocrine functions, responsible for secreting prostate fluid enriched with proteins, enzymes, lipids, and metal ions. The PG secretion protects sperm, reduces urethral acidity, and enhances sperm motility. The PG enzyme, prostatic acid phosphatase, participates in sperm nutrition. The PG also secretes high levels of zinc, which is believed to promote sperm viability [6]. Thus, the prostate's condition can affect the functioning of sex cells and, consequently, male fertility. Prostate inflammation negatively impacts fertility, while the central role of $Zn^{(2+)}$ and its citrate $Zn^{(2+)}$ helps regulate epithelial homeostasis and ejaculation function [25].

Despite the wide range of pharmaceutical drugs and various treatment protocols, managing prostatitis and its associated conditions remains a pressing issue today. Notably, research has emerged demonstrating the effectiveness of vitamin D. Despite its historical designation, vitamin D is not actually a vitamin but a hormone; in its activated state, it is a metabolically active steroidal, fat-soluble hormone (hormone D) in reproductive endocrinology [11]. This is due to the presence of its receptors in almost all tissues of the reproductive tract, enabling it to directly participate in their function, including the prostate [5, 10, 18].

Prostatopathy not only disrupts prostate function but also alters its morphological structure [9]. Therefore, it was crucial to study the histological structure of the PG under pathological conditions and its changes due to experimental correction with vitamin D, as well as to evaluate the effect of Prostatilen, a basic therapy drug for prostatitis known to positively influence spermatogenesis.

The above factors determined the study's objective - to assess the impact of cholecalciferol on the histological structure of the prostate gland in rats with experimental prostatitis and after its administration alone or in combination with a prostate protector.

Materials and methods

The effect of cholecalciferol on the morphological structure of the prostate gland was studied in sexually active seven-month-old Wistar rats weighing 250-300 g when used alone or in combination with a prostate protector under conditions of impaired reproductive function induced by experimental prostatitis (EP).

The study adhered to the national "General Ethical Principles of Animal Experiments" (Ukraine, 2001), which comply with the "European Convention for the Protection of Vertebrate Animals used for Experimental and other Scientific Purposes" (Strasbourg, 1985) [22], Protocol No. 3 of the meeting of Bioethics Commission No. 2 of the State Institution SI "V. Danilevsky Institute for Endocrine Pathology Problems of NAMS of Ukraine" dated May 10, 2023. Rats were kept under standard vivarium conditions with natural lighting, room temperature, unlimited access to drinking water, and a diet recommended for this species [14].

Experimental prostatitis was modeled by cryoinjury of the ventral part of the prostate gland using a Wartner cryo-device (manufactured by Omega Pharma International, Belgium) for 5 seconds. The treatment, lasting 21 days, began two weeks after the operation.

The Department of Pharmaceutical Technology of Medicines of the Laboratory of Analytical and Physicochemical Research of the State Institution SI "V. Danilevsky Institute for Endocrine Pathology Problems of NAMS of Ukraine" developed and produced new dosage forms of known active pharmaceutical ingredients. Solutions of vitamin D_3 (cholecalciferol) in apricot kernel oil were prepared from vitamin D_3 powder (China, batch CHG20062009, quality standard GB 9840-2017). As a comparison drug, 0.5 % rectal gel Prostatilen (Pr) was used, which, according to the patent, was made from the lyophilisate of bull prostate extract (Prostatilen-Biopharma lyophilisate for injections).

Vitamin D_3 (cholecalciferol) was administered orally at a dose of 4000 IU. The reference drug Prostatilen and the pharmaceutical composition with Prostatilen and vitamin D_3 were administered rectally in a volume of 0.5 ml using a medical catheter with a diameter of 3 mm into the upper rectum at a depth of 20-25 mm from the anus.

Rats with modeled prostatitis were divided into groups: EP (rats with cold experimental prostatitis without treatment, n=5), EP + seed oil (rats with experimental prostatitis receiving the solvent - apricot kernel oil), EP + vit. D_3 (*per os*) (rats with experimental prostatitis receiving vitamin D_3, n=7), EP + Pr (rec) (males with experimental prostatitis

receiving Prostatilen *per rectum*, n=10), EP + vit. D_3 (*per os*) + Pr (rec) (rats with experimental prostatitis receiving vitamin D_3 per os and Prostatilen gel *per rectum*, n=7), EP + (vit. D_3 + Pr) (rec) (rats with experimental prostatitis receiving Prostatilen gel with vitamin D_3 *per rectum*, n=8). Intact animals (Intact group, n=5) and sham-operated rats (Control group, n=11) were used as controls.

After euthanizing the animals through rapid decapitation, the prostate gland was removed and fixed in 10 % formalin. The material was subsequently dehydrated in alcohols of increasing strength and embedded in paraffin. Sections of 6-7 μm thickness were made from paraffin blocks using an MC-1 sledge microtome, mounted on glass slides, and stained with hematoxylin, eosin, and Van Gieson stains [3, 23]. In addition to general microscopy of the ventral lobe and the isthmus of the prostate gland, the following morphometric measurements were performed: 1) inflammation and fibrosis were assessed using a 4-point scale (based on a semi-quantitative visual evaluation of the histochemical reaction intensity according to Sokolovsky's method): 0 points - no signs; 1 point - mild signs; 2 points - moderate signs; 3 points - pronounced signs; 2) the number of terminal sections of prostatic glands with visually unchanged state, lumen dilation, and wall destruction were counted in the microscope field (lens 10, eyepiece 10) in several repeated consecutive fields of view; 3) the longitudinal diameter of the acini of the prostatic glands and the height of the epithelial cells lining their walls (μm) were measured on images of the studied areas of glandular parenchyma (eyepiece 10, lens 20) using the Toupcam Granum program [13, 16, 19].

The type of crystallization of the prostate fluid was determined based on gland impressions according to the method of Vartapetov B. A. and Demchenko O. M. [24]. Assessment of the "fern leaf" phenomenon allows for indirect evaluation of the androgen saturation level of the body.

A Granum L 30 (03) light microscope was used to examine the slides. Microscopic images were photographed with a Granum DCM 310 digital camera. Photographs were processed on a Pentium 2.4 GHz computer using the Toup View program.

Statistical analysis of the results was conducted using the "Statistica 6.0" software package with Student's t-test and the non-parametric analog of one-way analysis of variance, the Kruskal-Wallis test, and the Mann-Whitney test for qualitative and quantitative parameters [15].

Results

In the control group animals (sham-operated animals without cold injury to the prostate), as in intact males, the parenchyma of the ventral lobe and the isthmus zone between the ventral parts of the PG consisted of acini (terminal sections) of prostatic glands, predominantly oval or round in shape with clear contours and adequately tense walls.

The epithelium lining the walls is a single-layered high cuboidal or columnar epithelium, forming relatively small and infrequent folds in some acini (located closer to the isthmus between the ventral parts). The nuclei of epithelial cells are positioned basally, and the acinar lumens often contain an eosinophilic homogeneous secretion, which partially or fully fills the lumen. The density of acini of the prostatic glands and the presence of loose unstructured interacinar stroma depend on the location of the glands - whether in the lobe or the isthmus between the lobes (see Fig. 1, 2).

In the interacinar tissue, few cellular elements and blood

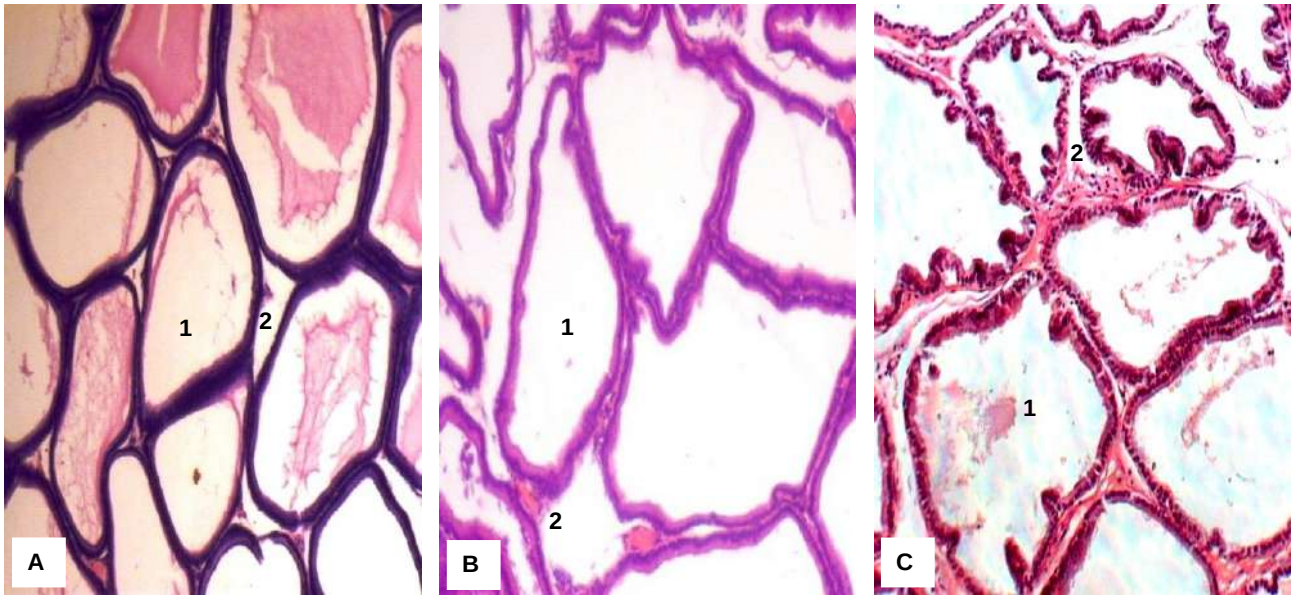

Fig. 1. Prostate gland of intact rats: A - central zone of the ventral lobe; B, C - isthmus zone. 1 - acini of the prostatic glands. 2 - interacinar stroma. A, B - hematoxylin-eosin staining, C - Van Gieson's picrofuchsin staining. x100.

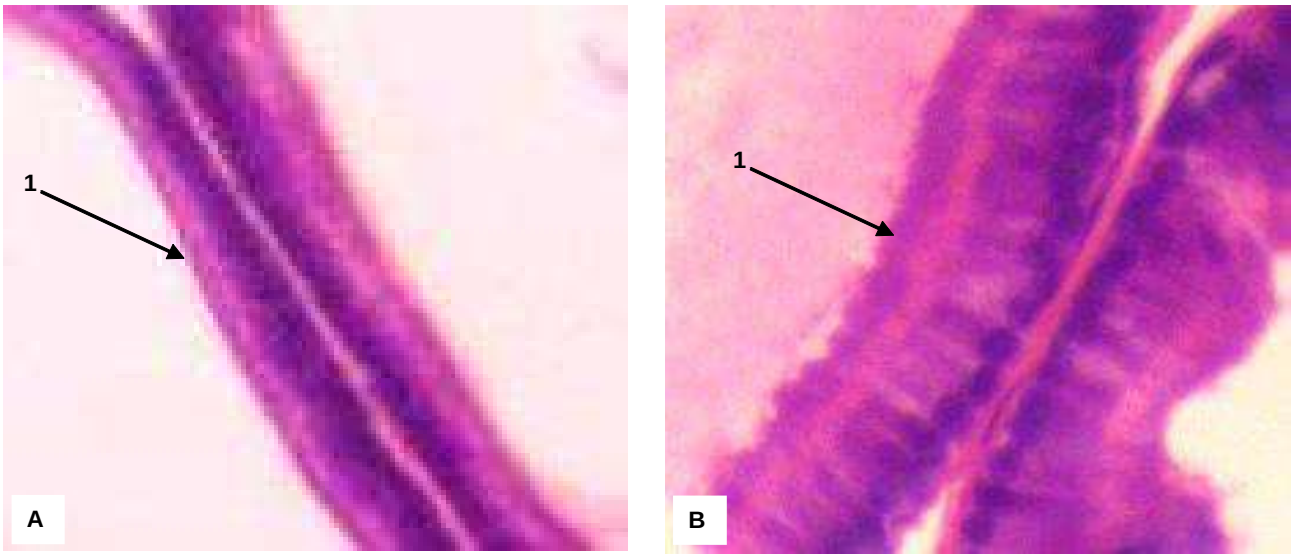

Fig. 2. Prostate gland of intact rats: A - central zone of the ventral lobe; B - isthmus zone. Typical height of the epithelial cells (1, arrows) lining the walls of the acini. Hematoxylin-eosin staining. x400.

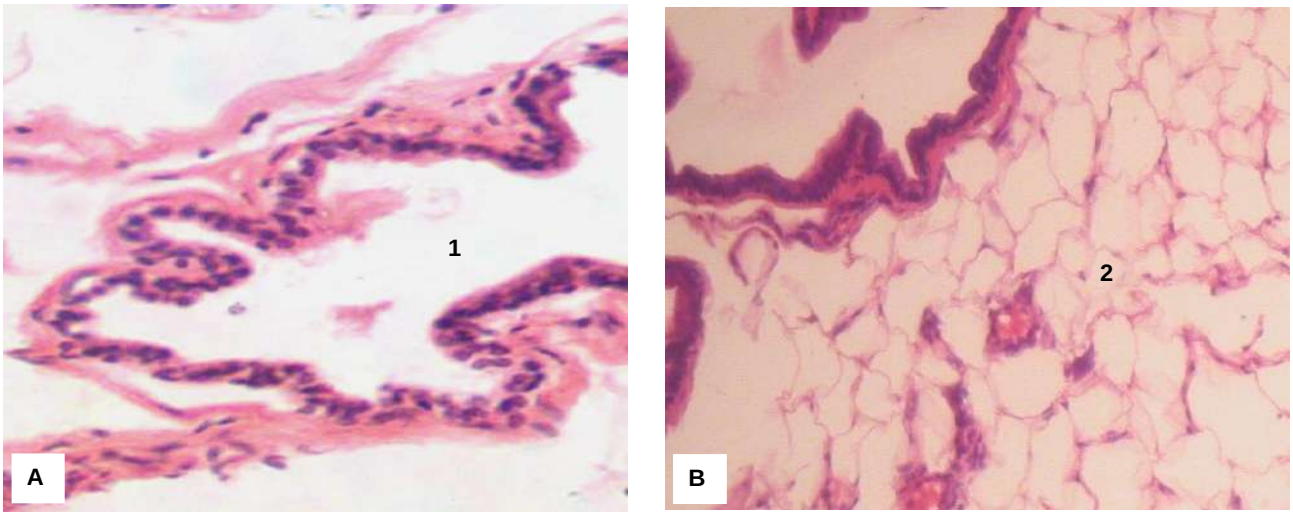

Fig. 3. Prostatic gland of intact rats: A - excretory duct (1) x400; B - paraprostatic adipose tissue (2), x200. Hematoxylin-eosin staining.

vessels are visible. Among the terminal sections of the glands, cross-sectional profiles of the prostatic ducts of varying sizes are often observed. The lumen of the ducts is sufficiently wide, and the epithelial cells lining their walls are cuboidal, arranged in several rows. The connective tissue around the ducts is moderately expressed. The serous-adipose tissue surrounding the gland remains unchanged (Fig. 3).

According to morphometric data, in the Intact and Control groups of rats, the central zone of the ventral part of the prostate gland predominantly consisted of unchanged terminal segments of prostatic glands (95.4% and 94.4%, respectively). The remaining acini had distended walls. In the isthmus zone, unchanged acini made up nearly 92.0%, with distended acini accounting for 6.2% and 7.1%, respectively. No destructively altered acini were detected. The average longitudinal diameter of the glandular acini in these areas was 81.97-85.34 μm. The height of the epithelial cells in the walls of the terminal segments of the glands was 9.285-9.437 μm (Fig. 4, 5).

In conditions of experimental prostatitis and cholecalciferol administration, changes in the histological structure of the prostate gland were observed. Twenty-eight days after cryogenic injury of the acini, most of the prostatic glands were significantly distended. The epithelial folds were less noticeable or completely absent, with a significantly thickened colloid often filling nearly the entire lumen of the acini. The walls of some terminal segments of the acini were focally destroyed, with dense protein masses mixed with clusters of macrophage-like cells nearby (Fig. 6).

Only a small portion of the terminal sections of the prostatic glands in the isthmus zone remained nearly unchanged. The epithelium lining the walls of the acini in

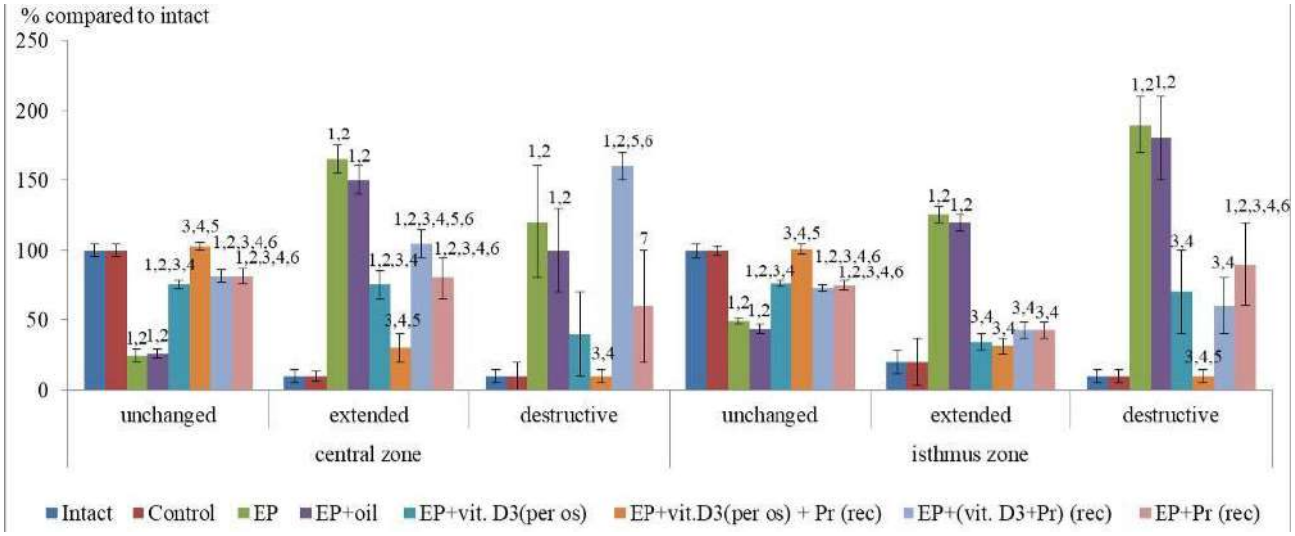

Fig. 4. Effect of cholecalciferol on the condition of terminal segments of prostatic glands in the ventral part of the PG in experimental rats.
Notes: here and in the next graph, 1 - statistically significant differences compared to the Intact group, p<0.05; 2 - statistically significant differences compared to the Control group, p<0.05; 3 - statistically significant differences compared to the EP group, p<0.05; 4 - statistically significant differences compared to the EP+oil group, p<0.05; 5 - statistically significant differences compared to the EP+vit.D_3 (*per os*) group, p<0.05; 6 - statistically significant differences compared to the EP+vit.D_3 (*per os*)+Pr (rec.) group, p<0.05; 7 - statistically significant differences compared to the EP+(vit.D_3+Pr) (rec.) group, p<0.05.

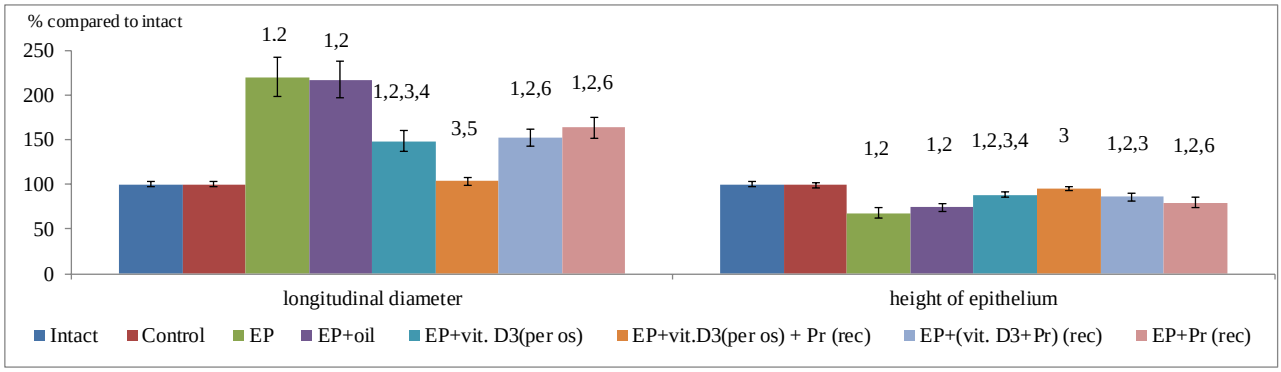

Fig. 5. Morphometric parameters of terminal segments of prostatic glands and semi-quantitative assessment of the condition of the interacinar stroma in the ventral part of the prostate gland in rats with experimental prostatitis.

the central zones of the lobe was flattened or low cuboidal. In the acini of the isthmus zone, the reduction in epithelial height was less pronounced; however, many acini showed epithelial cells with signs of vacuolar degeneration. The epithelium of the prostatic gland ducts was noticeably proliferated, with a narrowed lumen visible in some ducts (Fig. 7).

The interstitial stroma is locally swollen, infiltrated with proteinaceous material, and frequently shows focal productive inflammatory reaction. Among the inflammatory cells, lymphocytes, plasma cells, smooth muscle cells, and macrophages were visualized. There is often marked thickening of the interstitial stroma, with an increase in collagen content - signs of fibrosis. The collagen fibers are quite fuchsinophilic, often organized into small, moderately thick bundles (Fig. 8).

In the interstitial stroma, there are occasional remnants of hemorrhage in the form of hemolyzed erythrocytes; blood capillaries are engorged, and the walls of some blood vessels are thickened. In the lumen of isolated acini in the isthmus zone, among desquamated epithelial cells and colloid-like masses, rounded formations with acidophilic content - so-called amyloid bodies, which are precursors to prostatic concretions - are visible. In some rats, a productive inflammatory reaction was observed in the periprostatic adipose tissue (Fig. 9).

Our visual observations were confirmed by morphometric data. In both studied zones, the proportion of prostatic glands with unchanged terminal segments decreased to 27.0 % (central) and 40.8 % (isthmus). Glands with stretched acini accounted for 54.1 % and 40.8 % respectively in these zones. The relative proportion of glands with destructively altered acini increased to 18.9 % in the central zone and 18.4 % in the isthmus. The longitudinal diameter of the prostatic acini increased by 2.3 times, while the height of epithelial cells decreased by

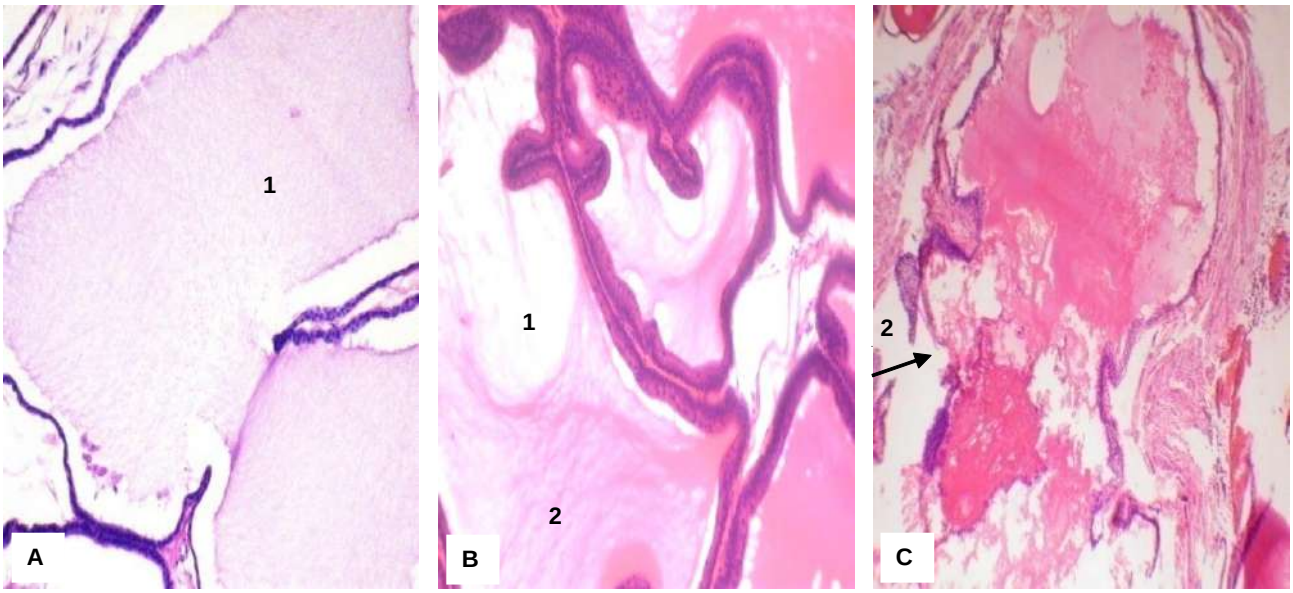

Fig. 6. Prostate gland of rats after cryotrauma: A - central zone of the ventral lobe; B, C - isthmus zone. Distension of prostatic gland acini (1), thickening of the colloid filling the acinar lumen (A, B, x100). Focal destruction (2, arrow) of the acini walls. (C, x200). Hematoxylin-eosin staining.

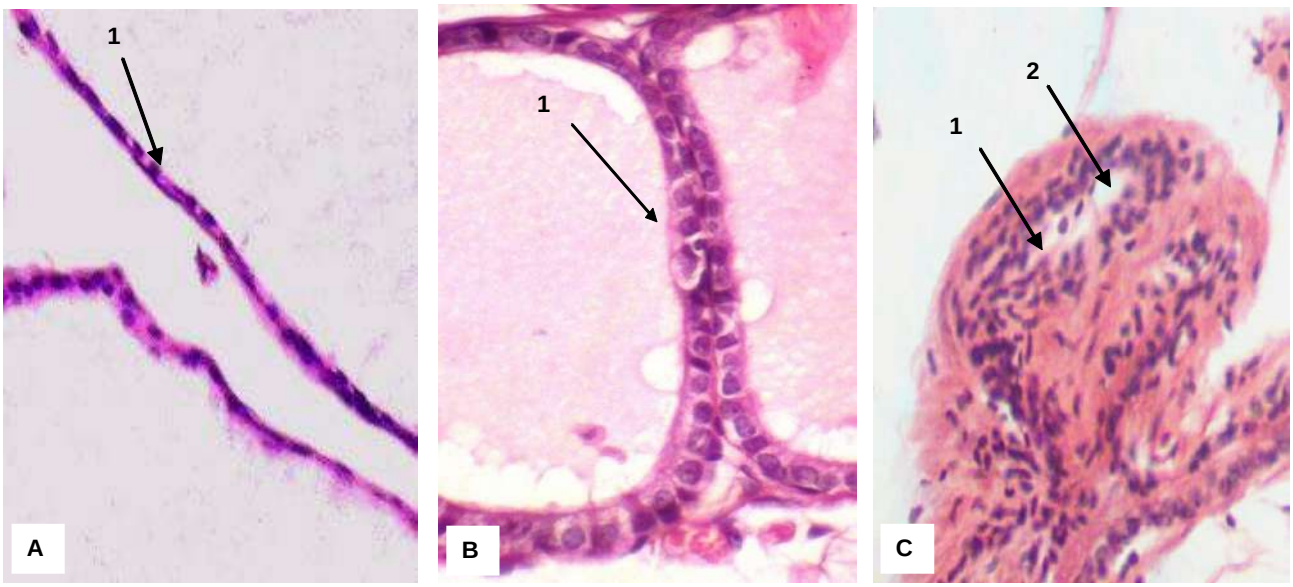

Fig. 7. Rat prostate after cryoinjury. Prostatic gland acini: A - central area of the ventral lobe (1, arrow - flattening of epithelial cells), B - isthmus zone (1, arrow - reduction in height, cell vacuolization); C - prostatic duct (epithelial proliferation (1) and lumen narrowing (2)). Hematoxylin-eosin staining. x400.

1.5 times (see Fig. 4, 5). The severity of the inflammatory reaction in the interstitial stroma was rated at 2.6 points, and the fibrosis of the interstitial and periacinar areas at 2.4 points.

Significant changes were also observed in the type of prostatic secretion crystallization. An increased angle of branch divergence from the main stem was noted, with crystals being thinner, smaller, and less numerous. The type of secretion crystallization in the group was rated at 2.0 points, indicating reduced androgenic saturation in these rats (Table 1).

Administration of seed oil (a solvent for vitamin D_3) following cryoinjury had a minimal effect on the microscopic condition of the rat prostate. Similar to the experimental prostatitis group, there was stretching of the acini, their destruction, thickening of the secretion, reduction in epithelial height, focal edema with inflammation of the stroma and periprostatic tissue, and signs of initial sclerosis of the interstitial stroma. In the interstitial stroma, blood capillaries were noticeably engorged, with some having thickened walls (Fig. 10, 11).

The morphometric parameters characterizing the

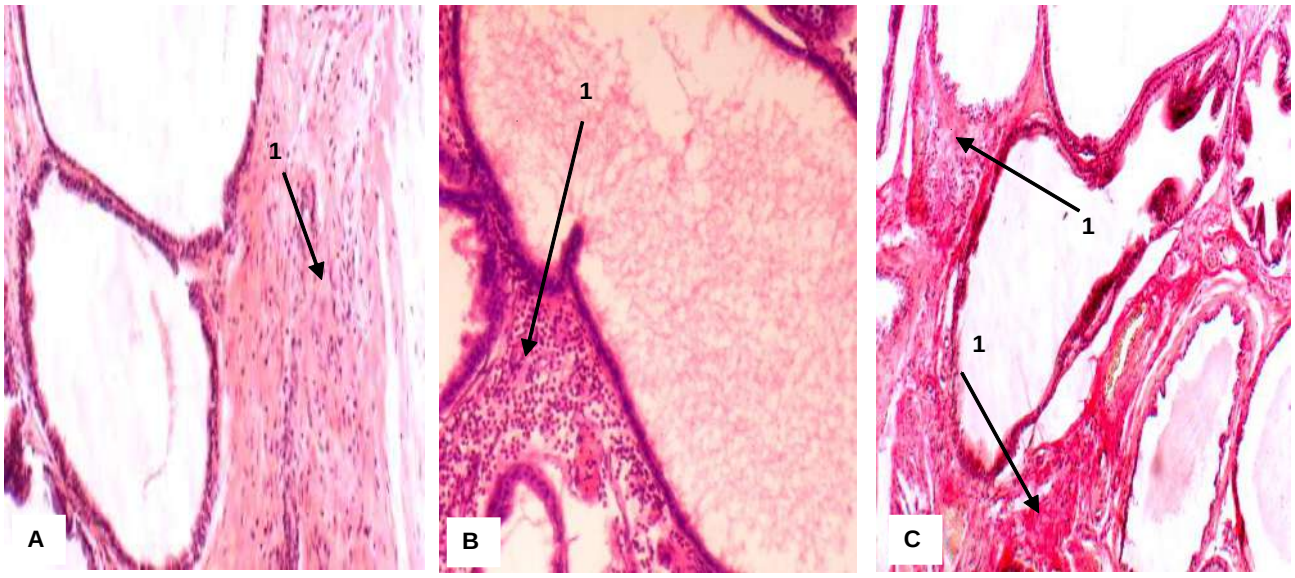

Fig. 8. Rat prostate after cryoinjury: A - central zone of the ventral lobe (fibrinoid edema of the interstitial stroma - 1); B, C - isthmus zone (inflammatory productive reaction in the interstitial stroma (B - 1), expansion and thickening of the interstitial stroma (C - 1)). A, B - Hematoxylin-eosin staining, C - Van Gieson's picrofuchsin staining. x100.

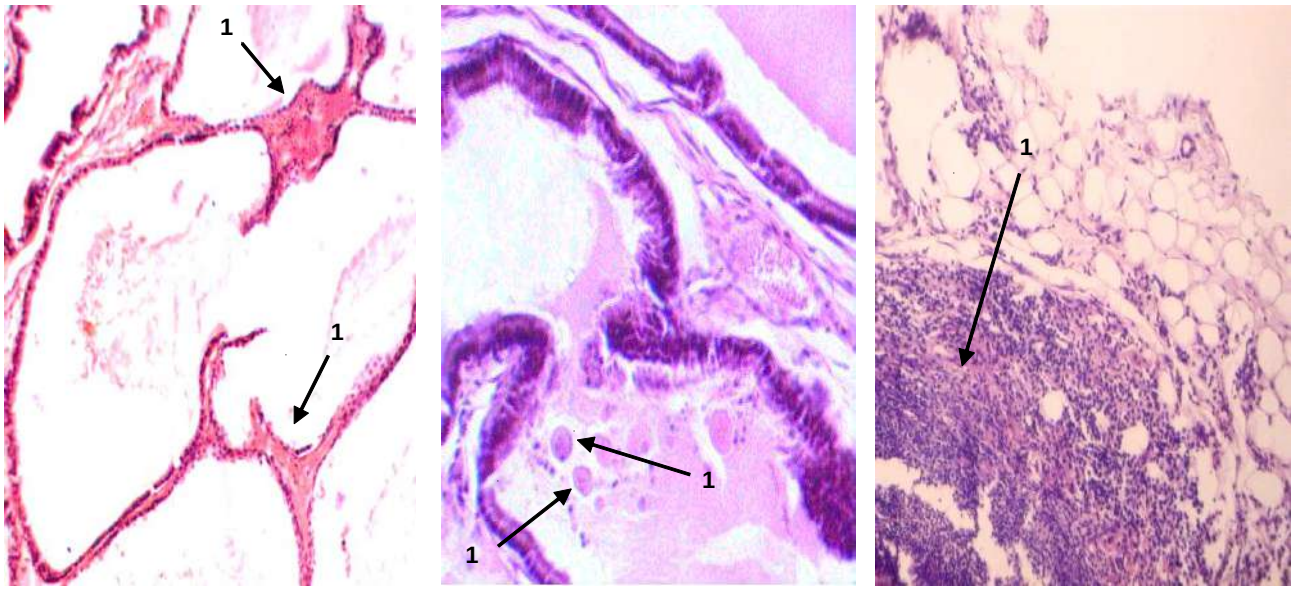

Fig. 9. Rat prostate after cryoinjury: A - remnants of hemorrhage in the interstitial stroma (1), x200; B - amyloid bodies in the lumen of an acinus (1), engorgement of blood capillaries, x250; C - productive inflammatory reaction in the periprostatic adipose tissue (1), x100. Hematoxylin-eosin staining.

condition of the glandular tissue (see Fig. 4, 5), as well as the type of crystallization of the glandular secretion (see Table 1), were practically similar to the control pathology (EP group).

After a two-week administration to rats with experimental prostatitis and administration of vitamin D_3 per os, it was established that part of the end sections of the prostatic glands in the studied areas was noticeably reduced in size, although they were stretched, few destructive structures were observed. Thickening of the secretion in the lumen was not observed in all acini. Visually, the height of the cells of the epithelial lining in many end sections of the prostatic glands (even in stretched ones) increased relative to that in animals with control pathology (Fig. 12).

However, quite often, especially in the area of the isthmus, with a visual reduction in the size of the acini themselves, an increase in the length and number of folds of their epithelial lining was noted, and sometimes the appearance of "subsidiary" acini was noted in the wall of the acini. The nuclei of epithelial cells in all acini were not clearly located in the basal part, but "advanced" in the direction of the center. The lining itself acquired a multi-row character. In addition, "vacuole-like" openings of various sizes took place in the epithelial cells, and destruction of

Table 1. The impact of cholecalciferol on type of crystallization of prostate gland secretion in rats with experimental prostatitis, ($\overline{x} \pm S\overline{x}$).

Group of animal, n	The type of crystallization of prostate gland secret, points
Intact, n=5	3.600±0.245
Control, n=11	3.400±0.245
EP (cryotrauma), n=5	2.000±0.211[1)]
EP+Apricot kernel oil, n=5	2.000±0.000[1)]
EP+vit. D_3(per os), n=7	2.437±0.095[1) 2)]
EP+vit. D_3(per os)+Pr(rec), n=7	2.670±0.048[1) 2)]
EP+(vit. D_3+Pr)(rec), n=8	2.534±0.021[1) 2)]
EP+Pr(rec), n=10	2.949±0.169[2) 3)]

Notes: 1) statistically significant differences compared to Control, $p<0.05$; 2) statistically significant differences compared to group EP+oil, $p<0.05$; 3) statistically significant differences compared to group EP+vit. D_3(per os), $p<0.05$.

the epithelial layer was observed in some acini (Fig. 13).

In the majority of rats, which received vitamin D_3 per os after cryotrauma, less pronounced swelling of the stroma and its plasmatic impregnation were observed. Some of the animals still had blood capillaries (locally) full of blood, and one rat had a perivascular inflammatory reaction, proliferation of the epithelium of some excretory ducts and narrowing of their lumen. However, the signs of the development of fibrosis in all examined males of this group were reduced (Fig. 14).

The morphometric indicators of the condition of the studied lobes of the gland basically confirmed the visual observations: the share of acini unchanged in size increased by 2.7-1.9 times, the number of stretched acini decreased by 2.6-2.9 times, destructively changed by 3.2-2.3 times. Accordingly, the longitudinal diameter of the acini decreased by 32.6 %, and the height of the epithelial cells increased by an average of 1.3 times compared to the group of rats with cold experimental prostatitis without treatment (see Fig. 4, 5).

Administration of the drug Prostatylen against the background of cryotrauma visually contributed to the preservation of a significant number of end sections of the prostatic glands, especially in the isthmus area. A reduced number of destructively changed terminal divisions of the prostatic glands was visually established (Fig. 15). The height of the epithelium of the acini varied depending on the degree of stretching of their walls. Cell nuclei are mostly located basally in one row (Fig. 16 A-B). In the interacinar stroma, the productive inflammatory reaction is significantly reduced or absent, however, in some cases, a rather pronounced inflammatory infiltration of the periprostatic tissue is observed. Decreased swelling and protein effusion of the stroma. In the group as a whole, the thickening of the inter-acinar stroma is weakly or moderately expressed, only in one case was a place (closer to the isthmus) with a sufficiently large connective tissue scar, in which areas with an unevenly expressed inflammatory reaction and remnants of acini can be seen. Van Gieson's picrofuchsin staining also shows an uneven distribution of bundles of collagen fibers. All this indicates that the zones in the connective tissue scar are more "old" and more "fresh" in terms of time of their appearance (Fig. 16 D-F).

Morphometric analysis showed that unchanged acini of prostatic glands became more compared to those in rats with prostatitis (by 2.7 times and by 1.8 times according to the studied zones); stretched acini became fewer (by 2.6

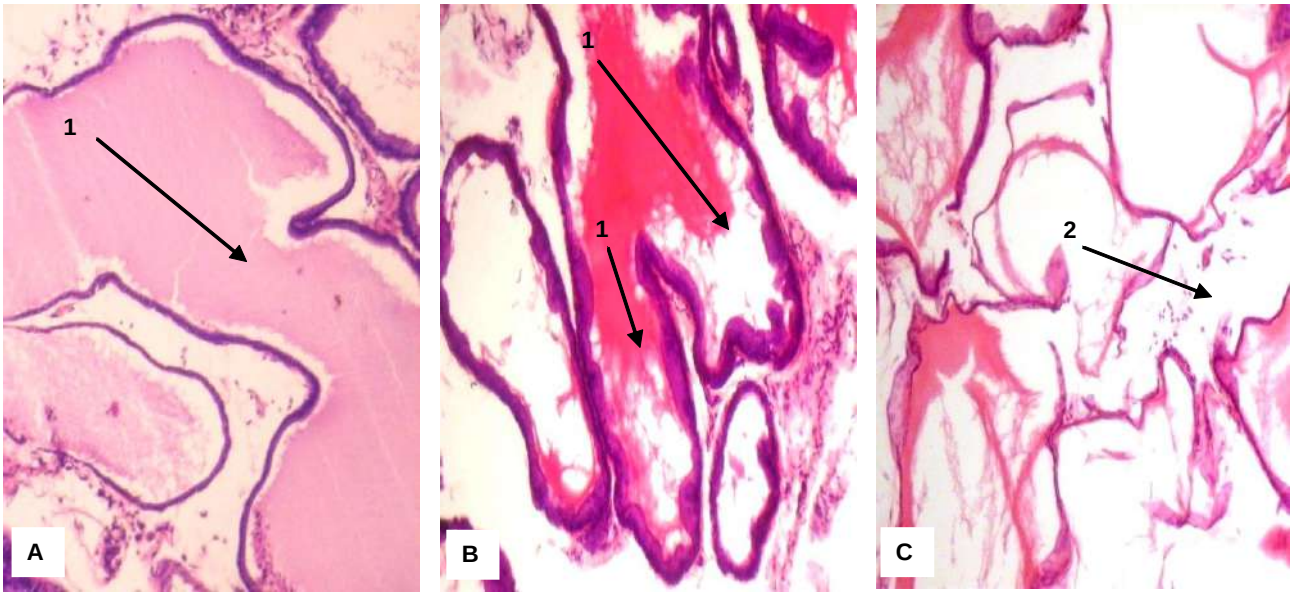

Fig. 10. Prostate gland of rats received Apricot kernel oil after cryotraumatizing: A - central zone of the ventral lobe; B, C - isthmus zone. The prostatic acini are stretched, and the colloid in the lumen is thickened (1); focal destruction of the acini (2). Hematoxylin-eosin staining. x200.

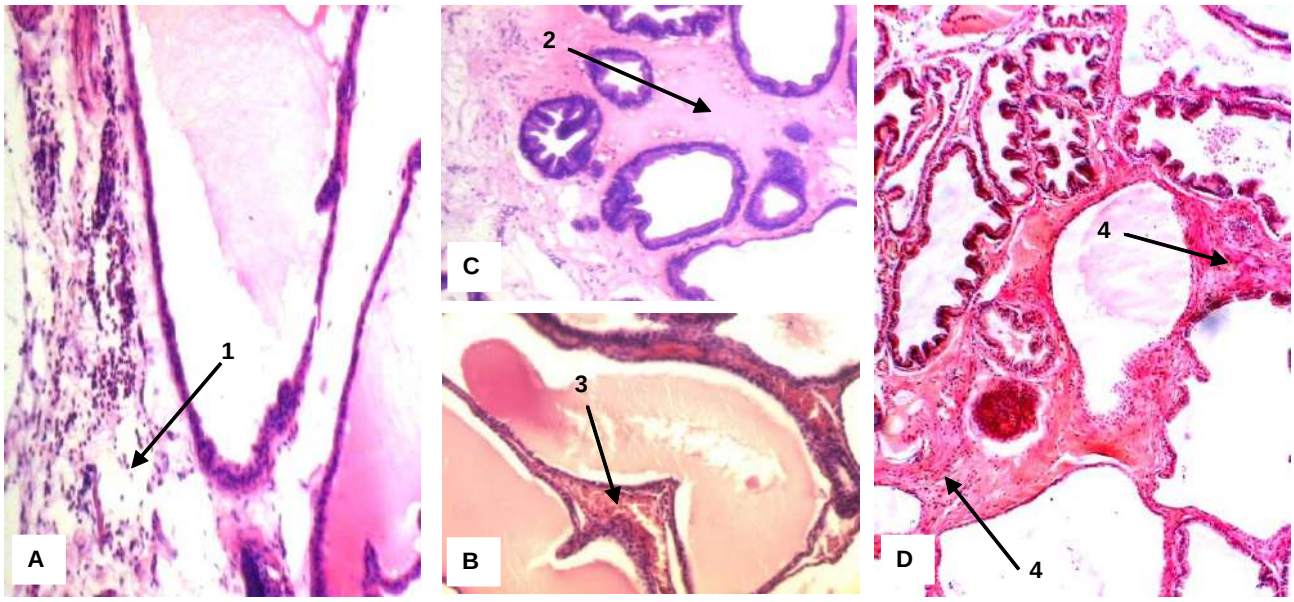

Fig. 11. Prostate gland of rats received Apricot kernel oil after cryotraumatizing: A, B - central zone of the ventral lobe; C, D - isthmus zone. Inflammation of the interstitial stroma (1), edema, plasma infiltration of the stroma (2), engorgement of blood capillaries (3), focal fibrosis of the stroma (4). A, B, C - Hematoxylin-eosin staining, D - Van Gieson's picrofuchsin staining. x200.

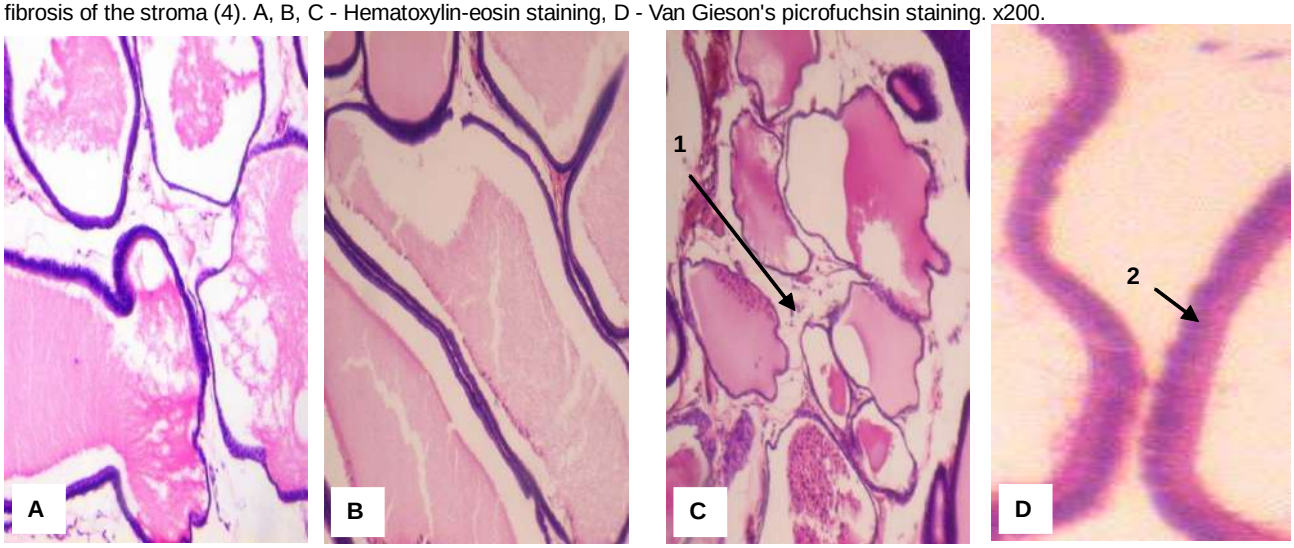

Fig. 12. Prostate gland of rats that received vitamin D_3 *per os* after cryotrauma: A - central zone of the ventral lobe; B, C - zone of the isthmus (C - 1 - small zone of destruction); D - the height of epithelial cells (2) is close to normal. Hematoxylin-eosin staining. A, B - x200, C - x100, D - x400.

times and 2.4 times). The number of destructively changed acini is significantly reduced (by 2.5-1.8 times). Their longitudinal diameter decreased by 25.5 %, and the height of the epithelium increased by 18.5 % compared to pathology. The inflammatory reaction (by 3.7 times) and signs of stroma thickening (by 2.5 times) significantly decreased (see Fig. 4, 5).

The combined administration of Prostatilen and cholecalciferol per os after cryotrauma of the prostate tissue led to the restoration of the typical size of the vast majority of acini of the prostatic glands both in the central zone and in the area of the isthmus between the ventral lobes of the prostate gland. Only single acini had a stretched appearance. Destruction of these structures was not noted. The number of folds of the epithelial lining and their size was close to the similar parameter of the intact group. The secret was not condensed. In most acini, the epithelial cells had a high cubic shape, the nuclei occupied a basal position, and the epithelium was single-layered (Fig. 17). Only in some acini (mainly the zone of the isthmus) the epithelium became multi-rowed, "vacuole-like" lightening was visualized in the cells. The epithelium of the excretory ducts was weakly proliferated, narrowing of the lumen of the ducts was not observed. There is no productive inflammatory reaction in the interacinar stroma, there is reduced edema and protein effusion.

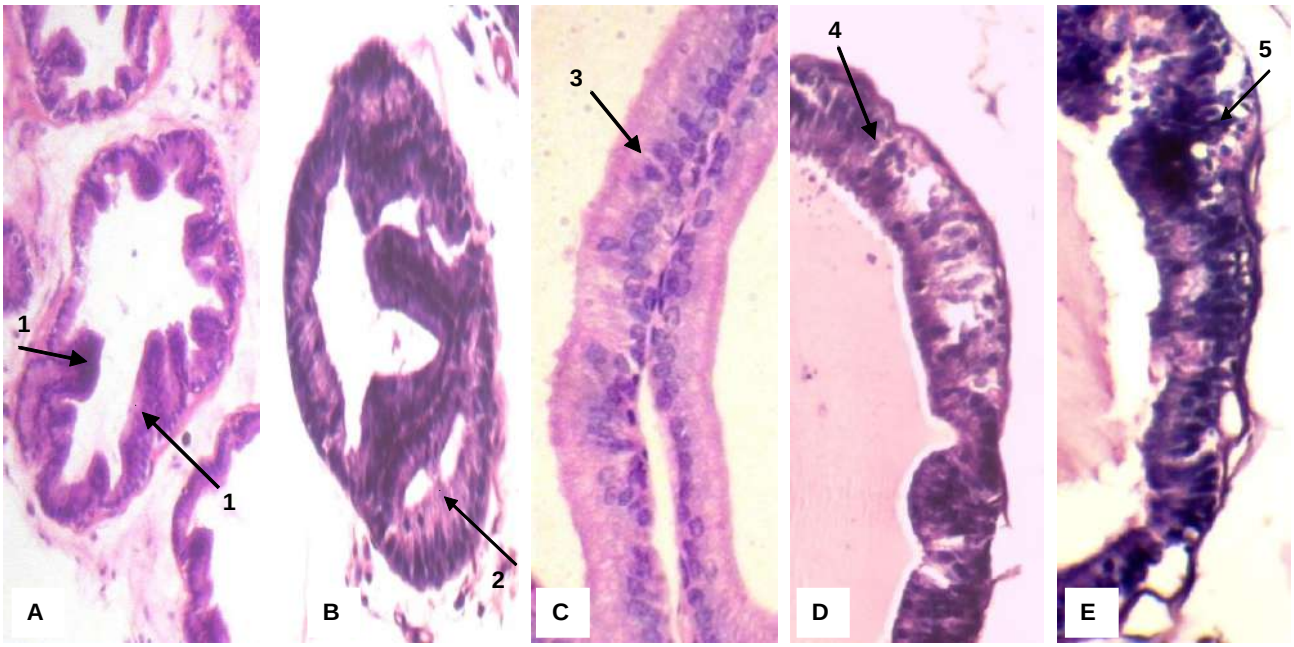

Fig. 13. Prostate gland of rats that received vitamin D_3 *per os* after cryotrauma: A - increase in the height and number of folds in the epithelial lining (1, arrows), x200; B - the appearance of "subsidiary" acini in the acini wall (2) x250; C, D - multi-rowed epithelium, shift of nuclei towards the center of cells (3), appearance of "vacuole-like" structures (4), x400; E - destruction of the epithelial layer (5) x400. Hematoxylin-eosin staining.

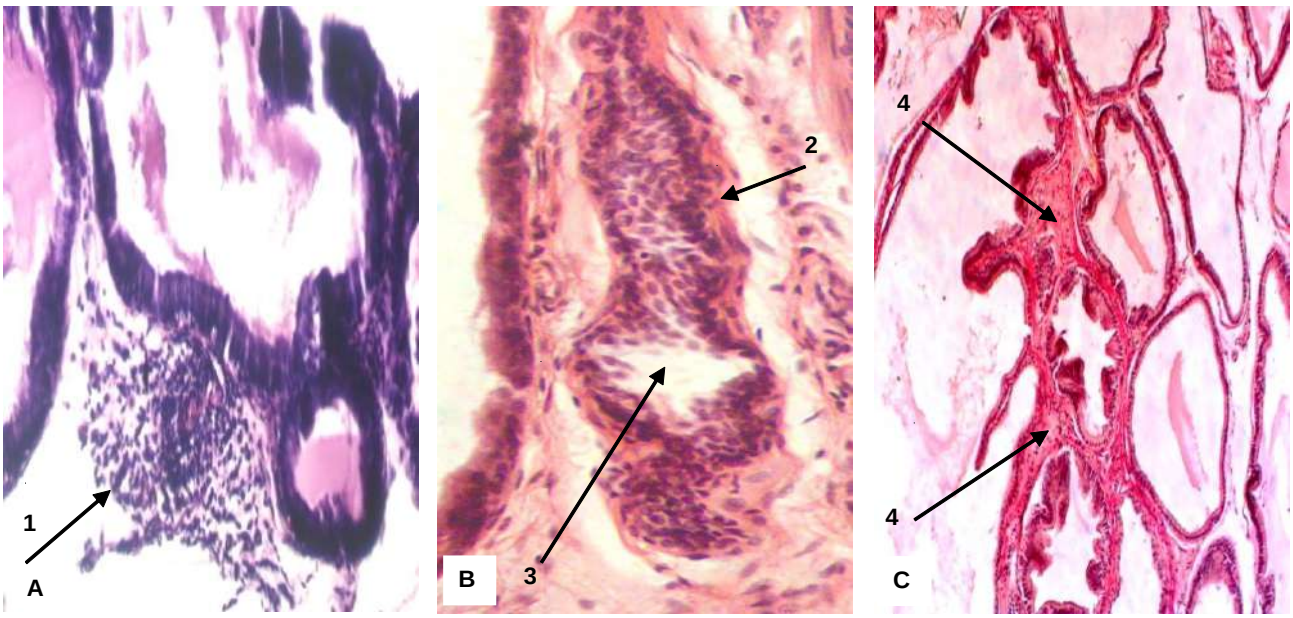

Fig. 14. Prostate gland of rats administered vitamin D_3 *per os* after cryotrauma. Isthmus zone. Perivascular inflammatory reaction (A, 1), proliferation of the epithelium of the excretory duct (2, arrow), narrowing of its lumen (B, 3), decrease, compared to the control, of signs of fibrosis of the interacinar stroma (C, 4). A, B - Hematoxylin-eosin staining, x250; C - Van Gieson's picrofuchsin staining, x100.

Figure 18 shows the intertubular stroma, which has the appearance of ordinary loose connective tissue with no signs of fibrosis.

According to the data of morphometry, unchanged acini of prostatic glands became more compared to the control pathology: by 3.4 times and by 2.2 times according to the studied zones; stretched acini became less by 7.2 times and 3.7 times, and the number of destructively changed acini decreased by more than 18 times (see Fig. 4). The longitudinal diameter of the acini decreased by 53.0 %, and the height of the epithelium increased by 40.0 % compared to the control pathology. The inflammatory reaction and signs of stroma thickening were significantly reduced (see Fig. 5).

After the combined administration of Pr with D3 (rec.), visually quite a significant part of the acini of the prostatic

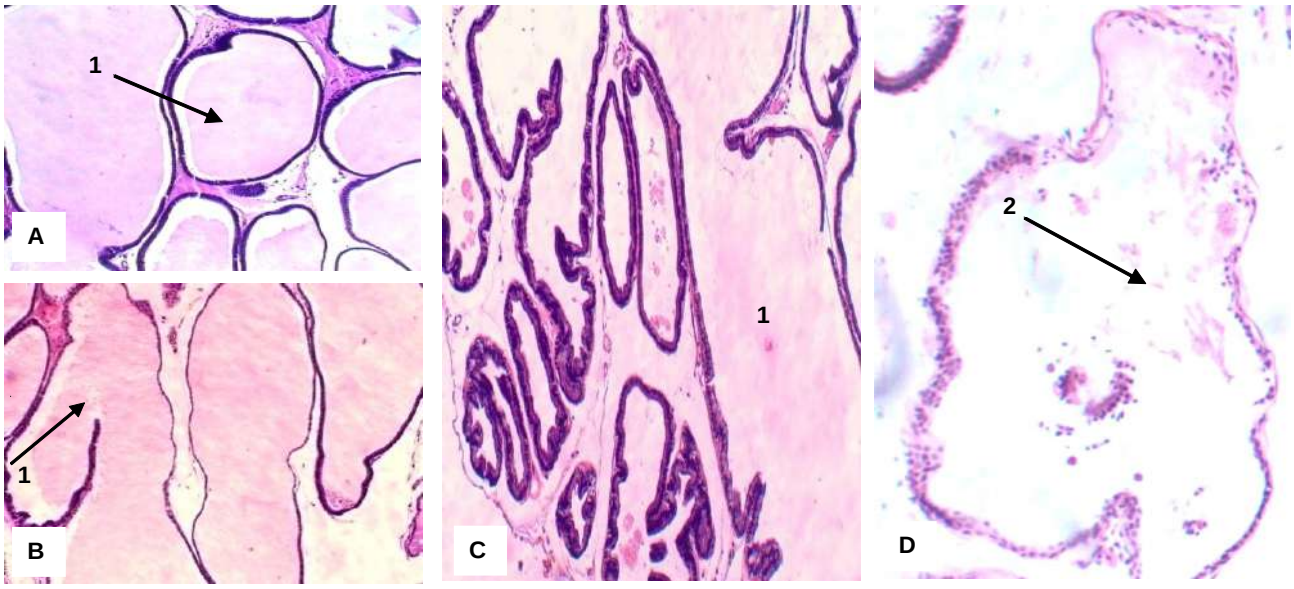

Fig. 15. Prostate gland of rats injected with Prostatylen after cryotrauma: central zone of the ventral lobe (A, B), isthmus zone (C, D). Different expressiveness of stretching of the terminal departments of the prostatic glands (1), destruction of some of them (2). Hematoxylin-eosin staining. A, B, C - x100, D - x200.

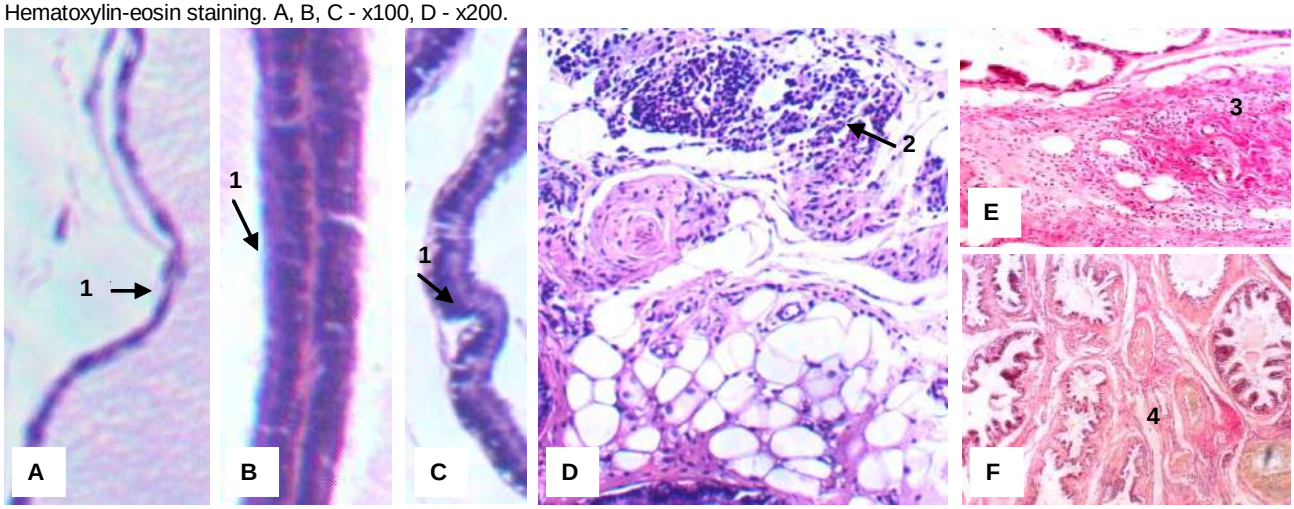

Fig. 16. Prostate gland of rats injected with Prostatylen after cryotrauma: fluctuations in the height of epithelial cells in the wall of the acini: A, B, C - central zone of the ventral lobe; B - zone of the isthmus (1, arrows); a focus of inflammation in the paraprostatic tissue (D, 2); different expressiveness of stroma fibrosis - connective tissue scar with remnants of small atrophied acini (E, 3), moderate thickening of the inter-acinar stroma (F, 4). A-D - Hematoxylin-eosin staining, E, F - Van Gieson's picrofuchsin staining. A-C - x 400, D - x250, E, F - x100.

glands, compared to the group after the administration of vitamin D3 per os and Prostatilen) remained stretched (Fig. 19).

More acini underwent destructive changes, although, compared to the control pathology, the positive effect on the state of the terminal departments of the prostatic glands was quite noticeable (see Fig. 19).

The epithelium lining the walls of the acini of the prostate varied in height from cylindrical-high-cuboidal to flattened. In a whole series of acini, the epithelium changed from single-layered to multi-layered, acquired "vacuole-like" lightening in the cytoplasm. Signs of cell proliferation and vacuolization were also observed in the epithelial lining of the excretory ducts (Fig. 20).

In the interacinar stroma, pronounced swelling, protein impregnation, and a rather noticeable inflammatory cellular reaction were often observed, both perivascularly and focally. An increase in smooth cells was observed among the cellular content. An increase in collagen fibers was indirectly visible - a sign of stroma fibrosis (Fig. 21).

When analyzing the morphometric data (see Fig. 4, 5), it was found that there were 2.5 times and 1.8 times more unchanged acini; stretched - 2.1 and 2.3 times less, destructive - 2.7 and 2.7 times less than in the control pathology according to the studied zones. The longitudinal diameter of the acini decreased by 30.6 %, the height of the

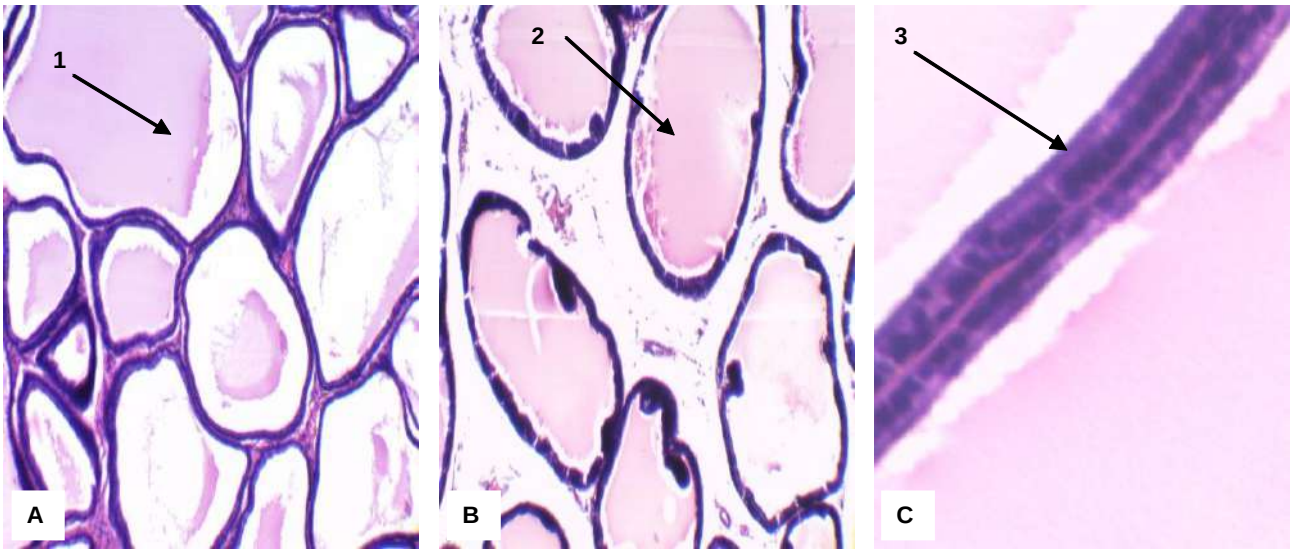

Fig. 17. Prostate gland of rats that received Prostatylen and cholecalciferol per os in combination after cryotrauma: restoration of the typical size of the vast majority of prostatic gland acini in the central zone of the ventral lobe (A, 1 - x200) and in the isthmus zone (B, 2 - x200); normal single-layer epithelium lining the walls of the acini (C, 3 arrow - x400). Hematoxylin-eosin staining.

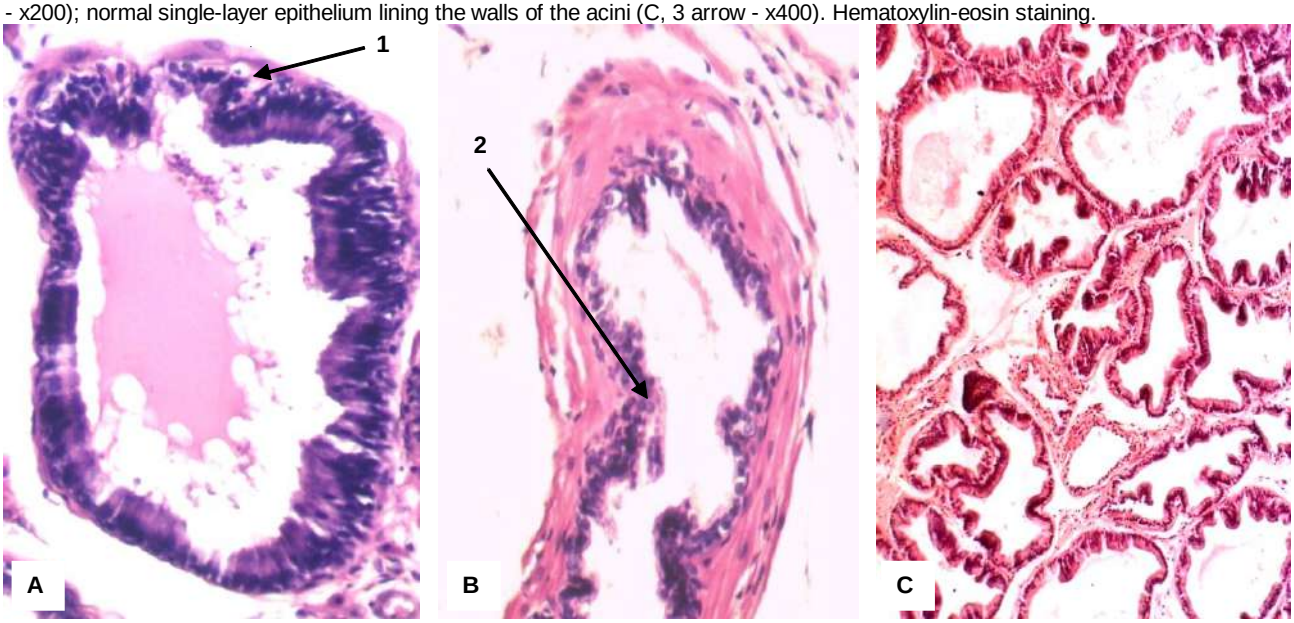

Fig. 18. Prostate gland of a rat that received Prostatylen and vitamin D3 per os in combination after cryotrauma: A - multi-row type of epithelium, "vacuole-like" light in the cytoplasm of cells (1, arrow), x250; B - weak proliferation of the excretory duct epithelium, normal lumen of the duct (2), x250; C - almost no signs of intertubular stroma fibrosis, x100. A, B - Hematoxylin-eosin staining, C - Van Gieson's picrofuchsin staining.

epithelium increased by 27.4 %.

Discussion

Thus, the microscopic picture of the PG in intact animals and control rats (sham-operated), established in this experimental work, corresponded to those described in the literature [29]. 28 days after cryoinjury, the glandular tissue of the ventral part of the PG and the isthmus between them showed signs of chronic prostatitis, characterized by dilation of the terminal sections of most prostatic glands, glandular epithelium atrophy, secretion thickening and stagnation, productive inflammatory response, and stromal thickening. Similar changes have been described in studies conducted at the SI "V. Danilevsky Institute for Endocrine Pathology Problems of NAMS of Ukraine", previously studying the significance of inflammation for the function and structure of the PG.

Acinar atrophy and the appearance of inflammatory infiltration in the connective tissue cells around the acini or in the prostate duct indicate the development of experimental prostatitis in rats [27]. Similar phenomena were observed by other researchers [21, 30]. The most direct sign of EP is inflammation of the PG. Pathomorphological observations confirmed the presence

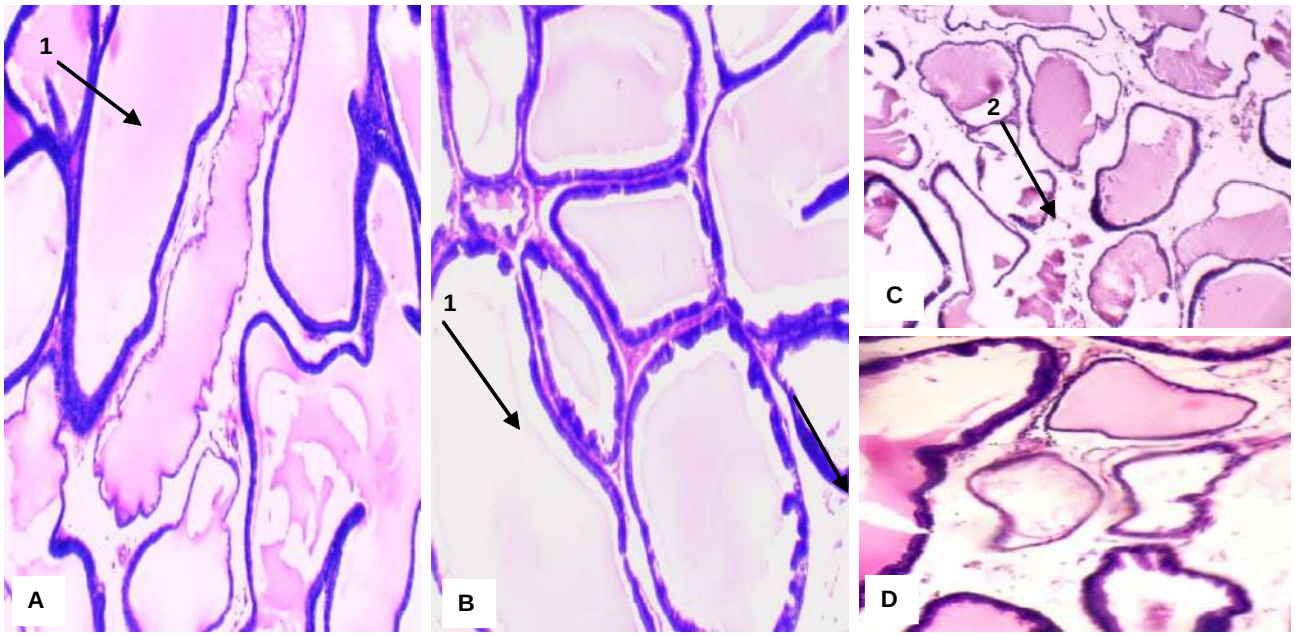

Fig. 19. Prostate gland of rats that were injected with Prostatylen and vitamin D3 rec. after cryotrauma: A, C - central zone of the ventral lobe; B, D - zone of the isthmus. Preservation of the stretched walls of part of the acini (1), destruction of some structures (2). Hematoxylin-eosin staining. x100.

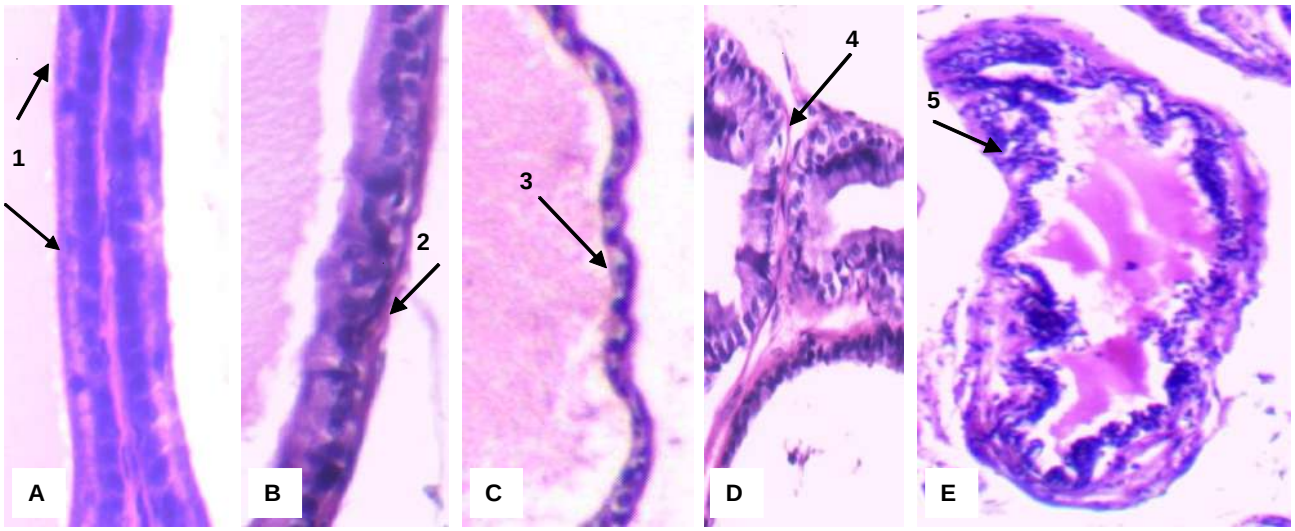

Fig. 20. Prostate gland of a rat, which was injected with Prostatylen and vitamin D3 rec. in combination after cryotrauma. Different state of the epithelium (A, 1 - normal; B, 2 - multi-row epithelium; C, 3 - flattening of epithelial cells; D, 4 - vacuolization of epithelial cells), E, 5 - moderate proliferation of the epithelium of the excretory duct. Hematoxylin-eosin staining. A-D - x400, E - x250.

of prostatitis, and a light microscope was used to confirm the presence of infiltration, inflammation, and identify the type of inflamed cells, as well as the presence of tissue edema, necrosis, detachment, disappearance, and flattening of the glandular epithelium [26].

As described in similar studies, morphological structure disruption of the PG under conditions of experimental cold prostatopathy is accompanied by reduced reproductive capacity in males. At the same time, the histological structure of the testes in rats with EP does not have such pronounced morphological disorders, and the spermatogenesis index in the gonads does not change [29].

It should be noted that under EP conditions, not only is the functioning of the prostate gland disrupted, as determined by the crystallization of its secretion (see Table 1), but its morphological structure also changes (see Figures 6-8). It was found that these animals also experience a disruption in generative function, as evidenced by significant changes in the spermogram parameters of sperm obtained from the epididymis, where they enter the ejaculate after maturation. Specifically, there is reduced sperm motility and decreased total gamete concentration with an increased percentage of pathological forms.

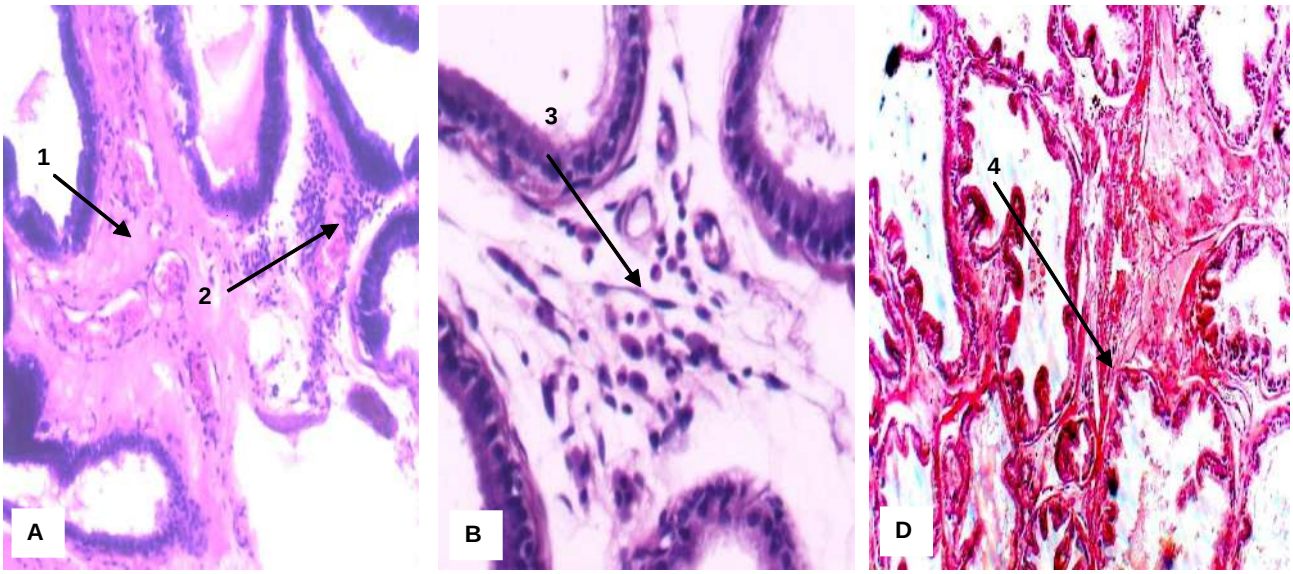

Fig. 21. Prostate gland of rats, which after cryotrauma were injected with Prostatylen and vitamin D3 rec. Zone of the isthmus: A - edema of the interacinar stroma, protein impregnation (1), perivascular inflammatory reaction (2), x200; B - enlargement of smooth cells in the layer of loose, unformed connective tissue (3), x400; C - stroma fibrosis (4), x100. A, B - Hematoxylin-eosin staining. C - Van Gieson's picrofuchsin staining.

Disruptions in the prostate gland state (e.g., changes in organ morphostructure and crystallization of its secretion in animals with cold experimental prostatitis) can be explained by decreased male sex hormone levels in these animals [29], whereas the impact on the histological structure of gonads in EP is not as significant as on the prostate structure. Meanwhile, intact females fertilized by males with EP had a lower pregnancy index and higher fetal loss during pregnancy. Therefore, it was important to investigate the state of the PG under prostatopathy conditions and its changes under the influence of experimental correction. Likely, reproductive disorders can be explained by impaired function and morphological structure of the PG [9].

Cholecalciferol administered per os at a dose of 4000 IU to animals with EP reduced the manifestations of atrophic and destructive processes, signs of tissue inflammation, and prostate stromal thickening. In terms of its impact on some of the above-mentioned signs, oral vitamin D_3 surpassed the reference drug Prostatilen. At the same time, after separate administration of cholecalciferol, specific changes were observed in the state of the epithelial cells lining the walls of the prostatic gland acini (irritation signs - displacement of nuclei to the center, the appearance of vacuoles and clearances in the cytoplasm, initial proliferation signs - acquiring multilayered structure, increased number and height of epithelial folds, presence of "secondary" acini), which may be potential precursors of further undesirable changes. The androgen saturation of these rats decreased based on the parameters of the disruption of prostate secretion crystallization (see Table 1).

The use of vitamin D_3 as monotherapy in animals with EP did not lead to significant changes in spermatogenesis parameters in both the testes and their appendages [29]. However, the separate use of cholecalciferol was effective in restoring fructose content in seminal vesicles, which was reduced in EP. This led to a positive result in reducing the total intrauterine losses of females fertilized by males with experimental prostatitis after correction with vitamin D alone.

Recent studies have proven the presence of vitamin D receptors in male spermatozoa. In addition, calcitriol has been shown to affect sperm protein phosphorylation, enhancing sperm viability. In men, the level of this parameter determines the qualitative and quantitative parameters of the ejaculate, including sperm motility and morphology. There is a correlation between low 25(OH)D levels and a decrease in the number of motile and morphologically normal spermatozoa. Thus, it can be assumed that vitamin D plays a crucial role in the processes of extratesticular sperm maturation, influencing capacitation and modulating male germ cell viability [2].

The combined administration of the studied substances via different routes-rectally with Prostatilen and orally with vitamin D_3 - showed a more positive effect on the histoarchitectonics of the prostatic glandular tissue in rats than separate oral administration of cholecalciferol. Changes in prostate epithelial cells were also significantly minimized. According to the prostate secretion crystallization data, androgen saturation in these animals increased significantly.

Interestingly, the complex use of cholecalciferol to improve fertility in vitro along with biologically active substances, as shown in studies by other authors [28], also leads to improved sperm motility, indicating the importance of components that enter the sperm along with

spermatozoa from the accessory sex glands. The qualitative composition of the secretion depends on the functional state of the prostate gland and its morphostructure.

Rectal administration of the pharmacological composition (vitamin D_3 + Prostatilen) was somewhat inferior to the previous combination, where cholecalciferol was used orally. At the same time, EP induced by cryoinjury did not significantly affect the histoarchitectonics of rat testes or quantitative spermatogenesis parameters during the study period. Visually, rats in the EP group and those receiving only vitamin D_3 per os showed mildly expressed signs of focal proliferation of hormone-producing cells. These signs were somewhat mitigated with separate administration of the reference drug, vitamin D_3 *per os*, and Prostatilen rectally along with it.

Summarizing the above and considering the fact that under EP conditions caused by the use of a cryo-agent, with pronounced changes in the prostate gland's morphological structure, the histological structure of the gonads changed insignificantly under all correction methods and solvent variants, while the spermogram showed improvement in fertility. This suggests that hypofertility caused by such experimental prostatopathy is primarily excretory, relative, and secondary. It is known that excretory infertility results from spermatozoa losing their properties in an aggressive environment. Such a situation can occur against the background of inflammatory diseases of the male reproductive system, its inflammation, disrupting sperm morphology, viability, and activity [20].

Thus, under conditions of EP in rats due to cold intraoperative prostate injury, significant changes in the prostate gland's morphological structure are observed. The obtained data indicate a prostate-protective effect of vitamin D per os at a dose of 4000 IU, manifested in reducing atrophic and destructive processes, signs of tissue inflammation, and prostate stromal thickening. A positive outcome was the reduction of gland fibrosis signs in all studied males in this group, with a significant decrease in the number of destructive changes and the longitudinal diameter of the terminal sections of the prostatic glands in the ventral part of the prostate gland in rats with EP. The addition of cholecalciferol to basic infertility therapy drugs has a more pronounced corrective effect on the morphological structure of the prostate, which is more significant than the separate use of Cholecalciferol and Prostatilen.

Conclusion

1. Experimental prostatopathy induced by intraoperative cold irrigation of the prostate gland leads to experimental prostatitis, which manifests as significant changes in the histological structure of the prostate gland and the type of crystallization of its secretion.

2. The study of prostate gland damage conducted on rats with induced experimental prostatitis demonstrated the effectiveness of adding vitamin D to treatment regimens for correcting reproductive function disorders in individuals with hypofertility.

3. In the histomorphological structure of the prostate gland in animals exposed to cryoinjury, the combined administration of vitamin D per os and Prostatilen reduced the signs of prostate fibrosis and restored the typical size of the majority of acini of the prostatic glands. There was a marked reduction in the inflammatory response and signs of stromal thickening, with morphometric indicators of the prostate gland within physiological norms, unlike the changes observed with the use of a single prostate protector, whose effect was less effective.

4. Rectal administration of the cholecalciferol composition with a prostate protector showed a positive effect on the gland damaged by cryoinjury in male rats, restoring its histostructure and reducing the intensity of inflammation.

5. The addition of cholecalciferol to the basic therapy drug Prostatilen enhances its prostate-protective properties, as confirmed by the histological study of the prostate gland, and is promising for promoting the restoration of overall reproductive function.

References

[1] Agarwal, A., Baskaran, S., Parekh, N., Cho, C. L., Henkel, R., Vij, S., ... & Shah, R. (2021). Male infertility. *The Lancet,* 397(10271), 319-333. doi: 10.1016/S0140-6736(20)32667-2

[2] Aquila, S., Guido, C., Perrotta, I., Tripepi, S., Nastro, A., & Ando, S. (2008). Human sperm anatomy: ultrastructural localization of 1alpha,25-dihydroxyvitamin D receptor and its possible role in the human male gamete. *Journal of Anatomy,* 213(5), 555-564. doi: 10.1111/j.1469-7580.2008.00975.x

[3] Bahriy, M. M., Dibrova, V. A., Popadynets, O. H., & Hryshchuk, M. I. (2016). *Методики морфологічних досліджень: Монографія [Methods of Morphological Research: Monograph].* Вінниця: Нова книга=Vinnytsya: A new book.

[4] Bhattacharjee, N. V., Schumacher, A. E., Aali, A., Abate, Y. H., Abbasgholizadeh, R., Abbasian, M., ... & Bahri, R. A. (2024). Global fertility in 204 countries and territories, 1950-2021, with forecasts to 2100: a comprehensive demographic analysis for the Global Burden of Disease Study 2021. *The Lancet*. doi: 10.1016/S0140-6736(24)00550-6

[5] Blajszczak, C. C., & Nonn, L. (2019). Vitamin D regulates prostate cell metabolism via genomic and non-genomic mitochondrial redox-dependent mechanisms. *The Journal of Steroid Biochemistry and Molecular Biology,* 195, 105484. doi: 10.1016/j.jsbmb.2019.105484

[6] Fullwood, N. J., Lawlor, A. J., Martin-Hirsch, P. L., Matanhelia, S. S., & Martin, F. L. (2019). An analysis of benign human prostate offers insights into the mechanism of apocrine secretion and the origin of prostasomes. *Scientific Reports,* 9(1), 4582. doi: 10.1038/s41598-019-40820-2

[7] Graziani, A., Grande, G., Martin, M., Ferraioli, G., Colonnello, E., Iafrate, M., ... & Ferlin, A. (2023). Chronic Prostatitis/Chronic Pain Pelvic Syndrome and Male Infertility. *Life,* 13(8), 1700. doi: 10.3390/life13081700

[8] Gritsulyak, B. V., Gritsulyak, V. B., Dolinko, N. P., Ivasyuk, I. J., Polivkan, M. Ya. I., Spaska, A. M., & Hallo, O. E. (2016). *Клінічна*

анатомія простати [Clinical anatomy of the prostate]. Івано-Франківськ=Ivano-Frankivsk.

[9] He, H., Luo, H., Xu, H., Qian, B., Zou, X., Zhang, G., … & Zou, J. (2023). Preclinical models and evaluation criteria of prostatitis. *Frontiers in Immunology,* 14, 1183895. doi: 10.3389/fimmu.2023.1183895

[10] Kaminsky, O. (2021). Дозування вітаміну D [Vitamin D dosage]. *International Journal of Endocrinology,* 17(5), 435-442. doi: 10.22141/2224-0721.17.5.2021.241524

[11] Keane, K. N., Cruzat, V. F., Calton, E. K., Hart, P. H., Soares, M. J., Newsholme, P., & Yovich, J. L. (2017). Molecular actions of vitamin D in reproductive cell biology. *Reproduction* (Cambridge, England), 153(1), R29-R42. doi: 10.1530/REP-16-0386

[12] Khmil, S. V., Mayorova, O. Y., & Dudchuk, I. V. (2020). Причини чоловічого безпліддя: питання та відповіді [Causes of male infertility: questions and answers]. *Актуальні питання педіатрії, акушерства та гінекології=Actual Problems of Pediatrics, Obstetrics and Gynecology,* (2), 91-97. doi: 10.11603/24116-4944.2019.2.10819.

[13] Kiernan, J. A. (2015). *Histological and histochemical methods: theory and practice.* Banbury: Scion Publishing.

[14] Kozhemiakin, Yu. M., Khromov, O. S., Filonenko, M. A., & Saifetdinova, G. A. (2002). *Науково-практичні рекомендації з утримання лабораторних тварин та роботи з ними [Scientific and Practical Recommendations for Keeping Laboratory Animals and Working with Them]*. Київ: Авіцена=Kyiv: Avicenna.

[15] Lapach, S. N., Gubenko, A. V., & Babich, P. N. (2000). *Статистические методы в медико-биологических исследованиях с использованием Excel [Statistical methods in biomedical research using Excel].* Киев: Морион=Kiev: Morion.

[16] Layton, C., Bancroft, J. D., & Suvarna, S. K. (2019). *Fixation of tissues. Bancroft's theory and practice of histological techniques.* St. Louis : Elsevier.

[17] Lurin, I., Seliukova, N., Koreneva, Y., Boiko, M., Misiura, K., & Nehoduiko, V. (2023). Зміни в ендокринній системі чоловіків з посттравматичним стресовим розладом, отриманим внаслідок бойової травми [The changes in the endocrine system of men with post-traumatic stress disoder due to combat operations]. *Problems of Endocrine Pathology,* 80(4), 66-76. doi: 10.21856/j-PEP.2023.4.08

[18] Maghsoumi-Norouzabad, L., Labibzadeh, M., Javid, A. Z., Hosseini, S. A., Kaydani, G. A., & Dastoorpur, M. (2022). The association of vitamin D, semen parameters, and reproductive hormones with male infertility: A cross-sectional study. *International Journal of Reproductive BioMedicine,* 20(4), 331-338. doi: 10.18502/ijrm.v20i4.10905

[19] Maynard, R., Downes, N., & Finney, B. (2014) *Histological techniques: an introduction for beginners in toxicology.* Cambridge: Royal Society of Chemistry.

[20] Nikiforov, O. A., Lomeyko, H. A., Lomaka, S. V., & Lavysh, I. A. (2014). Мужское бесплодие: актуальные вопросы физиологии, этиопатогенеза и диагностики нарушений репродуктивной системы у мужчин [Male infertility: actual questions of physiology, pathogenesis and diagnosis of disorders of the reproductive system in male]. *Запорізький медичний журнал=Zaporozhye Medical Journal,* 85(4), 69-76.

[21] Ravshanov, T. B., Zaichenko, G. V., Zaichenko, V. S., & Ruban, O. A. (2018). Фармакологічне дослідження супозиторіїв для лікування доброякісних захворювань передміхурової залози [Pharmacological study of suppositories for the treatment of benign diseases of the prostate gland]. *Web of Scholar,* 1(8,26), 51-57. doi: 10.31435/rsglobal_wos/30082018/6092

[22] Reznikov, O. G. (2003). Загальні етичні принципи експериментів на тваринах [The fundamental ethical principles of experiments on animals]. *Ендокринологія=Endocrinology*, 8(1), 142-145.

[23] Stefanov, O. V. (2001). *Доклінічні дослідження лікарських засобів [Preclinical studies of drugs]*. Київ: Авіцена=Kyiv: Avicenna.

[24] Vartapetov, B. A., & Demchenko, A. N. (1975) *Предстательная железа и возрастные нарушения половой деятельности [Prostate gland and age-related sexual disorders].* Київ=Kyiv.

[25] Verze, P., Cai, T., & Lorenzetti, S. (2016). The role of the prostate in male fertility, health and disease. *Nature Reviews Urology,* 13(7), 379-386. doi: 10.1038/nrurol.2016.89

[26] Wang, W., Naveed, M., Baig, M. M. F. A., Abbas, M., & Xiaohui, Z. (2018). Experimental rodent models of chronic prostatitis and evaluation criteria. *Biomedicine & Pharmacotherapy,* 108, 1894-1901. doi: 10.1016/j.biopha.2018.10.010

[27] Wang, X., Zhong, S., Xu, T., Xia, L., Zhang, X., Zhu, Z., ... & Shen, Z. (2015). Histopathological classification criteria of rat model of chronic prostatitis/chronic pelvic pain syndrome. *International Urology and Nephrology,* 47, 307-316. doi: 10.1007/s11255-014-0868-x

[28] Yilmazer, Y., Moshfeghi, E., Cetin, F., & Findikli, N. (2024). In vitro effects of the combination of serotonin, selenium, zinc, and vitamins D and E supplementation on human sperm motility and reactive oxygen species production. *Zygote*, 1-7. doi: 10.1017/S0967199424000029.

[29] Zaichenko, G. V., & Ravshanov, T. B. (2019). Морфоструктура передміхурової залози щурів при застосуванні супозиторіїв комбінованого складу з індол-3-карбінолом та меоксикамом [The morphostructure of the premixurous bud of the schuriv with frozen suppositories in a combined warehouse with indole-3-carbinol and meoxicam]. *Фітотерапія. Часопис=Phytotherapy. Chasopys,* 1, 37-44. doi: 10.33617/2522-9680-2019-1-37

[30] Zhang, M., Luo, C., Cui, K., Xiong, T., & Chen, Z. (2020). Chronic inflammation promotes proliferation in the prostatic stroma in rats with experimental autoimmune prostatitis: study for a novel method of inducing benign prostatic hyperplasia in a rat model. *World Journal of Urology,* 38, 2933-2943. doi: 10.1007/s00345-020-03090-6

МОРФОЛОГІЧНА БУДОВА ПЕРЕДМІХУРОВОЇ ЗАЛОЗИ ЗА УМОВ ЕКСПЕРИМЕНТАЛЬНОЇ ПРОСТАТОПАТІЇ ТА ПІСЛЯ ЗАСТОСУВАННЯ ХОЛЕКАЛЬЦИФЕРОЛУ У РІЗНИХ СХЕМАХ КОРЕКЦІЇ ГІПОФЕРТИЛЬНОСТІ

Мараховський І. О., Смолєнко Н. П., Коренєва Є. М., Бєлкіна І. О., Бречка Н. М., Бойко М. О., Лар'яновска Ю. Б., Бондаренко В. О.

Дія негативних чинників, стресу та умов сучасного життя ушкоджують чоловіче здоров'я та призводять до безпліддя. Причиною гіпофертильності часто є простатити. Сьогодні показано можливу роль вітаміну D в регуляції функціонування органів репродуктивної системи. Мета дослідження - визначити вплив холекальциферолу на гістологічну картину передміхурової залози щурів з експериментальним простатитом та після його застосування окремо або разом із простатопротектором. Експериментальний простатит викликали холодовим інтраопераційним ураженням передміхурової

залози. Для корекції простатиту вводили вітамін D_3 (холекальциферол) перорально у дозі 4000 МО. Простатопротектор (Простатилен, Пр) та фармацевтичну композицію з ним, а також вітамін D_3 вводили ректально. Щурів з модельованим простатитом було поділено на групи: ЕП (холодовий експериментальний простатит без лікування); ЕП + кісточкова олія (на тлі експериментального простатиту тварини отримували розчинник - олію абрикосових кісточок); ЕП + вім D_3 (per os) (на тлі експериментального простатиту тварини отримували вітамін D_3); ЕП + Пр(rec) (на тлі експериментального простатиту самцям вводили Простатилен per rectum); ЕП + вім. D_3 (per os) + Пр(rec) (на тлі експериментального простатиту тварини отримували вітамін D_3 (per os) та гель Простатилен (per rectum)); ЕП + (вім. D_3+Пр)(rec) (на тлі експериментального простатиту щурам per rectum вводили гель Простатилен з вітаміном D_3). В якості контролю були інтактні тварини (група Інтактні) та хибнооперовані щури (група Контроль). Парафінові зрізи передміхурової залози забарвлювали гематоксиліном, еозином та за методом Ван Гізона. Крім оглядової мікроскопії вентральних часток передміхурової залози та перешийку між ними вимірювали потужність гістохімічних реакцій, оцінювали виразність запалення та фіброзу, підраховували кількість кінцевих відділів простатичних залозок з візуально незміненим станом, з розширенням просвіту та з деструкцією стінки, вимірювали поздовжній діаметр ацинусів та висоту епітеліальних клітин простатичних залозок. Статистичний аналіз результатів здійснювали в стандартному пакеті програм "Statistica 6.0" з використанням t-критерію Стьюдента та застосовуючи непараметричний аналог однофакторного дисперсійного аналізу - критерій Краскела-Уоліса, а також критерій Мана-Уітні. Встановлено, що у щурів з експериментальним простатитом спостерігаються виразні зміни морфологічної будови передміхурової залози. Встановлено простатопротекторний ефект вітаміну D per os у дозі 4000 МО, котрий зменшував прояви атрофічних і деструктивних процесів, ознаки запалення тканини та огрубіння строми передміхурової залози. Знижувались ознаки розвитку фіброзу передміхурової залози у самців цієї групи, зменшувалась кількість деструктивних змін та повздовжнього діаметра кінцевих відділів простатичних залозок вентральної частки передміхурової залози щурів із експериментальним простатитом. Таким чином, додавання холекальциферолу до препаратів базової терапії неплідності має більш виражений корегувальний вплив на морфологічну будову простати, аніж окреме використання холекальциферолу та простатопротектору. Поєднання базової терапії з вітаміном D посилює простатопротекторні властивості останнього і є перспективним для відновлення репродуктивної функції загалом.

Ключові слова: *вітамін D, гістоструктура, морфометричні показники, холекальциферол, передміхурова залоза, простатит.*

Author's contribution

Marakhovskyi I. O. - research, review writing and editing, methodology and writing of the original draft, formal analysis and validation, data visualization.

Smolienko N. P. - research, review writing and editing, data visualization.

Korenieva Ye. M. - conceptualization, methodology and writing of the original draft review writing and editing, supervision, project administration.

Bielkina I. O. - research, formal analysis and validation, data visualization.

Brechka N. M. - research, review writing and editing, formal analysis and validation, data visualization.

Boiko M. O. - formal analysis and validation, data visualization.

Laryanovska Yu. B. - research, review writing and editing, formal analysis and validation.

Bondarenko V. O. - conceptualization, methodology and writing of the original draft, project administration.

DOI: 10.31393/morphology-journal-2024-30(3)-08 **Reports of Morphology, Vol. 30, №3, Pages 80-90**

ISSN 1818-1295 eISSN 2616-6194

REPORTS OF MORPHOLOGY

Official Journal of the Scientific Society of Anatomists, Histologists, Embryologists and Topographic Anatomists of Ukraine

journal homepage: https://morphology-journal.com

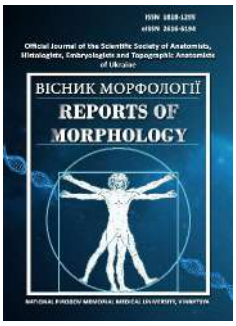

Morpho-topographic features of the course of gastric wall muscle fibers in the esophagogastric junction during sleeve gastrectomy

Kalashnikov O. O.[1], Usenko O. Yu.[2], Todurov I. M.[1], Hrynevych A. A.[1]

[1]State Scientific Institution "Center for Innovative Medical Technologies of the National Academy of Sciences of Ukraine", Kyiv, Ukraine
[2]State Institution "National scientific surgery center of surgery and transplantation named after O. O. Shalimov to National Academy of medical sciences of Ukraine", Kyiv, Ukraine

ARTICLE INFO
Received: 21 February 2024
Accepted: 07 August 2024

UDC: 626.33/329-092:616.33-089.87

CORRESPONDING AUTHOR
e-mail: kalashnikov.cimt@gmail.com
Kalashnikov O. O.

CONFLICT OF INTEREST
The authors have no conflicts of interest to declare.

FUNDING
This investigation is a part of the research project, which was funded by the National Academy of Sciences of Ukraine (Grant number 0120U105158).

DATA SHARING
Data are available upon reasonable request to corresponding author.

Sleeve gastrectomy, also known as vertical gastrectomy, is one of the most common and popular bariatric surgeries in the world. This surgery has become particularly popular in recent decades due to its effectiveness in reducing weight and improving associated metabolic disorders. However, despite the high effectiveness of this surgery, stapling line failure remains one of the most serious complications that can lead to severe consequences such as peritonitis, sepsis, and prolonged hospital stay. The study of the morphotopographic features of the course of the muscle fibers of the gastric wall in the area of the esophagogastric junction is relevant for understanding the mechanisms of suture failure and developing preventive measures. The aim of the study was to evaluate the morphotopographic features of the course of the gastric wall muscle fibers in the esophagogastric junction during sleeve gastrectomy. A comprehensive study of the anatomical and functional characteristics of the gastric muscle layer in the area of the esophagogastric junction was carried out. A significant change in the architectonics of the muscular layer is noted in the esophagogastric junction zone. The circular muscles predominate here, which indicates the functional adaptation of this area to the regulation of food passage. Taking into account the transition from the anatomical zone of the esophagus to the stomach, the appearance of new muscle layers was revealed due to the physiological specificity of the hollow organ. By sequential dissection of the muscle layers, using the methods of histological analysis and macroscopic morphometry, specific features of muscle fibers that affect the formation of the staple line were revealed, namely, a mostly parallel course of fibers in the area of the angle of His and crossed distally from it, the thickness of the muscle layer at the level of the angle of His prevails over the distal level. Thus, the results obtained are important for improving the surgical technique of sleeve gastrectomy, in particular, the choice of the optimal location and direction of the suture - the formation of a continuous "layer" of crossed muscle fibers of the gastric body, the transition of longitudinal esophageal muscle fibers to the bottom and the large curvature of the stomach, which, together with circular fibers, acquire a perpendicular orientation to the level of staple suture application.

Keywords: *sleeve gastrectomy, staple line leak, plastination, gastric wall, muscle fibers.*

Introduction

Sleeve gastrectomy (SG) is one of the most common and effective bariatric surgeries in the world to treat obesity and related metabolic disorders [4]. During this restrictive surgery, a gastric tube is formed by resecting almost most of the stomach along with hormone-producing areas, resulting in a decrease in the desire and ability to consume food in "preoperative" volumes, which consequently improves many parameters of metabolic homeostasis, such as carbohydrate and lipid profiles. Due to its technical simplicity, efficacy, and safety, SG is deservedly considered the surgery of choice for many patients who need a long-term solution to lose excess weight and improve overall health [1]. Thus, if in 2011 the percentage of SG of all bariatric surgeries performed was only 17.8 %, in 2018 this figure reached 61.4 % [1, 7].

But, like any surgical intervention, SG is not without its

drawbacks. Staple line failure (SLF) is one of the most life-threatening complications after this surgery [8, 16]. In the context of the postoperative period of patients who have undergone SG, it is extremely important to have constant clinical and laboratory monitoring aimed at assessing complications in order to formulate conclusions and strategies for correcting the stages and variations of surgical intervention [18].

Although the percentage of failure has decreased since the publication of the latest summit consensus, which analyzed each stage of the operation and all the key points that could affect the development of SLF, according to the latest data, the rate of this complication can reach up to 3 % [14, 27].

In order to prevent the occurrence of this complication, many studies have been conducted to investigate the thickness of the stomach wall, the scientific basis for choosing cassettes for stapling machines, the use of various synthetic materials and adhesives that were applied to the staple line for additional protection [21, 28]. However, the issue remains unresolved, because any tactical decisions that have a positive effect on complication rates are not morphologically justified. In addition, there are practically no publications devoted to the morphological study of the muscle layers of the esophagogastric junction.

The aim of the study - to evaluate the morphotopographic features of the course of the gastric wall muscle fibers in the esophagogastric junction during sleeve gastrectomy.

Materials and methods

The study was approved by the Commission on Bioethics Compliance in Experimental and Clinical Research at the State Scientific Institution "Center for Innovative Medical Technologies of the National Academy of Sciences of Ukraine" (Protocol No. 4 of October 26, 2023). All studies were based on the Declaration of Helsinki (6th edition, revised 2008, Seoul) and the Universal Declaration on Bioethics and Human Rights (2006).

The study was conducted within the framework of the research work of the State Scientific Institution "Center for Innovative Medical Technologies of the National Academy of Sciences of Ukraine" "The role and place of laparoscopic surgery in the treatment of patients with metabolic syndrome in ERAS protocols", state registration number 0120U105158. Samples for the study were collected on tissues obtained during autopsies in the pathology department of the Kyiv City Clinical Bureau of Forensic Medicine (Kyiv, Ukraine).

We collected 10 resected parts of the stomachs along with the lower third of the esophagus. The samples had no visible organic pathology. All samples were cleaned of gastric contents and blood residues. All specimens were placed in separate containers. In order to decolorize the samples and facilitate the subsequent extra- and intramural dissection, the specimens were filled with a solution of 30 % hydrogen peroxide in a ratio of 1/3. A thermal reaction was observed (specimen temperature -30°C), which instantly discolored the samples without denaturing the muscle protein. The standing time of the samples was 10 minutes.

After impregnation with hydrogen peroxide, the samples were rinsed under running water for 10 minutes. Visually - the effect of tissue emphysema and visible "oxygen dissection" of the serous membrane from the muscle membrane can be observed, the space between the layers of the stomach wall is filled with air bubbles (Fig. 1).

Fig. 1. Macro view of the resected part of the stomach. The method of "oxygen dissection": 1 - gas bubbles between the muscle wall and peritoneum, 2 - peritoneum.

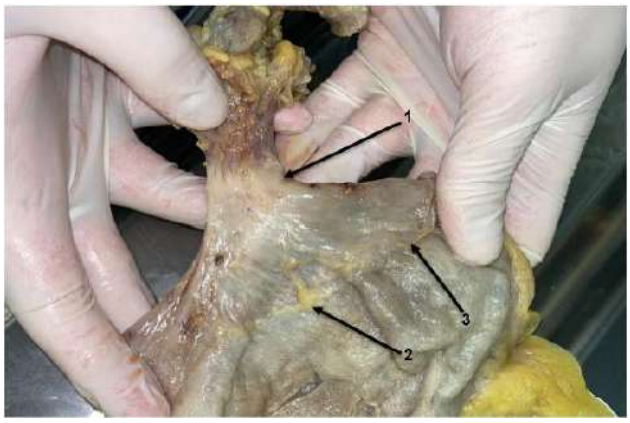

Fig. 2. Macro view of the resected part of the stomach. Surface dissection of the sample: 1 - gastroesophageal junction, 2 - perigastric fatty tissue, 3 - peritoneal margin.

All samples were immersed in a fixative solution of 300 ml of 37 % formalin and 700 ml of distilled water. The ratio "fixative solution"/samples was 5 times the original sample volume. The samples were immersed in the solution and covered with cotton wipes to prevent floating. The samples were fixed and stored in a refrigerator at a temperature of 0 to -1 °C. The solution and samples were kept in properly sealed containers at all times. The time of sample fixation was 5 days.

After fixation, the samples were removed and rinsed with plenty of running cold water for 2 hours. Then a surface preparation was performed.

Excess fat, connective tissue, remnants of the esophageal-diaphragmatic ligament, dissection and removal of blood vessels, n.vagus trunks were removed from the samples (Fig. 2).

After superficial dissection, we performed intramural intermuscular dissection of 8 samples with the isolation of the main layers of the gastric wall muscles in the body and esophagogastric junction. Thanks to the "oxygen dissection" method, it becomes possible to perform intramural dissections using sharp and blunt methods due to the loosening of dense intermuscular connections.

A long incision along the course of the outer fibers of the esophageal wall muscles was used to sequentially separate the longitudinal layer from the circular layer (Fig. 3).

Results

The right longitudinal fibers of the esophagus descended to become the longitudinal fibers of the stomach along the small curvature. The left longitudinal fibers of the esophagus and sometimes part of the circular fibers of the stomach descended to become the longitudinal fibers of the stomach along the great curvature of the stomach (Fig. 4).

As a result of precision dissection, it was found that in the area of the esophagogastric junction, the longitudinal muscles of the esophagus, together with the circular muscles of the stomach body, form a visually assessable continuous "layer" of intertwined fibers (Fig. 5). We came to the conclusion that dissection of individual layers in this topographic plane is impractical.

Immediately below the above-described "layer", the oblique muscle fibers with a deeper submucosal layer are clearly visualized (see Fig. 5).

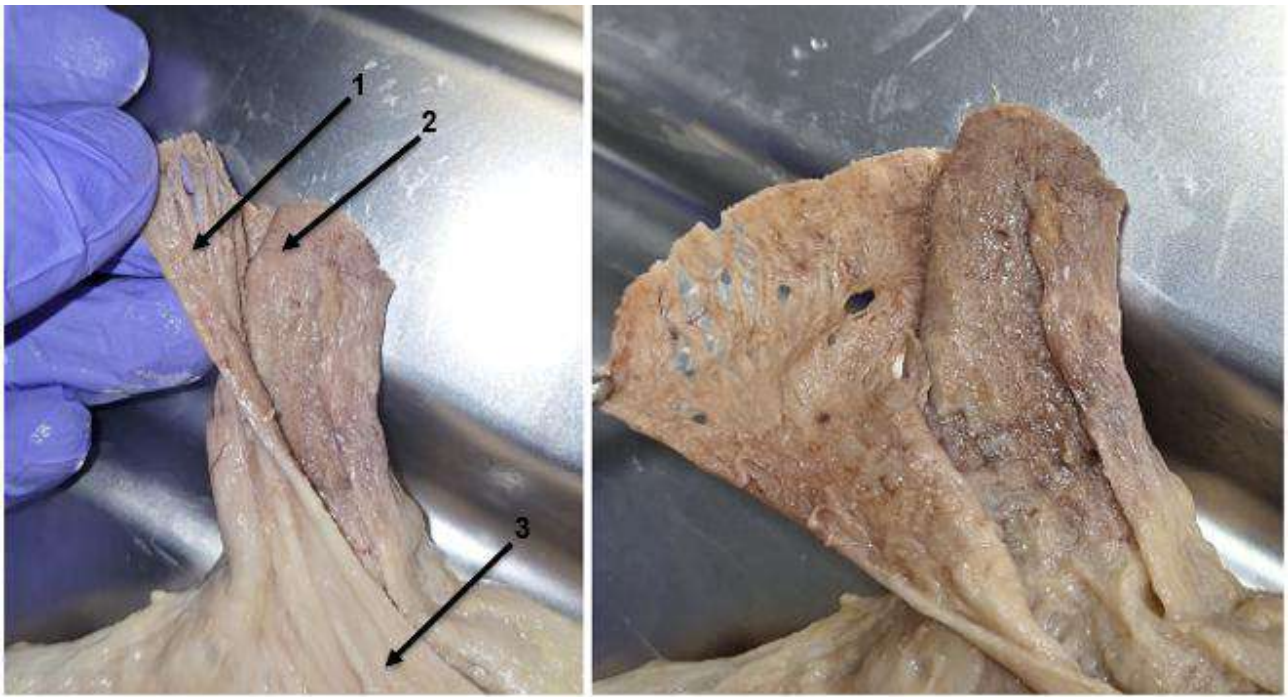

Fig. 3. Macro view of the resected part of the stomach. Separative dissection of the stomach muscle layers: 1 - longitudinal fibers of the esophagus, 2 - circular fibers of the esophagus, 3 - oblique fibers of the stomach.

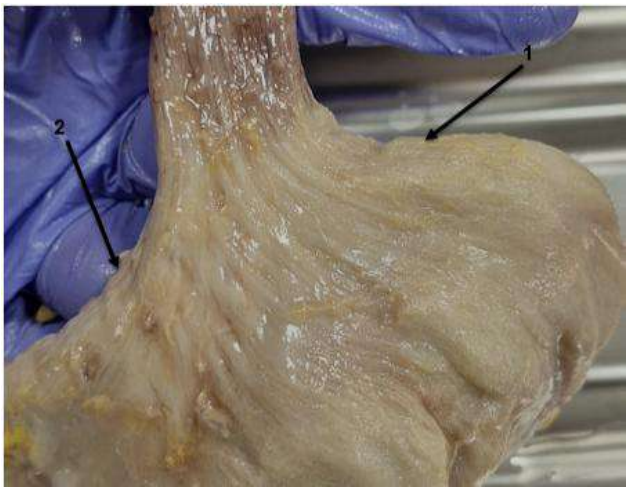

Fig. 4. Macro view of the resected part of the stomach. The course of longitudinal muscle fibers: 1 - transition of muscle fibers to the bottom and large curvature of the stomach, 2 - transition of muscle fibers to the small curvature of the stomach.

In the area of the esophagogastric junction, a change in the direction and orientation of the fibers of the circular layer of the esophageal muscles that passes to the stomach wall (the so-called sling fibers and clasp fibers, which together form the Helvecius collar) is visualized (Fig. 6).

On the other two samples, after preliminary surface dissection, a staple suture was performed with the intersection of the stomach wall in the area of the angle of His and at a distance of 1.5 cm from the angle of His, respectively, using a 36 Fr calibration probe (Fig. 7).

Two gastric tubes were formed and placed in 37 % formalin for 1 day for fixation, and subsequently intramural dissection was performed using the above method to visualize muscle fibers in the area of staple suture application (Fig. 8).

To demonstrate the separation of the muscle layers of the stomach wall in the esophagogastric junction and in the area of stapled sutures, the samples were stained layer by layer using food coloring of blue and red colors (5

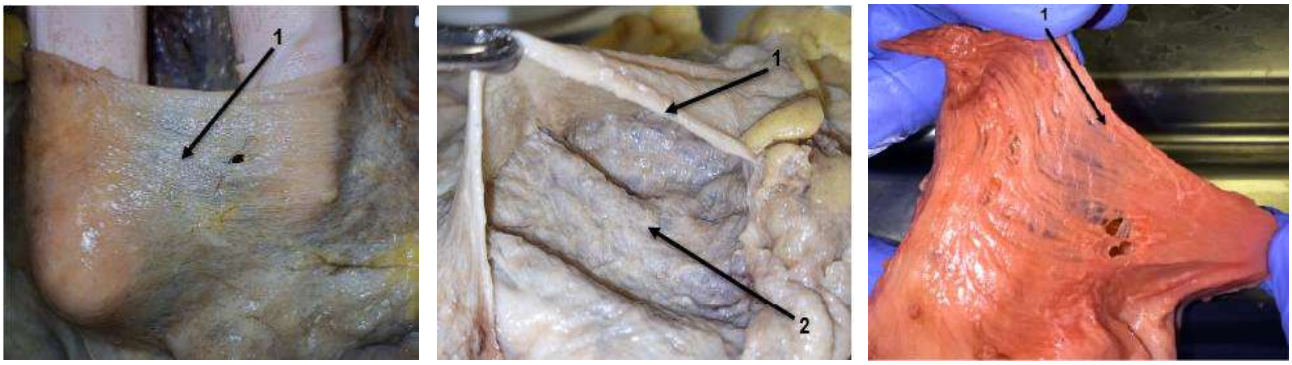

Fig. 5. Macro view of the resected part of the stomach. Muscle "layer": 1 - longitudinal and circular muscle fibers, 2 - oblique muscle fibers and submucosa.

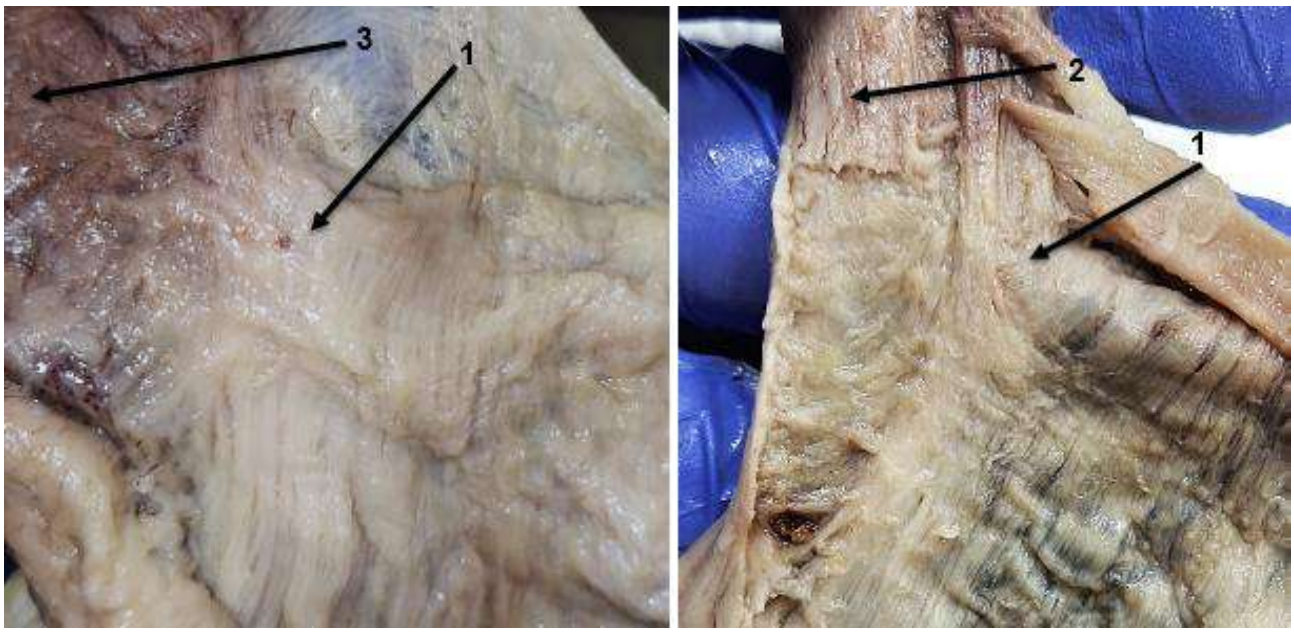

Fig. 6. Macro view of the resected part of the stomach. Intermuscular dissection: 1 - Helvecius collar, 2 - longitudinal muscle fibers of the esophagus, 3 - circular muscle fibers of the esophagus.

Fig. 7. Macro view of the resected part of the stomach. Stapler application: 1 - stapling at the level of the angle of His, 2 - stapling 1.5 cm distal to the angle of His.

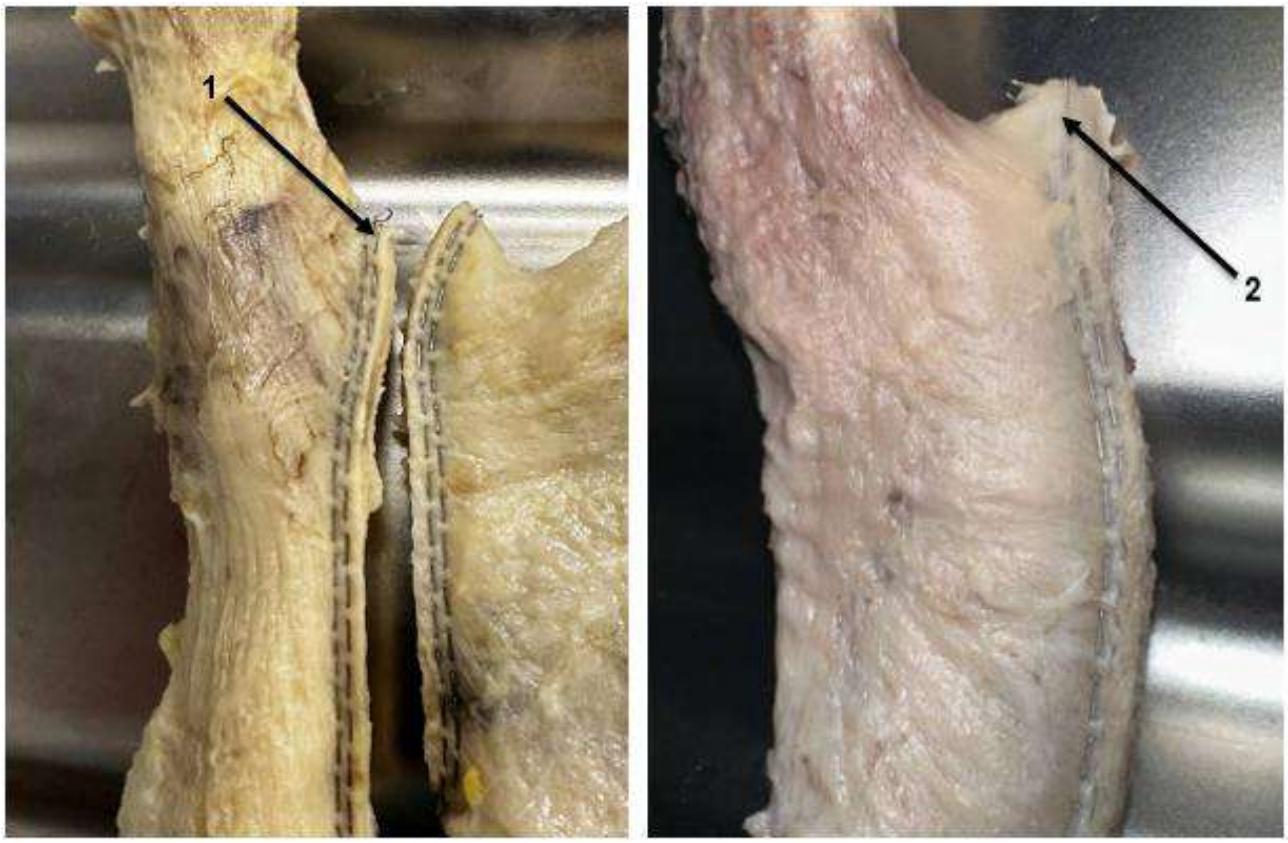

Fig. 8. Macro view of the resected part of the stomach. Stapled suture: 1 - level of the angle of His, 2 - 1.5 cm distal to the angle of His.

drops of dye per 100 ml of distilled water) (Fig. 9).

Different layers of the gastric tube muscle wall were visualized (Fig. 10).

In sample 1, it can be seen that most of the muscle

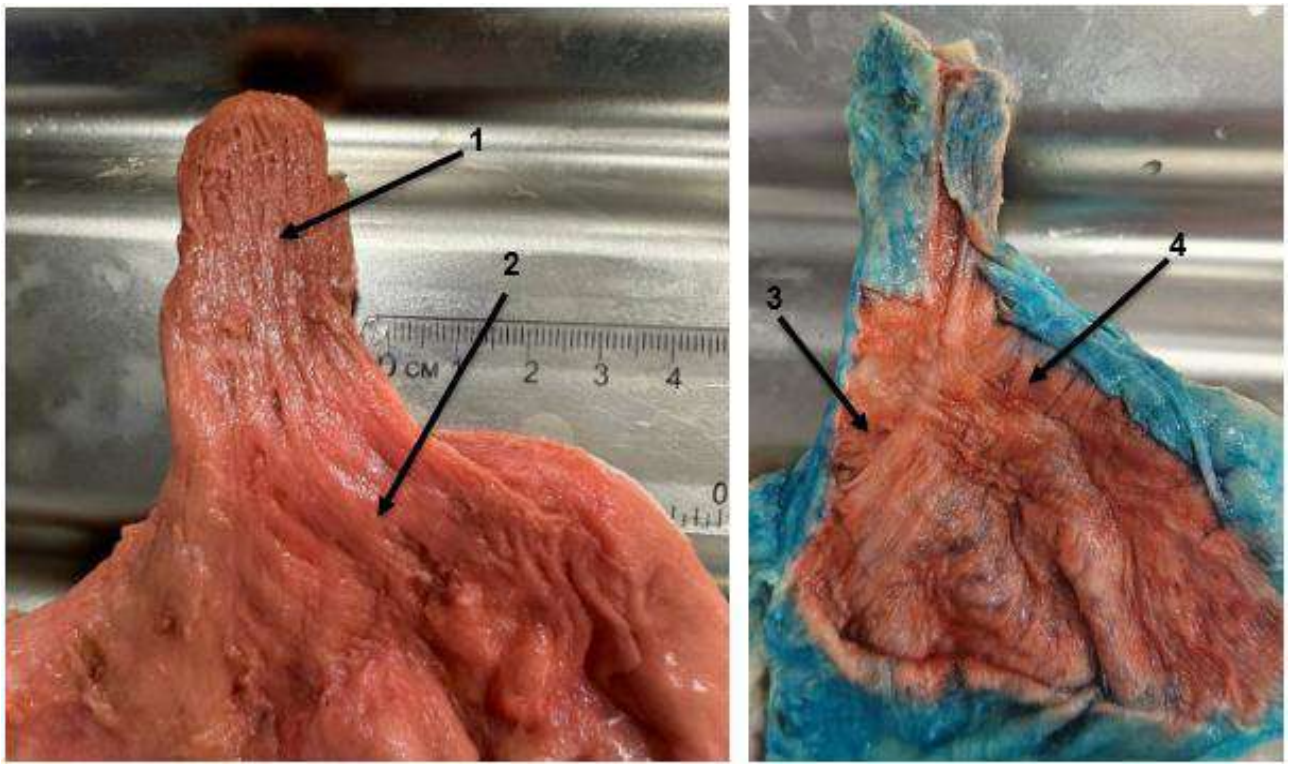

Fig. 9. Macro view of the resected part of the stomach. Stained muscle fibers of the samples: 1 - longitudinal muscle fibers of the esophagus, 2 - longitudinal muscle fibers of the stomach, 3 - circular muscle fibers of the stomach, 4 - oblique muscle fibers of the stomach.

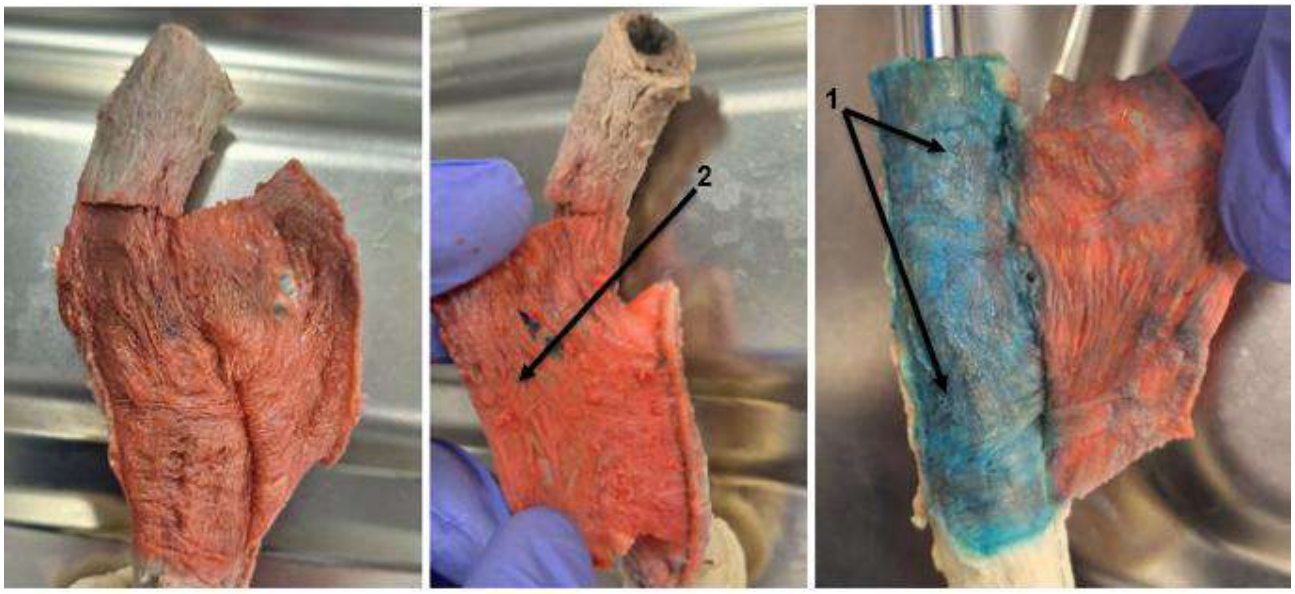

Fig. 10. Macro view of the resected part of the stomach. The result of intramural dissection of samples: 1 - circular muscle fibers of the esophagus and stomach, 2 - longitudinal muscle fibers of the esophagus and stomach

fibers run in a parallel and oblique direction to the staple suture. The longitudinal muscle fibers from the esophagus pass in the same direction to the formed gastric tube without changing orientation, the circular fibers of the esophagus at the transition to the gastric wall are also located almost longitudinally and parallel to the line of the staple suture (sling fibers and clasp fibers), the staple suture partially overlaps these fibers (Fig. 11).

In specimen 2, the direction of the longitudinal (external) muscle fibers visually changed, which, together with the circular gastric fibers, are oriented perpendicular to the staple line (Fig. 12).

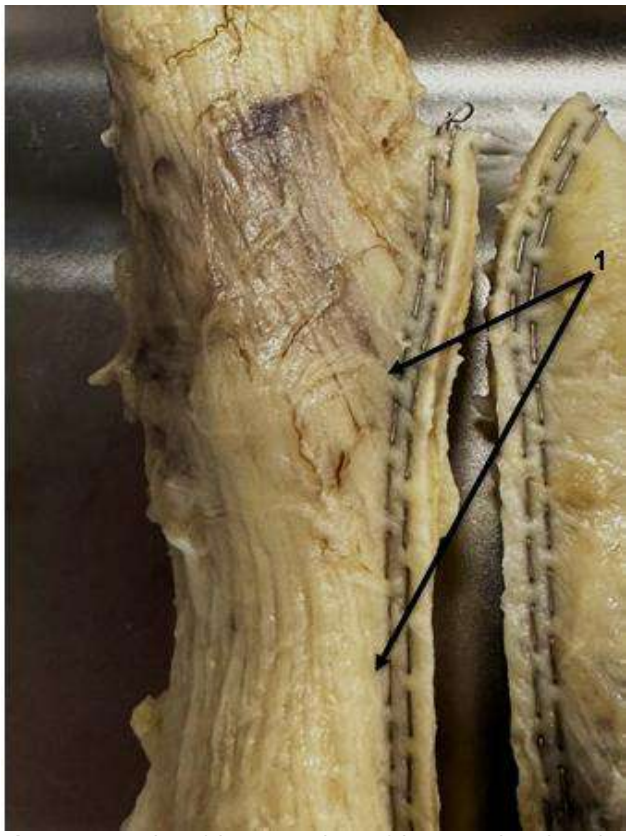

Fig. 11. Macro view of the resected part of the stomach. Orientation of the fibers to the staple suture applied to the angle of His: 1 - oblique and parallel orientation of the gastric muscle fibers to the staple suture.

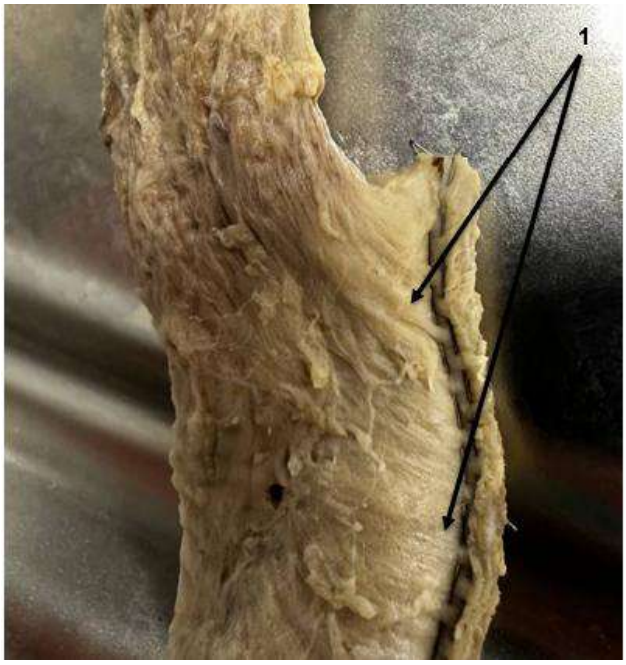

Fig. 12. Macro view of the resected part of the stomach. Orientation of the fibers to the staple suture applied 1.5 cm lateral to the angle of His: 1 - parallel orientation of the gastric muscle fibers to the staple suture.

Discussion

Obesity is a recognised modern pandemic and one of the most important risk factors for the development of a large number of life-threatening diseases. There are over 1 billion overweight adults worldwide and at least 300 million obese [22]. According to recent studies, the prevalence of obesity among the adult population has increased dramatically over the past decade. Researchers have demonstrated that obese people have a higher risk of developing a large number of comorbidities, a lower quality of life and increased mortality than those with a normal body mass index [5]. Although a healthy lifestyle seems to be the ideal option for losing weight, surgery remains the most effective and scientifically proven method for treating obesity.

Sleeve gastrectomy is a relatively new surgical technique and a leading method in metabolic surgery. SG is gaining popularity among bariatric surgeons around the world and has proven to be a successful method of achieving significant weight loss in a short period of time. After undergoing SG, patients can experience a variety of effects in the short term, including reduced body weight, improved blood pressure, reduced risks of stroke and cancer, and significant remission of obesity-related comorbidities, including type 2 diabetes mellitus, non-alcoholic fatty liver disease, cardiovascular disease, obstructive sleep apnoea, and non-obesity-related conditions such as gout, musculoskeletal disorders, ovarian dysfunction, and urinary incontinence [16].

This method of surgery removes a significant hormone-producing part of the stomach, which is responsible for appetite regulation. In recent years, SG has attracted considerable practical interest, mainly because this technique does not require various types of gastrointestinal anastomosis. It is minimally invasive and is considered less technically challenging than, for example, Roux-en-Y gastric bypass [16].

The most common and clinically significant complications of SG are SLF. The prevalence of these two complications is the same, and is 1-6 % [8, 17].

The rapidly growing number of different types of staplers and methods of forming gastric tube sutures creates a wide space for discussion on how the potential of these devices can be utilised during bariatric surgery with the lowest percentage of postoperative complications [2, 29].

SLF is a formidable complication after SG and often leads to prolonged postoperative treatment, increased morbidity and mortality [7]. This complication almost always occurs in the proximal part of the stapled suture within 1-2 cm of the esophagogastric junction (angle of His) [14]. Unfortunately, the exact pathophysiological mechanisms of this pathology have not yet been reflected in modern publications. Therefore, an understanding of the factors contributing to the occurrence of SLF can provide the necessary practical information to help reduce the incidence of this category of complications and assist in making tactical decisions during surgery. As of today, various mechanisms have been proposed that may

cause failure, but none of them is considered to be the main one. Wall ischaemia and intraluminal hypertension of the proximal gastric tube after SG are considered to be among the main causes of SLF [24]. Modern studies of the gastric wall and the staple suture line after SG are directed towards these two vectors. It is assumed that local ischaemia in the postoperative period is caused by hypoperfusion of the stapling suture zone wall and secondary arteriovenous insufficiency in the proximal gastric region. Other theories put forward include thermal injury to the wall or damage to the vascular network during excessive mobilisation in the esophagogastric junction zone [7, 9].

The high incidence of postoperative SLF has prompted surgeons around the world to change their surgical techniques. Some of these solutions include the use of larger diameter calibration probes (>36 Fr), the use of fibrin glue, reinforcing clips, coated cassettes and additional stitching of the staple suture area, selection of cassettes for the stapling machine [24].

However, there is still a debate in modern forums about how much to deviate from the angle of His when applying the edge stapler. The result of these discussions significantly reduced the level of major postoperative complications, but did not reduce them to 0, which provokes researchers to study in depth the morphology and pathophysiology of the stomach wall in the most compromised area of the oesophagogastric junction.

The main accent in the study of the nature of SLF is the morphological approach to assessing the thickness of the gastric wall in the fundus and oesophageal-gastric junction. Thus, C. Boeker et al. [4] in their observational study, which included 500 patients, measured the thickness of the gastric wall in the resected parts after SG. All histological blocks were prepared from the gastric wall near the proximal part of the last staple suture. The average thickness of the proximal gastric wall was 3172 μm in men and 2784 μm in women. In addition, 22 patients had SLF after surgery, which was 4.9 % (2.2 % in men and 6.6 % in women). In 90 % of cases, the failure was observed in the area of the angle of His, where the thickness of the muscle sheath was the proven cause. For the first time since 2014, a higher risk of SLF was reported in older patients ($p<0.05$) [4].

Elariny was one of the first to investigate and describe the thinning of the stomach wall from the pyloric region to the bottom in male patients. He noted that the greater thickness of the stomach wall in the area of the angle of His and the bottom is associated with the thickness of the muscularis [11]. The same conclusion was reached by van Rutte P. W. et al. in their study, where they additionally pointed out the thickness of the gastric wall in groups of patients with different body mass index [27].

The development of SLF is a consequence not only of the anatomical features of the stomach wall or surgical tactics, but also of the morbid background of obese patients. The most common multifactorial condition is metabolic syndrome, and its most important component is type II diabetes mellitus. This disease is very common and accounts for about 8.7 % of the general population [25].

The effect of long-term persistent type II diabetes on the innervation and morphology of the gastric wall has been described in many publications and is distinguished by separate pathological conditions. One of the most controversial and at the same time common conditions is diabetic gastroparesis, which occurs as a result of irreversible vagal neuropathy in long-standing and uncompensated type II diabetes [26].

Studies of the pathophysiology of this condition have shown that not only the neuropathy itself can influence the development of the above condition. The dysfunction of interstitial neurotransmitter cells, such as Cahal cells and fibroblast-like cells, makes it impossible to transmit action potentials from the nerve fibre to the smooth muscle tissue of the gastric wall, which in turn leads to persistent hypotension [20].

Long-standing neuromuscular dysfunction of the gastric wall will naturally develop into local and widespread fibrosis, which in turn will trigger a cascade of dysmetabolic and ischaemic changes that will eventually lead to thinning of the gastric wall. For example, Park K. S. et al. [20] found in their study that the incidence of moderate or severe wall fibrosis was 81.3 % in the group of patients with type II diabetes, and only 28.6 % in the control group. However, there was no clear association between the duration of diabetes mellitus and the degree of fibrosis ($p<0.05$).

Based on the results of these studies, it can be assumed that fibrosis and wall ischaemia will be unfavourable factors that will make it impossible to quickly heal and regenerate tissues in the most compromised area of the staple line after SG, the angle of His. This can naturally increase the risk of SLF, although it should be noted that these are not the only reasons for the development of this complication.

During our study, we found that for an in-depth study of the stomach wall as an anatomical specimen and possible pathologies, it is worth paying attention to the peculiarities of material preparation and fixation. The principle of preparing specimens for macroscopic and microscopic examination is significantly different. It is practically impossible to limit oneself to fixing the specimen for anatomical dissection and preparation due to the long work with bulky material.

At present, there is an incredibly wide range of chemical preservatives and variations in their use that allow anatomists to dissect anatomical objects without losing the structure, colour, and physical properties of the organ for a long time [6].

One of the newest and most promising methods of long-term fixation of human organs or body parts is the S10 and P40 plastination method, which has been the main method in most medical universities for 20 years due to its practicality in terms of working with anatomical specimens [23].

The plastination process consists of four main stages: fixation, dehydration, impregnation, and curing. The water and lipids of the biological tissue are completely replaced by polymers (silicone, polyester, epoxy) [13]. Even though

plastination offers many advantages, plastinated tissue is stiff and lacks natural elasticity, which is a disadvantage for teaching, learning, or clinical dissection [19].

Recently, a new modified type of plastination, the Elnady technique, was developed by Dr Fawzy Elnady [12] at the Department of Anatomy and Embryology, Faculty of Veterinary Medicine, Cairo University. This technique is superior to S10 plastination in several ways. The Elnady technique allows for preservation at room temperature, eliminating the need for expensive plastination laboratories. The technique is inexpensive and does not require proprietary chemicals. The specimens produced by Elnady technology are realistic, strong, soft and flexible [3].

We used Elnady's methodology only partially and with our own modifications in the process of preparation of specimens due to the priority given to dissection and preparation. When we started the process of preparing specimens for preservation, the main emphasis was placed on the "oxygen dissection" method, which was our main modification. There are no publications describing the effect of hydrogen peroxide on tissues during dissection. In their experiment, Echeverri D. and Acuña C. [10] described the irritating effect of hydrogen peroxide and sodium hypochloride (in combination and isolated) on the musculo-aponeurotic tissues of pigs in order to assess the effectiveness and speed of dissolution of necrotic and connective tissue masses in dental practice. The result of the study was the rapid dissolution of connective tissue (120 seconds) with the isolated use of 3 % hydrogen peroxide solution and the appearance of the effect of tissue emphysema.

We achieved a similar effect on our samples, where, in addition to emphysematous tissue dissection and dissolution of interstitial connective tissue adhesions, we obtained discolouration of muscle fibres without denaturation, which facilitated the process of further staining of the samples. The subsequent stages of preparation were identical to the Elnady method.

The gastric musculature has been described by many anatomists. Most of these descriptions have focused on the lower oesophageal sphincter area and have been based on dissection manometry and sectional images. In addition, there are various descriptions of the location and direction of the gastric muscle fibres in many textbooks. In 2020, Professor Mi-Sun Hur [15] published a fundamental descriptive study of the muscle architecture of the abdominal esophagus and stomach, including 60 specimens describing the variability of the course of different fibres.

Focusing on the area of the gastroesophageal junction, a reasonable addition to the above results of our study would be the data of Mi-Sun Hur [15], according to which in the area of the angle of His, the number of muscle fibres running parallel or oblique to the small curvature is much higher than that estimated 1-1.5 cm distal to the oesophageal-gastric junction; 1 cm distal to the angle of His, there is an asymmetric thickening of the stomach wall due to the muscle component, with a predominance of fibres with a perpendicular orientation to the large and small curvature of the stomach; unlike the esophagus, the muscle layers of the stomach are not separate but are interconnected starting from the oesophagogastric junction.

Based on our own and international studies, it can be assumed that when applying a staple suture at the level of the angle of His, the number of parallel fibres to the staple suture line will prevail over perpendicular fibres, in turn, the number of perpendicular and oblique fibres to the staple suture line will prevail over parallel fibres in the case of staple distalisation by 1.5 cm from the esophagogastric junction.

Our results indicate that distalization in stapling suturing in SG will be the main factor in more extensive tissue trauma, which in turn will lead to a full-fledged local inflammatory and regenerative cascade with a lower risk of SLF.

Conclusions

1. As a result of the precision dissection, it was found that in the area of the esophagogastric junction, the longitudinal muscles of the esophagus, together with the circular muscles of the stomach body, form a continuous 'layer' of intertwined fibres.

2. The right longitudinal fibres of the oesophagus descend to become the longitudinal fibres of the stomach along the small curvature. The left longitudinal fibres of the oesophagus and part of the circular fibres of the stomach descend to become the longitudinal fibres of the stomach along the great curvature of the stomach.

3. In the area of the oesophagogastric junction, a change in the direction and orientation of the fibres of the circular layer of the oesophageal muscles that passes to the stomach wall (the so-called sling fibres and clasp fibres, which together form the Helvecius collar) is visualized.

4. When applying a staple suture, during sleeve gastrectomy, at the level of the His angle, the number of parallel fibres to the staple suture line will prevail over perpendicular fibres, in turn, the number of perpendicular and oblique fibres to the staple suture line will prevail over parallel fibres in the case of staple distalisation by 1.5 cm from the esophagogastric junction.

References

[1] Angrisani, L., Santonicola, A., Iovino, P., Palma, R., Kow, L., Prager, G., ... & Shikora, S. (2024). IFSO Worldwide Survey 2020-2021: Current Trends for Bariatric and Metabolic Procedures. *Obesity Surgery,* 34(4), 1075-1085. doi: 10.1007/s11695-024-07118-3

[2] Barski, K., Binda, A., Kudlicka, E., Jaworski, P., & Tarnowski, W. (2018). Gastric wall thickness and stapling in laparoscopic sleeve gastrectomy - a literature review. *Videosurgery and Other Miniinvasive Techniques,* 13(1), 122-127. doi: 10.5114/wiitm.2018.73362

[3] Bernal, V., Aburto, P., Pérez, B., Gómez, M., & Gutierrez, J. C. (2022). A technical note of improvement of the Elnady technique for tissue preservation in veterinary anatomy. *Animals*, 12(9), 1111. doi: 10.3390/ani12091111

[4] Boeker, C., Schneider, B., Markov, V., Mall, J., Reetz, C., Wilkens,

L., ... & Köhler, H. (2021). Primary sleeve gastrectomy and leaks: the impact of fundus-wall thickness and staple heights on leakage-an observational study of 500 patients. *Frontiers in Surgery,* 8, 747171. doi: 10.3389/fsurg.2021.747171

[5] Bout-Tabaku, S., Gupta, R., Jenkins, T. M., Ryder, J. R., Baughcum, A. E., Jackson, R. D., ... & Michalsky, M. P. (2019). Musculoskeletal pain, physical function, and quality of life after bariatric surgery. *Pediatrics,* 144(6), e20191399. doi: 10.1542/peds.2019-1399

[6] Brenner, E. (2014). Human body preservation-old and new techniques. *Journal of anatomy,* 224(3), 316-344. https://doi.org/10.1111/joa.12160

[7] Catchlove, W., Liao, S., Lim, G., Brown, W., & Burton, P. (2022). Mechanism of staple line leak after sleeve gastrectomy via isobaric pressurisation concentrating stress forces at the proximal staple line. *Obesity Surgery,* 32(8), 2525-2536. doi: 10.1007/s11695-022-06110-z

[8] Debs, T., Petrucciani, N., Kassir, R., Sejor, E., Karam, S., Amor, I. B., & Gugenheim, J. (2018). Complications after laparoscopic sleeve gastrectomy: can we approach a 0 % rate using the largest staple height with reinforcement all along the staple line? Short-term results and technical considerations. *Surgery for Obesity and Related Diseases,* 14(12), 1804-1810. doi: 10.1016/j.soard.2018.08.028

[9] Delattre, J. F., Avisse, C., Marcus, C., & Flament, J. B. (2000). Functional anatomy of the gastroesophageal junction. *Surgical Clinics of North America*, 80(1), 241-260. doi: 10.1016/s0039-6109(05)70404-7

[10] Echeverri, D., & Acuña, C. (2012). Dissolution of connective tissue in sodium hypochlorite alone and in combination with 3 % hydrogen peroxide. *Int. J. Odontostomat,* 6(3), 263-266. doi: 10.4067/S0718-381X2012000300003

[11] Elariny, H., González, H., & Wang, B. (2005). Tissue thickness of human stomach measured on excised gastric specimens from obese patients. *Surgical Technology International,* 14, 119-124. PMID: 16525963

[12] Elnady, F. A. (2016). The Elnady Technique: An innovative, new method for tissue preservation. *ALTEX-Alternatives to Animal Experimentation*, 33(3), 237-242. doi: 10.14573/altex.1511091

[13] Henry, R. W., von Hagens, G., & Seamans, G. (2019). Cold temperature/Biodur®/S10/von Hagens'-Silicone plastination technique. Anatomia, Histologia, Embryologia, 48(6), 532-538. doi: 10.1111/ahe.12472

[14] Hughes, D., Hughes, I., & Khanna, A. (2019). Management of staple line leaks following sleeve gastrectomy-a systematic review. *Obesity Surgery,* 29(9), 2759-2772. doi: 10.1007/s11695-019-03896-3

[15] Hur, M. S. (2020). Muscular architecture of the abdominal part of the esophagus and the stomach. *Clinical Anatomy*, 33(4), 530-537. doi: 10.1002/ca.23427

[16] Kheirvari, M., Nikroo, N. D., Jaafarinejad, H., Farsimadan, M., Eshghjoo, S., Hosseini, S., & Anbara, T. (2020). The advantages and disadvantages of sleeve gastrectomy; clinical laboratory to bedside review. *Heliyon,* 6(2), e03496. doi: 10.1016/j.heliyon.2020.e03496

[17] Li, S., Jiao, S., Zhang, S., & Zhou, J. (2021). Revisional surgeries of laparoscopic sleeve gastrectomy. *Diabetes, Metabolic Syndrome and Obesity,* 575-588. doi: 10.2147/DMSO.S295162

[18] Mechanick, J. I., Apovian, C., Brethauer, S., Garvey, W. T., Joffe, A. M., Kim, J., ... & Still, C. D. (2020). Clinical practice guidelines for the perioperative nutrition, metabolic, and nonsurgical support of patients undergoing bariatric procedures-2019 update: cosponsored by American Association of Clinical Endocrinologists/American College of Endocrinology, The Obesity Society, American Society for Metabolic & Bariatric Surgery, Obesity Medicine Association, and American Society of Anesthesiologists. *Surgery for Obesity and Related Diseases,* 16(2), 175-247. doi: 10.4158/GL-2019-0406

[19] Musumeci, E., Lang, F. J. W., Duvoisin, B., & Riederer, B. M. (2003). Plastinated ethmoidal region: I. Preparation and applications in clinical teaching. *J Int Soc Plast,* 18, 23-28. doi: 10.56507/GILN1147

[20] Park, K. S., Cho, K. B., Hwang, I. S., Park, J. H., Jang, B. I., Kim, K. O., ... & Kwon, J. G. (2016). Characterization of smooth muscle, enteric nerve, interstitial cells of Cajal, and fibroblast-like cells in the gastric musculature of patients with diabetes mellitus. *World Journal of Gastroenterology,* 22(46), 10131-10139. doi: 10.3748/wjg.v22.i46.10131

[21] Parmer, M., Wang, Y. H. W., Hersh, E. H., Zhang, L., Chin, E., & Nguyen, S. Q. (2022). Management of staple line leaks after laparoscopic sleeve gastrectomy. *JSLS: Journal of the Society of Laparoscopic & Robotic Surgeons*, 26(3), e2022.00029. doi: 10.4293/JSLS.2022.00029

[22] Piché, M. E., Tchernof, A., & Després, J. P. (2020). Obesity phenotypes, diabetes, and cardiovascular diseases. *Circulation Research,* 126(11), 1477-1500. doi: 10.1161/CIRCRESAHA.120.316101

[23] Riederer, B. M. (2014). Plastination and its importance in teaching anatomy. Critical points for long-term preservation of human tissue. *Journal of Anatomy,* 224(3), 309-315. doi: 10.1111/joa.12056

[24] Saber, A. A., Azar, N., Dekal, M., & Abdelbaki, T. N. (2015). Computed tomographic scan mapping of gastric wall perfusion and clinical implications. *The American Journal of Surgery,* 209(6), 999-1006. doi: 10.1016/j.amjsurg.2014.05.023

[25] Shi, Y., & Hu, F. B. (2014). The global implications of diabetes and cancer. *The Lancet,* 383(9933), 1947-1948. doi: 10.1016/S0140-6736(14)60886-2

[26] Thazhath, S. S., Jones, K. L., Horowitz, M., & Rayner, C. K. (2013). Diabetic gastroparesis: recent insights into pathophysiology and implications for management. *Expert Eview of Gastroenterology & Hepatology,* 7(2), 127-139. doi: 10.1586/egh.12.82

[27] Van Rutte, P. W., Naagen, B. J., Spek, M., Jakimowicz, J. J., & Nienhuijs, S. W. (2015). Gastric Wall Thickness in Sleeve Gastrectomy Patients: Thickness Variation of the Gastric Wall. *Surgical Technology International,* 27, 123-128. PMID: 26680415

[28] Varban, O. A., Sheetz, K. H., Cassidy, R. B., Stricklen, A., Carlin, A. M., Dimick, J. B., & Finks, J. F. (2017). Evaluating the effect of operative technique on leaks after laparoscopic sleeve gastrectomy: a case-control study. *Surgery for Obesity and Related Diseases,* 13(4), 560-567. doi: 10.1016/j.soard.2016.11.027

[29] Vogt, C. D., & Panoskaltsis Mortari, A. (2020). Tissue engineering of the gastroesophageal junction. *Journal of Tissue Engineering and Regenerative Medicine*, 14(6), 855-868. doi: 10.1002/term.3045

МОРФО-ТОПОГРАФІЧНІ ОСОБЛИВОСТІ ХОДУ М'ЯЗОВИХ ВОЛОКОН СТІНКИ ШЛУНКА В ДІЛЯНЦІ СТРАВОХІДНО-ШЛУНКОВОГО ПЕРЕХОДУ ПРИ ВИКОНАННІ РУКАВНОЇ РЕЗЕКЦІЇ ШЛУНКА

Калашніков О. О., Усенко О. Ю., Тодуров І. М., Гриневич А. А.

Рукавна резекція шлунка, також відома як вертикальна гастректомія, є однією з найбільш поширених та популярних баріатричних операцій у світі. Ця операція стала особливо популярною в останні десятиліття завдяки своїй ефективності

в зменшенні ваги та покращенні супутніх метаболічних розладів. Однак, незважаючи на високу ефективність даної операції, неспроможність лінії степлерного шва залишається одним із найсерйозніших ускладнень, що може призвести до серйозних наслідків, таких як перитоніт, сепсис та подовжений термін перебування в стаціонарі. Дослідження морфо-топографічних особливостей ходу м'язових волокон стінки шлунка в ділянці стравохідно-шлункового переходу є актуальним для розуміння механізмів неспроможності шва та розробки профілактичних заходів. Мета роботи - оцінити морфо-топографічні особливості ходу м'язових волокон стінки шлунка в ділянці стравохідно-шлункового переходу при виконанні рукавної резекції шлунка. Проведено комплексне дослідження анатомо-функціональних характеристик м'язового шару шлунка в зоні стравохідно-шлункового переходу. В зоні стравохідно-шлункового переходу відзначається значна зміна в архітектоніці м'язового шару. Тут переважають колові м'язи, що свідчить про функціональну адаптацію цієї ділянки до регуляції пасажу їжі. З урахуванням переходу від анатомічної зони стравоходу до шлунку виявлено появу нових м'язових шарів що пояснюється фізіологічною специфікою порожнистого органу. Шляхом послідовної дисекції м'язових шарів, використовуючи методи гістологічного аналізу та макроскопічної морфометрії, виявлено специфічні особливості м'язових волокон, що впливають на формування лінії степлерного шва, а саме здебільшого паралельний хід волокон в зоні кута Гіса та схрещений дистальніше від нього, товщина м'язового шару на рівні кута Гіса переважає над дистальнішим рівнем. Таким чином, отримані результати мають важливе значення для вдосконалення хірургічної техніки рукавної резекції шлунка, зокрема щодо вибору оптимального розташування та напряму шва - формування суцільного "пласту" схрещених м'язових волокон тіла шлунка, перехід поздовжніх м'язових волокон стравоходу на дно та велику кривизну шлунка що разом з циркулярними волокнами набувають перпендикулярної орієнтації до рівня накладення степлерного шва.

Ключові слова: *рукавна резекція шлунка, неспроможність лінії степлерного шва, пластинація, стінка шлунка, м'язові волокна.*

Author's contribution

Kalashnikov O. O. - conceptualization, data curation, investigation, methodology, visualization, writing original draft.
Usenko O. Yu. - formal analysis, funding acquisition, project administration, supervision, validation.
Todurov I. M. - review & editing, formal analysis, funding acquisition, project administration, supervision, validation.
Hrynevych A. A. - conceptualization, investigation, methodology, visualization, writing original draft.

DOI: 10.31393/morphology-journal-2024-30(3)-09 Reports of Morphology, Vol. 30, №3, Pages 91-98

ISSN 1818-1295 eISSN 2616-6194

REPORTS OF MORPHOLOGY

Official Journal of the Scientific Society of Anatomists, Histologists, Embryologists and Topographic Anatomists of Ukraine

journal homepage: https://morphology-journal.com

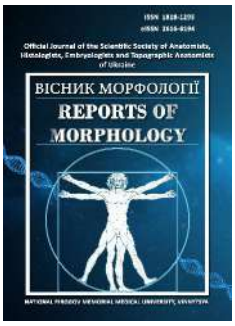

Characteristics of the hemomicrocirculatory channel of the ventricular myocardium in triptorelin-induced central deprivation of the synthesis of luteinizing hormone and correction of this condition by the introduction of quercetin

Voroshilova T. A., Shepitko V. I., Stetsuk E. V., Vilkhova O. V., Puzyryov G. S.
Poltava State Medical University, Poltava, Ukraine

ARTICLE INFO
Received: 02 February 2024
Accepted: 13 August 2024

UDC: 161.9:612.017 - 587.323.2

CORRESPONDING AUTHOR
e-mail: stetsuk78@gmail.com
Stetsuk Ye. V.

CONFLICT OF INTEREST
The authors have no conflicts of interest to declare.

FUNDING
Not applicable.

DATA SHARING
Data are available upon reasonable request to corresponding author.

The study of the microcirculatory channel of the connective tissue of the myocardium of the ventricles improves the understanding of the features of pathological processes, such as ischemia, hypoxia and remodeling of the myocardium, the evaluation of the effectiveness of drug therapy, as well as rehabilitation methods. The purpose of the study is to determine the changes in the hemomicrocirculatory channel of the ventricular myocardium in triptorelin-induced central deprivation of the synthesis of luteinizing hormone and the correction of this condition by the introduction of quercetin. The experiment was conducted on 60 sexually mature white male rats weighing 140-160 g. The rats were divided into 3 groups. 1 group - control, rats injected with physiological solution (10 animals). Group 2 - rats that were injected subcutaneously with diphereline (triptorelin embonate) at a dose of 0.3 mg of the active substance per kg of body weight for 365 days (25 animals). Group 3 - rats that were injected with a solution of triptorelin at the rate of 0.3 mg of the active substance per kg of body weight to simulate central deprivation of the synthesis of luteinizing hormone with the addition of quercitin to the diet using a gastric tube based on the body weight of the animals three times a week (25 animals). Animals were withdrawn from the experiment after 1, 3, 6, 9 and 12 months by overdose with ether anesthesia. A comprehensive study of histological preparations of the myocardium and quantitative calculation of the diameter of the vessels of the microcirculatory bed were carried out using a light microscope with a digital microfilter and software adapted for these studies. Statistical processing of the research results was carried out using the Microsoft Office Excel software and the Real Statistics 2019 extension. When analyzing the index of arteriole diameters in the group of animals that were injected with triptorelin after 1, 3, 6, 9 and 12 months, a significant increase in the diameter of arterioles was established compared to the control group animals, respectively, by 13.9 % - 40.8 % - 102.6 % - 112.6 % - 11.5 %; and in animals to which quercetin was administered against the background of triptorelin administration, it was established that this indicator after 1 month did not reliably differ from the similar one in the control group, and after 3, 6, 9 and 12 months it was reliably higher than in the control respectively by 11.5 % - 136.2 % - 101.1 % - 101.4 %. The analysis of the diameters of the venular link of the hemomicrocirculatory channel in the group of animals administered triptorelin showed a significant increase in the value of this indicator after 3, 6, 9 and 12 months compared to the control group, respectively by 20.0 % - 71.2 % - 57.8 % - 22.9 %; and in animals that were additionally injected with quercetin after 1 month, the diameter of venules was significantly reduced by 8.1% compared to the control, and after 3, 6, 9 and 12 months - respectively by 5.2 % - 87.5 % - 64.0 % - 50.4 % it was significantly greater than in control animals. Analysis of capillary diameters in the group of animals administered triptorelin showed a significant increase in the value of this indicator after 1, 3, 6 and 9 months compared to the control group, respectively by 23.9 % - 49.1 % - 61.8 % - 36.7 %; and in animals that were additionally injected with quercetin, the capillary diameter significantly increased compared

to the control after 3, 6, 9, and 12 months - by 22.3 % - 55.3 % - 17.1 % - 25.2 %, respectively. The conducted study showed that the introduction of triptorelin leads to structural and functional changes in the components of the microcirculatory channel of the myocardium of the ventricles of the heart, which are characterized by changes in the diameter of the arterial and venous links with a gradual increase in blood flow, the maximum of which is at the 6th month of the experiment in both experimental groups, but without impaired outflow in the group with the addition of quercitin.
Keywords: *heart, myocardium, hemomicrocirculatory channel, testosterone, luteinizing hormone, quercetin, triptorelin.*

Introduction

According to estimates of the World Health Organization, about a third of all deaths in the world during the last few years are caused by cardiovascular diseases [8, 21]. Most often, patients die from coronary heart disease, the main cause of which is atherosclerotic changes in the coronary arteries [20, 23]. Regarding non-coronarogenic diseases, which are caused by other factors, the first place is occupied by complications after the therapy of oncological diseases. The consequences of this therapy are manifested in the form of disorders of the hemomicrocirculatory channel of the connective tissue layer of the myocardium of the ventricles of the heart [22, 24, 28].

As you know, the space between cardiomyocytes is filled with loose fibrous connective tissue, which has a rather complex structure. It is the features of the structural organization that allow it to perform a number of important functions: nutrition, immune protection, coordination of contractile components of the myocardium. The components of the interstitium are vessels, elements of the nervous system, cells of connective tissue, the main substance and fibers [3]. They structurally integrate the myocardium and are a multifunctional system of interdependent elements that provides the formation of an environment for the normal functioning of working cardiomyocytes [4, 27].

The hemomicrocirculatory channel in the connective tissue of the myocardium of the ventricles is a complex and important vascular system that ensures the supply of oxygen and nutrients to the cells of the myocardium, as well as the effective removal of metabolic products. Arterioles, capillaries, and venules are classified as vessels of the hemomicrocirculatory channel. They penetrate deep into the connective tissue of the myocardium and provide blood supply to each cell of this area of the heart muscle [11, 17].

Studies of the hemomicrocirculatory channel of the connective tissue of the ventricular myocardium are quite relevant for modern medicine. The study of the hemomicrocirculatory channel improves the understanding of the features of pathological processes, such as ischemia, hypoxia, and remodeling of the myocardium, allows to evaluate the effectiveness of drug therapy, as well as rehabilitation methods [11, 13, 25].

Studies of the hemomicrocirculatory channel enable the development of new methods of visualization of microvessels and contribute to the improvement of diagnostics and surgical interventions [7, 30], as well as identify risk factors for the development of complications in cardiovascular diseases and take measures for their prevention [16].

Preparations based on triptorelin lead to disruption of the synthesis of luteinizing hormone and inhibition of testosterone production. This fact is of particular importance in the treatment of oncological pathology, in particular such as prostate cancer [25].

In turn, testosterone plays an important role in the functioning of the cardiovascular system, and its deficiency leads to an increased risk of cardiovascular mortality [30]. Testosterone replacement therapy can be used as an effective means of correcting these changes in the heart, although it works partially and not in all clinical cases [7]. The reason for such partial effectiveness may lie in the lack of data on the molecular mechanisms of changes that occur in the heart with testosterone deficiency.

Testosterone is involved in the regulation of protein activity. Some authors provide evidence that testosterone deficiency improves the condition of the heart after myocardial infarction [28]. Testosterone deficiency also prevents the development of myocardial hypertrophy in the late stages after myocardial infarction [20]. At the same time, testosterone deficiency can cause the development of oxidative stress and spread endothelial dysfunction, interfering with the production of nitric oxide [9]. Thus, the consequences of long-term testosterone deficiency caused by central deprivation of luteinizing hormone synthesis can lead to changes in the hemomicrocirculatory channel of the myocardial interstitium, which require detailed study.

Recently, the study of the antioxidant activity of quercetin has increasingly attracted the attention of scientists. It has been proven that the antioxidant activity of quercetin [2] is mainly based on the maintenance of oxidative balance. It is able to affect enzymatic activity, glutathione synthesis, signal transmission pathways, and reactive oxygen species caused by various environmental and toxicological factors [5, 6, 19].

Thus, studies of the microcirculatory channel of the connective tissue of the myocardium of the ventricles play a key role in modern medicine, helping to increase the effectiveness of treatment of cardiovascular diseases and improve the prognosis for patients.

The purpose of this study is to determine the changes in the hemomicrocirculatory channel of the ventricular myocardium during triptorelin-induced central deprivation of the synthesis of luteinizing hormone and to correct this condition by introducing of quercetin.

Materials and methods

The experiment was conducted on 60 sexually mature white male rats weighing 140-160 g. The material for the study was the ventricles of the hearts. The animals were divided into 3 groups. 1 group - control, rats injected with physiological solution (10 animals). Group 2 - rats injected subcutaneously with diphereline (triptorelin embonate) [26] at a dose of 0.3 mg of the active substance per kg of body weight for 365 days (25 animals). Group 3 - rats that were injected with a solution of triptorelin at the rate of 0.3 mg of the active substance per kg of body weight to simulate central deprivation of the synthesis of luteinizing hormone with the addition of quercitin to food with the help of a gastric probe based on the body weight of the animals three times a week (25 animals). Animals were withdrawn from the experiment after 1, 3, 6, 9 and 12 months by overdose with ether anesthesia. The animals were kept under standard conditions in the vivarium of the Poltava State Medical University. The study is a fragment of the scientific project "Experimental and morphological study of the influence of diphereline of cryopreserved placenta transplants on the morphofunctional state of a number of internal organs", state registration No. 0124U003358.

All research and euthanasia of experimental animals were carried out in accordance with the provisions of the "European Convention for the Protection of Vertebrate Animals Used for Experimental and Other Scientific Purposes" (Strasbourg, 1986), as well as with the "General Ethical Principles of Animal Experimentation" adopted by the First National Congress of bioethics (Kyiv, 2001).

The process of euthanasia of animals was carried out by overdose of ether anesthesia. Small fragments of the myocardium were fixed according to the generally accepted method and placed in paraffin blocks. Sections with a thickness of 4 μm were made from these blocks and stained with hematoxylin and eosin [1]. A comprehensive study of histological preparations was performed on a light microscope BIOREX-3#5605. Quantitative counting of the vessels of the microcirculatory bed was performed in the field of vision, by visual assessment, using a light microscope with a digital microfilter and software adapted for these studies. Photographs were taken using a DCM 900 digital microphotographic attachment using special software for these studies.

Statistical processing of the research results was carried out using Microsoft Office Excel software and the Real Statistics 2019 extension to it. The non-parametric Mann-Whitney test was used to determine the statistical significance of differences between groups. The difference was considered statistically significant at $p<0.05$.

Results

When studying the microscopic organization of the myocardium with the help of histological preparations of the heart ventricles of rats of both experimental groups, which were stained with hematoxylin-eosin, the following was established. The composition of the myocardium included cardiomyocytes and a connective tissue component. Representatives of different cell groups were clearly visualized in the connective tissue, and vessels of different diameters were also detected (Fig. 1B).

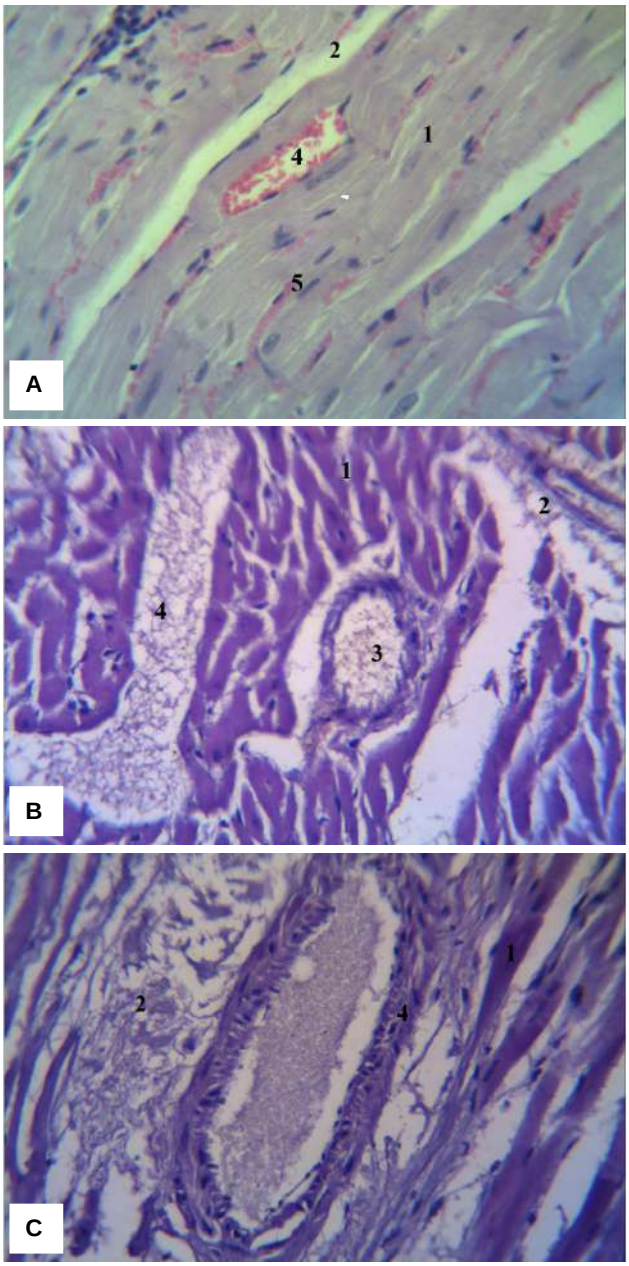

Fig. 1. Hemomicrocirculatory channel of the myocardium of the ventricles. A - control group. B - group with the introduction of triptorelin. C - group when quercetin is administered against the background of triptorelin. 1 - cardiomyocyte; 2 - myocardial interstitium; 3 - arteriole; 4 - venule; 5 - capillary. Hematoxylin-eosin staining. Lensx40. Eyepiecex15.

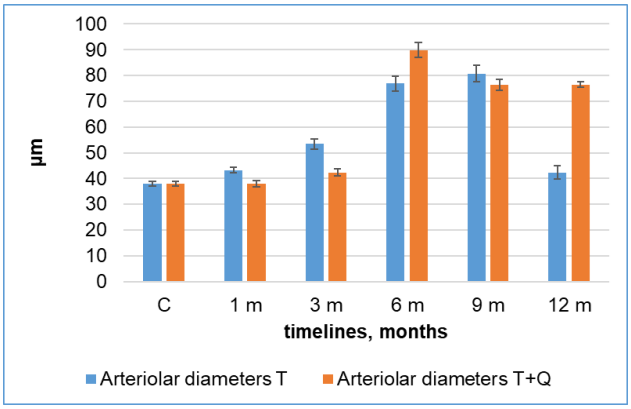

Fig. 2. The diameters of the arteriolar link of the hemomicrocirculatory bed in the group of animals with the introduction of triptorelin (T) and the group of animals that were injected with quercetin (T+Q) against the background of the introduction of triptorelin at different terms of the study.

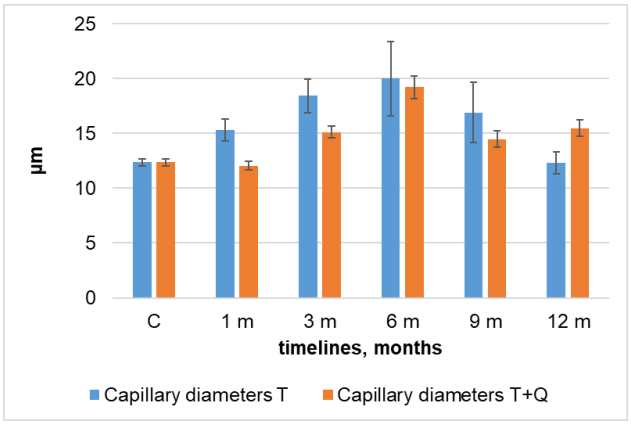

Fig. 3. The diameters of the capillary link of the hemomicrocirculatory channel in the group of animals with the introduction of triptorelin (T) and the group of animals that were injected with quercetin (T+Q) against the background of the introduction of triptorelin at different terms of the study.

The connective tissue component of the myocardium had a complex shape and organization, which changed depending on the response to the administration of triptorelin and triptorelin in combination with quercetin. Visual analysis of the ventricular myocardium showed diversity in the quantitative and qualitative appearance of arteriolar, capillary and venular links of the hemomicrocirculatory channel. As can be seen on histological preparations, arteriolar and venular links are located in the interstitial space, that is, in the connective tissue between the cardiomyocytes of the ventricles. And the capillary link was practically immersed in the very clusters of cardiomyocytes (Fig. 1A, 1B, 1C).

The arteriolar link of the hemomicrocirculatory channel was represented by arterioles. As can be seen in Figure 2, the parameter studied by us - the diameter of arterioles 1 month after administration of triptorelin is statistically significantly larger (43.22±1.09 µm, $p<0.05$) compared to the control group of rats (37.96±1.02 µm). After 3 months, a further increase in the diameter of the arterioles was observed (53.45±2.03 µm, $p<0.01$ compared to the control group). After 6 months of observation, a sharp increase in the diameter of the arterioles was found (76.91±2.93 µm, $p<0.001$ compared to the control group). After 9 months of observation, the value of this indicator continues to increase (80.71±3.12 µm, $p<0.001$ compared to the control group). At the end of the experiment (12 months), there was a sharp decrease in the diameter of arterioles (42.34±2.56 µm, $p<0.05$ compared to the control group).

When analyzing the index of the diameters of arterioles in the group of animals that received quercetin against the background of triptorelin administration (see Fig. 2), we found that this index after 1 month was not significantly different (38.04±1.23 µm, $p>0.05$) from the similar one in the control group (37.96±1.02 µm). After 3 months of observation, a statistically significant increase in this parameter was found (42.33±1.33 µm, $p<0.05$ compared to the control group). After 6 months of the study, a sharp increase in the diameter of arterioles was established (89.91±3.03 µm, $p<0.001$). After 9 months, the value of the diameter of arterioles decreases (76.33±2.17 µm), but remains significantly larger than in the control group of animals ($p<0.001$). After 12 months, this indicator was not significantly different from the previous period (76.44± 1.09 µm, $p<0.001$ compared to the control group).

The analysis of the diameters of the capillary link of the hemomicrocirculatory channel (Fig. 3), in the group of animals administered triptorelin showed that after 1 month of observation, a significant increase in the diameter of these vessels (12.37±0.33 µm, $p<0.05$) was observed when compared with the control group (15.33±1.02 µm). After 3 months, a significant increase in capillary diameters continued (18.44±1.54 µm, $p<0.05$ compared to the control group). The maximum increase in the value of this indicator was observed after 6 months (20.01±3.41 µm, $p<0.05$ compared to the control group). After 9 months, there was

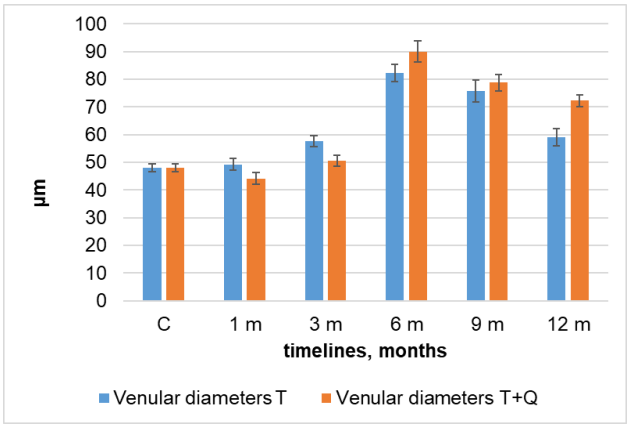

Fig. 4. The diameters of the venular link of the hemomicrocirculatory bed in the group of animals with the introduction of triptorelin (T) and the group of animals that were injected with quercetin (T+Q) against the background of the introduction of triptorelin at different terms of the study.

a slight decrease in the diameters of the microvessels of the exchange link (16.91±2.73 μm, p<0.05 compared to the control group). After 12 months, the diameters of the capillary link (12.33±0.98 μm) practically did not differ from similar indicators in the control group.

The analysis of the diameter of the capillary link in the group of animals that received quercetin against the background of triptorelin administration showed (see Fig. 3) that after 1 month the indicator was almost equal to that in the control group (12.04±0.39 μm and 12.37± 0.33 μm, respectively). After 3 months of observation, the diameters of the microvessels of the exchange link increased significantly (15.13±0.54 μm, p<0.05 compared to the control group). The maximum increase of this indicator was established after 6 months of observation (19.21±1.05 μm, p<0.001 compared to the control group). After 9 months, the capillary diameter significantly decreased (14.49±1.54 μm, p<0.05 compared to the control group). After 12 months, the capillary diameter was slightly higher than in the previous period (15.49±0.76 μm, p<0.05 compared to the control group).

Statistical analysis of indicators of the diameters of the venular link of the hemomicrocirculatory channel (Fig. 4) showed that in the group of animals administered triptorelin after 1 month of observation, the value of this indicator did not differ statistically significantly (49.22±2.12 μm, p>0.05) from the control group of animals (48.03 ±1.34 μm). After 3 months, a significant increase in the diameter of the venular link was established (57.62±2.08 μm, p<0.05 compared to the control group). After 6 months, there was a sharp increase in the diameter of the venules (82.23±3.09 μm, p<0.001 compared to the control group). After 9 months, a slight decrease of this indicator was established (75.77±4.08 μm, p<0.001 compared to the control group). After 12 months, a significant decrease in the diameter of the venules was established when compared with the previous period of the study (59.01±3.09 μm), at the same time, this indicator remained significantly higher than in the control group (p<0.05).

The analysis of the diameters of the venular link of the hemomicrocirculatory channel in the group of animals that received quercetin against the background of triptorelin administration (see Fig. 4) showed that after 1 month of observation, this indicator significantly decreased (44.12±2.07 μm, p<0.05) when compared with the control group (48.03±1.34 μm). After 3 months of observation, the diameter of the venules significantly increases compared to the previous period (50.55±1.98 μm, p<0.05 compared to the control group). After 6 months, a sharp increase in the diameter of the venules was established (90.05± 3.74 μm, p<0.001 compared to the control group). After 9 months, a decrease in the value of this indicator was noted (78.77±3.08 μm, p<0.001 compared to the control group). After 12 months, the venule diameter continued to decrease (72.23±2.04 μm, p<0.001 compared to the control group).

Discussion

In this article, we considered the structural features of the hemomicrocirculatory channel of the myocardium of the ventricles of the heart during long-term (12 months) blocking of the synthesis of releasing hormone with the help of the substance triptorelin through the "hypothalamus-pituitary-testis" system, namely testosterone - the vascular wall of the heart of male rats.

Testosterone deficiency in men is increasingly recognized in clinical settings, and its pathological correlates cause increased research interest worldwide [8, 12, 21, 26]. Both basic and clinical studies have provided evidence that testosterone affects the cardiovascular system in both health and disease. In particular, low serum testosterone is associated with an increased risk of cardiovascular disease in men. A recent powerful meta-analysis of prospective studies comparing men with baseline serum testosterone in the lower or upper quartiles confirmed that low testosterone is a predictor of cardiovascular mortality and morbidity in older men. In addition, an interaction between the endogenous total testosterone level and the structural and functional parameters of the heart was found, although the causal relationship was not clearly established [6, 18, 31].

In our work, we observed a tendency to increase the diameter of blood vessels, namely arterioles and venules with a maximum after 6 months of observation, with increased blood supply to the heart muscle and with proportional outflow in the group with the addition of quercetin. At the same time, in 1 group (without quercitin), slight blood stasis was detected. Which, in our opinion, indicates the compensatory effect of the quercetin drug on the vascular wall.

Testosterone is known to promote a global improvement in energy metabolism, administration of excess can cause excess reactive oxygen species along with oxidative damage, indicative of mitochondrial respiratory chain electron leakage and metabolic uncoupling. The myocardium, and actually cardiomyocytes and vascular myocytes are enriched with mitochondria, meaning their dependence on oxidative metabolism in order to maintain the high demand for ATP necessary to maintain physiological functions [9].

Due to its vasoprotective properties, reducing the inflammatory process in the endothelium and increasing the level of nitric oxide in endothelial cells, quercetin is potentially able to reduce the level of blood pressure [24, 30], which we actually observed in our experimental groups of animals when comparing the diameters of the hemomicrocirculatory channel. The tendency to increase the indicator turns out to be different, so in group 1 (without the addition of quercitin), it gradually increases, and in group 2 (with the addition of quercitin) it is more stable, compared to the control group, which indicates a positive effect of the use of quercitin on the structure of the heart in as a whole

The results obtained by us are consistent with the data

of some other experimental and clinical studies, which draw attention to the fact that the use of quercetin leads to a decrease in elevated blood pressure, heart rate, and improvement in the diastolic function of the left ventricle [10, 14]. It is assumed that the vasoprotective effects of quercetin are realized due to its ability to reduce the activity of the inflammatory process in the endothelium of vessels, to increase the activity of endothelial NO-synthase (eNOS), which, in turn, increases the level of nitric oxide in endothelial cells and leads to improved endothelial function [15, 29, 32].

The results obtained by us are a theoretical justification for the development of methods for correcting violations of the hemomicrocirculatory channel of the myocardium in the case of a pathological effect on the body of a dyshormonal state of central genesis: "hypothalamus-pituitary-testis-heart". Data on the functional morphology of the heart at the stages of adaptation to changes in the endocrine link expand the existing ideas about the causes of heart homeostasis disturbances.

Conclusion

Administration of triptorelin leads to structural and functional changes in the vascular wall of all sections of the hemomicrocirculatory bed of the myocardium of the ventricles of the heart. The most pronounced changes are determined in the period from 6 to 9 months of observation in both experimental groups. The introduction of quercetin has a positive effect on the structure of the capacitive link, which improves the outflow of blood from the tissues of the heart.

References

[1] Bahriy, M. M., Dibrova, V. A., Popadynets, O. H., & Hryshchuk, M. I. (2016). *Методики морфологічних досліджень: монографія [Methods of morphological research: monograph].* Вінниця: Нова книга - Vinnytsya: Nova knyha.

[2] Botte, M. C., Lerrant, Y., Lozach, A., Berault, A., Counis, R., & Kottler, M. L. (1999). LH down-regulates gonadotropin-releasing hormone (GnRH) receptor, but not GnRH, mRNA levels in the rat testis. *Journal of Endocrinology,* 162(3), 409-415. doi: 10.1677/joe.0.1620409

[3] Brüll, V., Burak, C., Stoffel-Wagner, B., Wolffram, S., Nickenig, G., Müller, C., ... & Egert, S. (2015). Effects of a quercetin-rich onion skin extract on 24 h ambulatory blood pressure and endothelial function in overweight-to-obese patients with (pre-)hypertension: a randomised double-blinded placebo-controlled cross-over trial. *British journal of nutrition*, 114(8), 1263-1277. doi: 10.1017/S0007114515002950

[4] Carteri, R. B., Kopczynski, A., Rodolphi, M. S., Strogulski, N. R., Wannmacher, C. M., Franceschi, I. D., ... & Portela, L. V. (2021). Anabolic-androgenic steroids impair mitochondrial function and redox status in the heart and liver of mice. *Steroids,* 172, 108861. doi: 10.1016/j.steroids.2021.108861

[5] Chekalina, N. (2017). Resveratrol has a positive effect on parameters of central hemodynamics and myocardial ischemia in patients with stable coronary heart disease. *Wiadomosci Lekarskie* (Warsaw, Poland: 1960), 70(2), 286-291. PMID: 29059644

[6] Crawford, E. D., & Schally, A. V. (2020). The role of FSH and LH in prostate cancer and cardiometabolic comorbidities. *The Canadian journal of urology*, 27(2), 10167-10173. PMID: 32333736

[7] David, A. V. A., Arulmoli, R., & Parasuraman, S. (2016). Overviews of biological importance of quercetin: A bioactive flavonoid. *Pharmacognosy reviews*, 10(20), 84-89. doi: 10.4103/0973-7847.194044

[8] do Val Lima, P. R., Ronconi, K. S., Morra, E. A., Rodrigues, P. L., Ávila, R. A., Merlo, E., ... & Ribeiro Júnior, R. F. (2023). Testosterone deficiency impairs cardiac interfibrillar mitochondrial function and myocardial contractility while inducing oxidative stress. *Frontiers in Endocrinology,* 14, 1206387. doi: 10.3389/fendo.2023.1206387

[9] Frankel, Y. D., Cherno, V. S., & Kostenko, V. O. (2024). Effect of Melatonin and Quercetin on Inflammation and Metabolism under Conditions of Round-the-clock Lighting and High-calorie Carbohydrate-lipid Diet. *Фізіологічний журнал=Fiziologichnyi Zhurnal,* 70(1), 43-51. doi: 10.15407/fz70.01.043

[10] Huang, Y. P., Peng, C., & Peter, R. E. (1991). Metabolism of gonadotropin-releasing hormone in goldfish: serum clearance and tissue uptake studies. *General and comparative endocrinology,* 84(1), 67-75. doi: 10.1016/0016-6480(91)90065-e

[11] Jebari-Benslaiman, S., Galicia-Garcia, U., Larrea-Sebal, A., Olaetxea, J. R., Alloza, I., Vandenbroeck, K., ... & Martin, C. (2022). Pathophysiology of atherosclerosis. *International journal of molecular sciences,* 23(6), 3346. doi: 10.3390/ijms23063346

[12] King, O., Cruz-Moreira, D., Sayed, A., Kermani, F., Kit-Anan, W., Sunyovszki, I., ... & Terracciano, C. M. (2022). Functional microvascularization of human myocardium in vitro. *Cell reports methods,* 2(9), 100280. doi: 10.1016/j.crmeth.2022.100280

[13] Kondratiuk, V. E., & Synytsia, Y. P. (2018). Effect of quercetin on the echocardiographic parameters of left ventricular diastolic function in patients with gout and essential hypertension. *Wiadomosci Lekarskie* (Warsaw, Poland: 1960), 71(8), 1554-1559. PMID: 30684340

[14] Konijnenberg, L. S., Luiken, T. T., Veltien, A., Uthman, L., Kuster, C. T., Rodwell, L., ... & van Royen, N. (2023). Imatinib attenuates reperfusion injury in a rat model of acute myocardial infarction. *Basic Research in Cardiology,* 118(1), 2. doi: 10.1007/s00395-022-00974-z

[15] Kozaeva, R., Klymenko, M. O., Katrushov, O. V., & Kostenko, V. O. (2022). Bioflavonoids as agents for correcting nitro-oxidative stress and salivary gland functions in rats exposed to alcohol during modeled lipopolysaccharide-induced systemic inflammatory response. *Wiadomosci Lekarskie* (Warsaw, Poland: 1960), 75(3), 685-690. doi: 10.36740/wlek202203121

[16] Kronenberg, F., Mora, S., Stroes, E. S., Ference, B. A., Arsenault, B. J., Berglund, L., ... & Catapano, A. L. (2022). Lipoprotein (a) in atherosclerotic cardiovascular disease and aortic stenosis: a European Atherosclerosis Society consensus statement. *European heart journal,* 43(39), 3925-3946. doi: 10.1093/eurheartj/ehac361

[17] Kwon, H. M., Hong, B. K., Jang, G. J., Kim, D. S., Choi, E. Y., Kim, I. J., ... & Schwartz, R. S. (1999). Percutaneous transmyocardial revascularization induces angiogenesis: a histologic and 3-dimensional micro computed tomography

study. *Journal of Korean medical science,* 14(5), 502-510. doi: 10.3346/jkms.1999.14.5.502

[18] Lesjak, M., Beara, I., Simin, N., Pintavć, D., Majkić, T., Bekvalac, K., ... & Mimica-Dukić, N. (2018). Antioxidant and anti-inflammatory activities of quercetin and its derivatives. *Journal of Functional Foods,* 40, 68-75. doi: 10.1016/j.jff.2017.10.047

[19] Litvinuková, M., Talavera-López, C., Maatz, H., Reichart, D., Worth, C. L., Lindberg, E. L., ... & Teichmann, S. A. (2020). Cells of the adult human heart. *Nature*, 588(7838), 466-472. doi: 10.1038/s41586-020-2797-4

[20] Nestulia, K. I., Ksonz, I. V., Makarenko, V. I., Makarenko, O. V., & Kostenko, V. O. (2024). Impact of quercetin on the organic matrix and biomechanical properties of rat mandible following its incomplete fracture during chronic alcohol intoxication. *Фізіологічний журнал=Fiziologichnyi Zhurnal,* 70(3), 51-58. doi: 10.15407/fz70.03.051

[21] Opryshko, V., Prokhach, A., Akimov, O., Riabushko, M., Kostenko, H., Kostenko, V., ... & Kostenko, V. (2024). Desmodium styracifolium: Botanical and ethnopharmacological insights, phytochemical investigations, and prospects in pharmacology and pharmacotherapy. *Heliyon.* 10(3), e25058. doi: 10.1016/j.heliyon.2024.e25058

[22] Reyes-Soffer, G., Ginsberg, H. N., Berglund, L., Duell, P. B., Heffron, S. P., Kamstrup, P. R., ... & American Heart Association Council on Arteriosclerosis, Thrombosis and Vascular Biology; Council on Cardiovascular Radiology and Intervention; and Council on Peripheral Vascular Disease. (2022). Lipoprotein (a): a genetically determined, causal, and prevalent risk factor for atherosclerotic cardiovascular disease: a scientific statement from the American Heart Association. *Arteriosclerosis, Thrombosis, and vascular biology,* 42(1), e48-e60. doi: 10.1161/ATV.0000000000000147

[23] Sciarrone, D. F., McLaughlin, R. A., Argarini, R., To, M. S., Naylor, L. H., Bolam, L. M., ... & Green, D. J. (2022). Visualising and quantifying microvascular structure and function in patients with heart failure using optical coherence tomography. *The Journal of Physiology,* 600(17), 3921-3929. doi: 10.1113/JP282940

[24] Shahjehan, R. D., & Bhutta, B. S. (2023). *Coronary Artery Disease*. In: StatPearls [Internet]. Treasure Island (FL): StatPearls Publishing. PMID: 33231974

[25] Su, C., Xia, T., Ren, S., Qing, S., Jing, D., Lian, H., ... & Xiang, Z. (2014). Effect of diazoxide preconditioning on cultured rat myocardium microvascular endothelial cells against apoptosis and relation of PI3K/Akt pathway. *Balkan medical journal,* 2014(1), 83-87. doi: 10.5152/balkanmedj.2013.8458

[26] Tan, Z., Zhao, Y., Zheng, Y., & Pan, Y. (2022). The effect of blood flow-restricted low resistance training on microvascular circulation of myocardium in spontaneously hypertensive rats. *Frontiers in Physiology,* 13, 829718. doi: 10.3389/fphys.2022.829718

[27] Tarasenko, L. M., Neporada, K. S., & Klusha, V. (2002). Stress-protective effect of glutapyrone belonging to a new type of amino acid-containing 1, 4-dihydropyridines on periodontal tissues and stomach in rats with different resistance to stress. *Bulletin of experimental biology and medicine,* 133, 369-371. doi: 10.1023/a:1016250121896

[28] Verheule, S., & Schotten, U. (2021). Electrophysiological consequences of cardiac fibrosis. *Cells,* 10(11), 3220. doi: 10.3390/cells10113220

[29] Xiao, J., & Bai, W. (2019). Bioactive phytochemicals. *Critical reviews in food science and nutrition,* 59(6), 827-829. doi: 10.1080/10408398.2019.1601848

[30] Xu, M. X., Wang, M., & Yang, W. W. (2017). Gold-quercetin nanoparticles prevent metabolic endotoxemia-induced kidney injury by regulating TLR4/NF-kB signaling and Nrf2 pathway in high fat diet fed mice. *International journal of nanomedicine,* 5(12), 327-345. doi: 10.2147/IJN.S212318

[31] Yang, B., Qiao, Y., Yan, D., & Meng, Q. (2024). Targeting Interactions between Fibroblasts and Macrophages to Treat Cardiac Fibrosis. *Cells,* 13(9), 764. doi: 10.3390/cells13090764

[32] Yelins' ka, A. M., Akimov, O. Y., & Kostenko, V. O. (2019). Role of AP-1 transcriptional factor in development of oxidative and nitrosative stress in periodontal tissues during systemic inflammatory response. *Український біохімічний журнал=Ukrainian biochemical journal,* 91(1), 80-85. doi: 10.15407/ubj91.01.080

ХАРАКТЕРИСТИКА ГЕМОМІКРОЦИРКУЛЯТОРНОГО РУСЛА МІОКАРДА ШЛУНОЧКІВ ПРИ ТРИПТОРЕЛІН-ІНДУКОВАНІЙ ЦЕНТРАЛЬНІЙ ДЕПРИВАЦІЇ СИНТЕЗУ ЛЮТЕЇНІЗУЮЧОГО ГОРМОНУ ТА КОРЕКЦІЇ ЦЬОГО СТАНУ ВВЕДЕННЯМ КВЕРЦЕТИНУ

Ворошилова Т. А., Шепітько В. І., Стецук Є. В., Вільхова О. В., Пузирьов Г. С.

Вивчення мікроциркуляторного русла сполучної тканини міокарда шлуночків покращує розуміння особливостей патологічних процесів, таких як ішемія, гіпоксія та ремоделювання міокарда, оцінювання ефективності медикаментозної терапії, а також методи реабілітації. Мета дослідження - встановлення змін гемомікроциркуляторного русла міокарда шлуночків при трипторелін-індукованій центральній депривації синтезу лютеїнізуючого гормону та корекції цього стану введенням кверцетину. Експеримент проведено на 60 статевозрілих білих щурах самцях масою 140-160 г. Щурів розділили на 3 групи. 1 група - контрольна, щури яким вводився фізіологічний розчин (10 тварин). 2 група - щури, яким підшкірно вводили диферелін (трипторелін ембонат) у дозі 0.3 мг діючої речовини на кг маси тіла протягом 365 днів (25 тварин). 3 група - щури, яким вводили розчин триптореліну із розрахунку 0.3 мг діючої речовини на кг маси тіла для моделювання центральної депривації синтезу лютеїнізуючого гормону з додаванням кверцитину до харчування за допомогою гастрального зонду з перерахунку на масу тіла тварин тричі на тиждень (25 тварин). Тварин виводили із експерименту через 1, 3, 6, 9 та 12 місяців шляхом передозування ефірним наркозом. Комплексне дослідження гістологічних препаратів міокарда та кількісний підрахунок діаметра судин мікроциркуляторного русла проводили за допомогою світлового мікроскопа з цифровим мікрофільтром та адаптованого для цих досліджень програмного забезпечення. Статистичну обробку результатів дослідження проводили за допомогою програмного забезпечення Microsoft Office Excel та розширення Real Statistics 2019. При аналізі показника діаметрів артеріол в групі тварин, яким вводили трипторелін через 1, 3, 6, 9 і 12 місяців встановлено достовірне збільшення діаметра артеріол порівняно з контрольною групою тварин відповідно на 13,9 % - 40,8 % - 102,6 % - 112,6 % - 11,5 %; а у тварин, яким на тлі введення триптореліну вводився кверцетин встановлено, що цей показник через 1 місяць достовірно не відрізнявся від аналогічного в групі контролю, а через 3, 6, 9 і 12 місяців достовірно був більший, ніж в контролі відповідно на 11,5 % - 136,2 % - 101,1 % - 101,4 %. Аналіз діаметрів венулярної ланки гемомікроциркуляторного русла в групі тварин, яким вводили трипторелін показав достовірне збільшення величини даного показника через 3, 6, 9 і 12 місяців порівняно з

контрольною групою відповідно на 20,0 % - 71,2 % - 57,8 % - 22,9 %; а у тварин яким додатково вводився кверцетин через 1 місяць діаметр венул на 8,1 % достовірно зменшувався порівняно з контролем, а через 3, 6, 9 і 12 місяців - відповідно на 5,2 % - 87,5 % - 64,0 % - 50,4 % був достовірно більшим, ніж у контрольних тварин. Аналіз діаметрів капілярів в групі тварин, яким вводили трипторелін показав достовірне збільшення величини даного показника через 1, 3, 6 і 9 місяців порівняно з контрольною групою відповідно на 23,9 % - 49,1 % - 61,8 % - 36,7 %; а у тварин яким додатково вводився кверцетин діаметр капілярів достовірно збільшувався порівняно з контролем через 3, 6, 9 і 12 місяців - відповідно на 22,3 % - 55,3 % - 17,1 % - 25,2 %. Проведене дослідження показало, що введення трипторелiну призводить до структурно функціональних змін компонентів мікроциркуляторного русла міокарда шлуночків серця, які характеризуються змінами діаметра артеріальних та венозних ланок із поступовим збільшенням кровонаповнення, максимум якого відзначено на 6 місяць експерименту в обох експериментальних групах, але без порушення відтоку в групі з додаванням кверцитину.

Ключові слова: с*ерце, міокард, гемомікроциркуляторне русло, тестостерон, лютеїнізуючий гормон, кверцетин, трипторелін.*

Author's contribution

Voroshilova T. A. - work concept and design, data collection and analysis, writing the article.
Shepitko V. I. - work concept and design.
Stetsuk Ye. V. - critical review, final approval of the article.
Vilkhova O. V. - responsibility for statistical analysis.
Puzyryov G. S. -- data collection and analysis.

DOI: 10.31393/morphology-journal-2024-30(3)-10 Reports of Morphology, Vol. 30, №3, Pages 99-106

ISSN 1818-1295 eISSN 2616-6194

REPORTS OF MORPHOLOGY

Official Journal of the Scientific Society of Anatomists, Histologists, Embryologists and Topographic Anatomists of Ukraine

journal homepage: https://morphology-journal.com

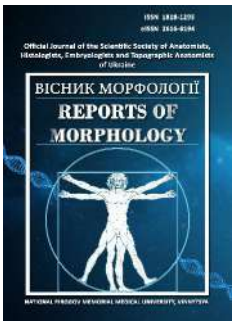

Stature estimation in male and female populations of India and Nigeria depending on other anthropometric parameters using multiple regression analysis

Usman A.[1,2], Gupta A.[1], Ghosal A.[3], Biswas A.[4], Adarsh K.[5]

[1]School of Basic and Applied Sciences, Galgotia's University, Greater Noida, Uttar Pradesh, India
[2]Department of Human Anatomy, College of Health Sciences, Umaru Musa Yar'adua University, Katsina, Dutsinma Road, Katsina State, Nigeria
[3]Department of Life Sciences, Red River College Polytechnic, Winnipeg, MB, Canada
[4]Orthogenetics Lab, All India Institute of Medical Sciences, New Delhi, India.
[5]Forensic Medicine & Faculty I/c Forensic Anthropology, All India Institute of Medical Sciences, New Delhi, India

ARTICLE INFO
Received: 04 March 2024
Accepted: 15 August 2024

UDC: 572.087.1

CORRESPONDING AUTHOR
e-mail: dradarshk@yahoo.com
Kumar Adarsh

CONFLICT OF INTEREST
The authors have no conflicts of interest to declare.

FUNDING
Not applicable.

DATA SHARING
Data are available upon reasonable request to corresponding author.

In cases of mass disasters, accidents, or criminal investigations where the identity of victims is unknown certain basic anthropological parameters are helpful in ascertaining these like race, sex, age and stature. Estimating stature using multiple body measurements such as shoulder breadth, foot length, thigh length, and knee height is a common approach in anthropometry and forensic anthropology. The presence of sex and population differences in anthropometric indicators allows these measurements to be used not only to estimate the stature of an individual, but also to determine sex, different races or populations based on skeletal remains. The purpose of the study is to develop and practically verify the work of regression equations for estimating stature depending on other anthropometric indicators of men and women of two ethnically diverse populations. For this study, anthropometric data were gathered from two distinct population groups: Indian (n=102) and Nigerian (n=205). Basic demographic details along with measurements of shoulder breadth, sitting shoulder height, sitting foot length, sitting knee height, and sitting thigh length were obtained using standardized techniques as per the established anthropometric protocols. Statistical analysis was performed using appropriate software packages such as SPSS, R, or SAS. The multiple regression method was used to estimate body length depending on other anthropometric indicators. As a result of the conducted multiple linear regression analysis, reliable relationships between stature and specific anthropometric measurements in Nigerian and Indian men and women were established. It was found that stature is highly likely to depend on knee height in a sitting position in Nigerian women (R^2=0.531, p<0.001), as well as hip length, foot length, and shoulder height in a sitting position in Indian men (R^2=0.725, p <0.001). Stature in Indian women reliably depends on hip length and foot length in a sitting position, and in Nigerian men - on hip length, foot length, shoulder width and shoulder height in a sitting position, but the regression equations have a coefficient of determination less than 0.5 (respectively, R^2=0.463, p<0.001 and R^2=0.405, p<0.001) and therefore do not have much significance for forensic purposes. Additional groups (30 people for each category) were used to test the obtained regression equations. The high correlation coefficients (0.6<r<0.75) observed in both test groups indicate the reliability of the regression models and the suitability of the selected anthropometric measurements for the estimation of stature in these populations. The obtained data emphasize the importance of taking into account factors specific to the population when developing regression equations for the estimation of stature and emphasize the usefulness of anthropometric measurements in predicting this indicator for different gender and demographic groups of the population, although their further verification on larger and more diverse samples is necessary.

Keywords: *regression analysis, stature estimation, anthropometric measurements, Nigerian and Indian men and women.*

Introduction

Natural disasters, including earthquakes and hurricanes, continue to pose significant threats to human life, making their impact on mortality a critical area of study, especially for forensic medicine. Global earthquake fatalities are directly correlated with population density, with a significant number of deaths occurring in regions with high population concentrations. Between 1970 and 2010, they estimate that earthquakes have caused approximately 1.4 million deaths worldwide, highlighting the devastating toll that seismic events can have on human populations. Similarly, the mortality following Hurricane Maria in Puerto Rico serves as a stark reminder of the deadly consequences of extreme weather events. Aftermath of the hurricane, from September 2017 to February 2018, there were approximately 4,645 excess deaths, underscoring the importance of accurate death reporting and investigation during such events. These figures illustrate that natural disasters lead to significant mortality, necessitating the involvement of forensic medicine in the investigation and classification of disaster-related deaths [8, 15].

Forensic anthropologists can use different body measurements to estimate the stature of the individual from skeletal remains in cases of mass disasters, accidents, or criminal investigations where the identity of victims is unknown [7, 17]. Pieces of evidence like fingerprints, shoeprints, or footprints are usually present at crime scenes but cases of mass grave sites like natural disasters, accidents, wars, and terror attacks leave unrecognizable dead bodies that need to be identified. Age, sex, stature, and ancestry are the foremost parameters for confirming biological profiles. Amongst them, the identification of sex and stature is the initial step in establishing a biological profile that narrows down the available pool of profiles. Different body parts like foot length, knee height, shoulder length and breadth etc. are used for the estimation of sex and stature of the unknown person thereby establishing its biological profile [14]. This can be done by establishing correlation values and using them to develop linear regression equations for the estimation of stature in a particular ethnic race. Equations for the estimation of sex and stature from measurements of body parts have been developed for populations of specific regions [24, 30]. However, varied populations and races have varied body proportions and parameters that alter the anthropometric stature estimation. Hence, there is a strict requirement for preparing a database that should be population specific as well as comparative for forensic investigation purposes.

Recently the utility of various anthropometric parameters using the anthropoid vertebral column as an alternate method in place of long bones for identifying human remains amongst diverse populations has been highlighted [6]. Many researchers have examined different body parameters to establish the stature of an individual in case of disintegrated body parts from any accident or disaster. The data includes stature estimation from the ulna, humerus, radius, tibia, femur, etc. which were well correlated with human stature in different populations [2, 3, 21, 25].

The purpose of our research is the development and practical verification of regression equations for estimating stature depending on other anthropometric indicators of men and women of two ethnically diverse populations.

Materials and methods

(a) Study Design, Inclusion, and Exclusion criteria

A cross-sectional comparative design to investigate anthropometric measurements and stature estimations in Indian and Nigerian populations has been presented. The study collected anthropometric data from 427 young and healthy participants with no physical impairments and from both populations. The two populations were randomly divided into two groups - the Discovery group (n=307; among them Nigerian=205; Indian=102) and the validation group (Nigerian=60; Indian=60). Ethical approval was obtained from the Institutional Review Board (IRB) of Galgotia's University, Greater Noida, Uttar Pradesh, India before data collection. Informed consent was obtained from all participants, and measures were taken to ensure the confidentiality and privacy of collected data.

Stature assessment was conducted using a stadiometer and standard measuring instruments, with measurements recorded in centimeters. All measurements were conducted in a controlled environment with optimal conditions and room temperature to ensure accuracy and consistency. As per the instructions, body swings were avoided during measurements to maintain the Frankfurt plane's horizon [19]. The individuals were requested to wear light clothing and no shoes during the measurements. All the data from each subject were collected twice to avoid observational errors and obtain a uniform data set.

(b) Measurement of Anthropometric parameters

Following the steps outlined in ISO7250-1, measurements of stature, sitting shoulder height, sitting foot length, shoulder breadth, sitting thigh length and sitting knee height. An intra-observer precision, pilot study was carried out to evaluate the validity of obtaining these measurements before the primary data collection. All measurements were within the permissible norms for relative technical error of measurement (rTEM) and coefficient of reliability (R), R>0.9 and rTEM<5 % [1, 10, 26].

Sitting thigh length (STL): the separation between the greater trochanter's proximal end and the lateral femoral condyle was recorded as the STL. The measurements were performed in the sitting position with a straight back, 90-degree flexion of the knee, and 30-45° of the hip, from the mid-inguinal point directed to the upper border of the patella on the ventral surface. The STL was recorded in the same pattern (right to left) irrespective of the dominant leg of each participant [4].

Sitting knee height (SKH): the vertical distance from the top of the kneecap to the foot resting on the floor was recorded as the SKH. The knee was flexed at 90° angles during the measurement. The SKH was recorded in the same pattern (right to left) irrespective of the dominant leg of each participant.

Sitting shoulder height (SSH): it was measured as the vertical distance from the top of the shoulder's acromion process to the participant's sitting surface. The SSH was taken for each participant consecutively at a standard sitting position.

Shoulder breadth (SB): it was measured horizontally in an acromial process from the left to the right of the shoulders.

Sitting Foot Length (SFL): the individual was seated comfortably on a flat surface with their legs extended and feet flat against a vertical surface, such as a wall. The individual's back was kept straight, and their feet were positioned perpendicular to the lower legs, forming a 90-degree angle at the ankles. Using a ruler or measuring tape, the length of the foot was measured from the posterior aspect of the heel (the back of the heel) to the tip of the longest toe (typically the first toe).

Stature was measured vertically. The distance was recorded from the highest point on the head to the floor after adjusting the head in the Frankfurt Horizontal (FH) plane while standing barefoot in the anatomical position.

(c) Statistical analysis

Statistical analysis for this study involved several steps to examine the relationship between anthropometric measurements and estimated stature, as well as to derive regression equations and validate their accuracy. Descriptive statistics were used to summarize the demographic characteristics of the study population, including mean, median, standard deviation, and range for continuous variables such as age and anthropometric measurements. Correlation analysis was performed to assess the relationships between anthropometric measurements (such as shoulder breadth, sitting shoulder height, sitting foot length, sitting thigh length, and sitting knee height) and estimated stature. Regression analysis was used to derive regression equations relating anthropometric measurements (seated hip length, seated knee height, seated shoulder height, seated shoulder width, and seated foot length) to body length in each population group (Indians and Nigerians). Multiple linear regression models were constructed to predict stature based on one or a combination of anthropometric measurements. Model fit statistics, such as R-squared, adjusted R-squared, and standard error of the estimate, were assessed to evaluate the goodness-of-fit and predictive accuracy of the regression models. The derived regression equations were validated using independent samples from the same population groups. The accuracy of the regression models was assessed by comparing predicted stature values obtained from the regression equations with actual stature values measured in the validation sample. Statistical analysis was conducted using appropriate software packages such as SPSS, R, or SAS.

Results

The overall characteristics of the Nigerian and Indian populations were examined in this study. Among the Nigerians group (n=205), the mean age was 22.2±3.1 years. In comparison, the Indian group (n=102) had a mean age of 21.7±3.3 years. Statistical analysis revealed that the difference in age between the two populations was not significant, indicating a similar age distribution among both groups.

Nigerian men had significantly greater values of hip length (p=0.0001) and foot length (p=0.0006) while sitting compared to their Indian counterparts (Table 1). On the contrary, Indian men had a significantly higher (p=0.0001) sitting shoulder height compared to Nigerian men (see Table 1).

Significant anthropometric differences between representatives of the Nigerian and Indian populations were also established among women (Table 2). In particular, Nigerian women have significantly higher values of thigh length (p=0.0001), foot length (p=0.0001) and shoulder width (p=0.0001) when sitting compared to Indian women (see Table 2). However, Indian women have significantly higher values (p=0.0001) of sitting shoulder height compared to Nigerian women (see Table 2).

Among Nigerian men, the following reliable correlations

Table 1. Anthropometric measurements of Nigerian and Indian men (M±σ, cm).

Anthropometric measurements	Nigerian Males (n=145)	Indian Males (n=53)	p-value
Stature	174.0±6.4	172.4±6.5	0.1136
Thigh length *	45.98±2.55	44.39±2.42	**0.0001**
Knee height *	55.99±3.63	55.26±2.70	0.1836
Foot length *	25.86±1.63	25.02±1.07	**0.0006**
Shoulder breadth *	37.89±3.77	37.02±3.12	0.1347
Shoulder height *	60.89±3.51	65.91±3.14	**0.0001**

Note: in this and the next table * - all measurements were taken while sitting.

Table 2. Anthropometric measurements of Nigerian and Indian women (M±σ, cm).

Anthropometric measurements	Nigerian Males (n=60)	Indian Males (n=49)	p-value
Stature	160.6±6.0	157.7±6.7	**0.0165**
Thigh length *	44.46±2.99	41.09±2.24	**0.0001**
Knee height *	50.76±2.76	50.58±2.31	0.7165
Foot length *	25.49±2.33	22.62±1.38	**0.0001**
Shoulder breadth *	42.23±5.27	32.47±2.13	**0.0001**
Shoulder height *	56.12±3.71	59.70±2.70	**0.0001**

Table 3. Linear regression analysis predicting different body measurements by body length and multiple regression model equations to estimate stature in Nigerian women.

Linear regression Equations for Stature estimation	R^2	S_{res}	p-value
Sitting Thigh Length = 10.55 + 0.211 x stature	0.181	2.73	<0.001
Sitting Knee Height = -3.145 + 0.336 x stature	0.532	1.91	<0.001
Sitting Foot Length = 12.67 + 0.080 x stature	0.042	2.30	0.116
Shoulder Breadth = 54.62 - 0.077 x stature	0.008	5.29	0.504
Sitting Shoulder Height = 33.03 + 0.144 x stature	0.054	3.64	0.074
Multiple regression analysis* for estimation of stature	R^2	Adj R^2	p-value
Stature=80.27 + 1.583 x SKH	0.531	0.526	<0.001

Note: in this and the following tables * - reverse stepwise method; Sres - Standardized Residuals; Adj R^2 - Adjusted R-squared.

Table 4. Linear regression analysis predicting different body measurements by body length and multiple regression model equations to estimate stature in Indian women.

Linear regression Equations for Stature estimation	R^2	S_{res}	p-value
Sitting Thigh Length = 12.31 + 0.183 x stature	0.302	1.90	<0.001
Sitting Knee Height = 24.95 + 0.163 x stature	0.234	2.05	<0.001
Sitting Foot Length = 3.906 + 0.119 x stature	0.333	2.30	0.116
Shoulder Breadth = 54.62 - 0.077 x stature	0.008	5.29	0.504
Sitting Shoulder Height = 33.03 + 0.144 x stature	0.054	3.64	0.074
Multiple regression analysis* for estimation of stature	R^2	Adj R^2	p-value
Stature= 62.06 + 1.165 x STL + 2.108 x SFL	0.463	0.439	<0.001

with body length were established: moderately strong positive (r=0.45 and r=0.40) with hip length and shoulder width in a sitting position, and weak positive (r=0.28) with shoulder height in a sitting position. Among Indian men, the following reliable correlations with body length were established: strong positive (r=0.75) with sitting foot length and moderate positive (r=0.55) with sitting shoulder height.

Among Nigerian women, the following reliable correlations with body length were established: strong positive (r=0.73) with knee height in a sitting position. Among Indian women, the following reliable correlations with body length were established: medium strength positive (r=0.55 in both cases) with hip length and foot length in a sitting position.

Linear regression analysis was used to estimate various parameters using body length as a predictor variable. Among Nigerian women, regression equations predicting sitting knee height and sitting hip length based on body length were found to be statistically significant (Table 3). However, the magnitude of the coefficient of determination (R^2) indicates that body length can effectively predict only sitting knee height. The length of the body also reliably and with high probability (R^2=0.531) depends only on the height of the knees when sitting (see Table 3).

In Indian women, regression equations predicting sitting knee height and sitting hip length based on body length were also found to be statistically significant (Table 4). However, in contrast to Nigerian women, the regression equation reliably estimates body length for sitting hip length and sitting foot length. Given that the coefficient of determination is less than 0.5 (R^2=0.463), this equation does not have an important practical value for the identification of this body parameter (see Table 4).

In Indian men, regression equations predicting knee height, hip length, foot length, shoulder width, and sitting shoulder height based on body length were found to be statistically significant (Table 5), and only for sitting shoulder

Table 5. Linear regression analysis predicting different body measurements by body length and multiple regression model equations to estimate stature in Indian men.

Linear regression Equations for Stature estimation	R^2	S_{res}	p-value
Sitting Thigh Length = 8.533 + 0.208 x stature	0.302	2.04	<0.001
Sitting Knee Height = -31.71 + 0.500 x stature	0.194	6.74	<0.05
Sitting Foot Length = 9.181 + 0.092 x stature	0.301	0.89	<0.001
Shoulder Breadth = 1.468 + 0.206 x stature	0.187	2.85	<0.05
Sitting Shoulder Height = 2.380 + 0.360 x stature	0.563	2.09	<0.001
Multiple regression analysis* for estimation of stature	R^2	Adj R^2	p-value
Stature=23.16 + 0.617 x STL + 1.748 x SFL + 1.184 x SSH	0.725	0.708	<0.0001

Table 6. Linear regression analysis predicting different body measurements by body length and multiple regression model equations for estimation of stature in Nigerian men.

Linear regression Equations for Stature estimation	R^2	S_{res}	p-value
Sitting Thigh Length = 14.12 + 0.183 x stature	0.212	2.27	<0.001
Sitting Knee Height = 24.67 + 0.182 x stature	0.105	3.45	<0.001
Sitting Foot Length = 8.107 + 0.102 x stature	0.164	1.51	<0.001
Shoulder Breadth = 54.62 - 0.077 x stature	0.008	5.29	0.504
Sitting Shoulder Height = 33.03 + 0.144 x stature	0.054	3.64	0.074
Multiple regression analysis* for estimation of stature	R^2	Adj R^2	p-value
Stature = 65.73 + 0.885 x STL + 0.667 x SFL + 0.432 x SB + 0.557 x SSH	0.405	0.388	<0.001

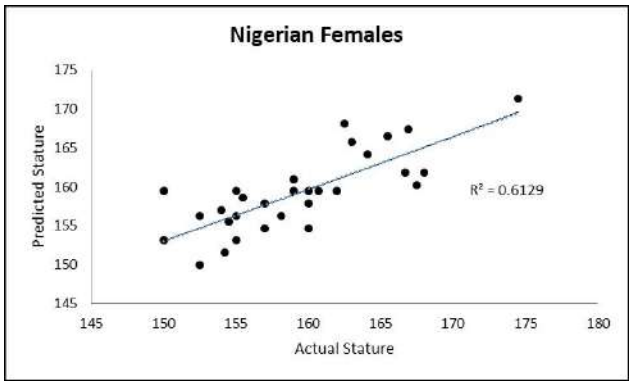

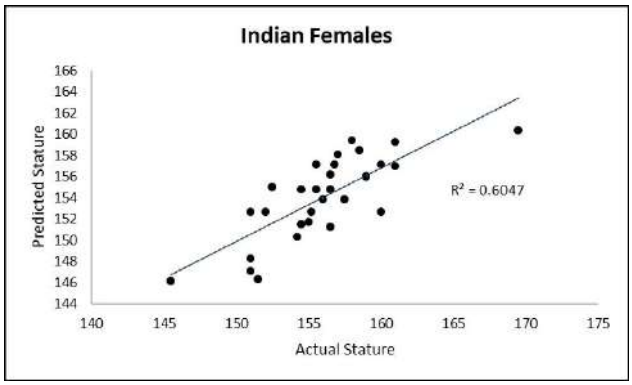

Fig. 1. Correlation plot between predicted and actual stature of Indian and Nigerian women for the control group.

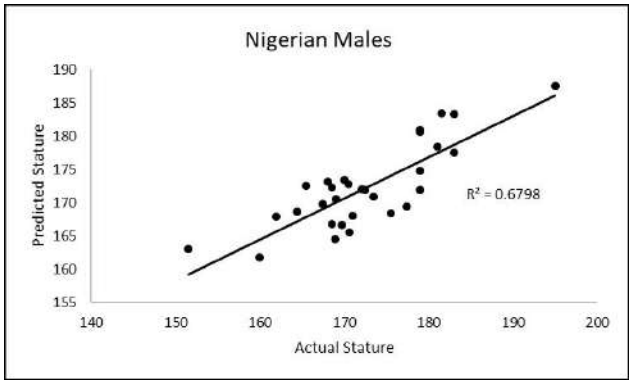

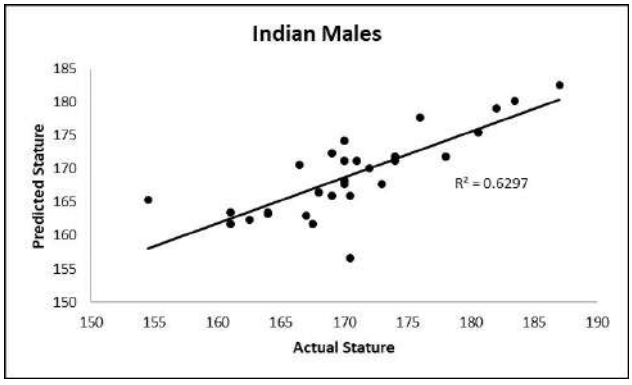

Fig. 2. Correlation plot between predicted and actual stature of Nigerian and Indian men for the control group.

height the coefficient of determination was greater than 0.5 (R^2=0.567). The multiple regression equation reliably estimates body length by sitting hip length, sitting foot length, and sitting shoulder height (see Table 5). Given that the coefficient of determination is higher than 0.5 (R^2=0.725), this equation has an important practical value for identifying body length in Indian men (see Table 5).

In Nigerian men, regression equations predicting sitting knee height, sitting hip length, and sitting foot length based on body length were found to be statistically significant (Table 6), and all equations had a coefficient of determination less than 0.5 (R^2= from 0.102 to 0.212). A multiple regression equation reliably estimates body length by hip length, foot length, shoulder width, and sitting shoulder height. Given that the coefficient of determination is less than 0.5 (R^2=0.405), this equation does not have an important practical value for identifying this body parameter (see Table 6).

An additional cohort of 60 individuals from both the Indian and Nigerian populations was used to test the equations derived from the original data set. Body length was predicted using the resulting equations, and then these predicted values were compared to actual body length measurements. By correlating predicted and actual body length values, the degree of correlation between estimated and observed values was determined, which provided insight into the accuracy and reliability of regression equations in estimating body length in these populations.

In women, predicted body length (derived from the equations in Tables 3 and 4) correlated with actual length at a level of 61 % for Nigerian women, and a concordance of 60 % was observed for Indian women (Fig. 1).

In the group of Nigerian men, the predicted length of the body corresponded to the actual length of the body at the level of 68%, and in the group of Indian men - at the level of 63 % (Fig. 2, see Tables 5 and 6).

Discussion

Thus, the results of multiple linear regression analysis revealed significant relationships between body length and specific anthropometric measurements within each gender and population group. Moreover, body length was highly likely to depend on knee height while sitting in Nigerian women (R^2=0.531, p<0.001), as well as hip length while sitting, foot length while sitting, and shoulder height while sitting in Indian men (R^2=0.725, p<0.001). Body length in Indian women and Nigerian men was also significantly related to sitting hip length and sitting foot length and sitting hip length, foot length, shoulder width and shoulder height, respectively, but the regression equations had coefficients of determination less than 0.5 and were therefore not significant for identification of body length (respectively R^2=0.463, p<0.001 and R^2=0.405, p<0.001).

A separate validation group consisting of 30 individuals for each category was used to test the resulting regression

equations. Correlation analysis between the predicted and actual value of body length revealed strong correlations (0.6<r<0.75), which indicates the appropriateness of the regression equations when predicting this indicator in these populations.

Firstly, the significant correlations observed between specific anthropometric measurements and stature highlight the importance of understanding the variability in body proportions across different demographic groups [28]. Furthermore, the differences observed in the correlation patterns between genders and populations suggest potential genetic, environmental, and cultural influences on body proportions [23]. For instance, the stronger correlation between sitting knee height and stature among Nigerian females may reflect unique physiological characteristics or lifestyle factors specific to this population group. Similarly, the distinct correlations observed in Indian males between sitting thigh length, sitting foot length, and sitting shoulder height with stature may be attributed to population-specific variations in body morphology.

The high correlation coefficients observed in both validation groups indicate the robustness of the regression models and the suitability of the selected anthropometric measurements for stature estimation. These results have important implications for forensic anthropology, where accurate stature estimation plays a crucial role in identifying individuals from skeletal remains. Additionally, they underscore the utility of anthropometric data in population health studies and anthropological research, providing valuable insights into variations in body proportions across different demographic groups.

However, it's essential to acknowledge the limitations of the study, including the relatively small sample size and the potential for measurement errors in anthropometric data collection. Although the manual approach has several advantages like it is a cost efficient and a simple procedure, however, its disadvantages cannot be ignored. The process is extremely time-consuming and the chances of human error are also high. So, in future there is a need to shift towards the automated methods for the anthropometric measurements.

Future research could focus on validating the regression equations in larger and more diverse population samples to enhance their generalizability and applicability. Overall, the findings contribute to our understanding of stature estimation methods and highlight the potential of anthropometric measurements in forensic and anthropological contexts.

Our study builds upon previous research conducted on Indian and Nigerian populations, which has elucidated the relationship between anthropometric measurements, body composition, and health outcomes within these demographic groups [9, 18, 20].

A. V. Marchenko et al. [16] explored the relationship between individual linear dimensions, odontometric, and cephalometric indicators. Their findings suggest that facial measurements, particularly those associated with dental arch morphology, play a crucial role in predicting stature. They demonstrated a significant correlation between the breadth of the face and height in young men with a wide face type.

The use of upper extremity measurements in stature estimation was examined by Uzun Ö. et al. [27], who found a strong correlation between arm length and stature. Their research highlighted that the arm span, forearm length, and hand length could predict stature with high accuracy. For instance, in their study, arm span showed a correlation coefficient (r) of 0.86, supporting its utility as a reliable predictor of height. A. Chandra et al. [5] focused on hand anthropometry and its relationship with stature, emphasizing the practical advantages of using hand dimensions for prediction models. The study found that hand length and palm width are significant indicators, with hand length showing a correlation coefficient of 0.82. This method is particularly useful when other measurements are not accessible. Similarly, Kamal R. and Yadav P. K. [12] demonstrated that foot and hand measurements could be effective in stature estimation in the Kori population of North India. They reported a strong correlation between hand length and stature (r=0.88), suggesting that these measurements could be applied broadly across populations with minor adjustments for ethnic differences.

P. Rai et al. [22] conducted a systematic review of stature estimation using physical anthropometry. Their comprehensive analysis reinforced the value of multiple body dimensions, including hand, foot, and craniofacial measurements, in developing accurate prediction models. This review underlines the importance of multi-dimensional approaches in forensic anthropology.

A. B. Yadav et al. [29] further investigated the role of facial anthropometry in stature estimation within the Indian population. Their regression analysis revealed that facial height and bizygomatic breadth provided reliable stature predictions, with a correlation coefficient of 0.75, underscoring the relevance of cephalometric measurements in height estimation. In the forensic domain, Khangura R. K. et al. [13] examined the use of odontometric parameters for stature estimation, particularly in forensic dental sciences. They identified four odontometric dimensions that showed strong correlations with stature, contributing to forensic identification practices.

Finally, Jervas E. et al. [11] studied the Igbos using cephalometric data and found that cephalo-facial anthropometry was highly effective in predicting stature. Their study highlighted that facial length and breadth could be used as non-invasive methods for estimating height, providing valuable tools in forensic reconstructions and identification.

Previous studies have demonstrated the significance of anthropometric parameters such as shoulder breadth, foot length, thigh length, and knee height in estimating stature and predicting health risks in diverse populations.

Additionally, research has highlighted the importance of considering genetic, environmental, and cultural factors in understanding variations in body proportions and health disparities among Indian and Nigerian populations. By extending this line of inquiry, our study contributes to the growing body of literature on anthropometry and stature estimation, providing valuable insights into the applicability of regression equations derived from specific anthropometric measurements in predicting stature across different demographic groups. Moreover, our findings underscore the utility of anthropometric measurements in forensic investigations, population health assessments, and anthropological research, thereby informing evidence-based interventions aimed at addressing health inequalities and promoting well-being within Indian and Nigerian populations.

Conclusion

In Indian and Nigerian men and women, reliable regression equations were constructed estimating body length as a function of knee height, hip length, foot length, shoulder width, and shoulder height in the sitting position. Only in Nigerian women and Indian men, body length was highly likely to depend on sitting knee height (R^2=0.531, p<0.001), as well as sitting hip length, sitting foot length, and sitting shoulder height (R^2=0.725, p<0.001). In Indian women and Nigerian men, the coefficients of determination of the regression equations were less than 0.5 (respectively R^2=0.463, p<0.001 and R^2=0.405, p<0.001) and therefore have no significant value in forensic medicine for determining body length. The revealed high correlation coefficients (0.6<r<0.75) observed in both test groups indicate the reliability of the constructed regression models.

References

[1] Ali, F. I., & Ahmed, A. A. (2020). Sexual and topological variability in palmprint ridge density in a sample of Sudanese population. *Forensic Science International: Reports,* 2, 100151. doi: 10.1016/j.fsir.2020.100151

[2] Asadujjaman, M., Molla, M. B. A., & Al Noman, S. N. (2019). Stature estimation from hand anthropometric measurements in Bangladeshi population. *Journal of forensic and legal medicine,* 65, 86-91. doi: 10.1016/j.jflm.2019.05.006

[3] Asadujjaman, M., Rashid, M. H. O., Rana, M. S., & Hossain, M. M. (2022). Stature estimation from footprint measurements in Bangladeshi adults. *Forensic Sciences Research,* 7(2), 124-131. doi: 10.1080/20961790.2020.1776469

[4] Bogin, B., & Varela-Silva, M. I. (2010). Leg length, body proportion, and health: a review with a note on beauty. *International journal of environmental research and public health,* 7(3), 1047-1075. doi: 10.3390/ijerph7031047

[5] Chandra, A., Chandna, P., Deswal, S., Mishra, R. K., & Kumar, R. (2015). Stature prediction model based on hand anthropometry. *International Journal of Biomedical and Biological Engineering,* 9(2), 201-207.

[6] Choong, C. L., Alias, A., Abas, R., Wu, Y. S., Shin, J. Y., Gan, Q. F., ... & Choy, K. W. (2020). Application of anthropometric measurements analysis for stature in human vertebral column: a systematic review. *Forensic Imaging,* 20, 200360. doi: 10.1016/j.fri.2020.200360

[7] Gunas, I. V., Shinkaruk-Dykovytska, M. M., Kotsyura, O. O., Orlovskiy, V. O., Dmytrenko, S. V., Shayuk, A. V., & Glushak, A. A. (2017). Differences of craniotype distribution and types of face among apparently healthy men from different regions of Ukraine. *Folia morphologica,* 76(3), 473-477. doi: 10.5603/FM.a2017.0017

[8] Holzer, T. L., & Savage, J. C. (2013). Global earthquake fatalities and population. *Earthquake Spectra,* 29(1), 155-175. doi: 10.1193/1.4000106

[9] Ibegbu, A. O., David, E. T., Hamman, W. O., Umana, U. E., & Musa, S. A. (2013). Association of hand length with height in Nigerian school children. *Journal of Biology and Life Sciences*, 4(2), 83-94. doi: 10.5296/jbls.v4i2.3025

[10] Jamison, P. L., & Ward, R. E. (1993). Brief communication: measurement size, precision, and reliability in craniofacial anthropometry: bigger is better. *American Journal of Physical Anthropology,* 90(4), 495-500. doi: 10.1002/ajpa.1330900409

[11] Jervas, E., Anibeze, C. I. P., Uloneme, G. C., & Anyanwu, G. E. (2015). Stature estimation of the Igbos using cephalo-facial anthropometry. *Journal of Forensic Research,* 6(4), 1-4. doi: 10.4172/2157-7145.1000295

[12] Kamal, R., & Yadav, P. K. (2016). Estimation of stature from different anthropometric measurements in Kori population of North India. *Egyptian journal of Forensic sciences,* 6(4), 468-477. doi: 10.1016/j.ejfs.2016.12.001

[13] Khangura, R. K., Sircar, K., & Grewal, D. S. (2015). Four odontometric parameters as a forensic tool in stature estimation. *Journal of forensic dental sciences,* 7(2), 132-136. doi: 10.4103/0975-1475.146367

[14] Kim, W., Kim, Y. M., & Yun, M. H. (2018). Estimation of stature from hand and foot dimensions in a Korean population. *Journal of forensic and legal medicine,* 55, 87-92. doi: 10.1016/j.jflm.2018.02.011

[15] Kishore, N., Marques, D., Mahmud, A., Kiang, M. V., Rodriguez, I., Fuller, A., ... & Buckee, C. O. (2018). Mortality in puerto rico after hurricane maria. *New England journal of medicine,* 379(2), 162-170. doi: 10.1056/NEJMsa1803972

[16] Marchenko, A. V., Shinkaruk-Dykovytska, M. M., Pozur, T. P., Gunas, V. I., & Orlovskiy, V. O. (2020). Models of individual linear dimensions necessary for the construction of the correct form of dental arches in young men with a wide face, depending on the features of odontometric and cephalometric indicators. *Wiadomosci Lekarskie* (Warsaw, Poland: 1960), 73(6), 1103-1107. doi: 10.36740/WLek202006104

[17] Marchenko, A. V., Prokopenko, O. S., Dzevulska, I. V., Zakalata, T. R., & Gunas, I. V. (2021). Mathematical modeling of teleroentgenographic parameters according to the method of Schwarz AM depending on the basic cephalometric parameters in Ukrainian young men and young women with different face types. *Wiadomosci Lekarskie* (Warsaw, Poland: 1960), 74(6), 1488-1492. PMID: 34159943

[18] Moorthy, T. N., Mostapa, A. M. B., Boominathan, R., & Raman, N. (2014). Stature estimation from footprint measurements in Indian Tamils by regression analysis. Egyptian Journal of Forensic Sciences, 4(1), 7-16. doi: 10.1016/j.ejfs.2013.10.002

[19] Navid, S., Mokhtari, T., Alizamir, T., Arabkheradmand, A., & Hassanzadeh, G. (2014). Determination of stature from upper arm length in medical students. *Anatomical Sciences Journal,* 11(3), 135-140.

[20] Pal, A., Aggarwal, P., Bharati, S., Panda, M., Datta, I., & Roy, P. (2014). Anthropometric measurements of the hand length and

their correlation with the stature in Eastern Indian population. *National Journal of medical research,* 4(04), 303-305.

[21] Paulis, M. G. (2015). Estimation of stature from handprint dimensions in Egyptian population. *Journal of forensic and legal medicine,* 34, 55-61. doi: 10.1016/j.jflm.2015.05.007

[22] Rai, P., Das, A., Agrawal, A. K., & Arora, D. (2020). Physical anthropometry in estimation of stature: A systematic review. *Int. J. Curr. Res. Rev,* 12, 75-79. doi: 10.31782/IJCRR.2020.122409

[23] Siegel, J. A., Saukko, P. J., & Houck, M. M. (2013). *Encyclopedia of forensic sciences.* Elsevier Ltd. All rights reserved. ISBN 978-0-12-382166-9

[24] Simon, S., Fischer, B., Rinner, A., Hummer, A., Frank, B. J., Mitterer, J. A., ... & Hofstaetter, J. G. (2023). Body height estimation from automated length measurements on standing long leg radiographs using artificial intelligence. *Scientific Reports,* 13(1), 8504. doi: 10.1038/s41598-023-34670-2

[25] Uhrová, P., Benuš, R., Masnicová, S., Obertová, Z., Kramárová, D., Kyselicová, K., ... & Neščáková, E. (2015). Estimation of stature using hand and foot dimensions in Slovak adults. *Legal medicine,* 17(2), 92-97. doi: 10.1016/j.legalmed.2014.10.005

[26] Ulijaszek, S. J., & Kerr, D. A. (1999). Anthropometric measurement error and the assessment of nutritional status. *British Journal of Nutrition,* 82(3), 165-177. doi: 10.1017/s0007114599001348

[27] Uzun, Ö., YegInoglu, G., Ertemoglu Öksüz, C., Kalkisim, Ş., & Zihni, N. (2019). Estimation of stature from upper extremity anthropometric measurements. *Journal of Clinical and Diagnostic Research,* 13, 9-15. doi: 10.7860/jcdr/2019/38372.12475

[28] Vercellotti, G., Piperata, B. A., Agnew, A. M., Wilson, W. M., Dufour, D. L., Reina, J. C., ... & Sciulli, P. W. (2014). Exploring the multidimensionality of stature variation in the past through comparisons of archaeological and living populations. *American Journal of Physical Anthropology,* 155(2), 229-242. doi: 10.1002/ajpa.22552

[29] Yadav, A. B., Kale, A. D., Mane, D. R., Yadav, S. K., & Hallikerimath, S. (2019). Stature estimation from regression analysis of facial anthropometry in Indian population. *Journal of Oral and Maxillofacial Pathology,* 23(2), 311. doi: 10.4103/jomfp.JOMFP_140_19

[30] Yeasmin, N., Asadujjaman, M., Islam, M. R., & Hasan, M. R. (2022). Stature and sex estimation from shoulder breadth, shoulder height, popliteal height, and knee height measurements in a Bangladeshi population. *Forensic Science International: Reports,* 5, 100258. doi: 10.1016/j.fsir.2022.100258

ОЦІНКА ДОВЖИНИ ТІЛА ЧОЛОВІЧОГО І ЖІНОЧОГО НАСЕЛЕННЯ ІНДІЇ ТА НІГЕРІЇ В ЗАЛЕЖНОСТІ ВІД ІНШИХ АНТРОПОМЕТРИЧНИХ ПАРАМЕТРІВ ЗА ДОПОМОГОЮ МНОЖИННОГО РЕГРЕСІЙНОГО АНАЛІЗУ

Usman A., Gupta A., Ghosal A., Biswas A., Adarsh K.

У випадках масових катастроф, аварій або кримінальних розслідувань, коли особу жертв не встановлено, деякі базові антропологічні параметри допомагають у визначенні таких характеристик, як раса, стать, вік і зріст. Оцінка зросту за допомогою кількох тілесних вимірювань, таких як ширина плечей, довжина стопи, довжина стегна та висота коліна, є загальним підходом в антропометрії та судовій антропології. Наявність статевих та популяційних відмінностей в антропометричних показниках дозволяє використовувати ці вимірювання не лише для оцінки зросту людини, а й для визначення статі, різних рас або популяцій на основі скелетних залишків. Метою дослідження є розробка та практична перевірка роботи регресійних рівнянь для оцінки зросту залежно від інших антропометричних показників чоловіків та жінок двох етнічно різних популяцій. Для цього дослідження були зібрані антропометричні дані від двох різних груп населення: індійців (n=102) і нігерійців (n=205). Були отримані основні демографічні дані, а також результати вимірювання ширини плечей, висоти плечей у сидячому положенні, довжини стопи в сидячому положенні, висоти колін і довжини стегна, використовуючи стандартизовані методики відповідно до встановлених антропометричних протоколів. Статистичний аналіз був проведений за допомогою відповідного програмного забезпечення, такого як SPSS, R або SAS. Для оцінки довжини тіла залежно від інших антропометричних показників використовувався метод множинної регресії. У результаті проведеного аналізу множинної лінійної регресії були встановлені достовірні зв'язки між зростом і певними антропометричними вимірами у нігерійських та індійських чоловіків і жінок. Було виявлено, що зріст з високою ймовірністю залежить від висоти коліна в сидячому положенні у нігерійських жінок (R^2=0,531, p<0,001), а також від довжини стегна, довжини стопи та висоти плечей у сидячому положенні у індійських чоловіків (R^2=0,725, p<0,001). Зріст індійських жінок достовірно залежить від довжини стегна та довжини стопи в сидячому положенні, а у нігерійських чоловіків - від довжини стегна, довжини стопи, ширини плечей та висоти плечей у сидячому положенні, але регресійні рівняння мають коефіцієнт детермінації менше ніж 0,5 (відповідно, R^2=0,463, p<0,001 і R^2=0,405, p<0,001), тому вони не мають значного значення для судових цілей. Додаткові групи (по 30 осіб для кожної категорії) були використані для перевірки отриманих регресійних рівнянь. Високі коефіцієнти кореляції (0,6<r<0,75), виявлені в обох тестових групах, свідчать про достовірність регресійних моделей та придатність обраних антропометричних вимірювань для оцінки зросту в цих популяціях. Отримані дані підкреслюють важливість урахування популяційних специфічних факторів при розробці регресійних рівнянь для оцінки зросту і наголошують на корисності антропометричних вимірювань у прогнозуванні цього показника для різних статевих і демографічних груп населення, хоча їх подальша перевірка на більших і більш різноманітних вибірках є необхідною.

Ключові слова: *регресійний аналіз, оцінка зросту, антропометричні вимірювання, нігерійські та індійськи чоловіки і жінки.*

Author's contribution

Usman A. - writing of original draft and methodology.
Gupta A. - supervision, project administration and data visualization.
Ghosal A. - conceptualization, formal analysis and validation.
Biswas A. - resources and software.
Adarsh K. - review writing and editing.

Signed for print 17.09.2024
Format 60x84/8. Printing offset. Order № 6683. Circulation 100.
Vinnytsia. Printing house “TVORY”, Nemyrivske shose St., 62a,
Vinnytsya, 21034
Phone: 0 (800) 33-00-90, (096) 97-30-934, (093) 89-13-852,
(098) 46-98-043
e-mail: tvory2009@gmail.com
http://www.tvoru.com.ua